ENVIRONMENTAL DRIVERS OF THE CORAL REEF ACCRETION-EROSION BALANCE IN PRESENT AND FUTURE OCEAN CONDITIONS

A DISSERTATION SUBMITTED TO THE GRADUATE DIVISION OF THE UNIVERSITY OF HAWAIʻI AT MĀNOA IN PARTIAL FULFILLMENT OF THE REQUIREMENTS FOR THE DEGREE OF

DOCTOR OF PHILOSOPHY

IN

ZOOLOGY (MARINE BIOLOGY)

AUGUST 2015

By

Nyssa J. Silbiger

Dissertation committee:

Megan Donahue, Chairperson
Ruth Gates
Florence Thomas
Robert Toonen
Stacy Jorgensen

This dissertation is dedicated to the memory of Matthew W. Beard. Although you left this world way too soon, your passion for science and coral reefs continues to drive me.

ACKNOWLEDGEMENTS

There are so many people that have supported me and helped me throughout my PhD. I am sincerely grateful to each and every one of you—these last 6 years would not have been the same without you all. First, and foremost, I am indebted to Dr. Megan Donahue, my wonderful PhD advisor and fearless leader. Megan has been the most supportive advisor. She is a brilliant ecologist, a total rock star in the field, an overall fun person to be around, and her enthusiasm for science is always evident and contagious. I feel so lucky to have gotten the opportunity to learn from her and I am very excited to continue to collaborate with her in the future. I also thank the rest of my brilliant committee members. All of my committee members were "second advisors" to me; they always took the time to talk with me no matter how busy they were. Dr. Rob Toonen was immensely helpful in putting together my NWHI chapter. He made sure that there was a spot for me on the research cruises and helped a lot with the community data methods and analysis. He is also one of the nicest and most supportive faculty members I know. Dr. Florence Thomas was a wonderful collaborator on many of my chapters. In particular, she made me think more deeply about hydrodynamic processes on the reefs. Dr. Ruth Gates really encouraged me to step back and think more about the "big picture" of my research. Her enthusiasm for coral reef research was always apparent. Dr. Stacy Jorgenson helped me to think more specifically about the importance of spatial-scale. Thank you all so much. You all really made my PhD an exciting journey.

I also need to thank the lovely ladies (and adopted ladies and gents) of the Donahue Lab. Megsie, Jamie, Chelsie, Courtney, Katie, Julie, Megan, and Iain have been the most fantastic lab mates. They provided such thoughtful advice in every lab meeting and were always super

encouraging. They also provided endless lab, field, and emotional support. I am very lucky to have gotten the opportunity to share a lab with each and every one of you.

I thank the countless people who helped me in the lab and in the field, especially those brave souls that came diving with me at 2am including (in no particular order): Scott Godwin, Holly Bolick, Matt Iacchei, Ily Iglesias, Maggie Sogin, CJ Bradley, Adrienne Copeland, Jessica Chen, Mary Donovan, Mareike Sudek, Iain Caldwell, Richard Coleman, Jessica Faith, Justin Miyano, Rebecca Maguire, Oscar Guadayol, Marlin Atkinson, Hollie Putnam, Chris Jury, Sherril Leon Soon, Ivor Williams, Rusty Brainard, Chip Young, John Burns, Eileen Nalley, Chelsie Counsell, Julie Zill, Mark Royer, Anne Rosinski, Kelsie DiPerna, Jason Jones, Keoki Stender, NOAA Ship Hi‘ialakai, UH Lapidary Facility, SOEST S-Lab, NOAA CRED, Nick Griffith, Megsie Siple, Jamie Caldwell, Kaleonani Hurley, Maya Walton, Dan Schar, Eric Tong, Jon Whitney and I am sure many more that I forgot to list here. A huge thank you to everyone at NOAA's Coral Reef Ecosystem Division for sharing their environmental data with me and providing logistical support for my 4th dissertation chapter. Thank you to all the crew on NOAA ship Hi‘ialakai for 4 summers of fun and safe cruises. Thank you to Mark Riccio and Fred von Stein at the Cornell Multiscale Imaging Facility for showing me the awesome applications of µCT scanning technology. Thank you to all the office and fiscal staff at HIMB and Biology. My dissertation greatly benefited from conversations with and edits from numerous people outside my committee including: Hollie Putnam, Matt Iacchei, Marlin Atkinson, Paul Jokiel, Margaret McManus, and the Donahue Lab.

Being able to live in Hawai‘i during my PhD was a blessing for many reasons. In addition to the obvious—great hiking trails, beautiful scenery, awesome surfing and diving—I was surrounded by the most wonderful people. Thank you to my Hawaiian ‘Ohana: "the melting

pot" (Maya Walton and Richard Coleman), Ily Iglesias, "The Team" (Maggie Sogin and Megan Ross), Hollie Putnam, Matt Iacchei, "The Donahue Lab Sorority", my many housemates over the years, Adrienne Copeland, Pat Curry, Angela Richards Doná, Sherril Leon Soon, Shark Mark, and many more. We have had so many crazy adventures, underwater pumpkin carving competitions, dance parties, catan battles, and just so many wonderful memories. Thank you for endless amounts of fun and laughter. Thank you to my "actual" family for putting up with me living on the other side of the world for the last six years. To my mom, Dianne, my dad, Randy, my sister, Erica, and my brother, Jason, you have all been so supportive of me throughout my entire life and I love you all very much. I could not have made it this far without your love and support.

Thank you to all my funding sources: Dr. Charles and Sandra Guest-Van Riper Endowed Student Travel Award for Graduate Students, Jessie D Kay Memorial Fellowship, National Oceanography and Atmospheric Administration Dr. Nancy Foster Scholarship Program, Travel Support for the Third International Symposium on a High CO_2-world, PADI Foundation Grant, University of Hawai‘i at Mānoa Graduate Student Research Grant, Dai Ho Chun Fund for Graduate Fellowships, University of Hawai‘i SeaGrant Program, Sigma Xi Grant in Aid of Research, NSF EPSCoR, Charles H. and Margaret B. Edmonson Research Fund, and the Kellogg Biological Station Grant for Summer Program. A very special thank you to the NOAA Nancy Foster Scholarship Program for providing a plethora of professional development opportunities, an amazing support system of scholars and program officers, funding, and, of course, welcoming me into the National Marine Sanctuaries family. The skills that I acquired and opportunities that I was afforded as a Nancy Foster Scholar changed the course of my graduate career.

Thank you!!

ABSTRACT

Worldwide, declines in coral cover and shifts in coral reef community composition have raised concerns about whether reef accretion will continue to exceed reef erosion. Reef persistence is influenced by global and local anthropogenic factors, such as ocean warming, acidification, eutrophication, and overfishing, as well as natural environmental variability. Predicting reef response to environmental stress requires an understanding of both natural and anthropogenic environmental drivers of reef accretion and erosion, and how these drivers interact at different spatiotemporal scales. In Chapters 2 and 3, I measured the variation in accretion, erosion, and net change rates along a natural gradient to determine the dominant environmental drivers of accretion-erosion rates at small spatial scales (tens of meters). In Chapter 4, I expanded the geographic range to 1000s of kilometers, measuring variation in accretion and erosion rates, as well as bioeroder community composition, across the Hawaiian Archipelago. In Chapter 5, I used a controlled mesocosm experiment to directly examine the effects of global anthropogenic drivers (i.e., temperature and ocean acidification) on the coral reef accretion-erosion balance. The results of my dissertation research highlight the significance of spatial scale in understanding reef dynamics and the differential responses of reef accretion and erosion to environmental drivers, which will change our predictions of net coral reef response to future environmental change. Further, my results suggest that increases in reef erosion, combined with expected decreases in calcification, could accelerate the shift of coral reefs to an erosion-dominated system in a high CO_2 world.

TABLE OF CONTENTS

LIST OF TABLES

LIST OF FIGURES

CHAPTER 1

INTRODUCTION: AN OVERVIEW OF THE CORAL REEF ACCRETION-EROSION BALANCE

Background

The value of coral reefs to human health and welfare is unequivocal. Coral reefs make up <0.1% of the global ocean (Reaka-Kudla et al. 1997), but they provide societal, economic, and health benefits to people world-wide. Coral reefs in Hawai‘i alone contribute over $33 billion to the US economy by supplying food, goods, tourism opportunities, and shoreline protection (Bishop et al. 2011); the strong, complex structural framework of coral reefs controls many of these economic and ecosystem resources. Corals form the structural framework of coral reef ecosystems, but other reef processes influence the integrity of this framework.

Coral reefs persist in a balance between reef growth (accretion) and reef breakdown (erosion). Corals and other calcifying organisms secrete calcium carbonate ($CaCO_3$) skeleton, while a diverse community of bioeroders erode reefs through grazing on and boring into the skeletal structure of the reef (Neumann 1966). Enhanced rates of bioerosion can compromise the function of the reef framework, undermining the mechanical stability (Scott and Risk 1988), structural complexity, and net accretion of coral reefs. Coral reefs absorb up to 90% of the energy from wind-driven waves (UNEP-WCMC 2006) providing natural shoreline protection to tropical ecosystems. When mechanical stability of coral reefs is compromised (Hutchings 1986), coastal property is more susceptible to storm damage and wave action (Reaka-Kudla et al. 1997). Structural complexity provides habitat and protection for reef organisms (Mumby and Wabnitz 2002), and reduced structural complexity can result in decreased abundance and diversity of fishes and invertebrates (Jones et al. 2004). Finally, if bioerosion exceeds accretion, coral reefs will drown as a result of sea-level rise. The services humans receive from coral reef ecosystems depend on the response of both erosion and accretion rates to local and global human impacts, including coastal development and increased atmospheric carbon dioxide.

The impact of human-induced stressors on corals has been extensively investigated. For example, coral cover, and general reef health, is negatively related to human population (Sandin et al. 2008; Williams et al. 2015). In response to climate change stressors, coral calcification declines in warmer, more acidic ocean conditions (reviewed in Hoegh-Guldberg et al. 2007; Pandolfi et al. 2011) though the species-specific responses are variable (Pandolfi et al. 2011). Notably, corals ability to adapt or acclimatize to changing conditions, particularly to rising sea surface temperature (SST) and CO_2, is a newer area research (Putnam 2012; van Oppen et al. 2015). Yet, the impacts of many stressors on secondary calcification and bioerosion are not well-described. In this dissertation, I explore the impacts of a suite of environmental variables on secondary accretion and erosion in both natural and simulated ocean conditions with a focus on rising SST and ocean acidity.

Bioeroder and secondary calcifier communities

Bioerosion rates are influenced by community composition. Bioeroding organisms may be classified into three functional groups: grazers (e.g., urchins and parrotfish), microborers (e.g., euendoliths), and macroborers (e.g., sponges, polychaetes, and bivalves). Grazers erode reefs externally by scraping $CaCO_3$ while foraging on the overlying algal or coral tissue. Micro- and macroborers erode reefs internally by boring, most frequently in areas where live coral tissue no longer covers the reef substrate (Highsmith 1981b). The relative rates of erosion from these functional groups differ among regions. For example, on the Great Barrier Reef, bioerosion rates from grazers, macroboreres, and microborers were 0.004, 0.13, and 0.15 kg $CaCO_3$ m^{-2} yr^{-1}, respectively, on an inshore reef, while an offshore reef had rates of 0.68, 0.03, and 1.4 kg $CaCO_3$ m^{-2} yr^{-1} in the same study (Tribollet and Golubic 2005). Among these three functional groups,

macroborers may be most diverse, consisting of hundreds of polychaete, sipunculan, sponge, and bivalve species with a range of life history strategies and morphological and chemical mechanisms for boring.

Secondary accretion rates are also influenced by community composition. All non-coral encrusters (e.g., CCA, bivalves, barnacles, and other calcifying sessile invertebrates) are considered secondary calcifiers, but CCA contributes the most to $CaCO_3$ production from this group (Perry et al. 2008). In fact, CCA is the dominant calcifier, inclusive of corals, in shallow, high energy, reef crest environments (Steneck and Adey 1976; Adey and Steneck 2001). In addition to contributing to the $CaCO_3$ budget, CCA helps maintain reef stability by cementing the reef together (Littler 1973; Camoin and Montaggioni 1994; Adey 1998) and producing chemical cues that induce settlement of many invertebrate larvae including several species of corals (Harrington et al. 2004; Price 2010). Similar to erosion, the relative cover of CCA can also differ across regions. In the Great Barrier Reef, CCA cover is highest in outer-shelf reefs where turf algae cover is lowest (Scott and Russ 1987; Klumpp and McKinnon 1989; Sweatman 1997).

Environmental drivers of the accretion-erosion balance

Secondary accretion and erosion rates differ across regions, but these patterns are driven by a suite of interacting chemical, physical, and biological drivers. The myriad of drivers complicates predictions of reef response to environmental variability and warrants an investigation that compares the relative influence of multiple parameters in a natural reef environment.

Chemical drivers: Many carbonate chemistry and nutrient parameters are known to drive patterns in accretion and erosion. In response to changing carbonate chemistry resulting from increased CO_2, erosion rates increase (Tribollet et al. 2009; Wisshak et al. 2012; Fang et al.

2013; Reyes-Nivia et al. 2013; Wisshak et al. 2013; Silbiger et al. 2014; DeCarlo et al. 2015; Enochs et al. 2015; Silbiger and Donahue 2015) and secondary accretion rates decrease (Jokiel et al. 2008; Diaz-Pulido et al. 2012; Johnson and Carpenter 2012; Comeau et al. 2013). Studies have also found a parabolic response between secondary calcification and CO_2 (Ries et al. 2009; Silbiger and Donahue 2015). Several studies show increased erosion in eutrophic relative to oligotrophic conditions (reviewed in Le Grand and Fabricius 2011) suggesting that erosion rates are particularly sensitive to nutrients, perhaps because many macroborers are filter feeders. Nutrients may increase secondary accretion via enhanced photosynthesis by calcifying algae and increased food availability to filter-feeding calcifying invertebrates (such as bivalves), but studies have also shown that high concentrations of phosphate could be damaging to CCA (Björk et al. 1995).

Physical drivers: SST, wave energy, and depth can influence secondary accretion and erosion. SST can increase metabolic performance in calcifying algae (Harley et al. 2012) or invertebrates (Huey and Kingsolver 1989) and thus increase accretion or erosion rates (Davidson et al. 2013; Fang et al. 2013; Wisshak et al. 2013). However, if a thermal maximum is reached or if temperature stress is combined with other stressors, increased temperature can be damaging, particularly to accreting organisms (Johnson and Carpenter 2012; Harvey et al. 2013; Silbiger and Donahue 2015). Wave energy can also impact accretion rates: Hamylton et al (2013) found an increase in carbonate production (including live coral, carbonate sand, green calcareous macroalgae, and encrusting calcified algae) with increasing wave energy (Hamylton et al. 2013). In response to depth, erosion rates are positively correlated with depth on Jamaican forereef sites (Perry 1998) and accretion rates of photosynthesizing calcifiers could be impacted by depth due to light limitations.

Biological drivers: Finally, biological parameters such as benthic cover and fish biomass can mediate accretion and erosion rates. Benthic cover can influence accretion and erosion rates through space availability for settling eroders or calcifiers. Reefs with a high density of dead coral or bare substrate will likely have high erosion rates because most eroders prefer dead coral (Highsmith 1981a; Hutchings 1986). Some eroders do colonize live coral, as well (see, Le Grand and Fabricius 2011; DeCarlo et al. 2015). The presence of secondary calcifiers, mainly CCA, can influence erosion by inhibiting the settlement of bioeroders; CCA seals off the substrate making it difficult for borers to penetrate the $CaCO_3$ skeleton (White 1980; Tribollet and Payri 2001). Herbivorous fish can directly influence erosion by removing $CaCO_3$ substrate while grazing for algae and can indirectly influence accretion by removing fleshy algae and relieving competitive interactions with CCA (Harley et al. 2012).

Patterns in accretion-erosion across spatial scales

Many of the studies describing the relationships between environmental drivers and accretion-erosion rates were conducted at spatial scales ranging from 1 to over 10,000 km. The relative importance of environmental drivers to accretion and erosion may change across spatial scale. A study in Kāneʻohe Bay, Hawaiʻi (~ 10 km) hypothesized that gradients in wave energy drove patterns in secondary calcifiers while gradients in eutrophication drove patterns in micro-bioerosion (Tribollet et al. 2006). In the Great Barrier Reef (~200 km), secondary calcification was correlated with grazing and microbioersion; grazing pressure also had the strongest influence on total erosion rates (Tribollet and Golubic 2005). A broader Pacific Basin (~16,000 km) study suggested ocean acidity regulated erosion rates in live corals, but the relationship between erosion and ocean acidity was mediated by nutrient concentrations (DeCarlo et al.

2015). Further, recent studies highlight the importance of local or small-scale within reef (~30 m) environmental variability and suggest that this variability could impact reef processes (Gagliano et al. 2010; Guadayol et al. 2014), such as accretion-erosion rates. To link environmental variability with reef response, we need to understand the spatial scales at which reefs are responding to environmental change, but there has yet to be a study that compares multiple accretion-erosion drivers on both broad and small spatial scales.

Could climate change tip the balance?

Though many environmental parameters influence accretion-erosion rates, the threat of climate change may have an overwhelming impact on the coral reef accretion-erosion balance. Rising anthropogenic CO_2 is increasing sea surface temperature (SST) and ocean acidity (Caldeira and Wickett 2003; Feely et al. 2004; Cubasch et al. 2013). Global SST has increased by 0.78 °C since pre-industrial times (Cubasch et al. 2013), and it is predicted to increase by another 0.8–5.7 °C by the end of this century (Van Vuuren et al. 2008; Meinshausen et al. 2011; Rogelj et al. 2012). The Hawai‘i Ocean Time-series detected a 0.075 decrease in mean annual pH at station ALOHA over the past 20 years (Doney et al. 2009) and there have been similar trends at stations around the world, including the Bermuda Atlantic Time-series and the European Station for Time-series Observations in the ocean (Solomon 2007). pH is expected to drop by an additional 0.14–0.35 pH units by the end of the twenty-first century (Bopp et al. 2013). All marine ecosystems are at risk from rising SST and decreasing pH (Hoegh-Guldberg et al. 2007; Doney et al. 2009; Hoegh-Guldberg and Bruno 2010), but coral reefs are particularly vulnerable to these stressors (reviewed in Hoegh-Guldberg et al., 2007).

CCA and coral calcification are predicted to decrease by 10 - 50% when pCO_2 doubles, as expected by 2100 (Kleypas and Langdon 2006) . Hoegh-Guldberg (1999) predicts bleaching events will increase with rising SST, reducing coral productivity and growth. Recent evidence supports this prediction: corals have shown a decrease in linear extension by 1.02% yr^{-1} and skeletal density by 0.36% yr^{-1} over 16 years in the Great Barrier Reef (Cooper et al. 2008) which was accompanied by a local increase in yearly temperature of approximately 0.4°C (Cooper et al. 2008) and a global increase in about 25ppm pCO_2 (Hawai‘i Ocean Time-series).

The relationship between ocean acidity and net reef calcification is an area of active research. Studies have found a positive relationship between net coral calcification and aragonite saturation state (Ω_{arg}; the concentration of calcium and carbonate ions in relation to a dissociation constant) (Langdon et al. 2000), suggesting that calcification will decline with the predicted decrease in Ω_{arg}. One study suggests that reefs with an Ω_{arg} of less than 3.25 will be net dissolving (Hoegh-Guldberg et al. 2007), but this number is highly debatable and, notably, reefs in Kāne‘ohe Bay with an Ω_{arg} of < 3 are still net calcifying (Shamberger et al. 2011). The puzzling question is why some reefs are in net dissolution when the water is still super-saturated with aragonite (i.e. Ω_{arg} >1; see,Yates and Halley 2006; Silverman et al. 2007). Dissolution or, perhaps, bioerosion may be more sensitive to changes in ocean acidity than calcification, leading to net dissolution in super-saturated waters. Erez et al. (2011) hypothesize that increased dissolution, rather than decreased accretion, maybe be the reason that net coral calcification is so sensitive to ocean acidification.

A handful of studies have examined the impact of rising SST and ocean acidity on individual groups of eroders, mainly *Clinoid* sponges (Wisshak et al. 2012; Fang et al. 2013; Wisshak et al. 2013; Enochs et al. 2015) and a community of photosynthesizing microborers

(Tribollet et al. 2009; Reyes-Nivia et al. 2013). These studies found that bioerosion increased under future climate change scenarios. Several studies have focused on tropical calcifying algae and have found decreased calcification (Kleypas and Langdon 2006; Jokiel et al. 2008; Semesi et al. 2009; Comeau et al. 2013; Johnson et al. 2014) and increased dissolution (Diaz-Pulido et al. 2012) with increasing ocean acidity and/or SST. However, the bioeroder and secondary calcifier communities are extremely diverse and an integrative study on the impacts of climate stressors incorporating a natural community of bioeroders and secondary calcifiers is lacking.

Objectives

The overall goal of my dissertation is to determine the dominant drivers of accretion-erosion rates and macroborer communities to test if the relationship between accretion-erosion rates and environmental drivers are conserved across space, and provide context for the effects of climate change on the accretion-erosion balance. I use a combination of field (Chapters 2-4) and laboratory experiments (Chapter 5) to address this goal. Further, I present a new technique for quantifying accretion-erosion rates to advance the study of accretion-erosion beyond the limits imposed by traditional methods. I demonstrate the use of micro computer-aided tomography (μCT), a powerful technology for creating 3-dimensional images of the internal structure of solid objects, to calculate bioerosion and secondary accretion rates with micrometer-scale precision and accuracy. My specific objectives are to:

1) compare pH with other known environmental predictors as possible drivers of net reef erosion on a small (local) spatial scale (Chapter 2);

2) individually test the relationship between accretion and erosion rates with previously described environmental correlates of the accretion-erosion balance (Chapter 3);

3) describe patterns and environmental drivers of accretion-erosion rates and macroborer communities across broad spatial scales (Chapter 4);

4) determine the impact of future climate scenarios on calcification, dissolution, and net community production rates from a natural community of secondary calcifiers and bioeroders (Chapter 5);

5) highlight the application of a novel μCT method to analyze accretion and erosion rates (Chapters 2 - 4).

REFERENCES

Adey WH (1998) Review—coral reefs: algal structured and mediated ecosystems in shallow, turbulent, alkaline waters. Journal of Phycology 34:393-406

Adey WH, Steneck RS (2001) Thermogeography over time creates biogeographic regions: a temperature/space/time-integrated model and an abundance-weighted test for benthic marine algae. Journal of Phycology 37:677-698

Bishop RC, Chapman DJ, Kanninen BJ, Krosnick JA, Leeworthy VR, Meade NF (2011) Total economic value for protecting and restoring Hawaiian coral reef ecosystems: Final report. US Department of Commerce, National Oceanic and Atmospheric Administration, National Ocean Service

Björk M, Mohammed S, Björklund M, A S (1995) Coralline alge, important coral reef builders threatened by pollution. Ambio 24:502-505

Bopp L, Resplandy L, Orr JC, Doney SC, Dunne JP, Gehlen M, Halloran P, Heinze C, Ilyina T, Séférian R, Tjiputra J, Vichi M (2013) Multiple stressors of ocean ecosystems in the 21st century: projections with CMIP5 models. Biogeosciences 10:3627-3676

Caldeira K, Wickett ME (2003) Oceanography: anthropogenic carbon and ocean pH. Nature 425:365-365

Camoin GF, Montaggioni LF (1994) High energy coralgal-stromatolite frameworks from Holocene reefs (Tahiti, French Polynesia). Sedimentology 41:655-676

Comeau S, Edmunds PJ, Spindel NB, Carpenter RC (2013) The responses of eight coral reef calcifiers to increasing partial pressure of CO_2 do not exhibit a tipping point. Limnol Oceanogr 58:388-398

Cooper TF, De 'Ath G, Fabricius KE, Lough JM (2008) Declining coral calcification in massive *Porites* in two nearshore regions of the northern Great Barrier Reef. Global Change Biology 14:529-538

Cubasch U, Wuebbles D, Chen D, Facchini MC, Frame D, Mahowald N, Winther J-G (2013) Climate Change 2013: The Physical Science Basis. Contribution of Working Group I to the Fifth Assessment Report of the Intergovernmental Panel on Climate Change In: Stocker TF, Qin D, Plattner G-K, Tignor M, Allen SK, Boschung J, Nauels A, Xia Y, Bex V, Midgley PM (eds), Cambridge, United Kingdom and New York, NY, USA.

Davidson TM, de Rivera CE, Carlton JT (2013) Small increases in temperature exacerbate the erosive effects of a non-native burrowing crustacean. Journal of Experimental Marine Biology and Ecology 446:115-121

DeCarlo TM, Cohen AL, Barkley HC, Cobban Q, Young C, Shamberger KE, Brainard RE, Golbuu Y (2015) Coral macrobioerosion is accelerated by ocean acidification and nutrients. Geology 43:7-10

Diaz-Pulido G, Anthony K, Kline DI, Dove S, Hoegh-Guldberg O (2012) Interactions between ocean acidification and warming on the mortality and dissolution of coralline alge. Journal of Phycology 48:32-39

Doney SC, Fabry VJ, Feely RA, Kleypas JA (2009) Ocean Acidification: The Other CO_2 Problem. Annual Review of Marine Science 1:169-192

Enochs IC, Manzello DP, Carlton RD, Graham DM, Ruzicka R, Colella MA (2015) Ocean acidification enhances the bioerosion of a common coral reef sponge: implications for the persistence of the Florida Reef Tract. Bulletin of Marine Science 91:000-000

Erez J, Reynaud S, Silverman J, Schneider K, Allemand D (2011) Coral calcification under ocean acidification and global change. In: Dubinski Z, Stambler N (eds) Coral Reefs: an ecosystem in transition. Springer,

Fang JKH, Mello-Athayde MA, Schönberg CHL, Kline DI, Hoegh-Guldberg O, Dove S (2013) Sponge biomass and bioerosion rates increase under ocean warming and acidification. Global Change Biology 19:3581-3591

Feely RA, Sabine CL, Lee K, Berelson W, Kleypas J, Fabry VJ, Millero FJ (2004) Impact of anthropogenic CO_2 on the $CaCO_3$ system in the oceans. Science 305:362-366

Gagliano M, McCormick MI, Moore JA, Depczynski M (2010) The basics of acidification: baseline variability of pH on Australian coral reefs. Marine Biology 157:1849-1856

Guadayol Ò, Silbiger NJ, Donahue MJ, Thomas FIM (2014) Patterns in Temporal Variability of Temperature, Oxygen and pH along an Environmental Gradient in a Coral Reef. PloS one 9:e85213

Hamylton SM, Pescud A, Leon JX, Callaghan DP (2013) A geospatial assessment of the relationship between reef flat community calcium carbonate production and wave energy. Coral reefs 32:1025-1039

Harley CDG, Anderson KM, Demes KW, Jorve JP, Kordas RL, Coyle TA, Graham MH (2012) Effects of climate change on global seaweed communities. Journal of Phycology 48:1064-1078

Harrington L, Fabricius K, De'Ath G, Negri A (2004) Recognition and selection of settlement substrata determine post-settlement survival in corals. Ecology 85:3428-3437

Harvey BP, Gwynn-Jones D, Moore PJ (2013) Meta-analysis reveals complex marine biological responses to the interactive effects of ocean acidification and warming. Ecology and evolution 3:1016-1030

Highsmith RC (1981a) Coral bioerosion at Enewetak- agents and dynamics. Internationale Revue Der Gesamten Hydrobiologie 66:335-375

Highsmith RC (1981b) Coral bioerosion - damage relative to skeletal density. American Naturalist 117:193-198

Hoegh-Guldberg O (1999) Climate change, coral bleaching and the future of the world's coral reefs. Marine and Freshwater Research 50:839-866

Hoegh-Guldberg O, Bruno JF (2010) The impact of climate change on the world’s marine ecosystems. Science 328:1523-1528

Hoegh-Guldberg O, Mumby PJ, Hooten AJ, Steneck RS, Greenfield P, Gomez E, Harvell CD, Sale PF, Edwards AJ, Caldeira K, Knowlton N, Eakin CM, Iglesias-Prieto R, Muthiga N, Bradbury RH, Dubi A, Hatziolos ME (2007) Coral reefs under rapid climate change and ocean acidification. Science 318:1737-1742

Huey RB, Kingsolver JG (1989) Evolution of thermal sensitivity of ectotherm performance. Trends in Ecology & Evolution 4:131-135

Hutchings PA (1986) Biological destruction of coral reefs- a review. Coral Reefs 4:239-252

Johnson MD, Carpenter RC (2012) Ocean acidification and warming decrease calcification in the crustose coralline alga *Hydrolithon onkodes* and increase susceptibility to grazing. J Exp Mar Biol Ecol 434:94-101

Johnson MD, Moriarty VW, Carpenter RC (2014) Acclimatization of the Crustose Coralline Alga *Porolithon onkodes* to Variable pCO_2. PLOS ONE 9:e87678

Jokiel PL, Rodgers KS, Kuffner IB, Andersson AJ, Cox EF, Mackenzie FT (2008) Ocean acidification and calcifying reef organisms: a mesocosm investigation. Coral Reefs 27:473-483

Jones GP, McCormick MI, Srinivasan M, Eagle JV (2004) Coral decline threatens fish biodiversity in marine reserves. Proceedings of the National Academy of Sciences of the United States of America 101:8251-8253

Kleypas J, Langdon C (2006) Coral reefs and changing seawater chemistry Coral Reefs and Climate Change: Science and Management. American Geophysical Union, Washington D.C.,

Klumpp DW, McKinnon AD (1989) Temporal and spatial patterns in primary production of a coral-reef epilithic algal community. Journal of Experimental Marine Biology and Ecology 131:1-22

Langdon C, Takahashi T, Sweeney C, Chipman D, Goddard J, Marubini F, Aceves H, Barnett H, Atkinson MJ (2000) Effect of calcium carbonate saturation state on the calcification rate of an experimental coral reef. Global Biogeochemical Cycles 14:639-654

Le Grand HM, Fabricius KE (2011) Relationship of internal macrobioeroder densities in living massive *Porites* to turbidity and chlorophyll on the Australian Great Barrier Reef. Coral Reefs 30:97-107

Littler MM (1973) The population and community structure of Hawaiian fringing-reef crustose Corallinaceae (Rhodophyta, Cryptonemiales). Journal of Experimental Marine Biology and Ecology 11:103-120

Meinshausen M, Smith SJ, Calvin K, Daniel JS, Kainuma MLT, Lamarque JF, Matsumoto K, Montzka SA, Raper SCB, Riahi K (2011) The RCP greenhouse gas concentrations and their extensions from 1765 to 2300. Climatic Change 109:213-241

Mumby PJ, Wabnitz CCC (2002) Spatial patterns of aggression, territory size, and harem size in five sympatric Caribbean parrotfish species. Environmental Biology of Fishes 63:265-279

Neumann AC (1966) Observations on coastal erosion in Bermuda and measurements of boring rate of sponge *Cliona lampa.* Limnology and Oceanography 11:92-108

Pandolfi JM, Connolly SR, Marshall DJ, Cohen AL (2011) Projecting coral reef futures under global warming and ocean acidification. Science 333:418-422

Perry CT (1998) Macroborers within coral framework at Discovery Bay, north Jamaica: species distribution and abundance, and effects on coral preservation. Coral Reefs 17:277-287

Perry CT, Spencer T, Kench PS (2008) Carbonate budgets and reef production states: a geomorphic perspective on the ecological phase-shift concept. Coral Reefs 27:853-866

Price N (2010) Habitat selection, facilitation, and biotic settlement cues affect distribution and performance of coral recruits in French Polynesia. Oecologia 163:747-758

Putnam HM (2012) Resilience and Acclimatization Potential of Reef Corals Under Predicted Climate Change Stressors. University of Hawai ʻi Mānoa p154

Reaka-Kudla ML, Wilson DE, Wilson EO (1997) Biodiversity II: understanding and protecting our biological resources. Joseph Henry Press

Reyes-Nivia C, Diaz-Pulido G, Kline D, Guldberg O-H, Dove S (2013) Ocean acidification and warming scenarios increase microbioerosion of coral skeletons. Global Change Biology 19:1919-1929

Ries JB, Cohen AL, McCorkle DC (2009) Marine calcifiers exhibit mixed responses to CO_2-induced ocean acidification. Geology 37:1131-1134

Rogelj J, Meinshausen M, Knutti R (2012) Global warming under old and new scenarios using IPCC climate sensitivity range estimates. Nature Climate Change 2:248-253

Sandin SA, Smith JE, DeMartini EE, Dinsdale EA, Donner SD, Friedlander AM, Konotchick T, Malay M, Maragos JE, Obura D (2008) Baselines and degradation of coral reefs in the northern Line Islands. PLoS One 3:e1548

Scott FFJ, Russ GGR (1987) Effects of grazing on species composition of the epilithic algal community on coral reefs of the central Great Barrier Reef. Marine Ecology Progress Series-pages: 39: 293-304

Scott PJB, Risk MJ (1988) The effect of Lithophaga (Bivalvia, Mytilidae) boreholes on the strength of the coral *Porites lobata*. Coral Reefs 7:145-151

Semesi IS, Kangwe J, Björk M (2009) Alterations in seawater pH and CO_2 affect calcification and photosynthesis in the tropical coralline alga, *Hydrolithon* sp.(Rhodophyta). Estuarine, Coastal and Shelf Science 84:337-341

Shamberger KEF, Feely RA, Sabine CL, Atkinson MJ, DeCarlo EH, Mackenzie FT, Drupp PS, Butterfield DA (2011) Calcification and organic production on a Hawaiian coral reef. Marine Chemistry 127:64-75

Silbiger NJ, Donahue MJ (2015) Secondary calcification and dissolution respond differently to future ocean conditions. Biogeosciences 12:567-578

Silbiger NJ, Guadayol, xd, Thomas FIM, Donahue MJ (2014) Reefs shift from net accretion to net erosion along a natural environmental gradient. Marine Ecology Progress Series 515:33-44

Silverman J, Lazar B, Erez J (2007) Community metabolism of a coral reef exposed to naturally varying dissolved inorganic nutrient loads. Biogeochemisty 84:67-82

Solomon S (2007) Climate change 2007-the physical science basis: Working group I contribution to the fourth assessment report of the IPCC. Cambridge University Press

Steneck RS, Adey WH (1976) The role of environment in control of morphology in *Lithophyllum congestum*, a Caribbean algal ridge builder. Botanica Marina 19:197-216

Sweatman HHPA (1997) Long-term monitoring of the Great Barrier Reef. Status Report Number 2

Tribollet A, Payri C (2001) Bioerosion of the coralline alga *Hydrolithon onkodes* by microborers in the coral reefs of Moorea, French Polynesia. Oceanologica Acta 24:329-342

Tribollet A, Golubic S (2005) Cross-shelf differences in the pattern and pace of bioerosion of experimental carbonate substrates exposed for 3 years on the northern Great Barrier Reef, Australia. Coral Reefs 24:422-434

Tribollet A, Langdon C, Golubic S, Atkinson M (2006) Endolithic microflora are major primary producers in dead carbonate substrates of Hawaiian coral reefs. Journal of Phycology 42:292-303

Tribollet A, Godinot C, Atkinson M, Langdon C (2009) Effects of elevated $pCO_{(2)}$ on dissolution of coral carbonates by microbial euendoliths. Global Biogeochemical Cycles 23:GB3008

UNEP-WCMC (2006) In the front line: Shoreline protection and other ecosystem services from mangroves and coral reefs, Cambridge, UK 33

van Oppen MJH, Oliver JK, Putnam HM, Gates RD (2015) Building coral reef resilience through assisted evolution. Proceedings of the National Academy of Sciences 112:2307-2313

Van Vuuren DP, Meinshausen M, Plattner GK, Joos F, Strassmann KM, Smith SJ, Wigley TML, Raper SCB, Riahi K, De La Chesnaye F (2008) Temperature increase of 21st century mitigation scenarios. Proceedings of the National Academy of Sciences 105:15258-15262

White J (1980) Distribution, recruitment and development of the borer community in dead coral on shallow Hawaiian reefs. University of Hawaii at Manoa,

Williams GJ, Gove JM, Eynaud Y, Zgliczynski BJ, Sandin SA (2015) Local human impacts decouple natural biophysical relationships on Pacific coral reefs. Ecography

Wisshak M, Schönberg CHL, Form A, Freiwald A (2012) Ocean acidification accelerates reef bioerosion. Plos One 7:e45124-e45124

Wisshak M, Schönberg CHL, Form A, Freiwald A (2013) Effects of ocean acidification and global warming on reef bioerosion—lessons from a clionaid sponge. Aquatic Biology 19:111-127

Yates KK, Halley RB (2006) CO_3^{2-} concentration and pCO_2 thresholds for calcification and dissolution on the Molokai reef flat, Hawaii. Biogeosciences 3:357-369

CHAPTER 2

REEFS SHIFT FROM NET ACCRETION TO NET EROSION ALONG A NATURAL ENVIRONMENTAL GRADIENT

Submitted as: Silbiger, NJ, Guadayol, Ò, Donahue, MJ, Thomas, FIM (2014). Reefs shift from net accretion to net reef erosion along a natural environmental gradient. *Marine Ecology Progress Series,* 14: 33-44

ABSTRACT

Coral reefs persist in an accretion-erosion balance and ocean acidification resulting from anthropogenic CO_2 emissions threatens to shift this balance in favor of net reef erosion. Corals and calcifying algae, largely responsible for reef accretion, are vulnerable to environmental changes associated with ocean acidification, but the direct effects of lower pH on reef erosion has received less focus, particularly in the context of known drivers of bioerosion and natural variability. Here, we examine the balance between reef accretion and erosion along a well-characterized natural environmental gradient in Kāne'ohe Bay, Hawai'i using experimental blocks of coral skeleton. Comparing before and after μCT scans to quantify net accretion and erosion, we show that, at the small spatial scale of this study (10s of meters), pH was a better predictor of the accretion-erosion balance than environmental drivers suggested by prior studies, including resource availability, temperature, distance from shore, or depth. In addition, this study highlights the fine-scale variation of pH in coastal systems and the importance of microhabitat variation on reef accretion and erosion processes. We demonstrate significant changes in both the mean and variance of pH on the order of meters, providing the local context for global increases in pCO_2. Our findings suggest that increases in reef erosion, combined with expected decreases in calcification, will accelerate the shift of coral reefs to an erosion-dominated system in a high CO_2 world. This shift will make reefs increasingly susceptible to storm damage and sea-level rise, threatening the maintenance of the ecosystem services that coral reefs provide.

INTRODUCTION

Ocean acidification is threatening the persistence of coral reef ecosystems (Hoegh-Guldberg et al. 2007). The oceans have absorbed ~30% of the anthropogenic increase in carbon dioxide (CO_2), resulting in a decrease in the pH of ocean water ("ocean acidification") and a shift in the chemical equilibrium towards dissolution (Caldeira & Wickett 2003, Feely et al. 2004, Sabine et al. 2004). Current IPCC models predict changes in pH for the open ocean, but these mean predictions are problematic for coral reefs, which are embedded in highly variable coastal ecosystems

(Gagliano et al. 2010, Hofmann et al. 2011) where restricted water motion, terrestrial influences, and feedbacks between benthic productivity and calcification strongly influence the physicochemical environment (Yates et al. 2007, Drupp et al. 2011, Massaro et al. 2012, Duarte et al. 2013, Smith et al. 2013). In this variable coastal environment, coral reef organisms experience biologically-relevant daily variation in pH (Price et al. 2012) and the magnitude of this variation changes over small spatial scales (meters to tens of meters that are relevant to individual organisms) (Guadayol et al. 2014). This natural spatial and temporal variation can exceed the 0.07-0.33 pH unit increase predicted for the global oceans in the 21st century (Bopp et al. 2013), demonstrating the need to study reef processes on finer spatial and temporal scales than prior studies and presenting an opportunity to examine ecological responses to environmental variation *in situ*. Here, we take advantage of the high spatial variability in lagoon reef systems and directly measure net reef accretion and erosion in experimental blocks of coral skeleton along a natural environmental gradient.

Coral reef ecosystems persist in a balance between accretion and erosion; this balance is vulnerable to observed and predicted changes in ocean carbonate chemistry. While the response of calcifying organisms to ocean acidification is variable (Ries et al. 2009), calcification rates for most tropical coral species and other reef calcifiers decline with increasing pCO_2 (Kroeker et al. 2010, Pandolfi et al. 2011). However, these demonstrated declines may underestimate the impact of ocean acidification because net reef accretion, or growth, depends not only on the constructive process of reef calcification, but also the destructive processes of reef dissolution and bioerosion – the removal of lithic substrate by bioeroding organisms (Neumann 1966). For reefs to persist, reef accretion must exceed erosion. Reef erosion by a diverse community of grazers (fish and urchins) and internal eroders (sponges, marine worms, bivalves, and microboring flora) plays a major role in the calcium carbonate ($CaCO_3$) budget (reviewed in Hutchings 1986). Reef eroders are responsible for 90% of coral reef sediment production and just over half of these sediments are re-incorporated back into the coral framework (Hubbard et al. 1990). In addition, bioerosion increases the porosity of the coral reef framework, which provides shelter for cryptic organisms (Moran & Reaka 1988) but also reduces mechanical stability (Scott & Risk 1988).

Reef bioerosion rates respond strongly to eutrophication (e.g. Rose & Risk 1985, Edinger et al. 2000, Holmes 2000, Holmes et al. 2000, Le Grand & Fabricius 2011) and substrate type (Highsmith 1981, Risk et al. 1995, Edinger & Risk 1996, Perry 1998, Schönberg 2002) . Distance from shore (Risk et al. 1995, Tribollet et al. 2002) and depth (Perry 1998, Le Grand & Fabricius 2011, Schmidt & Richter 2013) are also common correlates of bioerosion rates. However, the *in situ* response of erosion rates to pH and temperature – variables most relevant to climate change – remains poorly characterized. Recent reviews suggest that reef erosion will increase in a high CO_2 world (Hoegh-Guldberg et al. 2007, Guinotte & Fabry 2008, Andersson & Gledhill 2013) and that reefs may shift from an accretion-dominated to an erosion-dominated state (Silverman et al. 2009), making reefs more susceptible to storm damage and sea-level rise (Hutchings 1986). Yet, there is little field data testing this for a pH-driven shift from accretion to erosion *in situ*. Laboratory studies of bioerosion response to ocean acidification have focused on specific bioeroding groups and shown increases in the penetration depth and erosion rates of microboring flora (Tribollet et al. 2009, Reyes-Nivia et al. 2013) and the boring sponge, *Cliona orientalis* (Wisshak et al. 2012, 2013, Fang et al. 2013), under elevated pCO_2 conditions. Field studies have been indirect or strongly confounded by other environmental variables: Fabricius et al. (2011) showed that the density of externally visible borer orifices in live *Porites* sp. were higher in closer proximity to CO_2 seeps in Papua New Guinea (Fabricius et al. 2011). Manzello et al. (2008) compared three sites in the eastern tropical Pacific and found that erosion rates were higher at sites with frequent upwelling of water with a low aragonite saturation state (Manzello et al. 2008), but these upwelling sites also had high nutrients and low temperature: temperature and nutrients are both known drivers of bioerosion (Le Grand & Fabricius 2011, Davidson et al. 2013).

Here, we take advantage of the natural pH variation in coral reef ecosystems emphasized by recent studies (Gagliano et al. 2010, Hofmann et al. 2011, Guadayol et al. 2014) and directly measure net reef accretion and erosion using experimental blocks of coral skeleton in response to natural pH variation. This experimental approach integrates a natural, early successional community of bioeroders (including internal eroders and external grazers) and reef calcifiers, but excludes accretion

by corals. We characterize net erosion along a 32m onshore-offshore transect on a fringing reef within Kāne‘ohe Bay (O‘ahu, Hawai‘i), a lagoon system with naturally high spatiotemporal variability in pH (Guadayol et al. 2014). Because recent studies have demonstrated that pH variability correlates with calcification rates on coral reefs (Price et al. 2012), we measure spatial variation in both the mean and temporal variability of environmental parameters that are potential drivers of the accretion-erosion balance at 21 locations along the reef transect (Figure 1). To calculate net reef accretion and erosion, we use micro-computed tomography (μCT) to create high resolution (100 μm), 3-dimensional density profiles of experimental $CaCO_3$ blocks before and after deployment (Figure 2). Previous studies have used μCT to visualize bioerosion by sponges (Schönberg & Shields 2008) and to examine coral skeletal morphology (Roche et al. 2011); here, we apply this technology in a novel way to quantify net accretion and erosion more precisely than buoyant weight methods. Using a model-comparison framework, we compare pH with other known drivers and correlates of the accretion-erosion balance, including resource availability for filter feeding bioeroders, temperature, depth, and distance from shore.

MATERIALS AND METHODS

***Study site*:** Our study site is located in Kāne‘ohe Bay, O‘ahu on the windward (eastern) side of Moku o Lo‘e (Coconut Island), adjacent to the Hawai‘i Institute of Marine Biology (Figure S1; N21°25.975', W157°47.175'). This fringing reef is dominated by *Porites compressa* and *Montipora capitata*, with occasional colonies of *Pocillopora damicornis, Fungia scutaria,* and *Porites lobata*. Kāne‘ohe Bay is a protected, semi-enclosed embayment; the residence time can be >1 month in the protected southern portion of Kāne‘ohe Bay, where our study was located (Lowe et al. 2009a). Wave action is low (Smith et al. 1981, Lowe et al. 2009b,a), and currents are mild (5cm s^{-1} maximum) and tidally driven (mean and maximum tidal ranges are 0.7 and 1.1m, respectively) (Lowe et al. 2009b,a). Daily averages in pH, temperature, and O_2 in the Kāne‘ohe Bay waters just offshore our site ranged from 7.83 - 8.03, 21.84-27.86 °C, and 5.82-7.81 mg L^{-1}, respectively, during our study period (Guadayol et al., 2014; Table S1).

***Experimental Design*:** Twenty-one experimental blocks were deployed along a 32m transect,

stratified between reef flat and reef slope (Figure 1e). Blocks were deployed from March 31, 2011 to April 10, 2012 (Figure S2). Water samples for nutrients, chlorophyll *a*, total alkalinity (TA), and pH were collected directly above each block four times within 24 hours in September, December, and April in order to capture both diel and seasonal variability in the environment. In addition to discrete water samples, we measured high frequency (0.1 min^{-1}) variation in temperature and depth using a continuous sensor stationed over each block for a minimum of two weeks. These short time series were normalized to a continuous time series from a permanent station positioned adjacent to the transect, allowing comparison of the micro-environments at each block (Guadayol et al. 2014). Spatial variation in the mean and variance of environmental parameters across the transect allowed us to compare potential drivers of the accretion-erosion balance (Figures 1, S3-S4, and Table 1).

***Experimental Blocks*:** Blocks were cut from dead pieces of massive *Porites* sp. skeleton collected above the high-tide mark from beaches around O'ahu. Only coral pieces with obvious calices and no visible external borings were selected. Coral pieces were cut into a 5cm x 5cm x 2cm blocks, soaked in freshwater, and then autoclaved to remove any living organisms. Because substrate skeletal density can influence reef bioerosion rates (Highsmith 1981, Schönberg 2002), we used blocks with similar skeletal densities. The average skeletal density of each coral block was 1.57 ± 0.07(sd) g cm^{-3}. The skeletal density of *Porites lobata* ranges from 1.27 - 1.66 g cm^{-3} on O'ahu and ranges from 1.15 - 1.95 g cm^{-3} across the Hawaiian Archipelago (Grigg 1982).

***μCT*:** Net accretion and erosion rates were calculated using μCT (Figure 2). μCT is an x-ray technology that non-destructively images the external and internal structures of solid objects, resulting in a three-dimensional array of object densities. Previous studies have used single CT scans to analyze bioerosion (Becker & Reaka-Kudla 1996, Beuck et al. 2007, Schönberg & Shields 2008, Crook et al. 2013). Here, we use μCT in a novel way by comparing pre- and post-deployment scans. This technique allows us to calculate a very accurate rate for net accretion-erosion and to account for and digitally remove the effect of any pre-existing borings in the experimental substrate. Further, we can visualize new erosion scars by external and internal eroders and new growth

by secondary calcifiers in 3D –information that cannot be acquired from traditional buoyant weight techniques. We used an eXplore CT120 μCT (GE Healthcare Xradia, Inc) at the Cornell University Imaging Multiscale CT Facility to scan blocks before and after deployment (voltage = 100kV, current = 50mA). Angular projections were acquired in a full 360° rotation in 0.5° increments; two images at each angle were acquired and averaged. A three-dimensional array of isotropic voxels at 50 μm resolution was generated using the GE Console Software. These 50 μm voxels were averaged to 100μm for data analysis. The intensity value in each voxel is directly related to the density of the object at that voxel. A global threshold value of 200 Hounsfield Units (HU) was used to separate $CaCO_3$ from air and remove any effects of partial volume averaging at the coral block-air interface (Roche et al. 2010). The number of voxels exceeding this threshold was multiplied by the voxel size (100μm)^3 to give the total volume of $CaCO_3$. We measured net accretion-erosion as the change in volume of $CaCO_3$ from before and after scans. Note that this volumetric analysis measures changes at the voxel sale of 50μm, which was then averaged to 100μm, and, therefore, may underestimate erosion by microborers, which make erosion scars between 1 and 100μm (**?**). The values were square-root transformed to meet model assumptions of normality, and one block with a large aggregation of oysters was excluded from the analysis.

***Environmental parameters: potential predictors and correlates of net reef erosion*:**

Previous studies have identified nutrient concentration (e.g. Rose & Risk 1985, Edinger et al. 2000, Holmes 2000, Holmes et al. 2000, Le Grand & Fabricius 2011), chlorophyll (Le Grand & Fabricius 2011), temperature (Davidson et al. 2013), pH (Tribollet et al. 2009, Wisshak et al. 2012, Reyes-Nivia et al. 2013, Wisshak et al. 2013, Fang et al. 2013) and depth (Perry 1998, Le Grand & Fabricius 2011, Schmidt & Richter 2013) as possible drivers of accretion-erosion balance. Here, we compared the effect of these environmental parameters on net accretion-erosion by collecting both discrete water samples (pH, TA, nitrate (NO_3^-), nitrite (NO_2^-), ammonium (NH_4^+), phosphate (PO_4^{3-}), and chlorophyll *a*) and data from continuous sensors (temperature and depth) along the transect. The discrete water samples were collected directly above each block within two days of spring tide at 08:00, 14:00, 20:00, and 02:00 on September 10-11, 2011, December 12-13, 2011,

and April 4-5, 2012. All discrete water samples were collected on snorkel or SCUBA using 60 and 120ml plastic syringes. Syringes and storage vials were all pre-cleaned in a 10% HCl bath for 24 hours and rinsed three times with MilliQ water; during sample collection and processing, they were rinsed three times with sample water. The environment was sampled more continuously for temperature and depth (sampling rate of ~ 0.1 min^{-1}) using one permanent and two mobile monitoring stations. Two mobile stations were deployed at a time, one on the reef flat and one on the reef slope, to get simultaneous measurements at two different blocks on the transect. Mobile stations (Sonde 600XLM, YSI Incorporated) were positioned 5 to 10cm above each block for a two-week period between May 2011 and March 2012. Blocks were sampled in random order, ensuring that the spatial gradient along the transect was not systematically confounded by temporal trends or seasonality (Guadayol et al. 2014). The permanent monitoring station (Sonde 6600-V2-4, YSI) was mounted to a pole a few meters away from the transect, downward facing at 1.7m depth over a 3m deep bottom, with sensors for temperature, depth, conductivity, pH, and O_2 to characterize the background water column conditions for the duration of the experiment. All multi-parametric probes were calibrated periodically using standard procedures and calibration solutions. The permanent station was recovered, cleaned, calibrated, and re-deployed 3 times during the study, and the mobile station probes were calibrated 7 times. Pre-calibration measurements of commercial standard solutions were conducted to detect sensor drift, although none was found for the period of study. The background water column data are reported in Guadayol et al. (2014).

Nutrients and Chlorophyll: Water samples collected for nutrients were immediately filtered through combusted 25mm glass fiber filters (GF/F 0.7µm) and transferred into 50ml plastic centrifuge tubes. Nutrient samples were frozen and later analyzed for NO_3^-, NO_2^-, NH_4^+, and PO_4^{3-} on a Seal Analytical AA3 HR Nutrient Analyzer at the UH SOEST Lab for Analytical Chemistry (Table S2). GF/F filters were folded in half, wrapped in aluminum foil, and frozen for chlorophyll *a* analysis using a Turner Designs 10AU Benchtop Fluorometer (Table S2). The ratio of dissolved inorganic nitrogen to dissolved inorganic phosphate (DIN:DIP) was used as a proxy for resource quality available to filter feeders (Hauss et al. 2012), assuming that elemental composi-

tion of planktonic prey will be influenced by elemental composition of the water column, and was calculated from ($[NO_3^-]$ + $[NO_2^-]$ + $[NH_4^+]$):$[PO_4^{3-}]$) .

pH and TA: Mean and variance in pH at each block was calculated from water samples along the transect. Water samples for pH were immediately transferred into 25ml borosilicate glass vials, brought to a constant temperature of 25°C in a water bath, and immediately analyzed using an m-cresol dye addition spectrophotometric technique and calibrated against a Tris buffer of known pH from the Dickson Lab at Scripps Institute of Oceanography (Table S2). TA was fixed with 100 μL of $HgCl_2$ and analyzed using open cell potentiometric titrations on a Mettler T50 autotitrator and calibrated against a Certified Reference Material following Dickson et al. (2007) protocols. *In situ* pH and all other carbonate parameters (see Table S1) were estimated using CO2SYS (van Heuven et al. 2011) with the following parameters: pH_t, TA, temperature, and salinity. The K1K2 dissociation constants were from Mehrbach (1973) (refit by Dickson & Millero (1987)) and HSO_4 dissociation constants were taken from Uppström (1974) and Dickson (1990). Accuracy for TA and pH was better than 0.8% and 0.04%, respectively, and the precision was 3.55 µEq and 0.004 pH units.

Temperature: Temperature sensors (YSI 6560) were thermistors with manufacturer-reported accuracy of ±0.15°C and resolution of 0.01°C (YSI Incorporated 2011). Average differences in temperature along the transect were small and measured as a relative anomaly from the permanent station: $((\bar{x}_{mobile} - \bar{x}_{permanent})/\bar{x}_{permanent})$. To measure relative variability in temperature across the transect, we calculated the covariance in temperature between the mobile and permanent sensor arrays over a two-week period and compared this covariance across the transect.

Depth and Distance from Shore: Depth is the average depth measured at each block over the two week deployment of the mobile station. Distance from shore is the along-transect distance.

***Model Selection*:** Our goal was to compare pH with other known drivers and correlates of the accretion-erosion balance. In a model selection framework, we used Akaike Information Criterion (AIC) values to rank candidate models, accounting for both fit and complexity. Carefully constructed model selection avoids problems associated with multiple hypothesis testing that are

common in stepwise regression, such as arbitrary α levels and uninterpretable functional relationships (Johnson & Omland 2004, Anderson 2008). Here, we used AICc (AIC corrected), which is recommended for sample sizes less than 30 (Anderson 2008). While the model with the smallest AICc value (ΔAICc=0) is the "best" of the models considered, models with ΔAICc <4 have some empirical support; models with a ΔAICc >10-12 are less plausible (Anderson 2008).

Good inference from multivariate analyses is confounded by collinearity among environmental variables. Many of the environmental variables were collinear along the transect (Figure S5); thus, we removed collinearity by using the residuals of a regression of each environmental variable against depth and distance from shore. Correlation coefficients for raw environmental data and the residual environmental data are shown in Figure S5. Model selection with all raw data is also presented in the supplemental material (Table S3).

We compared models for 5 specific hypotheses about the accretion-erosion balance (carbonate chemistry, resource availability, temperature, depth, and distance from shore) to test which of these drivers had the strongest relationship to net accretion-erosion (Table 1). We used pH to test how carbonate chemistry influenced net accretion-erosion rates. Carbonate chemistry parameters are inherently correlated, and pH had the strongest relationship of the carbonate chemistry parameters (Table S4). The pH model includes both the mean and variance of the discrete pH samples from each block. The resource availability model includes the means and variances of DIN:DIP ratios (a proxy for resource quality) and chlorophyll *a* (a measure of resource quantity) from the discrete water samples. The temperature model included the mean relative temperature anomaly of each block from the permanent station and temperature covariance between the mobile and permanent stations. The final two models were individual models for depth and distance from shore. These linear models were compared to a full model that includes the means and variances of every parameter stated above (Table 1). Environmental data that did not meet the assumptions of normality were log-transformed and net erosion data were square-root transformed.

RESULTS

There were considerable differences in both the mean and variance of pH and nutrients across

the 32m transect. Mean pH increased from 7.84 to 7.91 and the coefficient of variation decreased from 0.013 to 0.0032 from onshore to offshore (Figure 1b, Tables S1, S5). Mean DIN:DIP decreased from 87.5 to 42.4 and the coefficient of variation increased from 0.36 to 0.59 (Figure 1d, Table S5) from onshore to offshore. Chlorophyll *a* and temperature remained relatively constant across the spatial gradient (Figure 1a,c, Table S5).

We compared models of pH, resource availability, temperature, depth, and distance from shore as drivers of net accretion and erosion (Table 1, Figures S3, S4). The pH model best explained patterns in the accretion-erosion balance along the transect in both the residual and raw data models (Tables 1, S3, Figure 3). Accretion was higher on the deeper reef slope, where pH is higher and less variable (Figures 1, S6, S7). Removing the effects of depth and distance from shore, pH was an even better predictor of the accretion-erosion balance (Figures 3, S3), particularly on the reef flat, and it explains 64% of the variation in net accretion-erosion over a one year deployment (Table 1). The second best model, the depth model (ΔAIC_c = 16.30), explained only 6% of the variance (Table 1, Figure S7), followed by the distance model which explained only 2% of the variance. While the resource availability model described 18% of the variance in the data, it also had a larger number of parameters (6, including mean and variance for both DIN:DIP and chlorophyll *a*) and, therefore, ranked sixth in model parsimony.

We also tested whether the mean or variance in pH was a better predictor of net accretion-erosion. Mean pH was the best model, explaining 64% of the variance (Table 1) and had a strong negative relationship with net accretion-erosion (Figure 3). pH was also a better predictor of net accretion-erosion than TA, pCO_2, and DIC, but these highly collinear carbonate chemistry parameters did have some empirical support and explained between 42-58% of the variance in net accretion-erosion (Table S4).

DISCUSSION

Spatial and temporal variation in pH across the transect:

Across the transect, pH had a range of 0.33 pH units at the most variable site and 0.08 pH units at the least variable site over the year (Table S1). The organisms at these sites experience a natural

variation in pH that is within the range that mean pH is predicted to decrease for the 21st century (Bopp et al. 2013). Indeed, this pH range is not unique to our transect, but is typical of other shallow coral reef sites in the Pacific. For example, pH at the CRIMP2 buoy, a slightly deeper (~3m) nearby reef site located in central Kāne'ohe Bay, ranged from 7.90-8.13 over a 2.5 year study (Drupp et al. 2013). On a Palmyra reef terrace, pH ranged from 7.85-8.10 (Hofmann et al. 2011) and pH spanned 0.39 units in a study examining the spatial variability in microhabitats on the Great Barrier Reef (Gagliano et al. 2010). Additionally, Gagliano et al. (2010) found a similar inshore-offshore pattern: mean pH was lower and more variable inshore compared to offshore sites, though their study was conducted over a much larger spatial scale. The patterns in the means and variances here and in other studies arise from both physical and biological processes including: tidal mixing with offshore waters, P/R cycles, and reef metabolism (Hurd et al. 2011, Kleypas et al. 2011), upwelling events (Leichter et al. 2003, Manzello et al. 2008), and porewater advection from permeable sediments (Santos et al. 2011). We saw a very strong correlation between pH variance and distance from shore (Figure S6), suggesting that tidal mixing was an important contributor to the spatial variation in pH, although we did not specifically test this hypothesis. Using the residual values that remove the effect of distance and depth from pH eliminates the impact of this large scale mixing, leaving the effect of small scale processes (such as local P/R and turbulent mixing) on pH. The raw pH data model explained 48% of the variance in net accretion-erosion (Table S3), but the residual model was an even better fit (Table 1), suggesting that small-scale physicochemical differences in microhabitats may strongly influence the patterns of accretion and erosion on coral reefs. The results of this study suggest that differences in microhabitat variability may be more important to the accretion-erosion balance than larger-scale processes. A better characterization of microhabitat variability (see Guadayol et al. 2014) and how this microhabitat variation impacts reefs will help us predict reef responses to climate change in the context of natural variability.

***Implications for the accretion-erosion balance of coral reefs*:**

Our results show that differences in the seawater chemistry on the scale of meters can have a substantial influence on the accretion-erosion balance. The majority of the blocks below a mean

pH of 7.88 were net eroding (Figure S3), a pH value likely to be more prevalent with the predicted 0.3-0.4 pH unit reduction in oceanic pH (Orr et al. 2005, Bopp et al. 2013). Previous studies on coral reefs have shown shifts from net accretion to erosion after major disturbances, such as ENSO events or hurricanes (Perry et al. 2008). Our data indicate that pH is a significant driver of net reef erosion and that, as mean pH decreases, erosion rates will increase. The pH model ranked higher than the distance, depth, and resource availability models; prior studies where depth, distance, and resource availability were stronger predictors of bioerosion were performed on much larger spatial scales and covered a greater range of values (e.g., Perry 1998, Holmes et al. 2000, Tribollet et al. 2002, Le Grand & Fabricius 2011, Schmidt & Richter 2013). For instance, a prior study showing a strong response of bioerosion to resource availability had mean chlorophyll *a* values ranging from 0.25 to 1.24 μg L^{-1} across their comparison sites (Holmes et al. 2000); mean chlorophyll *a* ranged only from 0.14 to 0.31 μg L^{-1} in this study (Figure 1). Results from the current study are in agreement with recent lab (Tribollet et al. 2009, Reyes-Nivia et al. 2013, Wisshak et al. 2012, 2013, Fang et al. 2013) and field experiments (Manzello et al. 2008, Fabricius et al. 2011, Crook et al. 2013) suggesting that erosion rates will increase with ocean acidification. However, this is the first study to directly test the relationship between the accretion-erosion balance and pH, using a natural pH gradient, and compare this relationship to other known drivers and correlates of reef accretion and erosion.

The bioeroder community is diverse and has a number of mechanisms for boring, including chemical dissolution and mechanical erosion. Individual species respond differently to environmental parameters and, thus, influence the accretion-erosion balance through changes in individual bioerosion rates and in community composition. For example, previous studies have found that boring sponges and bivalves respond positively to eutrophication, while the response of polychaetes is more variable (Le Grand & Fabricius 2011). Filter feeding sponges and bivalves are positively correlated with eutrophic sites in the Bahamas (Rose & Risk 1985), Barbados (Holmes et al. 2000), the Red Sea (Kleemann 2001), the Great Barrier Reef (Osorno et al. 2005, Tribollet & Golubic 2005) and the eastern Pacific (Fonseca E et al. 2006); bivalve abundances are also corre-

lated with high water velocity (Cantera et al. 2003, Londono-Cruz et al. 2003). In contrast, deposit feeding polychaetes in the Great Barrier Reef are more abundant at eutrophic sites (Osorno et al. 2005), while suspension feeding polychaetes are more abundant in oligotrophic sites (Le Bris et al. 1998). In addition, there are strong successional dynamics in these communities, and patterns of succession are location specific. In the Great Barrier Reef, microborers and polychaetes are the initial colonizers followed by sipunculans, bivalves, and then sponges (Hutchings 1986); it may take up to three years for sponges to fully colonize dead substrate (Tribollet & Golubic 2005). In the Caribbean, the suggested successional pattern of bioeroders is algae, fungi, clionid sponges, polychaetes, bivalves, barnacles, and then sipunculans (Risk & MacGeachy 1978). In Hawai'i, an 18 month study in Kāne'ohe Bay found no obvious successional patterns (White 1980), but likely captured only the initial successional stages. Our study highlights the influence of pH on the accretion-erosion balance after one year, the early-successional stage of this community, and future studies should include multi-year comparisons to test if this pattern holds. In a previous Kāne'ohe Bay study that used similar blocks, the most abundant organisms after a one-year deployment were polychaetes (Spionidae were the most abundant and largest polychaete borers) and sipunculans (White 1980). These were the most common taxa in our study, as well. Parrotfish erosion was also evident on our blocks. Common secondary calcifiers in our community were crustose coralline algae (*Hydrolithon* spp.), barnacles, and the oyster *Crassostrea gigas*.

Our results highlight the value of using of μCT as a tool to calculate accretion and erosion rates on coral reefs. μCT provides a more sensitive measure of net accretion-erosion in the field than previously published methods (e.g. Edinger & Risk 1996, Tribollet et al. 2009, Perry et al. 2012), and it is directly comparable across studies. Prior studies have used single CT scans to calculate skeletal density (Bosscher 1993), skeletal porosity (Roche et al. 2010), and linear extension (Crook et al. 2013); here, we used μCT in a novel way by comparing before and after images to calculate the precise volume of $CaCO_3$ removed or accreted. As reef erosion and coral growth are often decoupled on coral reefs (Edinger et al. 2000), quantification of net erosion must complement measures of coral growth for a more complete picture of coral reef health.

Although chemical dissolution will accelerate in future decades as tropical coral reefs shift to less-saturated aragonite conditions (van Woesik et al. 2013), bioerosion is currently the main driver of reef loss (Andersson & Gledhill 2013). The mechanisms by which ocean acidification may enhance bioerosion rates include lower coral skeletal densities (Hoegh-Guldberg et al. 2007, Cooper et al. 2008), making it easier for bioeroders to penetrate the coral skeleton (Edinger & Risk 1996, Dumont et al. 2013), though this point is debated in the literature (see, Highsmith 1981, Schönberg 2002, Hernández-Ballesteros et al. 2013); increased growth rates of photosynthesizing bioeroders (Tribollet et al. 2009); declines in crustose coralline algae (Jokiel et al. 2008), which can inhibit settlement and growth of micro- and macroborers (Tribollet & Payri 2001); and increased susceptibility of calcifiers to grazers (Johnson & Carpenter 2012). In addition, many boring organisms excrete acidic compounds, raising the possibility that a reduction in ocean pH could make it less metabolically costly to lower pH at the site of erosion.

The combination of slower coral growth (Hoegh-Guldberg et al. 2007, Kroeker et al. 2010, Pandolfi et al. 2011) and higher erosion rates with ocean acidification could act synergistically to hinder reef growth. In the Caribbean, erosion rates are highest in areas where coral cover is low (Perry et al. 2013), indicating that the same drivers that negatively impact corals may also promote erosion. Further, given the strong relationship between bioerosion and local anthropogenic impacts like sedimentation and nutrient run-off (Edinger et al. 2000, Le Grand & Fabricius 2011), the combined effect of these local impacts with decreases in pH in the global oceans could be devastating to reefs world-wide. This study portrays how coral reef ecosystems may change under predicted increases in ocean acidity: an existing community of reef secondary calcifiers and bioeroders showed a shift from net accretion to net erosion along a naturally occurring, within-reef gradient of high to low pH.

ACKNOWLEDGMENTS: We are grateful to C.J. Bradley, J. Chen, R. Coleman, A. Copeland, K. DiPerna, M. Donovan, N. Griffith, K. Hurley, M. Iacchei, I. Iglesias, M. Siple, E. M. Sogin, M. Sudek, J. Sziklay, M. Walton, and the Point Lab for help with data collection. We thank M. Riccio and F. von Stein from the Cornell University μCT Facility for Imaging and Preclinical Research,

R. Briggs from UH SOEST Lab for Analytical Chemistry, and the UH lapidary facility. Funding for this project came from NOAA Office of National Marine Sanctuaries-HIMB partnership (MOA #2009-039/7932), National Science Foundation EPSCoR Hawaii, NOAA Dr. Nancy Foster Scholarship to N.J.S., Sigma-Xi GIAR to N.J.S., and by Hawaii Sea Grant #1889 to F.I.M.T and #1847 to M.J.D. and F.I.M.T. Comments from H. Putnam, C. Jury, E. Wolkovich, and three anonymous reviewers improved this manuscript. This is HIMB contribution #xxxx, SOEST #xxxx, and SeaGrant #xxxx

References

Anderson DR (2008) Model based inference in the life sciences: a primer on evidence. Springer

Andersson A, Gledhill D (2013) Ocean acidification and coral reefs: Effects on breakdown, dissolution, and net ecosystem calcification. Ann Rev of Mar Sci 5:321–348

Becker L, Reaka-Kudla M (1996) The use of tomography in assessing bioerosion in corals. In: Proc 8th Int Coral Reef Symp, vol. 2, pp. 1819–1824

Beuck L, Vertino A, Stepina E, Karolczak M, Pfannkuche O (2007) Skeletal response of *Lophelia pertusa* (scleractinia) to bioeroding sponge infestation visualised with micro-computed tomography. Facies 53:157–176

Bopp L, Resplandy L, Orr JC, Doney SC, Dunne JP, Gehlen M, Halloran P, Heinze C, Ilyina T, Séférian R, Tjiputra J, Vichi M (2013) Multiple stressors of ocean ecosystems in the 21st century: projections with CMIP5 models. Biogeosciences 10:6225–6245

Bosscher H (1993) Computerized-tomography and skeletal density of coral skeletons. Coral Reefs 12:97–103

Caldeira K, Wickett ME (2003) Oceanography: anthropogenic carbon and ocean pH. Nature 425:365–365

Cantera JRK, Orozco C, Londono-Cruz E, Toro-Farmer G (2003) Abundance and distribution patterns of infaunal associates and macroborers of the branched coral (*Pocillopora damicornis*) in Gorgona Island (eastern tropical Pacific). Bull of Mar Sci 72:207–219

Cooper TF, De 'Ath G, Fabricius KE, Lough JM (2008) Declining coral calcification in massive *Porites* in two nearshore regions of the northern Great Barrier Reef. Glob Change Biol 14:529–538

Crook ED, Cohen AL, Rebolledo-Vieyra M, Hernandez L, Paytan A (2013) Reduced calcification and lack of acclimatization by coral colonies growing in areas of persistent natural acidification. Proc Natl Acad Sci U S A 110:11044–11049

Davidson TM, de Rivera CE, Carlton JT (2013) Small increases in temperature exacerbate the erosive effects of a non-native burrowing crustacean. J Exp Mar Biol Ecol 446:115 – 121

Dickson AG (1990) Standard potential of the reaction:$AgCl(s) + 12H2(g) = Ag(s) + HCl(aq)$, and and the standard acidity constant of the ion HSO_4^- in synthetic sea water from 273.15 to 318.15 k. The Journal of Chemical Thermodynamics 22:113–127

Dickson A, Millero F (1987) A comparison of the equilibrium constants for the dissociation of carbonic acid in seawater media. Deep Sea Research Part A Oceanographic Research Papers 34:1733–1743

Dickson A, Sabine C, Christian JR (2007) Guide to Best Practices for Ocean CO_2 Measurements. PICES Special Publication 3

Drupp P, De Carlo EH, Mackenzie FT, Bienfang P, Sabine CL (2011) Nutrient inputs, phytoplankton response, and CO_2 variations in a semi-enclosed subtropical embayment, Kaneohe Bay, Hawaii. Aquat Geochem 17:473–498

Drupp PS, De Carlo EH, Mackenzie FT, Sabine CL, Feely RA, Shamberger KE (2013) Compar-

ison of CO_2 dynamics and air–sea gas exchange in differing tropical reef environments. Aquat Geochem :1–27

Duarte CM, Hendriks IE, Moore TS, Olsen YS, Steckbauer A, Ramajo L, Carstensen J, Trotter JA, McCulloch M (2013) Is ocean acidification an open-ocean syndrome? Understanding anthropogenic impacts on seawater pH,. Estuaries and Coasts 36:1–16

Dumont CP, Lau DC, Astudillo JC, Fong KF, Chak ST, Qiu JW (2013) Coral bioerosion by the sea urchin *Diadema setosum* in Hong Kong: Susceptibility of different coral species. J Exp Mar Biol Ecol 441:71 – 79

Edinger EN, Limmon GV, Jompa J, Widjatmoko W, Heikoop JM, Risk MJ (2000) Normal coral growth rates on dying reefs: Are coral growth rates good indicators of reef health? Mar Pollut Bull 40:404–425

Edinger EN, Risk MJ (1996) Sponge borehole size as a relative measure of bioerosion and paleoproductivity. Lethaia 29:275–286

Fabricius K, Langdon C, Uthicke S, Humphrey C, Noonan S, De'ath G, Okazaki R, Muehllehner N, Glas M, Lough J (2011) Losers and winners in coral reefs acclimatized to elevated carbon dioxide concentrations. Nature Clim Change 1:165–169

Fang JK, Mello-Athayde MA, Schönberg CH, Kline DI, Hoegh-Guldberg O, Dove S (2013) Sponge biomass and bioerosion rates increase under ocean warming and acidification. Glob Change Biol 19:3581–3591

Feely RA, Sabine CL, Lee K, Berelson W, Kleypas J, Fabry VJ, Millero FJ (2004) Impact of anthropogenic CO_2 on the $CaCO_3$ system in the oceans. Science 305:362–366

Fonseca E AC, Dean HK, Cortes J (2006) Non-colonial coral macro-borers as indicators of coral reef status in the south pacific of costa rica. Revista De Biologia Tropical 54:101–115

Gagliano M, McCormick MI, Moore JA, Depczynski M (2010) The basics of acidification: baseline variability of pH on Australian coral reefs. Mar Biol 157:1849–1856

Grigg RW (1982) Darwin point: A threshold for atoll formation. Coral Reefs 1:29–34

Guadayol Ò, Silbiger NJ, Donahue MJ, Thomas FI (2014) Patterns in temporal variability of temperature, oxygen and pH along an environmental gradient in a coral reef. Plos One 9:e85213

Guinotte JM, Fabry VJ (2008) Ocean acidification and its potential effects on marine ecosystems. Year in Ecology and Conservation Biology 1134:320–342

Hauss H, Franz J, Sommer U (2012) Changes in N: P stoichiometry influence taxonomic composition and nutritional quality of phytoplankton in the Peruvian upwelling. J Sea Res 73:74–85

Hernández-Ballesteros LM, Elizalde-Rendón EM, Carballo JL, Carricart-Ganivet JP (2013) Sponge bioerosion on reef-building corals: Dependent on the environment or on skeletal density? J of Exp Mar Biol Ecol 441:23–27

Highsmith RC (1981) Coral bioerosion - damage relative to skeletal density. Am Nat 117:193–198

Hoegh-Guldberg O, Mumby PJ, Hooten AJ, Steneck RS, Greenfield P, Gomez E, Harvell CD, Sale PF, Edwards AJ, Caldeira K, Knowlton N, Eakin CM, Iglesias-Prieto R, Muthiga N, Bradbury RH, Dubi A, Hatziolos ME (2007) Coral reefs under rapid climate change and ocean acidification. Science 318:1737–1742

Hofmann G, Smith J, Johnson K, Send U, Levin L, Micheli F, Paytan A, Price N, Peterson B, Takeshita Y, Matson P, Crook E, Kroeker K, Gambi M, Rivest E, Frieder C, Yu P, Martz T (2011) High-frequency dynamics of ocean pH: A multi-ecosystem comparison. Plos One 6:e28983

Holmes KE (2000) Effects of eutrophication on bioeroding sponge communities with the description of new West Indian sponges, *Cliona* spp.(Porifera: Hadromerida: Clionidae). Invertebrate Biology 119:125–138

Holmes KE, Edinger EN, Hariyadi, Limmon GV, Risk MJ (2000) Bioerosion of live massive corals and branching coral rubble on Indonesian coral reefs. Mar Pollut Bull 40:606–617

Hubbard DK, Miller AI, Scaturo D (1990) Production and cycling of calcium carbonate in a shelf-edge reef system (St. Croix, United States, Virgin Islands)- application to the nature of reef systems in the fossil record. Journal of Sediment Petrol 60:335–360

Hurd CL, Cornwall CE, Currie K, Hepburn CD, McGraw CM, Hunter KA, Boyd PW (2011) Metabolically induced pH fluctuations by some coastal calcifiers exceed projected 22nd century ocean acidification: a mechanism for differential susceptibility? Glob Change Biol 17:3254–3262

Hutchings PA (1986) Biological destruction of coral reefs- a review. Coral Reefs 4:239–252

Johnson MD, Carpenter RC (2012) Ocean acidification and warming decrease calcification in the crustose coralline alga *Hydrolithon onkodes* and increase susceptibility to grazing. J Exp Mar Biol Ecol 434:94–101

Johnson JB, Omland KS (2004) Model selection in ecology and evolution. Trends Ecol Evol 19:101–108

Jokiel PL, Rodgers KS, Kuffner IB, Andersson AJ, Cox EF, Mackenzie FT (2008) Ocean acidification and calcifying reef organisms: a mesocosm investigation. Coral Reefs 27:473–483

Kleemann K (2001) The pectinid bivalve *Pedum spondyloideum* (gmelin 1791): Amount of surface and volume occupied in host corals from the Red Sea. Marine Ecology-Pubblicazioni Della Stazione Zoologica Di Napoli I 22:111–133

Kleypas JA, Anthony K, Gattuso JP (2011) Coral reefs modify their seawater carbon chemistry–case study from a barrier reef (Moorea, French Polynesia). Glob Change Biol 17:3667–3678

Kroeker KJ, Kordas RL, Crim RN, Singh GG (2010) Meta-analysis reveals negative yet variable effects of ocean acidification on marine organisms. Ecol Lett 13:1419–1434

Le Bris S, Le Campion-Alsumard T, Romano JC (1998) Characteristics of epilithic and endolithic algal turf exposed to different levels of bioerosion in french polynesian coral reefs. Oceanologica Acta 21:695–708

Le Grand HM, Fabricius KE (2011) Relationship of internal macrobioeroder densities in living massive *Porites* to turbidity and chlorophyll on the Australian Great Barrier Reef. Coral Reefs 30:97–107

Leichter JJ, Stewart HL, Miller SL (2003) Episodic nutrient transport to Florida coral reefs. Limnol Oceanogr 48:1394–1407

Londono-Cruz E, Cantera JR, Toro-Farmer G, Orozco C (2003) Internal bioerosion by macroborers in *Pocillopora* spp. in the tropical eastern Pacific. Mar Ecol Prog Ser 265:289–295

Lowe RJ, Falter JL, Monismith SG, Atkinson MJ (2009a) A numerical study of circulation in a coastal reef-lagoon system. J Geophys Res 114:C06022

Lowe RJ, Falter JL, Monismith SG, Atkinson MJ (2009b) Wave-driven circulation of a coastal reef-lagoon system. J Phys Oceanogr 39:873–893

Manzello DP, Kleypas JA, Budd DA, Eakin CM, Glynn PW, Langdon C (2008) Poorly cemented coral reefs of the eastern tropical Pacific: Possible insights into reef development in a high-CO_2 world. Proc Natl Acad Sci U S A 105:10450–10455

Massaro RF, De Carlo EH, Drupp PS, Mackenzie FT, Jones SM, Shamberger KE, Sabine CL, Feely RA (2012) Multiple factors driving variability of CO_2 exchange between the ocean and atmosphere in a tropical coral reef environment. Aquat Geochem 18:357–386

Mehrbach C (1973) Measurement of the apparent dissociation constants of carbonic acid in sea-water at atmospheric pressure. Limnol Oceanogr 18:897–907

Moran DP, Reaka ML (1988) Bioerosion and availability of shelter for benthic reef organisms. Mar Ecol Progr Ser 44:249–263

Neumann AC (1966) Observations on coastal erosion in Bermuda and measurements of boring rate of sponge *Cliona lampa*. Limnol Oceanogr 11:92–108

Orr JC, Fabry VJ, Aumont O, Bopp L, Doney SC, Feely RA, Gnanadesikan A, Gruber N, Ishida A, Joos F, Key RM, Lindsay K, Maier-Reimer E, Matear R, Monfray P, Mouchet A, Najjar RG, Plattner GK, Rodgers KB, Sabine CL, Sarmiento JL, Schlitzer R, Slater RD, Totterdell IJ, Weirig MF, Yamanaka Y, Yool A (2005) Anthropogenic ocean acidification over the twenty-first century and its impact on calcifying organisms. Nature 437:681–686

Osorno A, Peyrot-Clausade M, Hutchings PA (2005) Patterns and rates of erosion in dead *Porites* across the Great Barrier Reef (Australia) after 2 years and 4 years of exposure. Coral Reefs 24:292–303

Pandolfi JM, Connolly SR, Marshall DJ, Cohen AL (2011) Projecting coral reef futures under global warming and ocean acidification. Science 333:418–422

Perry CT (1998) Macroborers within coral framework at Discovery Bay, north Jamaica: species distribution and abundance, and effects on coral preservation. Coral Reefs 17:277–287

Perry C, Edinger E, Kench P, Murphy G, Smithers S, Steneck R, Mumby P (2012) Estimating rates of biologically driven coral reef framework production and erosion: a new census-based carbonate budget methodology and applications to the reefs of Bonaire. Coral Reefs 31:1–16

Perry C, Murphy G, Kench P, Smithers S, Edinger E, Steneck R, Mumby P (2013) Caribbean-wide decline in carbonate production threatens coral reef growth. Nat Commun 4:1402

Perry CT, Spencer T, Kench PS (2008) Carbonate budgets and reef production states: a geomorphic perspective on the ecological phase-shift concept. Coral Reefs 27:853–866

Price N, Martz T, Brainard R, Smith J (2012) Diel variability in seawater pH relates to calcification and benthic community structure on coral reefs. PloS one 7:e43843

Reyes-Nivia C, Diaz-Pulido G, Kline D, Guldberg OH, Dove S (2013) Ocean acidification and warming scenarios increase microbioerosion of coral skeletons. Glob Change Biol 19:1919–1929

Ries JB, Cohen AL, McCorkle DC (2009) Marine calcifiers exhibit mixed responses to CO_2-induced ocean acidification. Geology 37:1131–1134

Risk M, MacGeachy J (1978) Aspects of bioerosion of modern caribbean reefs [*Cliona vermifera, Montastrea annularis*]. Revista de Biologia Tropical 26:85–105

Risk MJ, Sammarco PW, Edinger EN (1995) Bioerosion in *Acropora* across the continental-shelf of the Great Barrier Reef. Coral Reefs 14:79–86

Roche RC, Abel RA, Johnson KG, Perry CT (2010) Quantification of porosity in *Acropora pulchra* (Brook 1891) using x-ray micro-computed tomography techniques. J Exp Mar Biol Ecol 396:1 – 9

Roche R, Abel R, Johnson K, Perry C (2011) Spatial variation in porosity and skeletal element characteristics in apical tips of the branching coral *Acropora pulchra* (Brook 1891). Coral reefs 30:195–201

Rose CS, Risk MJ (1985) Increase in *Cliona delitrix* infestation of *Montastrea cavernosa* heads on an organically polluted portion of the Grand Cayman fringing-reef. Marine Ecology-Pubblicazioni Della Stazione Zoologica Di Napoli I 6:345–363

Sabine CL, Feely RA, Gruber N, Key RM, Lee K, Bullister JL, Wanninkhof R, Wong C, Wallace DW, Tilbrook B, et al. (2004) The oceanic sink for anthropogenic CO_2. Science 305:367–371

Santos IR, Glud RN, Maher D, Erler D, Eyre BD (2011) Diel coral reef acidification driven by porewater advection in permeable carbonate sands, Heron Island, Great Barrier Reef. Geophys Res Lett 38:L03604

Schmidt GM, Richter C (2013) Coral growth and bioerosion of *Porites lutea* in response to large amplitude internal waves. PloS one 8:e73236

Schönberg CH (2002) Substrate effects on the bioeroding demosponge *Cliona orientalis*. 1. Bioerosion rates. Mar Ecol 23:313–326

Schönberg CH, Shields G (2008) Micro-computed tomography for studies on *Entobia*: transparent substrate versus modern technology. In: Current Developments in Bioerosion, Springer, pp. 147–164

Scott PJB, Risk MJ (1988) The effect of *Lithophaga (Bivalvia, Mytilidae)* boreholes on the strength of the coral *Porites lobata*. Coral Reefs 7:145–151

Silverman J, Lazar B, Cao L, Caldeira K, Erez J (2009) Coral reefs may start dissolving when atmospheric CO_2 doubles. Geophys Res Lett 36:L05606

Smith SV, Kimmerer WJ, Laws EA, Brock RE, Walsh TW (1981) Kaneohe Bay sewage diversion experiment- perspectives on ecosystem responses to nutritional perturbation. Pac Sci 35:279–402

Smith JE, Price NN, Nelson CE, Haas AF (2013) Coupled changes in oxygen concentration and pH caused by metabolism of benthic coral reef organisms. Mar Biol 160:1–11

Tribollet A, Decherf G, Hutchings PA, Peyrot-Clausade M (2002) Large-scale spatial variability in bioerosion of experimental coral substrates on the Great Barrier Reef (Australia): importance of microborers. Coral Reefs 21:424–432

Tribollet A, Godinot C, Atkinson M, Langdon C (2009) Effects of elevated pCO_2 on dissolution of coral carbonates by microbial euendoliths. Global Biogeochem Cycles 23:GB3008

Tribollet A, Golubic S (2005) Cross-shelf differences in the pattern and pace of bioerosion of experimental carbonate substrates exposed for 3 years on the northern Great Barrier Reef, Australia. Coral Reefs 24:422–434

Tribollet A, Payri C (2001) Bioerosion of the coralline alga *Hydrolithon onkodes* by microborers in the coral reefs of Moorea, French Polynesia. Oceanologica Acta 24:329–342

Uppström LR (1974) The boron/chlorinity ratio of deep-sea water from the pacific ocean. In: Deep Sea Research and Oceanographic Abstracts, vol. 21, pp. 161–162

van Heuven S, Pierrot D, Rae J, Lewis E, Wallace D (2011) MATLAB Program Developed for CO2 System Calculations. ORNL/CDIAC-105b. Carbon Dioxide Information Analysis Center, Oak Ridge National Laboratory, U.S. Department of Energy, Oak Ridge, Tennessee.

van Woesik R, van Woesik K, van Woesik L, van Woesik S (2013) Effects of ocean acidification on the dissolution rates of reef-coral skeletons. PeerJ 1:e208

White J (1980) Distribution, recruitment and development of the borer community in dead coral on shallow Hawaiian reefs. Ph.D. thesis, University of Hawaii at Manoa

Wisshak M, Schönberg CH, Form A, Freiwald A (2012) Ocean acidification accelerates reef bioerosion. Plos One 7:e45124

Wisshak M, Schönberg C, Form AU, Freiwald A (2013) Effects of ocean acidification and global warming on reef bioerosion - lessons from a clionaid sponge. Aquat Biol 19:111–127

Yates KK, Dufore C, Smiley N, Jackson C, Halley RB (2007) Diurnal variation of oxygen and carbonate system parameters in Tampa Bay and Florida Bay. Mar Chem 104:110–124

Table1: Model Selection: k is the number of parameters in the model, -log($\mathcal{L}$) is the negative log likelihood of the model, AIC_c is the Akaike Information Criterion corrected, ΔAIC_c is the difference from the lowest AIC_c value, R^2 is the proportion of total variance explained by the model, and Rank is the rank of the model with 1 being the best fit. Each model is a linear regression of net reef erosion versus the means ($\overline{X}$) and variances ($Var(X)$) of each parameter. The Resource Availability Model includes DIN:DIP and chlorophyll *a* concentration and the Full Model includes means and variances for all listed environmental parameters. The ranges for each environmental parameter are included in Tables S5. The lower table shows a model selection for pH mean versus variance.

	k	-log($\mathcal{L}$)	AICc	ΔAIC	R^2	Rank
pH $Y \sim \overline{pH} + Var(pH)$	4	-30.46	68.42	0.00	0.64	1
Depth $Y \sim \overline{Depth}$	3	-40.01	84.73	16.30	0.06	2
Distance $Y \sim Distance$	3	-40.40	85.50	17.08	0.02	3
Temperature $Y \sim \overline{Temp} + Covar(Temp)$	4	-40.42	88.33	19.91	0.03	4
Resource Availability $Y \sim \overline{Chl} + Var(Chl) + \overline{N:P} + Var(N:P)$	6	-38.91	92.11	23.68	0.18	5
Full Model $Y \sim \overline{pH} + Var(pH) + \overline{Temp} + Covar(Temp) + \overline{Chl} + Var(Chl) +$ $\overline{N:P} + Var(N:P) + \overline{Depth} + Distance$	12	-25.92	106.84	38.42	0.82	6
pH Mean $Y \sim \overline{pH}$	3	-30.41	65.52	0.00	0.64	1
pH Mean and Variance $Y \sim \overline{pH} + Var(pH)$	4	-30.46	68.42	2.90	0.64	2
pH Variance $Y \sim Var(pH)$	3	-39.34	83.39	17.87	0.12	3

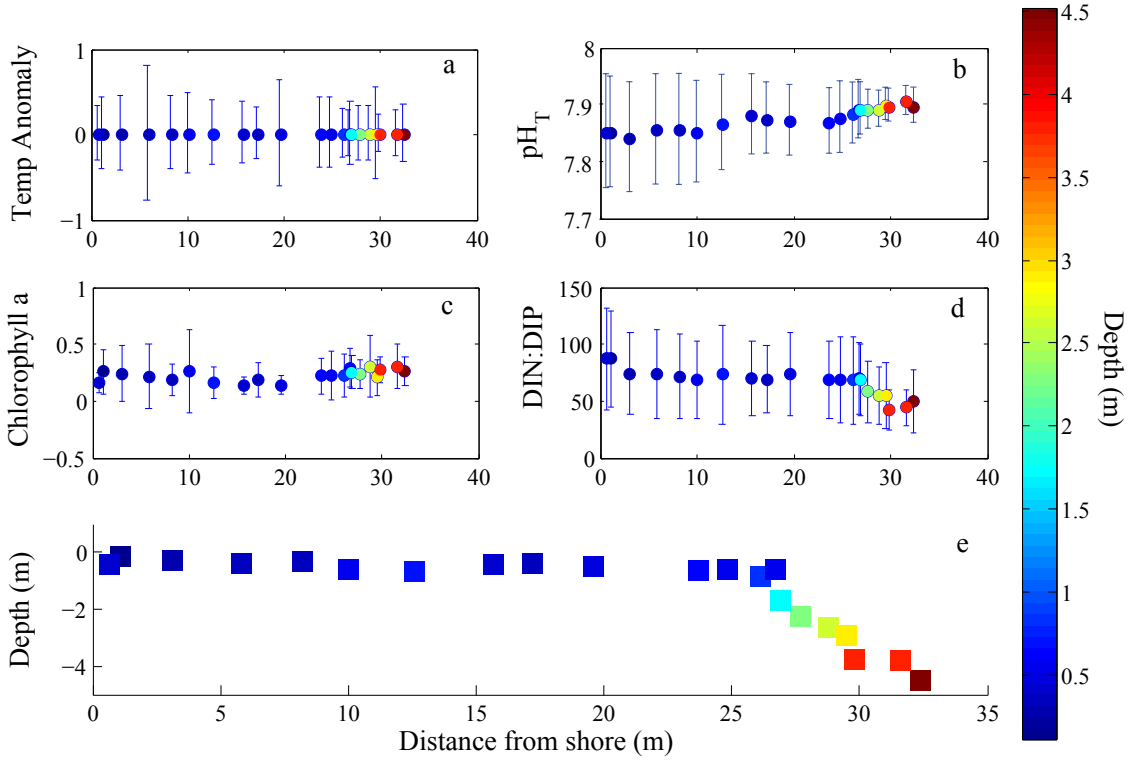

Figure 1: **Environmental parameters measured at 21 points along the transect.** Plots represent the mean (circles) and variability (error bars are standard deviation) of the environmental along the transect for a) relative temperature anomalies, b) pH (total scale), c) chlorophyll *a* (μg L^{-1}) , and d) DIN:DIP at e) the location of each experimental block. X-axes are distance (m) across the transect with 0 being closest to shore, and colors represent depth (m).

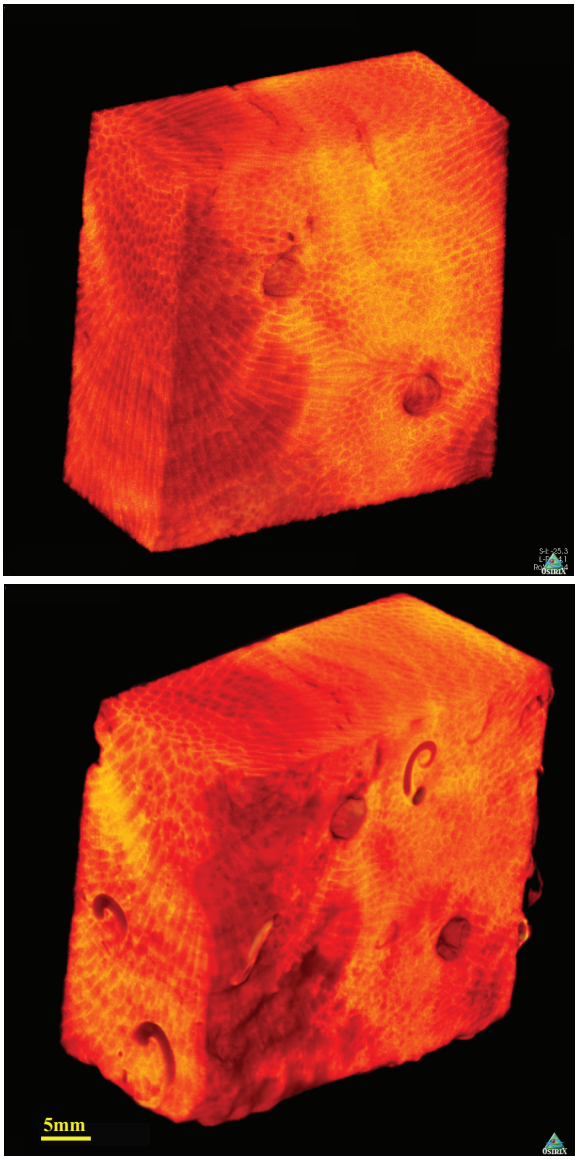

Figure 2: **μCT scan.** Visualization of μCT scan of an experimental block before (top) and after one year deployment (bottom). Scale bar is 5mm long.

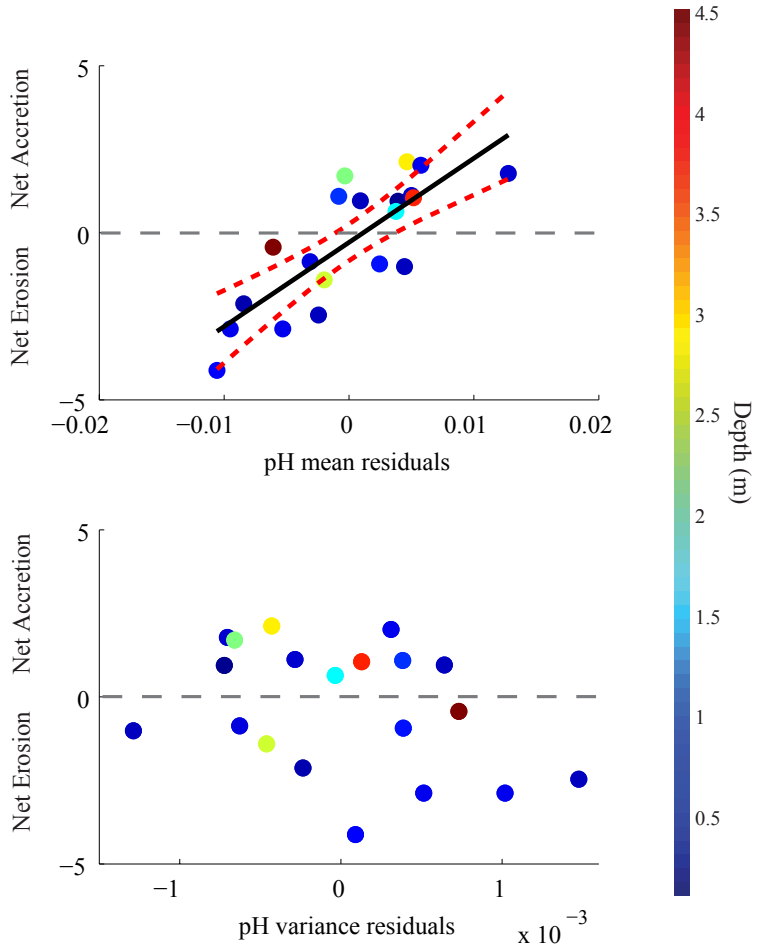

Figure 3: **pH versus net erosion.** Best fit model and 95 % confidence intervals for percent change in volume of experimental blocks (N=20) versus a) mean pH residuals ($y = 251.81x - 0.29$, $R^2 = 0.64$) and b) pH variance residuals ($y = -960.66x - 0.27$, $R^2 = 0.12$). Both pH mean and variance were regressed against depth and distance from shore, and the residuals were used in the analysis and this figure. Percent change in volume for each block was square-root transformed to meet model assumptions.

SUPPLEMENTAL MATERIAL

Tables S1-S5

Figure S1-S7

Movie S1

References

Table S1: **The mean, min, and max for total alkalinity, pH, dissolve inorganic carbon, and pCO_2 at each block**

	Distance from shore (m)	TA Mean	Min	Max	pH Mean	Min	Max	DIC Mean	Min	Max	pCO_2 Mean	Min	Max
1	0.67	2165.28	2095.47	2222.46	7.85	7.70	8.03	1962.93	1831.92	2075.01	658.21	383.34	975.33
2	1.10	2163.19	2113.80	2227.00	7.85	7.69	8.02	1961.63	1834.68	2074.01	658.52	395.77	996.26
3	3.10	2165.79	2089.75	2257.98	7.84	7.70	8.02	1968.44	1810.13	2074.89	675.79	390.79	977.94
4	5.80	2162.67	2101.46	2221.84	7.86	7.72	8.03	1959.19	1812.66	2067.66	650.87	377.19	925.28
5	8.20	2160.20	2092.45	2217.20	7.86	7.71	8.03	1956.83	1806.26	2073.59	650.54	378.85	951.15
6	10.00	2162.44	2088.65	2249.94	7.85	7.72	8.01	1961.16	1810.32	2063.16	655.33	392.98	932.32
7	12.60	2153.50	2077.01	2215.51	7.87	7.75	8.00	1945.46	1805.26	2037.73	623.31	402.03	842.97
8	15.70	2148.80	2075.69	2216.86	7.88	7.79	7.99	1934.68	1816.87	2011.11	594.41	422.67	755.96
9	17.20	2151.65	2085.82	2219.42	7.88	7.79	7.98	1940.73	1834.68	2017.91	603.99	433.50	749.74
10	19.60	2146.80	2069.79	2219.24	7.87	7.78	7.97	1938.05	1822.68	2007.47	608.75	444.06	772.08
11	23.70	2144.53	2047.65	2226.42	7.87	7.78	7.97	1936.70	1802.80	2013.38	609.36	442.48	773.40
12	24.80	2149.03	2053.58	2220.95	7.88	7.79	7.99	1937.61	1800.69	2018.77	600.94	418.94	749.22
13	26.10	2153.33	2050.84	2224.86	7.89	7.82	7.98	1938.42	1800.55	1997.31	588.57	431.89	697.11
14	26.70	2159.52	2053.77	2221.09	7.89	7.81	7.98	1940.97	1802.36	2000.49	579.44	432.34	709.40
15	26.90	2161.51	2079.12	2222.29	7.89	7.83	7.98	1942.22	1818.32	2003.07	576.89	427.54	678.45
16	27.70	2170.00	2109.46	2234.96	7.89	7.83	7.95	1950.99	1876.65	2009.64	579.44	483.75	673.61
17	28.80	2166.87	2116.02	2222.18	7.89	7.83	7.94	1947.64	1877.44	2002.80	576.77	497.79	676.40
18	29.50	2174.30	2126.05	2232.07	7.90	7.85	7.95	1950.49	1892.00	2000.87	565.53	498.45	650.80
19	29.80	2190.64	2139.22	2294.06	7.90	7.84	7.95	1966.69	1897.06	2078.80	573.38	498.68	664.07
20	31.60	2182.22	2138.47	2239.22	7.91	7.86	7.94	1954.90	1903.00	1998.34	558.39	504.33	628.52
21	32.40	2187.85	2149.13	2236.12	7.90	7.83	7.94	1964.11	1910.03	2006.13	573.09	511.54	678.21

Table S2: **Parameters and methods used to measure environmental data.** LoD is level of detection.

Parameter	Method	Instrument	LoD
Nitrate	Armstrong et al (1967); Grasshoff et al (2009)	Seal Analytical AA3 HR Nutrient Autoanalyzer	0.04μmol/l
Nitrite	Armstrong et al (1967); Grasshoff et al (2009)	Seal Analytical AA3 HR Nutrient Autoanalyzer	0.01μmol/l
Ammonium	Kérouel and Aminot (1997)	Seal Analytical AA3 HR Nutrient Autoanalyzer	0.02μmol/l
Phosphate	Murphy and Riley (1962)	Seal Analytical AA3 HR Nutrient Autoanalyzer	0.02μmol/l
Chlorophyll *a*	Arar and Collins (1997); Welschmeyer (1994)	Turner Designs 10AU Benchtop and Field Fluorometer	0.025μg/l
Temperature	Guadayol et al (2014)	Sonde 600XLM, YSI Incorporates	N/A
Total Alkalinity	Dickson et al (2007) SOP 3b	Mettler T50 autotitrator	N/A
pH	Dickson et al (2007) SOP 6b	MolecularDevices SpectraMax M2	N/A

Table S3: **Model selection of raw data with all carbonate chemistry parameters.**

	k	-log($\mathcal{L}$)	AICc	ΔAIC	R^2	Rank
pH	4	-34.17	75.84	0.00	0.48	1
pCO_2	4	-35.19	77.89	2.04	0.42	2
DIC	4	-38.22	83.94	8.10	0.22	3
TA	4	-38.38	84.26	8.41	0.21	4
Depth	3	-40.01	84.73	8.88	0.06	5
Distance	3	-40.40	85.50	9.66	0.02	6
Temperature	4	-40.03	87.56	11.71	0.07	7
Resource Availability	6	-40.03	94.34	18.50	0.09	8
Full Model	18	-12.23	364.46	288.62	0.98	9

Table S4: **Model selection of residual data with all carbonate chemistry parameters.**

	k	-log($\mathcal{L}$)	AICc	ΔAIC	R^2	Rank
pH	4	-30.46	68.42	0.00	0.64	1
TA	4	-32.05	71.60	3.17	0.58	2
pCO_2	4	-32.31	72.13	3.70	0.57	3
DIC	4	-35.27	78.04	9.62	0.42	4
Depth	3	-40.01	84.73	16.30	0.06	5
Distance	3	-40.40	85.50	17.08	0.02	6
Temperature	4	-40.42	88.33	19.91	0.03	7
Resource Availability	6	-38.91	92.11	23.68	0.18	8
Full Model	18	-12.23	364.46	296.04	0.98	9

Table S5: **List of parameters and parameter ranges across all sampling days and sites.**

Parameter	Range
Mean Temperature Anomaly	-0.0064 - 0.008
Chlorophyll *a* (μg L^{-1})	0.019 - 1.36
DIN:DIP	14.56 - 173.75
pH$_T$	7.69 - 8.032
Distance (m)	0.67 - 32.4
Depth (m)	0.12 - 4.52

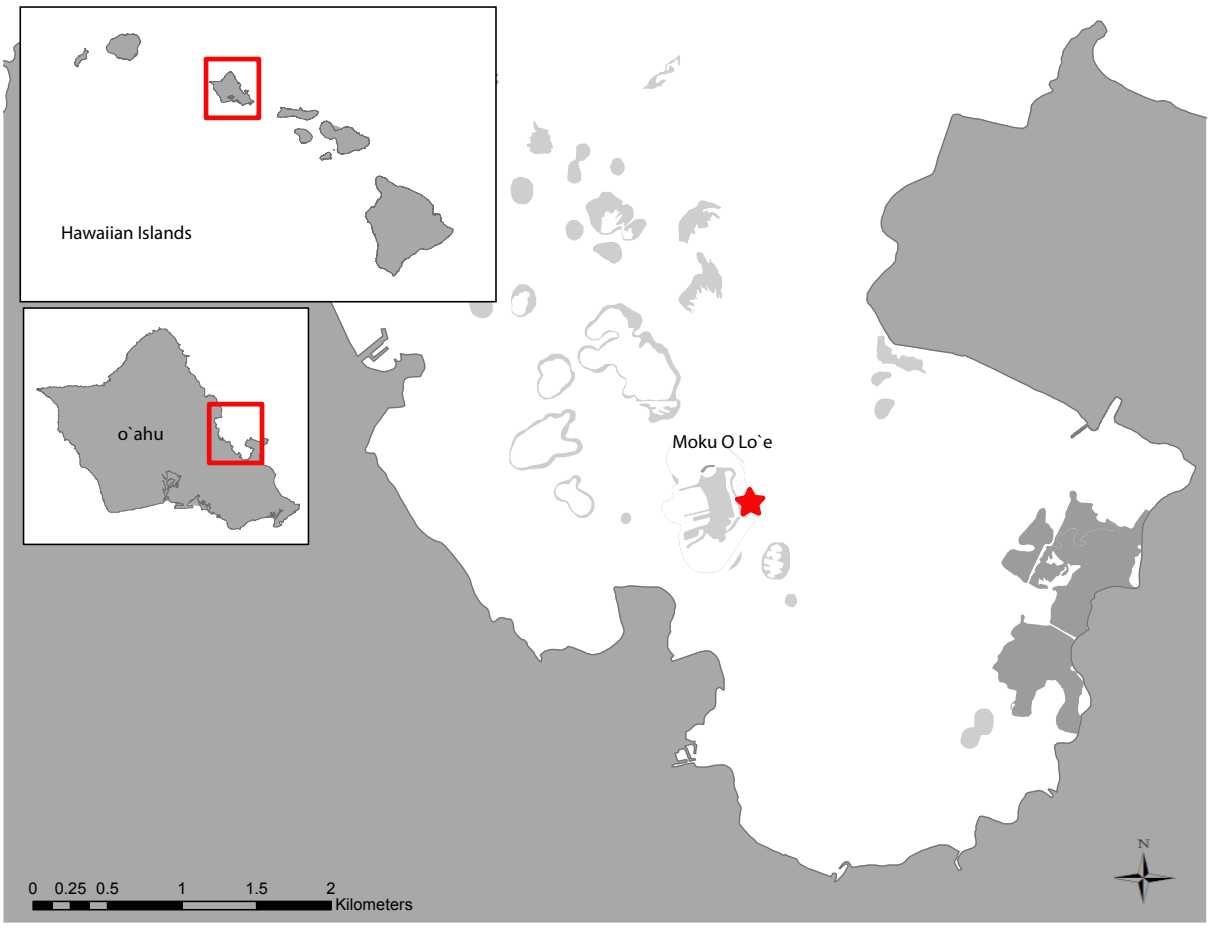

Figure S1: **Map of Kāneʻohe Bay.** Red star represents the location of the study site. Insets on upper left are the Main Hawaiian Islands and the island of O'ahu.

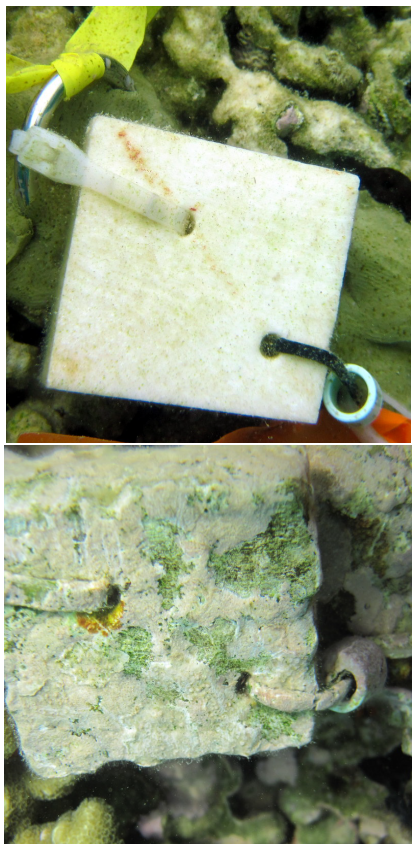

Figure S2: Experimental blocks. Images of experimental blocks attached to substrate immediately after deployment (top) and one year later (bottom).

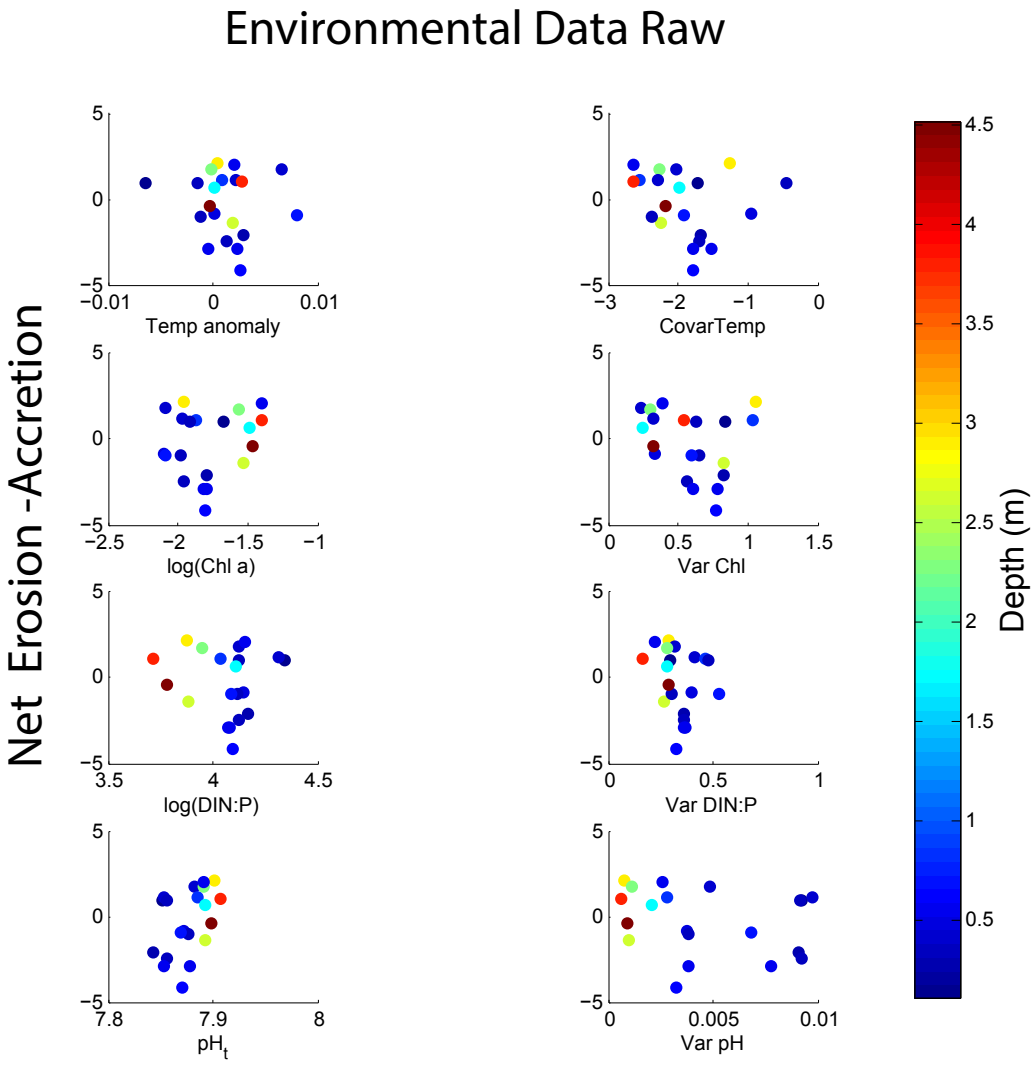

Figure S3: **Net accretion-erosion (square-root transformed) versus raw environmental data.** All positive values on the y-axis are net accretion and all negative values are net erosion.

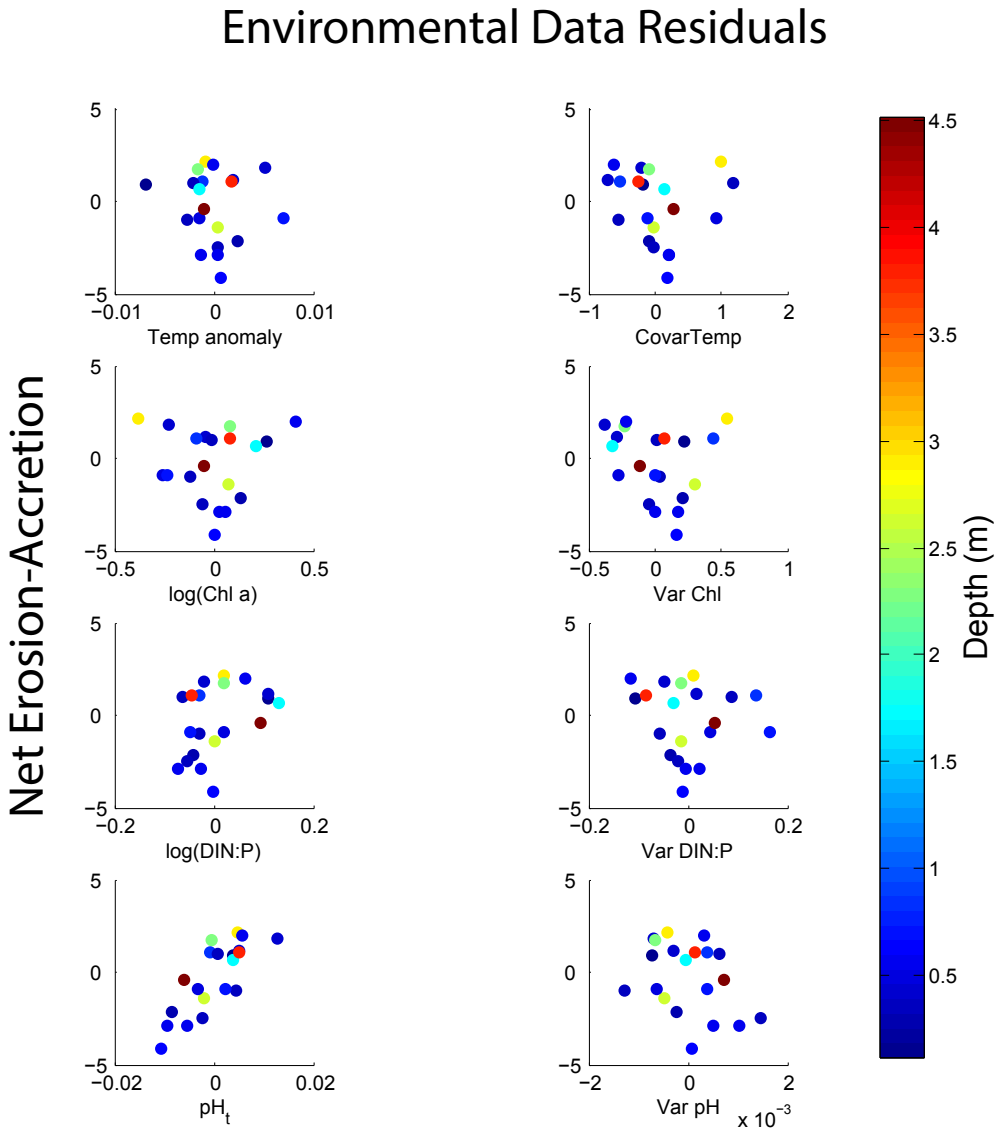

Figure S4: **Net accretion-erosion (square-root transformed) versus residual environmental data.** All positive values on the y-axis are net accretion and all negative values are net erosion.

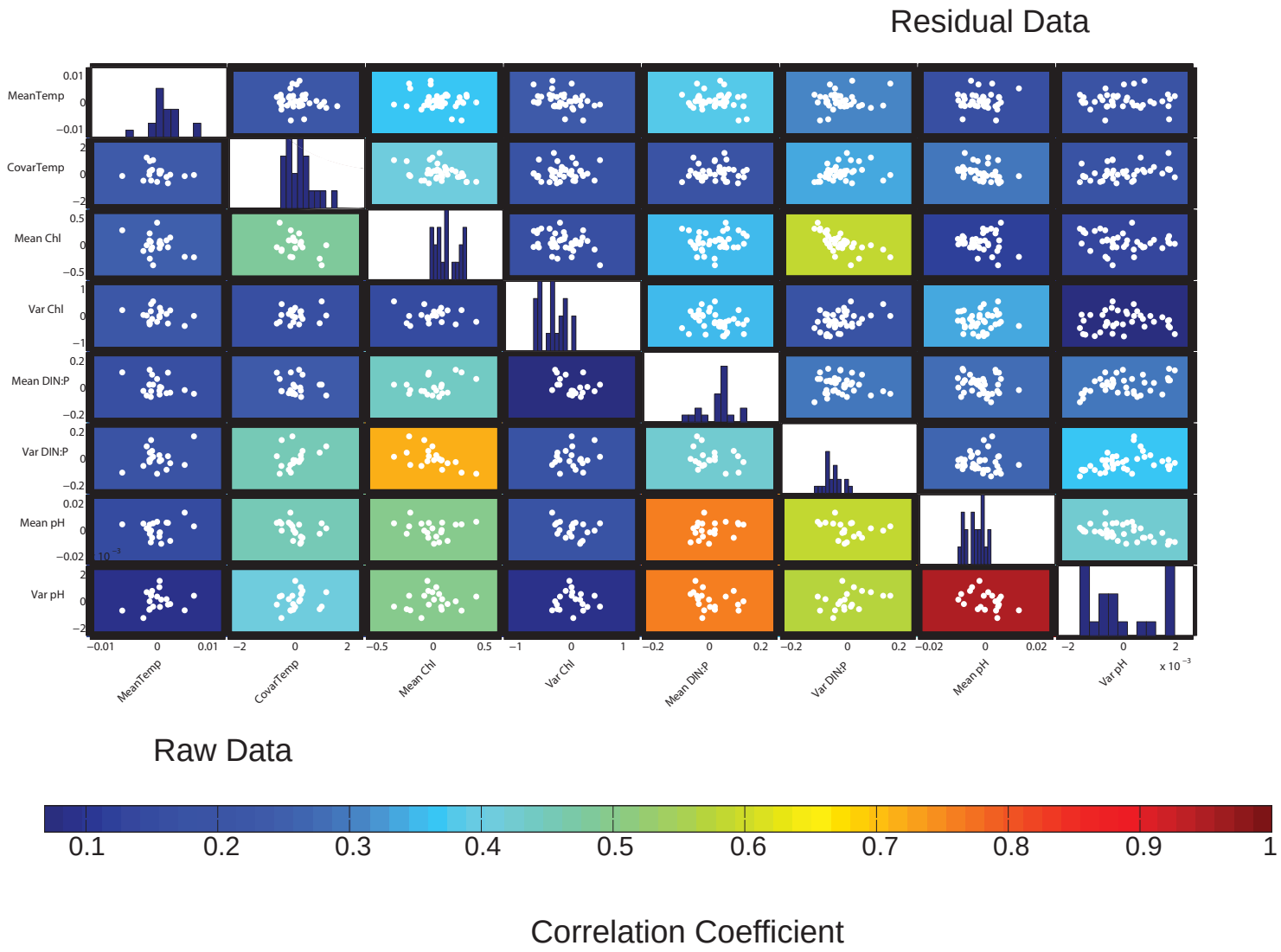

Figure S5: **Matrix of correlation coefficients for environmental data.** Blue background is low correlation and red background is highly correlated. Subplots on the bottom are for the non-manipulated raw environmental data and subplots above the white line are correlation coefficients of residuals from a multiple regression for each parameter against distance from shore and depth.

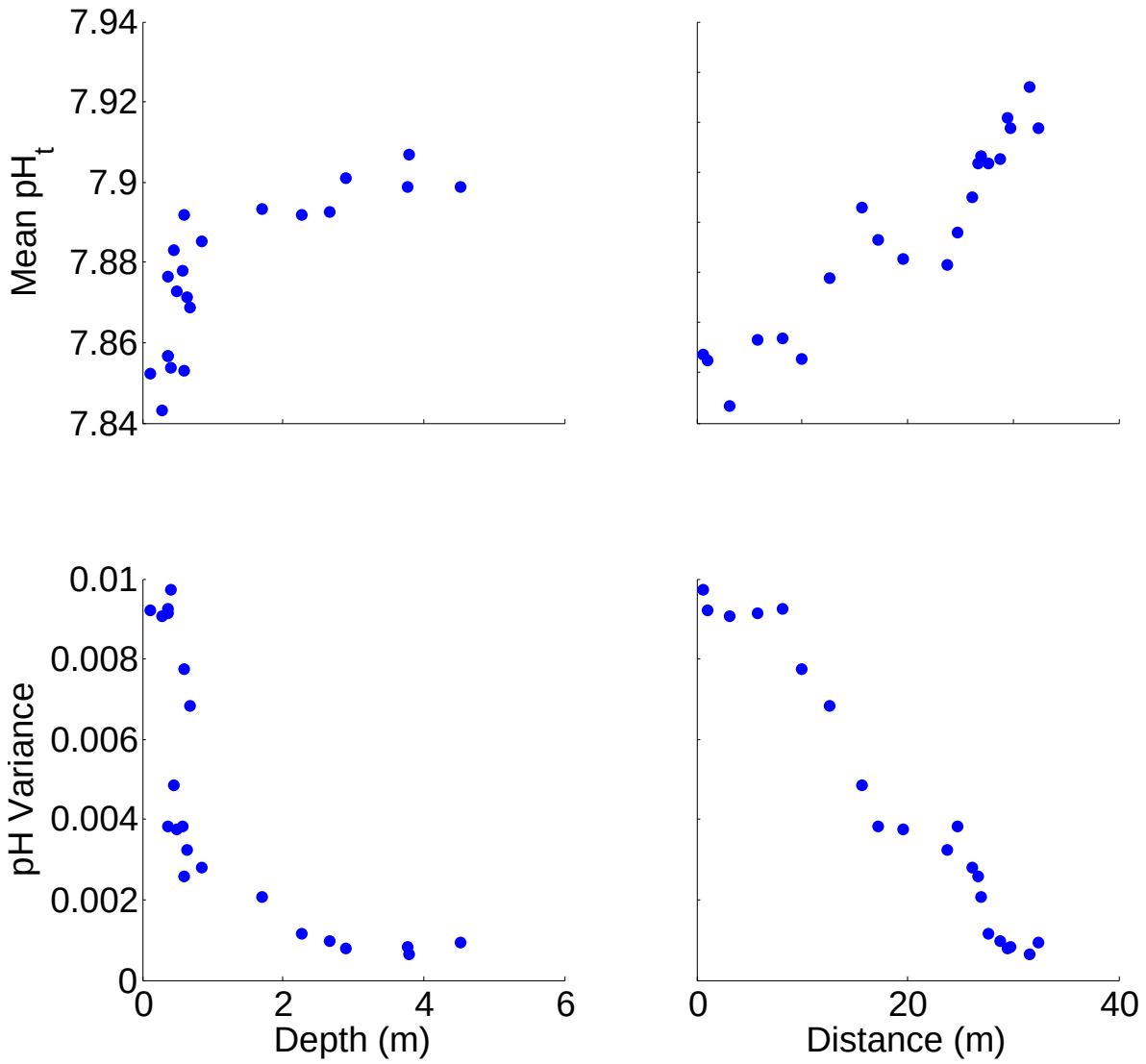

Figure S6: **pH mean (top) and variance (bottom) for each site versus depth (left) and distance from shore (right) across the transect.**

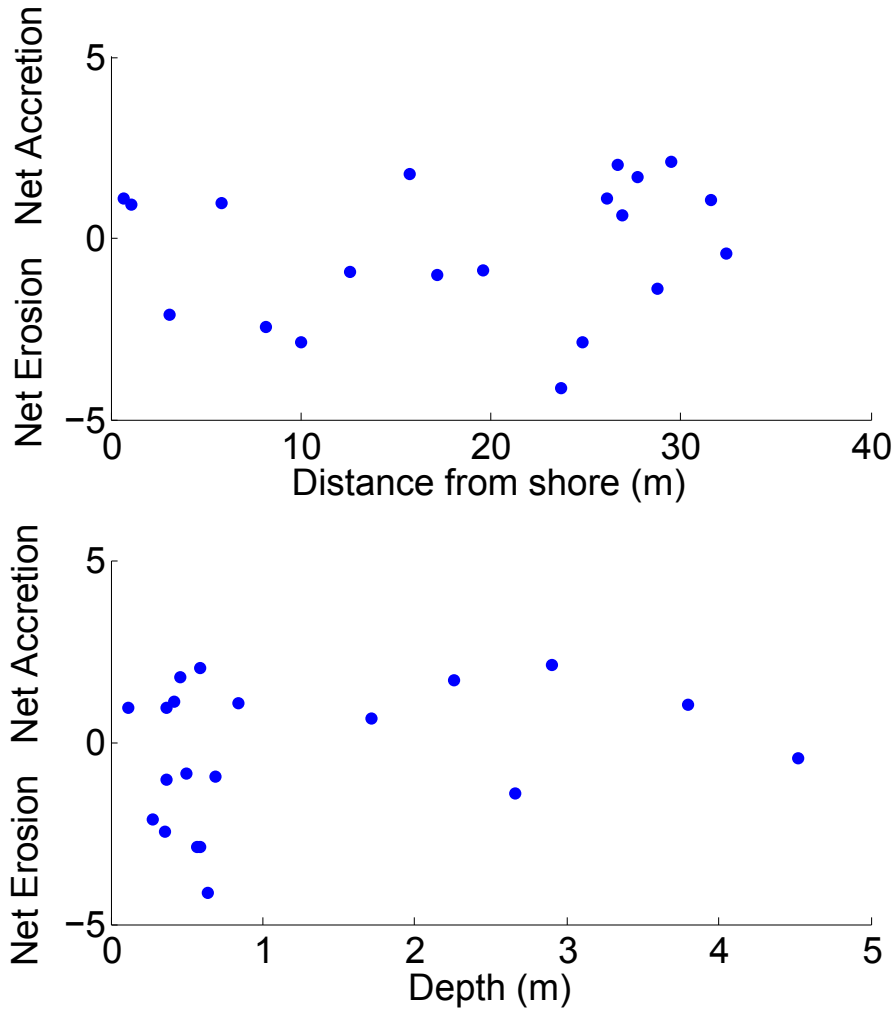

Figure S7: **Net accretion and erosion (square-root transformed) versus distance from shore (top) and depth (bottom).** All positive values on the y-axis are net accretion and all negative values are net erosion. There is no significant relationship between net accretion-erosion and distance from shore or depth.

Movie S1: Three dimensional μCT video of an experimental block after deployed on the reef for one year. This video was created by Mark Riccio at the Cornell University μCT Facility for Imaging and Preclinical Research.

REFERENCES

Arar EJ, Collins GB (1997) Method 445.0: In vitro determination of chlorophyll *a* and pheophytin a in marine and freshwater algae by fluorescence. United States Environmental Protection Agency, Office of Research and Development, National Exposure Research Laboratory

Armstrong F, Stearns C, Strickland J (1967) The measurement of upwelling and subsequent biological process by means of the technicon autoanalyzer R and associated equipment. In: Deep Sea Research and Oceanographic Abstracts, 14: 381-389

Dickson A, Sabine C, Christian JR (2007) Guide to Best Practices for Ocean CO2 Measurements. PICES Special Publication 3

Grasshoff K, Kremling K, Ehrhardt M (1999) Methods of seawater analysis. third, completely revised and extended edition. Wiley-VCH, Weinheim 77(89):160

Guadayol Ò, Silbiger NJ, Donahue MJ, Thomas FIM (2014) Patterns in temporal variability of temperature, oxygen, at pH and along an environmental gradient in a coral reef. Plos One 9:e85213

Kérouel R, Aminot A (1997) Fluorometric determination of ammonia in sea and estuarine waters by direct segmented flow analysis. Mar Chem 57:265-75

Murphy J, Riley J (1962) A modified single solution method for the determination of phosphate in natural waters. Anal Chim Acta 27:31-36

Welschmeyer NA (1994) Fluorometric analysis of chlorophyll *a* in the presence of chlorophyll b and pheopigments. Limnol Oceanogr 39:1985-1992

CHAPTER 3

RANKING THE IMPACT OF MULTIPLE ENVIRONMENTAL STRESSORS ON CORAL REEF EROSION AND SECONDARY ACCRETION

Submitted as: Silbiger, NJ, Guadayol, Ò, Donahue, MJ, Thomas, FIM (*submitted*) Ranking the impact of multiple environmental stressors on coral reef erosion and secondary accretion.

ABSTRACT:

Ocean acidification threatens to shift coral reefs from net accreting to net eroding. While corals build reefs through accretion of calcium carbonate ($CaCO_3$) skeletons, net reef growth depends on bioerosion by grazers and borers and on secondary calcification by crustose coralline algae and other calcifying invertebrates. Primary calcification, secondary calcification, and erosion processes respond differently to climate change stressors; therefore, the combined accretion-erosion response is uncertain. Using a a new micro-computed tomography (μCT) method, we measured the simultaneous response of secondary accretion and bioerosion along an environmental gradient. We saw that bioerosion rates ranged from 0.02 to 0.91 kg m^{-2} yr^{-1} and secondary accretion rates ranged from 0.01 to 0.4 mm yr^{-1} across a 32m transect. Co-located measures of secondary accretion and bioerosion had different environmental drivers: bioerosion rates were highly sensitive to ocean acidity while secondary accretion rates were most sensitive to physical drivers. These results suggest that bioerosion likely plays a more significant role in the shift from net accretion to net erosion on coral reefs than previously thought.

SIGNIFICANCE STATEMENT

Corals build reefs though the accretion of calcium carbonate skeletons, but the structural complexity, mechanical stability and net growth of coral reefs also depends on the response of secondary calcification and bioerosion to local and global anthropogenic disturbances. Here, we highlight the importance of these two under-studied reef processes and rank the dominant environmental drivers of secondary accretion and bioerosion along a natural reef gradient. We also present a novel μCT method to calculate highly accurate rates of secondary accretion and bioerosion from the same experimental substrate. Our study emphasizes how important it is to consider both accretion and erosion processes in future work that seek to predict the fate of coral reefs under a changing climate.

INTRODUCTION

Human-induced changes in ocean chemistry (1–9), temperature (1, 5, 9, 10), and water quality (3, 11–16) are threatening the net growth of coral reefs (1, 11, 17). Predictions for how reefs will respond to changing ocean conditions are often only based on the response of reef building corals (17, 18), but coral reef bioerosion from borers and grazers and secondary accretion from crustose coralline algae and other encrusting invertebrates are also critical processes for reef sustainability (19). There are several gaps in our knowledge about the response of coral reefs to future ocean conditions and, particularly, whether reef accretion will continue to exceed reef erosion. For example, there remains substantial uncertainty about the following: 1) Will primary accretion, secondary accretion, and reef erosion respond similarly to environmental drivers and will their responses combine to accelerate reef loss?

Studies that examine accretion or erosion processes individually have found varying responses to environmental stress. In a field experiment, coral calcification and bioerosion had different functional relationships with land-based pollution (15). Laboratory experiments focusing on climate stressors (i.e. temperature and ocean acidity) have found that bioerosion is linearly related to ocean acidity and temperature (5–9), but that calcification exhibits both linear (17, 20) and parabolic (5, 17, 20, 21) responses. These complex individual responses challenge our ability to predict the net response of coral reefs to environmental change. 2) How will multiple environmental stressors impact individual reef processes? Many environmental parameters interact to drive patterns in accretion and erosion, including ocean acidity (1–9), temperature (1, 5, 9, 10), nutrients(3, 11–14), and gradients of human influence (e.g., chlorophyll, turbidity, sedimentation) (15, 16). This myriad of drivers complicates the predictions of reef response to climate change. 3) How does local, natural variability contextualize global changes in the accretion-erosion balance? Shallow coral reef ecosystems persist in highly variable physicochemical environments (22–24) driven by tidal flushing, photosynthesis and respiration, ground-water inputs, and other benthic biological processes (25–30). Little is known about how climate change interacts with this naturally variable environment to drive patterns accretion and erosion. Here, we address each of these knowledge gaps by leveraging a natural environmental gradient in Kāne‘ohe Bay to rank the impact of multiple environmental stressors on simultaneous measures of secondary accretion and reef bioerosion.

The physicochemical variability of reefs in Kāne‘ohe Bay, Hawai‘i has been extensively investigated (22, 27, 31). Like many reefs around the globe (23–25, 32, 33), Kāne‘ohe Bay has persistent areas of natural acidification that reach the low open-ocean pH values expected by the end of the 21st century (4, 22).Using a space-for-time framework, we can leverage this natural variability to predict how reefs will respond to ocean acidification in the context of a naturally variable environment. Prior work in Kāne‘ohe Bay demonstrates that net reef erosion (calculated as the percent change in volume of experimental blocks) is driven by natural changes in pH and that reefs could shift from net accretion to net erosion with increasing ocean acidity (4). To compliment previous findings, we rank the importance of different environmental parameters (Figure 1) to individual measures of secondary accretion and bioerosion along this same environmental gradient. We calculate high-precision bioerosion and secondary accretion rates, using a new μCT analysis (Figure 2), by comparing before and after μCT scans of blocks from a year-long deployment.

In prior studies using experimental substrates, pre and post deployment buoyant weights have been used to calculate changes in density, mass, or volume (reviewed in Table S1), but this method is unable to distinguish between secondary accretion and bioerosion processes. Imaging methodologies in 2-dimensions and, more recently, 3-dimensions (CT and μCT) can separate accretion and bioerosion on slabs or cores of reef (Table S1), but rates are difficult to estimate because the time the substrate became available to bioeroders and secondary calcifiers is unknown. Here, we develop a new analysis that uses μCT to separate secondary accretion and bioerosion from the same experimental substrate exposed to the same environmental variation over the same time-scale (Figure 2).

Our μCT method also allows for a 3D visualization of the experimental blocks that highlights specific areas of secondary accretion and bioerosion (See Movies S1 and S2 in Supplement). Using μCT, we calculate secondary accretion and bioerosion rates from experimental blocks that were deployed along a 32 m reef transect (Figure S1). Patterns in carbonate chemistry, nutrients, chlorophyll *a*, temperature, and depth were characterized along this same transect (Figure 1; described in Silbiger et al. 2014 (4)) and these data were incorporated into models that address five specific hypotheses about the accretion-erosion balance (carbonate chemistry, resource availability, temperature, light availability (depth), and hydrodynamics (distance from shore and depth)). We use a model selection approach to test which of these drivers has the strongest relationship to secondary accretion and bioerosion and we find new results that are different from those obtained using previously published methods.

RESULTS AND DISCUSSION

Environmental data: The environmental gradient is detailed in Silbiger et al. (2014) (4) and described briefly here. There were considerable differences in the mean and variance in pH and DIN:DIP across the gradient (Figure 1e-f). pH mean increased from 7.84 to 7.91 across the transect. At the least variable site pH ranged from 7.84 to 7.94 and at the most variable site pH ranged from 7.76 to 8.02 during the year deployment (Figures 1g,h and S2). Mean DIN:DIP decreased from 87.5 to 42.4 and the coefficient of variation increased from 0.36 to 0.59 (Figure 1e,f). Chl *a* and temperature anomalies remained relatively constant (Figure 1a-d).

Bioerosion Rates:

Bioerosion rates increased by nearly two orders of magnitude across our 32 m transect, ranging from 0.02 to 0.91 kg m^{-2} yr^{-1} (Figure S3p). These bioerosion rates are similar to rates at other Pacific reefs sites. For example, a recent study saw bioerosion rates ranging from 0 to 0.6 kg m^{-2} yr^{-1} at remote reefs across the Pacific (3). Interestingly, the range of bioerosion rates on our transect encompassed their Pacific wide study, highlighting the importance of small-scale within-reef variability. The pH model best predicted patterns in bioerosion along the transect explaining 54% of the variance (Table 1a, Figure 3). Bioerosion rates were highest in areas of the reef with the lowest pH (Table 1a and Figure 3). The second best model, the distance and depth model, had low empirical support ($\Delta AIC_c = -13.78$) and explained only 9% of the variance (Table 1a) and was followed by the temperature model which explained only 7% of the variance in bioerosion rates. While the resource availability model described 21% of the variance in the data, it also had a larger number of parameters (6, including mean and variance for both DIN:DIP and chlorophyll *a*) and, therefore, ranked fourth in model parsimony. The full model, which included the means and variances of all parameters, described 79% of the variance in bioerosion rates indicating that the environmental data we collected adequately described patterns in bioerosion rates across our transect. Any additional environmental parameter would at most only explain 21% of the variance in bioerosion.

Indeed, all the parameters in these models interact with each other to drive patterns in bioerosion, but when

ranking individual parameters pH was the dominant driver. It is becoming clear that ocean acidity facilitates erosion (4–9), but the mechanisms that control this relationship are still not well known. Several studies suggest that ocean acidification could enhance chemical erosion (5, 6, 8) because many bioeroders erode the coral skeleton by secreting acidic compounds. Lower pH in the overlaying water-column might make it metabolically easier for the bioeroders to reduce pH at the site of erosion and therefore promote erosion.

Secondary Accretion Rates:

Secondary accretion rates ranged from 0.01 to 0.4 mm yr^{-1} across the transect (Figure S4p). These rates are slightly lower than secondary accretion rates from a Kāne'ohe Bay study that saw 2 mm crusts of CCA after a 6 mo. exposure, possibly due to differences in grazing between study sites or the size of the experimental blocks (34). For secondary accretion, pH was not the best predictor for patterns in accretion across the transect ($R^2 = 0.13$; Table 1b). Rather, the distance from shore and depth model ranked highest explaining 23% of the variance in the data (Figure 4). Differences in light and hydrodynamics along the transect could be mediating the relationship between secondary accretion and distance from shore and depth. Notably, our accretion rates were limited to secondary calcifiers such as CCA and encrusting invertebrates that are not light dependent (e.g., oysters and barnacles), and excluded corals. We did not measure light or photosynthetically active radiation across our transect, but our deepest site was only 4.5m deep, and, therefore, it is unlikely that light was limiting across the transect. Further, distance from shore explained more of the variation in secondary accretion than depth (23% vs 13%; Figure 4) and there is a tight correlation between distance from shore and turbulent kinetic energy dissipation rate ($R^2 = 0.88$, Figure S5), suggesting that hydrodynamics, rather than light, may be driving the patterns in accretion. Hydrodynamic energy (e.g., turbulence, wave action, tidal mixing) could impact secondary accretion in several ways: 1) both the delivery of dissolved compounds and particulates are positively correlated with hydrodynamic parameters increasing nutrient availability for benthic organisms (35, 36), 2) increased flow could promote accretion by facilitating settlement of benthic invertebrate larval recruits, such as oysters and barnacles (37), and 3) different exchange, or mixing, rates with offshore waters could impact accretion by replenishing food supplies and removing waste (38). On our reef transect, the furthest offshore sites on the reef slope were constantly mixed with offshore deep water masses, whereas the water inside the reef flat was sometimes isolated. Therefore, large-scale mixing is a likely mechanism driving the patterns between accretion and distance from shore. Lastly, the full model explained 90% of the variance in secondary accretion. Again, this indicates that the measured parameters adequately described patterns in secondary accretion. Any additional parameter would only add at most 10% explanatory power to the over-all model.

Advancing methods for examining secondary accretion and bioerosion

Our new μCT method shows that secondary accretion and bioerosion processes are driven by different environmental parameters. Indeed, accretion and erosion rates on coral reefs are controlled by different organisms, so it is not surprising that they respond to different environmental parameters. Yet, this is the first study to simul-

taneously measure secondary accretion and bioerosion on the same time-scale and correlate them with multiple drivers of the accretion-erosion balance. In a prior study, we used before and after μCT scans to calculate a net change in volume (4). In the present study, we advance this method and subtract before and after scans to separate differences in secondary accretion and bioerosion. With μCT we can calculate how much volume is added or removed from an experimental block to the accuracy of the scan (here, 100 μm). We also compared the volume of the pre-deployment blocks calculated with μCT to the volume calculated using buoyant weight and the data are in close agreement: the volumes calculated from μCT are nearly identical to standard buoyant weight methods (Figure S6; F_{19} = 859, p<0.001, R^2 = 0.98, $y = 0.96x + 1.9$) and provides a more complete analysis of secondary accretion and bioerosion processes.

Secondary accretion versus bioerosion in a high CO_2 world

Our data indicate that bioerosion is more sensitive to ocean acidity than secondary accretion. Both the R^2 values (0.54 vs 0.13) and the effect size of the pH model (Figure 5) were highest for bioerosion. For a 0.1 increase in pH, we saw a 2.35 kg m^{-2} yr^{-1} increase in bioerosion compared to a 0.77 mm yr^{-1} decrease in secondary accretion indicating that bioerosion responded more strongly to pH than secondary accretion. Bioerosion also responded to pH mean 1.7$\times$ more strongly than pH variance. In a prior study, we saw a shift from net accretion to net erosion with increasing ocean acidity (4), but we were unable to uncover the underlying mechanisms driving this shift. Here, our data indicate that reef erosion (and dissolution), rather than reef accretion, may be driving the negative relationship between ocean acidification and net calcification of coral reefs, and recent studies support this hypothesis (5, 39, 40). In a laboratory experiment, chemical dissolution from bioeroders was more strongly correlated with ocean acidity than secondary calcification (5). In a field study, live coral and mollusc calcification was unaffected by natural acidification at CO_2 vents in the Mediterranean at normal temperatures, but dissolution of dead skeletons increased with decreasing pH (39). Here, we demonstrate that bioerosion is more sensitive to ocean acidity than secondary accretion along a natural environmental gradient. Our results and those from previous studies (3–7, 9) provide compelling evidence that erosion rates will increase under future ocean conditions. The sensitivity of erosion to ocean acidification could tip the balance of coral reefs in favor of net reef erosion in a more acidic ocean.

Materials and Methods

***(a) Experimental Design*:** Our study site is located in Kāne‘ohe Bay, O‘ahu on the windward (eastern) side of Moku o Lo‘e. We used the same environmental gradient as Silbiger et al. (2014) (4), which we briefly describe here (see supplement for full description of methods). Twenty-one experimental blocks were deployed along a 32 m transect, stratified between reef flat and reef slope (Figure S1). Experimental blocks were cut from dead pieces of massive *Porites* sp. skeleton into 5cm x 5cm x 2cm blocks, soaked in freshwater, and then autoclaved to remove

any living organisms. The average skeletal density of each experimental block was 1.57 ± 0.07(sd) g cm^{-3}. Blocks were deployed from March 31, 2011 to April 10, 2012. We collected both discrete water samples (pH, TA, nitrate, nitrite, ammonium, phosphate, and chlorophyll *a*) and data from continuous sensors (temperature and depth) along the transect. Water samples were collected directly above each block four times within 24 hours in September, December, and April in order to capture both diel and seasonal variability in the environment. Continuous sensors were stationed over each block for a minimum of two weeks to calculate high frequency (0.1 min^{-1}) variation in temperature and depth. These short time series were normalized to a continuous time series from a permanent station positioned adjacent to the transect, allowing comparison of the micro-environments at each block (22).

***(b)* μ*CT*:** Secondary accretion and bioerosion rates were calculated using μCT (Figure 2). μCT is an X-ray technology that non-destructively images the external and internal structures of solid objects, resulting in a three-dimensional array of object densities. We used an eXplore CT120 μCT (GE Healthcare Xradia, Inc) at the Cornell University Imaging Multiscale CT Facility (Figure 2.1-2) to scan blocks before and after deployment (voltage = 100kV, current = 50mA). A three-dimensional array of isotropic voxels at 50 μm^3 resolution was generated using the GE Console Software and were averaged to 100 μm^3 for data analysis. We used a threshold of 200 Hounsfield Units to separate coral from air (4) (Figure 2.3). The pre and post-deployment scans were aligned using an intensity-based registration technique (Figure 2.4), converted to binary (Figure 2.5), and subtracted from one another resulting in a matrix of 0's, 1's, and -1's (Figure 2.5). All positive values were new pixels added to the post-deployment scan which indicate secondary accretion, negative values were pixels that were lost and indicate bioerosion, and zeros meant there was no change at that pixel between the two scans. All values were summed and multiplied by the resolution of the scan to obtain the volume lost or gained per block (Figure 2.6).

***(c) Rates*:** Bioerosion and secondary accretion rates were calculated using the following equations: Bioerosion Rate (kg m^{-2} yr^{-1}) $= (Vol_i \times \rho_i)/(SA_i \times Time)$ and Secondary Accretion Rate (mm yr^{-1}) $= Vol_i/(SA_i \times Time)$, where i represents an individual block, Vol is the volume lost (bioerosion) or gained (secondary accretion) in m^3, SA is the surface area of the pre-deployment blocks (m^2), ρ is the skeletal density of the pre-deployment block (kg m^{-3}), and $Time$ is the deployment time (years). Secondary accretion rates were converted from m to mm per year to compare with literature values.

***(d) Model Selection*:** Our goal was to compare pH with other known drivers and correlates of the accretion-erosion balance. Many of the environmental variables were collinear along the transect; thus, we removed collinearity by using the residuals of a regression of each environmental variable against log(depth) and distance from shore(4). Correlation coefficients for raw environmental data and the residual environmental data are available in Silbiger et al. 2014 (4).

We used a model selection framework to compare models for five specific hypotheses about the accretion-erosion balance and test which of these drivers had the strongest relationship to secondary accretion and bioerosion (Table 1). In a model selection framework, Akaike Information Criterion (AIC) values are used to rank candidate

models, accounting for both fit and complexity. Carefully constructed model selection avoids problems associated with multiple hypothesis testing that are common in stepwise regression, such as arbitrary α levels and uninterpretable functional relationships (41, 42). Here, we used the corrected AIC (AICc), which is recommended for sample sizes <30 (42). While the model with the smallest AICc value (ΔAICc = 0) is the 'best' of the models considered, models with an ΔAICc value of <4 have some empirical support (42). We used pH to test how carbonate chemistry influenced secondary accretion and bioerosion rates. Carbonate chemistry parameters are inherently correlated, and pH had the strongest relationship of the carbonate chemistry parameters (Table S2). The pH model includes both the mean and variance of the discrete pH samples from each block. The resource availability model includes the means and variances of DIN:DIP ratios (a proxy for resource quality) and chlorophyll *a* (a measure of resource quantity) from the discrete water samples. The temperature model included the mean relative temperature anomaly of each block from the overlaying water column and temperature covariance between the block and overlaying water column. The final model was the combination of log(depth) and distance from shore. These linear models were compared to a full model that includes the means and variances of every parameter stated above (Table 1). Environmental data that did not meet the assumptions of normality were log-transformed, secondary accretion and bioerosion data were square-root transformed to meet assumptions of normality, and one block with a large aggregation of oysters was excluded from the analysis. Figures showing secondary accretion (Figure S4) and bioerosion (Figure S3) versus the means and variances of all environmental parameters are available in the supplement.

Data Accessibility: Data will be made publicly available after acceptance.

Competing Financial Interests: We have no competing interests.

Author Contributions: NJS, OG, MJD, FIMT conceived and designed the experiment. NJS, OG conducted the field work. NJS did the μCT analysis. NJS, MJD, OG ran the statistical analyses. NJS wrote the paper. NJS, OG, FIMT, MJD edited the paper.

Acknowledgments: We are grateful to C.J. Bradley, J. Chen, R. Coleman, A. Copeland, K. DiPerna, M. Donovan, N. Griffith, K. Hurley, M. Iacchei, I. Iglesias, M. Siple, E.M. Sogin, M. Sudek, J. Sziklay, M. Walton, and the Point Lab for help with data collection. We thank M. Riccio and F. von Stein from the Cornell University μCT Facility for Imaging and Preclinical Research, R. Briggs from UH SOEST Laboratory for Analytical Biochemistry, and the UH lapidary facility. This is HIMB contribution #, SOEST #, and SeaGrant #.

Funding: Funding for this project came from NOAA Office of National Marine Sanctuaries-HIMB partnership (MOA #2009-039/7932), National Science Foundation EPSCoR Hawai'i, NOAA Dr. Nancy Foster Scholarship to N.J.S., Sigma-Xi GIAR to N.J.S., and by Hawai'i Sea Grants #1889 to F.I.M.T and #1847 to M.J.D. and F.I.M.T.

This paper is funded in part by a grant/cooperative agreement from the National Oceanic and Atmospheric Administration, Project No. R/IR-18, which is sponsored by the University of Hawai'i Sea Grant College Program, School of Ocean and Earth Science and Technology, under Institutional Grant No. NA09OAR4170060 Office of Sea Grant, Department of Commerce. The views expressed herein are those of the author(s) and do not necessarily reflect the views of NOAA or any of its subagencies.

References

[1] Hoegh-Guldberg O, et al. (2007) Coral reefs under rapid climate change and ocean acidification. *Science* 318:1737–1742.

[2] Andersson A, Gledhill D (2013) Ocean acidification and coral reefs: effects on breakdown, dissolution, and net ecosystem calcification. *Ann Rev of Mar Sci* 5:321–348.

[3] DeCarlo TM, et al. (2014) Coral macrobioerosion is accelerated by ocean acidification and nutrients. *Geology* pp G36147–1.

[4] Silbiger NJ, Guadayol Ò, Thomas FI, Donahue MJ (2014) Reefs shift from net accretion to net erosion along a natural environmental gradient. *Marine Ecology Progress Series* 515:33–44.

[5] Silbiger N, Donahue M (2015) Secondary calcification and dissolution respond differently to future ocean conditions. *Biogeosciences* 12:567–578.

[6] Wisshak M, Schönberg CH, Form A, Freiwald A (2012) Ocean acidification accelerates reef bioerosio. *Plos One* 7:e45124.

[7] Tribollet A, Godinot C, Atkinson M, Langdon C (2009) Effects of elevated pCO_2 on dissolution of coral carbonates by microbial euendoliths. *Global Biogeochem Cycles* 23:GB3008.

[8] Reyes-Nivia C, Diaz-Pulido G, Kline D, Guldberg OH, Dove S (2013) Ocean acidification and warming scenarios increase microbioerosion of coral skeletons. *Glob Change Biol* 19:1919–1929.

[9] Fang JK, et al. (2013) Sponge biomass and bioerosion rates increase under ocean warming and acidification. *Glob Change Biol* 19:3581–3591.

[10] Davidson TM, de Rivera CE, Carlton JT (2013) Small increases in temperature exacerbate the erosive effects of a non-native burrowing crustacean. *J Exp Mar Biol Ecol* 446:115 – 121.

[11] Fabricius KE (2005) Effects of terrestrial runoff on the ecology of corals and coral reefs: review and synthesis. *Marine pollution bulletin* 50:125–146.

[12] Risk MJ, Sammarco PW, Edinger EN (1995) Bioerosion in *Acropora* across the continental-shelf of the Great Barrier Reef. *Coral Reefs* 14:79–86.

[13] Holmes KE, Edinger EN, Hariyadi, Limmon GV, Risk MJ (2000) Bioerosion of live massive corals and branching coral rubble on Indonesian coral reefs. *Mar. Pollut. Bull.* 40:606–617.

[14] Tribollet A, Golubic S (2005) Cross-shelf differences in the pattern and pace of bioerosion of experimental carbonate substrates exposed for 3 years on the northern Great Barrier Reef, Australia. *Coral Reefs* 24:422–434.

[15] Edinger EN, et al. (2000) Normal coral growth rates on dying reefs: Are coral growth rates good indicators of reef health? *Mar. Pollut. Bull.* 40:404–425.

[16] Le Grand HM, Fabricius KE (2011) Relationship of internal macrobioeroder densities in living massive *Porites* to turbidity and chlorophyll on the Australian Great Barrier Reef. *Coral Reefs* 30:97–107.

[17] Pandolfi JM, Connolly SR, Marshall DJ, Cohen AL (2011) Projecting coral reef futures under global warming and ocean acidification. *Science* 333:418–422.

[18] Silverman J, Lazar B, Cao L, Caldeira K, Erez J (2009) Coral reefs may start dissolving when atmospheric CO_2 doubles. *Geophys. Res. Lett.* 36:L05606.

[19] Przeslawski R, Ahyong S, Byrne M, Woerheide G, Hutchings P (2008) Beyond corals and fish: the effects of climate change on noncoral benthic invertebrates of tropical reefs. *Global Change Biology* 14:2773–2795.

[20] Comeau S, Edmunds P, Spindel N, Carpenter R (2013) The responses of eight coral reef calcifiers to increasing partial pressure of co2 do not exhibit a tipping point. *Limnol. Oceanogr* 58:388–398.

[21] Castillo KD, Ries JB, Bruno JF, Westfield IT (2014) The reef-building coral siderastrea siderea exhibits parabolic responses to ocean acidification and warming. *Proceedings of the Royal Society B: Biological Sciences* 281:20141856.

[22] Guadayol Ò, Silbiger NJ, Donahue MJ, Thomas FI (2014) Patterns in temporal variability of temperature, oxygen and pH along an environmental gradient in a coral reef. *Plos One* 9:e85213.

[23] Hofmann G, et al. (2011) High-frequency dynamics of ocean pH: A multi-ecosystem comparison. *Plos One* 6:e28983.

[24] Rivest EB, Gouhier TC (2015) Complex environmental forcing across the biogeographical range of coral populations. *PloS one* 10:e0121742.

[25] Shamberger KE, et al. (2014) Diverse coral communities in naturally acidified waters of a western pacific reef. *Geophysical Research Letters* 41:499–504.

[26] Yates KK, Dufore C, Smiley N, Jackson C, Halley RB (2007) Diurnal variation of oxygen and carbonate system parameters in Tampa Bay and Florida Bay. *Mar Chem* 104:110–124.

[27] Drupp P, De Carlo EH, Mackenzie FT, Bienfang P, Sabine CL (2011) Nutrient inputs, phytoplankton response, and CO_2 variations in a semi-enclosed subtropical embayment, Kaneohe Bay, Hawaii. *Aquat Geochem* 17:473–498.

[28] Massaro RF, et al. (2012) Multiple factors driving variability of CO_2 exchange between the ocean and atmosphere in a tropical coral reef environment. *Aquat Geochem* 18:357–386.

[29] Duarte CM, et al. (2013) Is ocean acidification an open-ocean syndrome? Understanding anthropogenic impacts on seawater pH,. *Estuaries and Coasts* 36:1–16.

[30] Smith JE, Price NN, Nelson CE, Haas AF (2013) Coupled changes in oxygen concentration and pH caused by metabolism of benthic coral reef organisms. *Mar Biol* 160:1–11.

[31] Lowe RJ, Falter JL, Monismith SG, Atkinson MJ (2009) Wave-driven circulation of a coastal reef-lagoon system. *J. Phys. Oceanogr.* 39:873–893.

[32] Manzello DP, et al. (2008) Poorly cemented coral reefs of the eastern tropical Pacific: Possible insights into reef development in a high-CO_2 world. *Proc. Natl. Acad. Sci. U. S. A.* 105:10450–10455.

[33] Crook ED, Cohen AL, Rebolledo-Vieyra M, Hernandez L, Paytan A (2013) Reduced calcification and lack of acclimatization by coral colonies growing in areas of persistent natural acidification. *Proc Natl Acad Sci U S A* 110:11044–11049.

[34] Tribollet A, Langdon C, Golubic S, Atkinson M (2006) Endolithic microflora are major primary producers in dead carbonate substrates of Hawaiian Coral Reefs. *Journal of Phycology* 42:292–303.

[35] Nowell A, Jumars P (1984) Flow environments of aquatic benthos. *Annual review of ecology and systematics* pp 303–328.

[36] Butman CA, Geyer WR (1989) The importance of boundary-layer flows in supplying phytoplankton to the benthic suspension feeder, *Mytilus edulis* l. *Limnol. Oceanogr* 34:19–36.

[37] Abelson A, Denny M (1997) Settlement of marine organisms in flow. *Annual Review of Ecology and Systematics* pp 317–339.

[38] Smith S (1984) Phosphorus versus nitrogen limitation in the marine environment. *Limnology and Oceanography* 29:1149–1160.

[39] Rodolfo-Metalpa R, et al. (2011) Coral and mollusc resistance to ocean acidification adversely affected by warming. *Nature Climate Change* 1:308–312.

[40] Erez J, Reynaud S, Silverman J, Schneider K, Allemand D (2011) in *Coral reefs: an ecosystem in transition* (Springer), pp 151–176.

[41] Johnson JB, Omland KS (2004) Model selection in ecology and evolution. *Trends Ecol Evol* 19:101–108.

[42] Anderson DR (2008) *Model based inference in the life sciences: a primer on evidence* (Springer).

[43] Dumont CP, et al. (2013) Coral bioerosion by the sea urchin *Diadema setosum* in Hong Kong: Susceptibility

Table 1: Model Selection: k is the number of parameters in the model, -log($\mathcal{L}$) is the negative log likelihood of the model, AIC_c is the Akaike Information Criterion corrected, ΔAIC_c is the difference from the lowest AIC_c value, R^2 is the proportion of total variance explained by the model, and Rank is the rank of the model where 1 is the best fit.

[1]

Model Parameters	**k**	**-log($\mathcal{L}$)**	**AICc**	**ΔAIC**	**R^2**	**Rank**
(a) Model selection for bioerosion vs environmental parameters						
pH	4	-13.34	-18.97	0	0.54	1
$Y \sim \overline{pH} + Var(pH)$						
Depth & Distance	4	-6.34	-5.19	13.78	0.09	2
$Y \sim \overline{Depth} + Distance$						
Temperature	4	-6.11	-5.19	14.26	0.07	3
$Y \sim \overline{Temp} + Covar(Temp)$						
Resource Availability	6	-7.44	-0.60	18.38	0.21	4
$Y \sim \overline{Chl} + Var(Chl) + \overline{DIN : DIP} + Var(DIN : DIP)$						
Full	12	-18.61	17.79	36.76	0.79	5
$Y \sim \overline{pH} + Var(pH) + \overline{Temp} + Covar(Temp) + \overline{Chl} +$ $Var(Chl) + \overline{DIN : DIP} + Var(DIN : DIP) + \overline{Depth} +$ $Distance$						
(b) Model selection for secondary accretion vs environmental parameters						
Depth & Distance	4	-16.19	-24.89	0	0.23	1
pH	4	-15.00	-22.51	2.38	0.13	2
Temperature	4	-14.32	-21.15	3.74	0.07	3
Resource Availability	6	-14.13	-13.97	10.91	0.08	4
Full	12	-33.81	-12.62	12.26	0.90	5

[1] Each model is a linear regression of bioerosion versus the means ($\overline{X}$) and variances ($Var(X)$) or covariance ($Cov(X)$) of each parameter. The Resource Availability Model includes DIN:DIP and chlorophyll *a* concentration and the Full Model includes means and variances or covariance for all listed environmental parameters. Environmental data are the residuals from a regression between each parameter versus log(depth) and distance from shore. Secondary accretion and bioerosion rates were square-root transformed to meet model assumptions. The upper table is the model selection for bioerosion and the lower table is the model selection for accretion. The ranges for each environmental parameter are included in Silbiger et al. 2014 (4).

Figure Legends:

Figure 1: Environmental data. Means and variances for temperature anomalies (a-b), chlorophyll *a* (c-d), DIN:DIP (e-f), and pH_t (g-h) along the transect (N=21).

Figure 2: Schematic illustrating the μCT methods. 1. Experimental blocks were cut from dead *Porites lobata* skeleton and sent to the Cornell University Multiscale CT facility for Imaging and Preclinical Research for pre-deployment scans. Blocks were scanned at a resolution of 50 μm^3 and then averaged to 100 μm^3 for data analysis. 2. Pre-scanned blocks were deployed along the reef transect for one year, retrieved, and scanned a second time. 3. During data analysis a threshold of 200 Hounsfield Units (shown by the grey line) was set to remove edge effects and separate $CaCO_3$ fom air. Figure shows histograms for a pre-deployment block (green) and a post-deployment block (magenta). The inset shows the histograms of the blocks after thresholding. 4. Pre and post-deployment scans were aligned using image registration tools in MATLAB's Image Processing Toolbox. Images are pre and post-deployment scans overlayed on top of each other before (left) and after (right) image registration. 5. Images were converted to binary (white is a value of 1 and black is a value of 0) and subtracted from each other. All positive values (red) were new pixels and were counted as secondary accretion and all negative values (blue) were lost pixels and counted as bioerosion. Values of zero (green) correspond to areas where there were no changes between pre and post-deployment scans. 6. We calculated secondary accretion by summing all positive values and bioerosion by summing all negative values in the subtracted image. Images are 3D representations highlighting only secondary accretion (left) and bioerosion (right). See supplement for 3D movies of secondary accretion (Movie S1) and bioerosion (Movie S2). Image credits: N. Silbiger and M. Riccio.

Figure 3: pH versus bioerosion. Best fit model and 95 % confidence intervals for bioerosion (kg $CaCO_3$ m^{-2} yr^{-1}) of experimental blocks (N=20) versus mean pH residuals ($y = -22.45x + 0.55$, $R^2 = 0.54$). pH mean was regressed against log(depth) and distance from shore, and the residuals were used in the analysis and this figure. Bioerosion rate for each block was square-root transformed to meet model assumptions. Color represents depth (m) along the transect with blue representing blocks closest to shore and red representing blocks the farthest.

Figure 4: Depth and distance from shore versus secondary accretion. Best fit model and 95 % confidence intervals for secondary accretion (mm $CaCO_3$ yr^-1) of experimental blocks (N=20) versus a) distance from shore (m) ($y = 0.0055x + 0.29$, $R^2 = 0.23$) and b) log(depth) (m) ($y = 0.048x + 0.41$, $R^2 = 0.14$). Accretion rate for each block was square-root transformed to meet model assumptions.

Figure 5: Mean pH effect size for secondary accretion and bioerosion. The effect size was calculated as the absolute value of the slope for mean pH in each model.

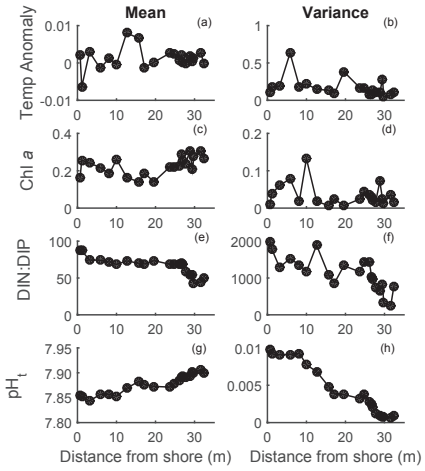
Mean
Variance
(a)
(b)
(c)
(d)
(e)
(f)
(g)
(h)
Temp Anomaly
Chl a
DIN:DIP
pH t
Distance from shore (m)
Distance from shore (m)

Figure 1

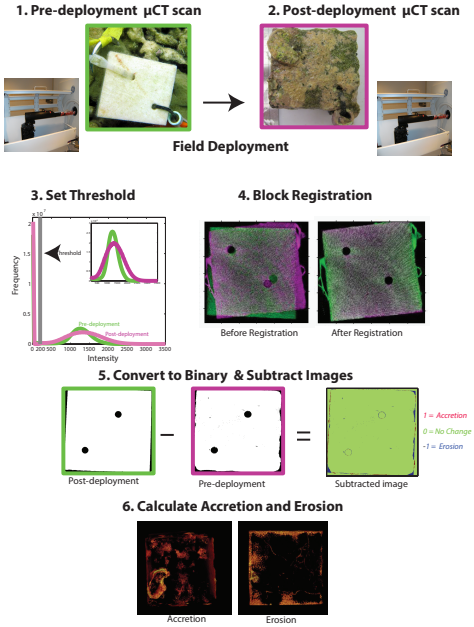
1. Pre-deployment µCT scan
2. Post-deployment µCT scan
Field Deployment
3. Set Threshold
Frequency
Intensity
Threshold
Pre-deployment
Post-deployment
4. Block Registration
Before Registration
After Registration
5. Convert to Binary & Subtract Images
Post-deployment
Pre-deployment
Subtracted image
1 = Accretion
0 = No Change
-1 = Erosion
6. Calculate Accretion and Erosion
Accretion
Erosion

Figure 2

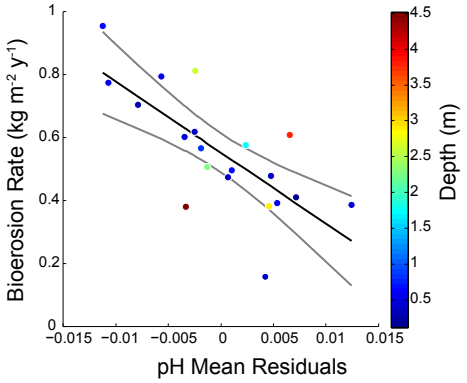
Bioerosion Rate (kg m-2 y-1)
pH Mean Residuals
Depth (m)
1
0.8
0.6
0.4
0.2
0
−0.015
−0.01
−0.005
0
0.005
0.01
0.015
4.5
4
3.5
3
2.5
2
1.5
1
0.5

Figure 3

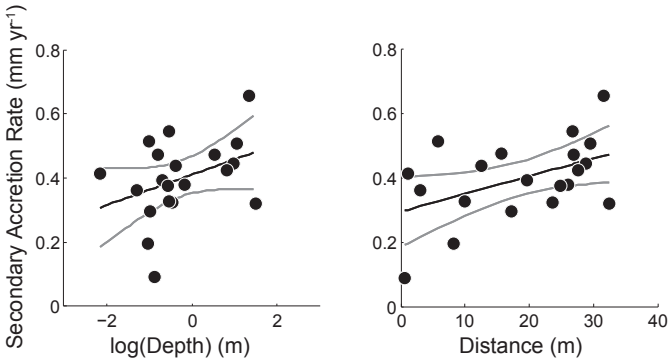
Secondary Accretion Rate (mm yr-1)
0.8
0.6
0.4
0.2
0
−2
0
2
log(Depth) (m)
0.8
0.6
0.4
0.2
0
0
10
20
30
40
Distance (m)

Figure 4

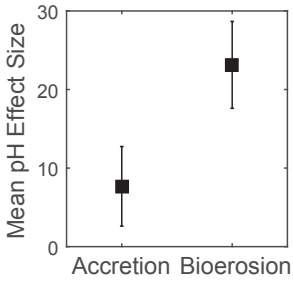

Figure 5

SUPPLEMENTAL MATERIAL

Tables S1-S2

Detailed Methods

Figures S1-S4

References from Supplemental Material

Movie S1 and S2

Table S1: Traditional Field Methods for bioerosion Measurements: A table highlighting different methods published in the primary literature, a short description of each method, benefits and constraints of each method, and selected publications

Method for measuring reef bioerosion	**Method Description**	**Benefits**	**Constraints**	**Publications**
Change in weight, height, volume, or density of experimental block	Deploy blocks of $CaCO_3$ on a reef for a set time and measure the difference in weight, height, volume, or density between the pre- and post-deployment blocks.	• Calculates an accurate rate because the block deployment time is known. • Erosion rate is inclusive of both internal and external eroders.	• Measures a net change in the block and confounds accretion and erosion processes. • Blocks need to be deployed for approx. 5 years to incude late succesional stage eroders.	(6, 8, 43–47)
Casts or Molds	Impregnate samples with epoxy resign and dissolve sample with dilute HCl. Results in 3D cast of bioerosion scars.	• Separates accretion and erosion. • Visualize boring scars in 3D	• Only estimate a bioerosion rate because the actual time when $CaCO_3$ becomes available is unknown.	(48–50)
X-ray and other 2-dimensional image analyses	Collect live coral cores or dead coral rubble, cut the sample into slabs, and take a picture, X-ray, or trace erosion scars onto a piece of paper.	• Separates accretion and erosion. • Using reef samples, as opposed to experimental blocks, likely includes an advanced succesional stage of eroders and calcifiers.	• Only estimates a bioerosion rate because the actual time when $CaCO_3$ becomes available is unknown. • Results may under- or over-estimate erosion rates depending on where the slab was cut.	(13–15, 32, 46, 51–70)
Count grazing scars by eroding fish	Track parrotfish, note when they remove $CaCO_3$ from the reef, and measure volume of grazing scar.	• Able to calculate grazing rates based on size or species of fish.	• Only accounts for parrotfish erosion.	(71–73)
Count bore holes along a reef transect	Count bore holes from bieoroding animals on the surface of live or dead coral *in situ*.	• Inexpensive and quick. • Includes counts of different types of macroeroders.	• Only accounts for macroborers large enough to make a hole that is visible without magnification. • Only estimates a bioerosion rate because the actual time when $CaCO_3$ becomes available to borers is unknown.	(16, 74, 75)

Scanning Electron Microscopy (SEM)	Millimeter sections of a sample are cut with a diamond blade saw, embedded with resin, etched with dilute HCl, and sometimes coated in platinum. Surface area bioeroded from each sample is quantified with 2D image analysis.	• Very high resolution images of microboring	• Only uses a very small sample for this analysis. • Only accounts for microerosion. • Results are highly dependent on where cuts are made.	(14, 48–52, 60, 76–79)
Single CT or μCT scan	Scan live or dead coral cores using a CT or μCT scanner.	• Separates accretion from erosion • Visualizes erosion scars in 3D • Calculates accretion from measuring coral annulae	• Only estimates a bioerosion rate because the actual time when $CaCO_3$ becomes available is unknown.	(3, 33, 80–83)
Before and after μCT scan	See methods section.	• High resolution 3D measure of both accretion and erosion. • Visualizes boring scars in 3D. • Using before and after scans allows for the removal of any pre-existing boring scars. • Calculates an accurate rate since deployment time is known.	• Blocks need to be deployed for a long period of time to quantify late succesional stage bioeroders. • Can be costly depending on resolution of scan	(4), Present Study

Table S2: Bioerosion Model Selection with all carbonate parameters: k is the number of parameters in the model, -log($\mathcal{L}$) is the negative log likelihood of the model, AIC_c is the Akaike Information Criterion corrected, ΔAIC_c is the difference from the lowest AIC_c value, R^2 is the proportion of total variance explained by the model, and Rank is the rank of the model with 1 representing the best fit. Each model is a linear regression of total bioerosion versus the means ($\overline{X}$) and variances ($Var(X)$) or covariance ($Cov(X)$) of each parameter. The Resource Availability Model includes DIN:DIP and chlorophyll *a* concentration and the Full Model includes means and variances or covariances for all listed environmental parameters. Environmental data are the residuals from a regression between each parameter versus log(depth) and distance from shore. Bioerosion rates were square-root transformed to meet model assumptions.The ranges for each environmental parameter are included in Silbiger et al. 2014.

	k	**-log($\mathcal{L}$)**	**AICc**	**ΔAIC**	**R^2**	**Rank**
pH	4.00	-13.24	-18.97	0.00	0.54	1
pCO_2	4.00	-12.02	-16.54	2.43	0.49	2
TA	4.00	-9.52	-11.55	7.43	0.34	3
DIC	4.00	-8.65	-9.79	9.18	0.28	4
Depth & Distance	4.00	-6.35	-5.19	13.78	0.09	5
Temperature	4.00	-6.11	-4.71	14.26	0.07	6
Resource Availability	6.00	7.44	-0.60	18.38	0.21	7
Full	18.00	-37.25	265.50	284.47	0.99	8

Detailed Methods:

***Study site*:** Our study site is located in Kāne‘ohe Bay, O‘ahu on the windward (eastern) side of Moku o Lo‘e (Coconut Island), adjacent to the Hawai‘i Institute of Marine Biology; N21°25.975', W157°47.175'). This fringing reef is dominated by *Porites compressa* and *Montipora capitata*, with occasional colonies of *Pocillopora damicornis, Fungia scutaria,* and *Porites lobata*. Kāne‘ohe Bay is a protected, semi-enclosed embayment; the residence time can be >1 month in the protected southern portion of Kāne‘ohe Bay, where our study was located (84). Wave action is low (31, 84, 85), and currents are slow (5cm s^{-1} maximum) and tidally driven (mean and maximum tidal ranges are 0.7 and 1.1m, respectively) (31, 84). Daily averages in pH, temperature, and O_2 in the Kāne‘ohe Bay waters just offshore our site ranged from 7.83 - 8.03, 21.84-27.86 °C, and 5.82-7.81 mg L^{-1}, respectively, during our study period (22).

Environmental Parameters:

The discrete water samples were collected directly above each block within two days of spring tide at 08:00, 14:00, 20:00, and 02:00 on September 10-11, 2011, December 12-13, 2011, and April 4-5, 2012. All discrete water samples were collected on snorkel or SCUBA using 60 and 120ml plastic syringes. Syringes and storage vials were all pre-cleaned in a 10% HCl bath for 24 hours and rinsed three times with MilliQ water; during sample collection and processing syringes were rinsed three times with sample water. The environment was sampled more continuously for temperature and depth (sampling rate of ~ 0.1 min^{-1}) using one permanent and two mobile monitoring stations. Two mobile stations were deployed at a time, one on the reef flat and one on the reef slope, to get simultaneous measurements at two different blocks on the transect. Mobile stations (Sonde 600XLM, YSI Incorporated) were positioned 5 - 10cm above each block for a two-week period between May 2011 and March 2012. Blocks were sampled in random order, ensuring that the spatial gradient along the transect was not systematically confounded by temporal trends or seasonality (22). The permanent monitoring station (Sonde 6600-V2-4, YSI) was mounted to a pole a few meters away from the transect, downward facing at 1.7m depth over a 3m deep bottom, with sensors for temperature, depth, conductivity, pH, and O_2 to characterize the background water column conditions for the duration of the experiment. All multi-parametric probes were calibrated periodically using standard procedures and calibration solutions. The permanent station was recovered, cleaned, calibrated, and re-deployed 3 times during the study, and the mobile station probes were calibrated 7 times. Pre-calibration measurements of commercial standard solutions were conducted to detect sensor drift, although none was found for the period of study. Environmental data from the transect are reported in Silbiger et al. (2014)(4) and background water column data are reported in Guadayol et al. (2014) (22).

Nutrients and Chlorophyll: Water samples collected for nutrients were immediately filtered through combusted 25 mm diameter glass fiber filters (GF/F 0.2 µm) and transferred into 50 ml plastic centrifuge tubes. Nutrient samples were frozen and later analyzed for NO_3^-, NO_2^-, NH_4^+, and PO_4^{3-} on a Seal Analytical AA3 HR Nutrient Analyzer at the UH SOEST Laboratory for Analytical Chemistry. GF/F filters were folded in half, wrapped

in aluminum foil, and frozen for chlorophyll *a* analysis using a Turner Designs 10AU Benchtop Fluorometer. The ratio of dissolved inorganic nitrogen to dissolved inorganic phosphate (DIN:DIP) was used as a proxy for resource quality available to filter feeders (86), assuming that elemental composition of planktonic prey will be influenced by elemental composition of the water column, and was calculated from ($[NO_3^-]$ + $[NO_2^-]$ + $[NH_4^+]$):$[PO_4^{3-}]$) .

pH and TA: Mean and variance in pH at each block was calculated from water samples along the transect. Water samples for pH were immediately transferred into 25 ml borosilicate glass vials, brought to a constant temperature of 25°C in a water bath, and immediately analyzed using an m-cresol dye addition spectrophotometric technique and calibrated against a Tris buffer of known pH from the Dickson Laboratory at Scripps Institution of Oceanography. TA was fixed with 100 μL of $HgCl_2$ and analyzed using open cell potentiometric titrations on a Mettler T50 autotitrator and calibrated against a Certified Reference Material following Dickson et al. (2007) (87) protocols. *In situ* pH and all other carbonate parameters were estimated using CO2SYS (88) with the following parameters: pH_t, TA, temperature, and salinity. The K1K2 dissociation constants were from Mehrbach (1973) (89) (refit by Dickson and Millero (1987) (90)) and HSO_4^- dissociation constants were taken from Uppstrom (1974) (91) and Dickson (1990) (92). Accuracy for TA and pH was better than 0.8% and 0.04%, respectively, and the precision was 3.55 µEq and 0.004 pH units.

Temperature: Temperature sensors (YSI 6560) were thermistors with manufacturer-reported accuracy of ±0.15°C and resolution of 0.01°C (YSI Incorporated 2011). Average differences in temperature along the transect were small and measured as a relative anomaly from the permanent station: $((\bar{x}_{mobile} - \bar{x}_{permanent})/\bar{x}_{permanent})$. To measure relative variability in temperature across the transect, we calculated the covariance in temperature between the mobile and permanent sensor arrays over a two-week period and compared this covariance across the transect.

Depth and Distance from Shore: Depth is the average depth measured at each block over the two week deployment of the mobile station. Distance from shore is the along-transect distance.

Turbulent Kinetic Energy Dissipation Rate (ϵ): Acoustic doppler velocimeters (Vectrino Field, Nortek A.S.) were deployed 5-10 cm above the blocks along with the multiparametric sondes measuring temperature and depth at 11 of the 21 stations. Unfortunately one of the velocimeters broke during deployment, and flow data could not be acquired for the rest of the stations and therefore was not included in the model selection. However, given the tight correlation between ϵ and distance from shore ($R^2 = 0.88$), distance from shore was used as a proxy for the hydrodynamic gradient.

Spikes were removed following a 3D phase-space thresholding technique (93, 94) in the beam coordinates. Values with correlations <60 were also removed (95). Gaps were linearly interpolated when shorter than 10 measurements. Empirical orthogonal functions (EOF) were used to align coordinates to streamwise/cross-stream axes for the entire sampling period

Turbulent kinetic energy dissipation rates (ϵ; $m^2 s^{-3}$) for each segment were estimated from the spectra using

the inertial subrange dissipation method (96). Briefly, data was partitioned in 10 minutes intervals, the same sampling period as the multiparameter sonde measuring temperature and depth. For each segment, data was further partitioned into 180 second segments of uninterrupted data, from which the fast fourier transforms were obtained. A smoothed spectra was generated by averaging all the raw spectra. The inertial subrange was identified in the log transformed spectra as the segment that best fit a -5/3 model, with a minimum coefficient of determination (R^2) of 0.75, and encompassing at least one order of magnitude of frequencies. Fits were evaluated using F statistics and R^2. To account for the effect of advection by current and waves on the turbulent spectra, we used a generalized frozen turbulence model (97). All calculations were done using MATLAB.

μCT: We used an eXplore CT120 μCT (GE Healthcare Xradia, Inc) at the Cornell University Imaging Multi-scale CT Facility (Figure 2.1,1.2) to scan blocks before and after deployment (voltage = 100kV, current = 50mA). Angular projections were acquired in a full 360° rotation in 0.5° increments; two images at each angle were acquired and averaged creating a three-dimensional array of isotropic voxels at 50 μm^3 which was then averaged to 100 μm^3. Pre- and post-deployment scans were aligned, or registered, using an intensity-based image registration algorithm from the MATLAB ®Image Processing Toolbox. Mattes Mutual Information metric maximizes the number of corresponding pixels with similar intensity values (98) which was used to describe the accuracy of the registration. We used the One Plus One Evolutionary Optimizer, an iterative algorithm that maximizes the best registration results by perturbing the parameters between iterations (99), as our optimization technique. A global threshold value was set at an intensity value of 200 to separate $CaCO_3$ from air and remove any effects of partial volume averaging at the coral block-air interface (4). Intensity values are directly correlated with skeletal density at each pixel. The number of voxels exceeding this threshold was used in calculating secondary accretion and bioerosion. After the images were registered, both pre- and post-deployment scans were converted to binary, such that any positive intensity value (a pixel with $CaCO_3$) was assigned a one and all other values (air) were assigned a zero. The two images were then subtracted from one another giving a matrix of 1's, 0's, and -1's. I n the subtracted matrix, all pixels with a value of one represented areas of new $CaCO_3$ (accretion) and all values of negative one were areas where $CaCO_3$ was removed (bioerosion). A value of zero meant there was no change at that pixel between the before and after scans. Converting images to binary is the most conservative way to calculate secondary accretion and bioerosion; it does not account for any change in skeletal density, but rather an absolute loss of $CaCO_3$. Subtracting the two raw images, without converting to binary, would potentially over-estimate secondary accretion and bioerosion due to partial volume averaging of surrounding pixels or a change in skeletal density due to chemical dissolution. To calculate secondary accretion and bioerosion rates, all positive and negative values were summed in the subtracted matrix and multiplied by the voxel size (100 $\mu m)^3$ to give the total volume of $CaCO_3$ gained or lost, respectively. These values were then normalized to the surface area of the pre-deployment block and multiplied by the skeletal density and are expressed as kg $CaCO_3$ m^{-2} yr^{-1} for bioerosion and mm $CaCO_3$ yr^{-1} for secondary accretion. Bulk skeletal density of pre-deployment blocks was calculated using the

buoyant weight technique. Surface area was calculated following methods by Legland et al. 2011(100). Note that this volumetric analysis measures changes at the voxel scale of 100 μm^3, and, therefore, may underestimate bioerosion by microborers, which make erosion scars between 1 and 100 μm (76).

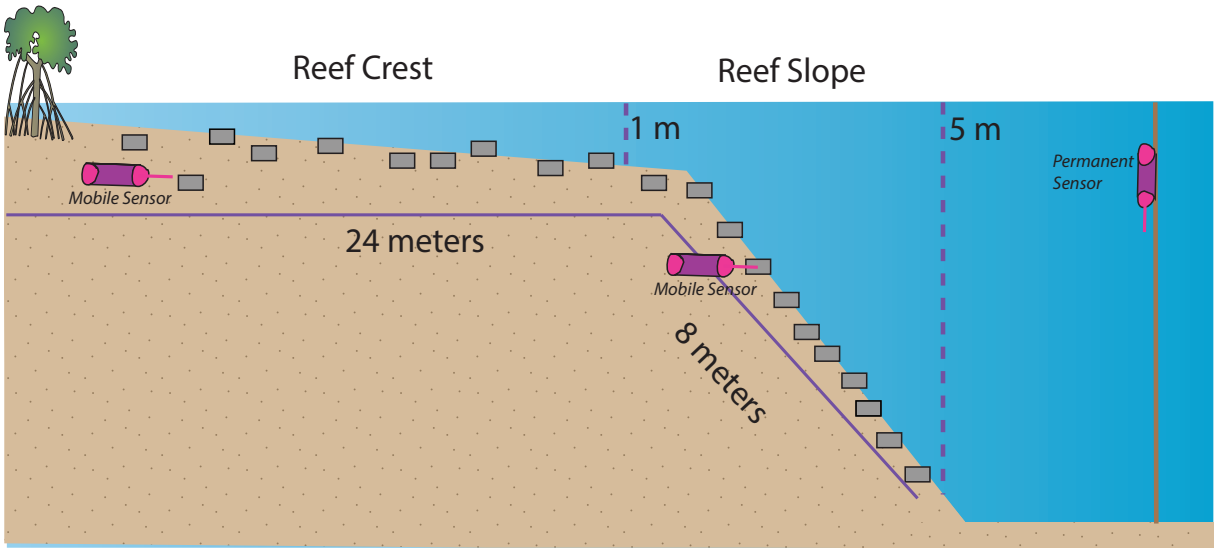

Figure S1: Schematic of reef transect. Experimental blocks (grey rectangles) were stratified between reef flat and reef slope along a 32 m transect and were deployed for one year. The depth ranged from 0.5 to 4.5 m. Discrete environmental samples were collected directly above each experimental block. Continuous sensors were stationed over each block for a minimum of two weeks (mobile sensors) and were normalized to a continuous time series from a permanent sensor station (Permanent sensors).

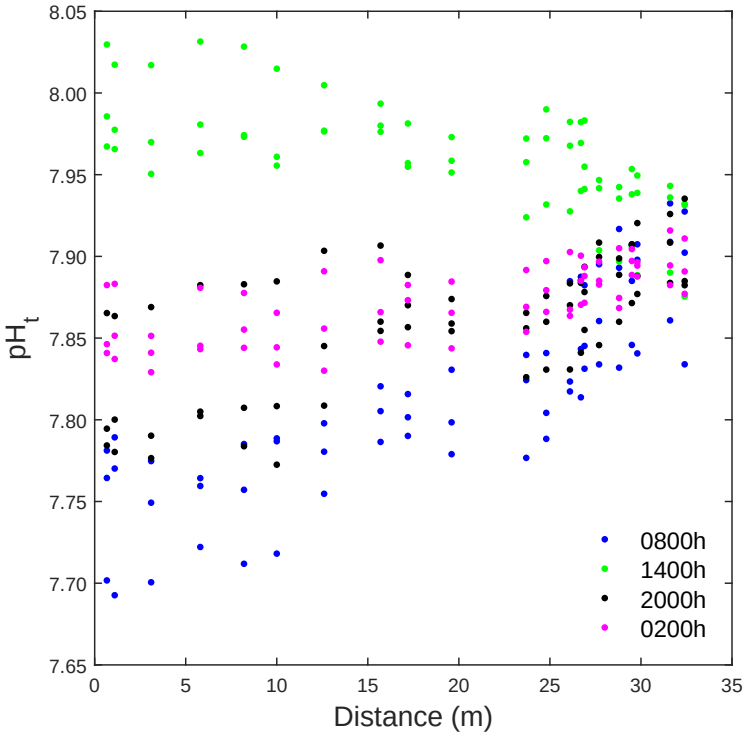

Figure S2: All discrete pH samples from September, December, and April sampling periods across the transect. Each dot is one sample and there are 12 samples per each of the 21 blocks. The colors represent collection times where blue, green, black, and magenta represent 0800h, 1400h, 2000h, and 0200h.

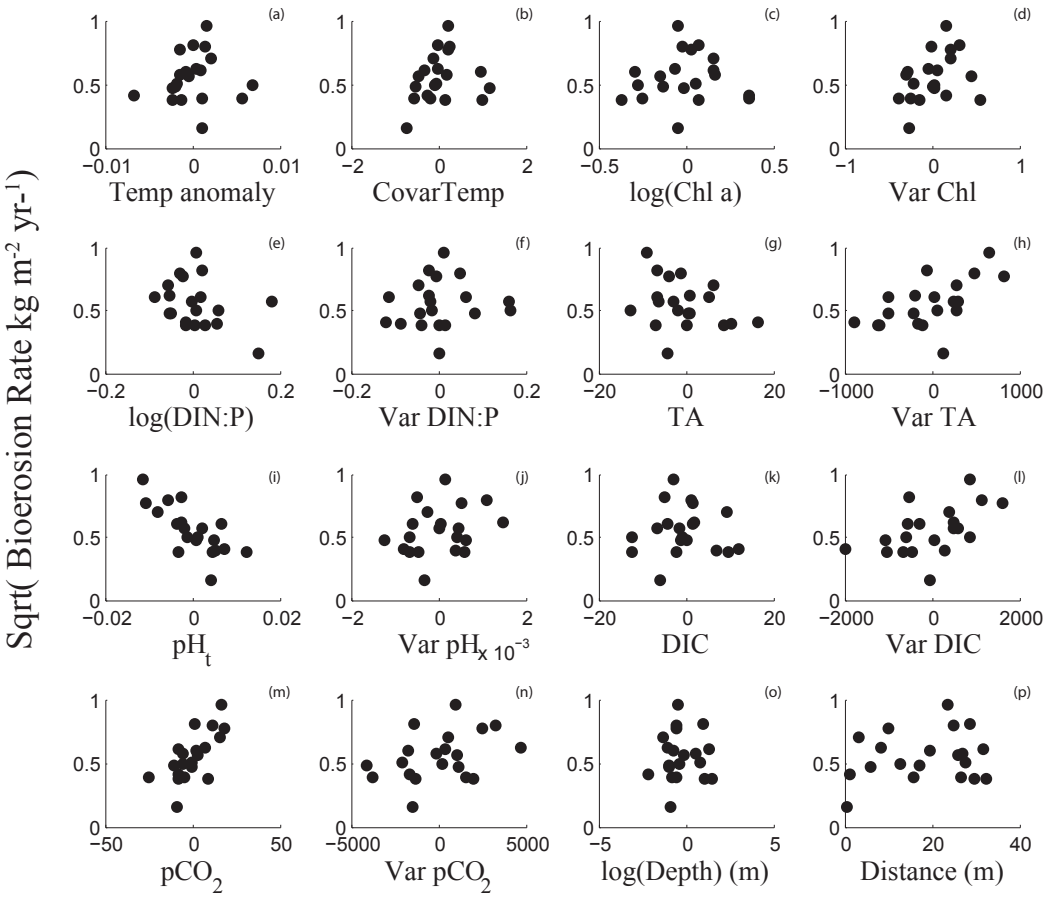

Figure S3: Bioerosion versus the means and variances of all environmental parameters. Environmental parameters were regressed against log(depth) and distance from shore and the residuals from those regressions are used in this figure.

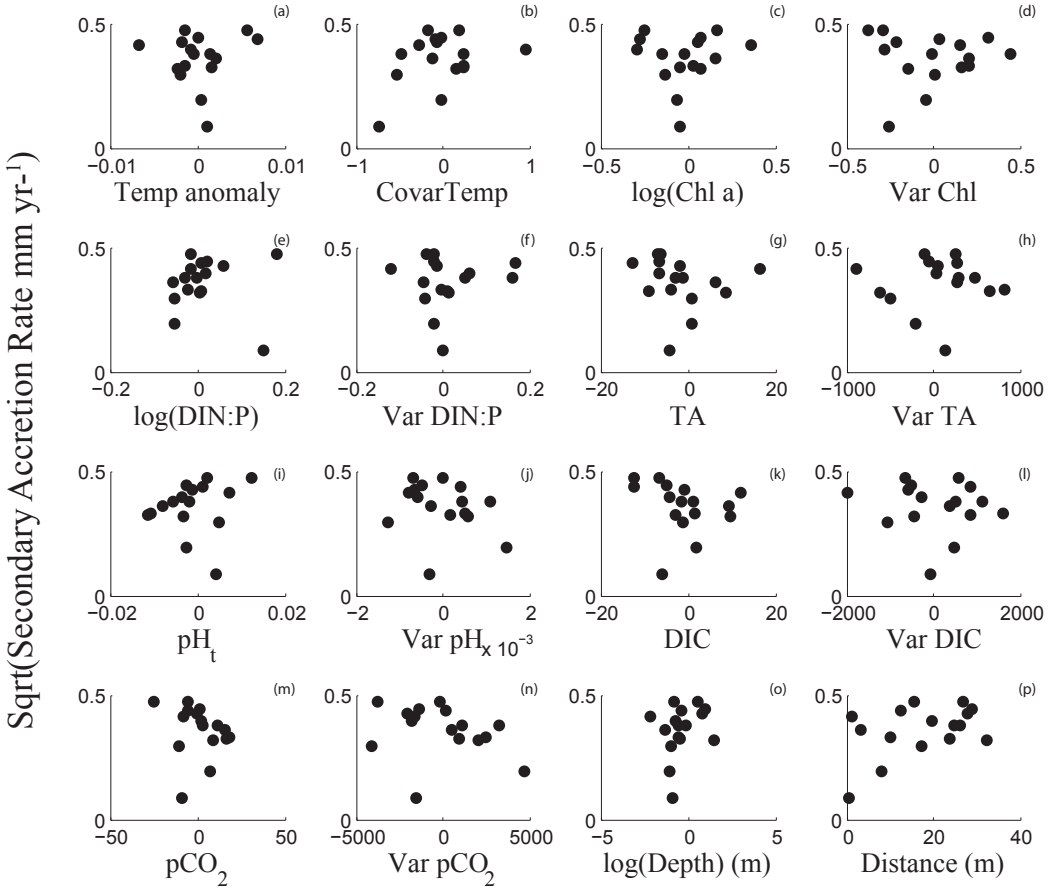

Figure S4: Secondary accretion versus the means and variances of all environmental parameters. Environmental parameters were regressed against log(depth) and distance from shore and the residuals from those regressions are used in this figure.

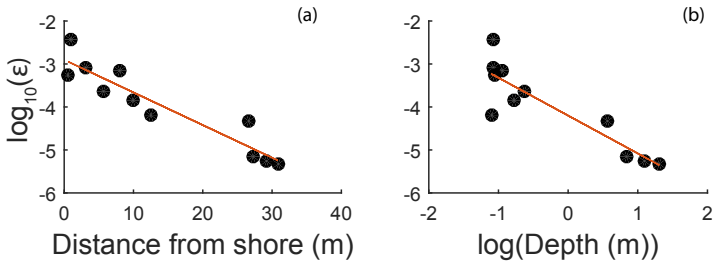

Figure S5: Turbulent kinetic energy dissipation rate (ϵ) ($m^2 s^{-3}$) versus (a) distance from shore (b) and depth (n=11). Turbulence was measured at 11 of the 21 sites and there was a significant relationship between ϵ and distance from shore ($F_{11,9} = 63.1$, p<0.0001, R^2=0.88) and depth ($F_{11,9} = 35.0$, p=0.0002, R^2=0.80).

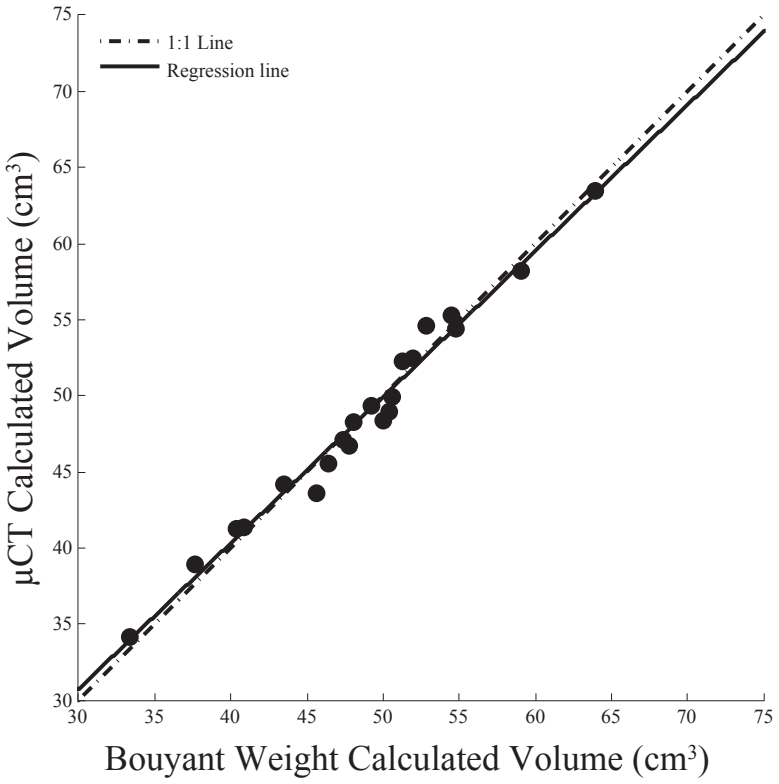

Figure S6: Comparison of calculated volumes (cm^3) using the buoyant weight and μCT methods described in this paper. Black circles are volumes calculated from the pre-deployment experimental blocks. We used a linear regression to test the relationship between the buoyant weight and μCT methods. The pre-deployment volumes calculated from each method are highly co-linear (F_{19} = 859, p<0.001, R = 0.98,$y = 0.96x + 1.9$)

Movie Legends

MovieS1: 3D visualization of μCT scan highlighting secondary accretion onto a block.

MovieS2: 3D visualization of μCT scan highlighting bioerosion from a block.

Full Reference List

References

[1] Hoegh-Guldberg O, et al. (2007) Coral reefs under rapid climate change and ocean acidification. *Science* 318:1737–1742.

[2] Andersson A, Gledhill D (2013) Ocean acidification and coral reefs: effects on breakdown, dissolution, and net ecosystem calcification. *Ann Rev of Mar Sci* 5:321–348.

[3] DeCarlo TM, et al. (2014) Coral macrobioerosion is accelerated by ocean acidification and nutrients. *Geology* pp G36147–1.

[4] Silbiger NJ, Guadayol Ò, Thomas FI, Donahue MJ (2014) Reefs shift from net accretion to net erosion along a natural environmental gradient. *Marine Ecology Progress Series* 515:33–44.

[5] Silbiger N, Donahue M (2015) Secondary calcification and dissolution respond differently to future ocean conditions. *Biogeosciences* 12:567–578.

[6] Wisshak M, Schönberg CH, Form A, Freiwald A (2012) Ocean acidification accelerates reef bioerosio. *Plos One* 7:e45124.

[7] Tribollet A, Godinot C, Atkinson M, Langdon C (2009) Effects of elevated pCO_2 on dissolution of coral carbonates by microbial euendoliths. *Global Biogeochem Cycles* 23:GB3008.

[8] Reyes-Nivia C, Diaz-Pulido G, Kline D, Guldberg OH, Dove S (2013) Ocean acidification and warming scenarios increase microbioerosion of coral skeletons. *Glob Change Biol* 19:1919–1929.

[9] Fang JK, et al. (2013) Sponge biomass and bioerosion rates increase under ocean warming and acidification. *Glob Change Biol* 19:3581–3591.

[10] Davidson TM, de Rivera CE, Carlton JT (2013) Small increases in temperature exacerbate the erosive effects of a non-native burrowing crustacean. *J Exp Mar Biol Ecol* 446:115 – 121.

[11] Fabricius KE (2005) Effects of terrestrial runoff on the ecology of corals and coral reefs: review and synthesis. *Marine pollution bulletin* 50:125–146.

[12] Risk MJ, Sammarco PW, Edinger EN (1995) Bioerosion in *Acropora* across the continental-shelf of the Great Barrier Reef. *Coral Reefs* 14:79–86.

[13] Holmes KE, Edinger EN, Hariyadi, Limmon GV, Risk MJ (2000) Bioerosion of live massive corals and branching coral rubble on Indonesian coral reefs. *Mar. Pollut. Bull.* 40:606–617.

[14] Tribollet A, Golubic S (2005) Cross-shelf differences in the pattern and pace of bioerosion of experimental carbonate substrates exposed for 3 years on the northern Great Barrier Reef, Australia. *Coral Reefs* 24:422–434.

[15] Edinger EN, et al. (2000) Normal coral growth rates on dying reefs: Are coral growth rates good indicators of reef health? *Mar. Pollut. Bull.* 40:404–425.

[16] Le Grand HM, Fabricius KE (2011) Relationship of internal macrobioeroder densities in living massive *Porites* to turbidity and chlorophyll on the Australian Great Barrier Reef. *Coral Reefs* 30:97–107.

[17] Pandolfi JM, Connolly SR, Marshall DJ, Cohen AL (2011) Projecting coral reef futures under global warming and ocean acidification. *Science* 333:418–422.

[18] Silverman J, Lazar B, Cao L, Caldeira K, Erez J (2009) Coral reefs may start dissolving when atmospheric CO_2 doubles. *Geophys. Res. Lett.* 36:L05606.

[19] Przeslawski R, Ahyong S, Byrne M, Woerheide G, Hutchings P (2008) Beyond corals and fish: the effects of climate change on noncoral benthic invertebrates of tropical reefs. *Global Change Biology* 14:2773–2795.

[20] Comeau S, Edmunds P, Spindel N, Carpenter R (2013) The responses of eight coral reef calcifiers to increasing partial pressure of co2 do not exhibit a tipping point. *Limnol. Oceanogr* 58:388–398.

[21] Castillo KD, Ries JB, Bruno JF, Westfield IT (2014) The reef-building coral siderastrea siderea exhibits parabolic responses to ocean acidification and warming. *Proceedings of the Royal Society B: Biological Sciences* 281:20141856.

[22] Guadayol Ò, Silbiger NJ, Donahue MJ, Thomas FI (2014) Patterns in temporal variability of temperature, oxygen and pH along an environmental gradient in a coral reef. *Plos One* 9:e85213.

[23] Hofmann G, et al. (2011) High-frequency dynamics of ocean pH: A multi-ecosystem comparison. *Plos One* 6:e28983.

[24] Rivest EB, Gouhier TC (2015) Complex environmental forcing across the biogeographical range of coral populations. *PloS one* 10:e0121742.

[25] Shamberger KE, et al. (2014) Diverse coral communities in naturally acidified waters of a western pacific reef. *Geophysical Research Letters* 41:499–504.

[26] Yates KK, Dufore C, Smiley N, Jackson C, Halley RB (2007) Diurnal variation of oxygen and carbonate system parameters in Tampa Bay and Florida Bay. *Mar Chem* 104:110–124.

[27] Drupp P, De Carlo EH, Mackenzie FT, Bienfang P, Sabine CL (2011) Nutrient inputs, phytoplankton response, and CO_2 variations in a semi-enclosed subtropical embayment, Kaneohe Bay, Hawaii. *Aquat Geochem* 17:473–498.

[28] Massaro RF, et al. (2012) Multiple factors driving variability of CO_2 exchange between the ocean and atmosphere in a tropical coral reef environment. *Aquat Geochem* 18:357–386.

[29] Duarte CM, et al. (2013) Is ocean acidification an open-ocean syndrome? Understanding anthropogenic impacts on seawater pH,. *Estuaries and Coasts* 36:1–16.

[30] Smith JE, Price NN, Nelson CE, Haas AF (2013) Coupled changes in oxygen concentration and pH caused by metabolism of benthic coral reef organisms. *Mar Biol* 160:1–11.

[31] Lowe RJ, Falter JL, Monismith SG, Atkinson MJ (2009) Wave-driven circulation of a coastal reef-lagoon system. *J. Phys. Oceanogr.* 39:873–893.

[32] Manzello DP, et al. (2008) Poorly cemented coral reefs of the eastern tropical Pacific: Possible insights into reef development in a high-CO_2 world. *Proc. Natl. Acad. Sci. U. S. A.* 105:10450–10455.

[33] Crook ED, Cohen AL, Rebolledo-Vieyra M, Hernandez L, Paytan A (2013) Reduced calcification and lack of acclimatization by coral colonies growing in areas of persistent natural acidification. *Proc Natl Acad Sci U S A* 110:11044–11049.

[34] Tribollet A, Langdon C, Golubic S, Atkinson M (2006) Endolithic microflora are major primary producers in dead carbonate substrates of Hawaiian Coral Reefs. *Journal of Phycology* 42:292–303.

[35] Nowell A, Jumars P (1984) Flow environments of aquatic benthos. *Annual review of ecology and systematics* pp 303–328.

[36] Butman CA, Geyer WR (1989) The importance of boundary-layer flows in supplying phytoplankton to the benthic suspension feeder, *Mytilus edulis* l. *Limnol. Oceanogr* 34:19–36.

[37] Abelson A, Denny M (1997) Settlement of marine organisms in flow. *Annual Review of Ecology and Systematics* pp 317–339.

[38] Smith S (1984) Phosphorus versus nitrogen limitation in the marine environment. *Limnology and Oceanography* 29:1149–1160.

[39] Rodolfo-Metalpa R, et al. (2011) Coral and mollusc resistance to ocean acidification adversely affected by warming. *Nature Climate Change* 1:308–312.

[40] Erez J, Reynaud S, Silverman J, Schneider K, Allemand D (2011) in *Coral reefs: an ecosystem in transition* (Springer), pp 151–176.

[41] Johnson JB, Omland KS (2004) Model selection in ecology and evolution. *Trends Ecol Evol* 19:101–108.

[42] Anderson DR (2008) *Model based inference in the life sciences: a primer on evidence* (Springer).

[43] Dumont CP, et al. (2013) Coral bioerosion by the sea urchin *Diadema setosum* in Hong Kong: Susceptibility of different coral species. *J. Exp. Mar. Biol. Ecol.* 441:71 – 79.

[44] Londoño-Cruz E, Cantera JR, Toro-Farmer G, Orozco C (2003) Internal bioerosion by macroborers in pocillopora spp. in the tropical eastern pacific. *Marine ecology. Progress series* 265:289–295.

[45] Márquez JC, Zea S (2012) Parrotfish mediation in coral mortality and bioerosion by the encrusting, excavating sponge cliona tenuis. *Marine Ecology* 33:417–426.

[46] Reaka-Kudla M, Feingold J, Glynn W (1996) Experimental studies of rapid bioerosion of coral reefs in the galapagos islands. *Coral Reefs* 15:101–107.

[47] Rützler K (1975) The role of burrowing sponges in bioerosion. *Oecologia* 19:203–216.

[48] Carreiro-Silva M, McClanahan T, Kiene W (2009) Effects of inorganic nutrients and organic matter on microbial euendolithic community composition and microbioerosion rates. *Marine Ecology Progress Series*.

[49] Carreiro-Silva M, McClanahan T, Kiene W (2005) The role of inorganic nutrients and herbivory in controlling microbioerosion of carbonate substratum. *Coral Reefs* 24:214–221.

[50] Golubic SS, Brent G, Lecampion T (1970) Scanning electron microscopy of endolithic algae and fungi using a multipurpose casting-embedding technique. *Lethaia* 3:203–209.

[51] Chazottes V, Campion-Alsumard TL, Peyrot-Clausade M (1995) Bioerosion rates on coral reefs: interactions between macroborers, microborers and grazers (moorea, french polynesia). *Palaeogeography, Palaeoclimatology, Palaeoecology* 113:189–198.

[52] Chazottes V, Le Campion-Alsumard T, Peyrot-Clausade M, Cuet P (2002) The effects of eutrophication-related alterations to coral reef communities on agents and rates of bioerosion (reunion island, indian ocean). *Coral Reefs* 21:375–390.

[53] Harney JN, Fletcher CH (2003) A budget of carbonate framework and sediment production, kailua bay, oahu, hawaii. *Journal of Sedimentary Research* 73:856–868.

[54] Hernández-Ballesteros LM, Elizalde-Rendón EM, Carballo JL, Carricart-Ganivet JP (2013) Sponge bioerosion on reef-building corals: Dependent on the environment or on skeletal density? *J of Exp Mar Biol Ecol* 441:23–27.

[55] Highsmith RC (1981) Coral bioerosion - damage relative to skeletal density. *Am Nat* 117:193–198.

[56] Moran DP, Reaka ML (1988) Bioerosion and availability of shelter for benthic reef organisms. *Mar Ecol Progr Ser* 44:249–263.

[57] Perry CT (1998) Macroborers within coral framework at Discovery Bay, north Jamaica: species distribution and abundance, and effects on coral preservation. *Coral Reefs* 17:277–287.

[58] Rose CS, Risk MJ (1985) Increase in *Cliona delitrix* infestation of *Montastrea cavernosa* heads on an organically polluted portion of the Grand Cayman fringing-reef. *Marine Ecology-Pubblicazioni Della Stazione Zoologica Di Napoli I* 6:345–363.

[59] Scott PJB, Risk MJ (1988) The effect of *Lithophaga (Bivalvia, Mytilidae)* boreholes on the strength of the coral *Porites lobata*. *Coral Reefs* 7:145–151.

[60] Tribollet A, Decherf G, Hutchings PA, Peyrot-Clausade M (2002) Large-scale spatial variability in bioerosion of experimental coral substrates on the Great Barrier Reef (Australia): importance of microborers. *Coral Reefs* 21:424–432.

[61] Hein FJ, Risk MJ (1975) Bioerosion of coral heads: inner patch reefs, florida reef tract. *Bulletin of Marine Science* 25:133–138.

[62] Highsmith RC (1981) Coral bioerosion at enewetak: agents and dynamics. *Internationale Revue der gesamten Hydrobiologie und Hydrographie* 66:335–375.

[63] Hutchings P, Peyrot-Clausade M, Osnorno A (2005) Influence of land runoff on rates and agents of bioerosion of coral substrates. *Marine pollution bulletin* 51:438–447.

[64] Nava H, Carballo JL (2008) Chemical and mechanical bioerosion of boring sponges from mexican pacific coral reefs. *Journal of Experimental Biology* 211:2827–2831.

[65] Pari N, Peyrot-Clausade M, Hutchings PA (2002) Bioerosion of experimental substrates on high islands and atoll lagoons (french polynesia) during 5 years of exposure. *Journal of Experimental Marine Biology and Ecology* 276:109–127.

[66] Risk M, Sammarco P, Edinger E (1995) Bioerosion in acropora across the continental shelf of the great barrier reef. *Coral reefs* 14:79–86.

[67] Sammarco PP, Risk MM, et al. (1990) Large-scale patterns in internal bioerosion of *Porites*: cross continental shelf trends on the gbr. *Marine Ecology Progress Series-pages: 59: 145-156*.

[68] MacGeachy J (1977) *Factors controlling sponge boring in Barbados reef corals* Vol. 2, pp 477–483.

[69] Sammarco PW, Risk MJ, Rose C (1987) Effects of grazing and damselfish territoriality on internal bioerosion of dead corals: indirect effects. *Journal of Experimental Marine Biology and Ecology* 112:185–199.

[70] Peyrot-Clausade M, et al. (1999) Bioerosion in the carbonate budget of two indo-pacific reefs: La reunion (indian ocean) and moorea (pacific ocean). *gen* 1999:01–30.

[71] Alwany MA, Thaler E, Stachowitsch M (2009) Parrotfish bioerosion on egyptian red sea reefs. *Journal of Experimental Marine Biology and Ecology* 371:170–176.

[72] Bellwood D (1995) A direct estimate of bioerosion by two parrotfish species *Chlorurus gibbus* and *Chlorurus sordidus* on the great barrier reef, australia. *Marine Biology* 121:419–429.

[73] Ong L, Holland KN (2010) Bioerosion of coral reefs by two hawaiian parrotfishes: species, size differences and fishery implications. *Marine biology* 157:1313–1323.

[74] Kiene W, Hutchings P (1994) Bioerosion experiments at lizard island, great barrier reef. *Coral reefs* 13:91–98.

[75] Edinger EN, RISK MJ (1996) Sponge borehole size as a relative measure of bioerosion and paleoproductivity. *Lethaia* 29:275–286.

[76] Tribollet A (2008) *Current Developments in Bioerosion*, ed Max Wisshak LT (Springer-Verlag Berlin Heudelberg), pp 67–94.

[77] Godinot C, Tribollet A, Grover R, Ferrier-Pagès C (2012) Bioerosion by euendoliths decreases in phosphate-enriched skeletons of living corals. *Biogeosciences Discussions* 9:2425–2444.

[78] Le Campion-Alsumard T, Golubic S, Hutchings P (1995) Microbial endoliths in skeletons of live and dead corals: Porites lobata (moorea, french polynesia). *Oceanographic Literature Review* 42.

[79] Zubia M, Peyrot-Clausade M (2001) Internal bioerosion of *Acropora formosa* in réunion (indian ocean): microborer and macroborer activities. *Oceanologica Acta* 24:251–262.

[80] Becker L, Reaka-Kudla M (1996) *The use of tomography in assessing bioerosion in corals* Vol. 2, pp 1819–1824.

[81] Hassan M, Dullo W, Fink A (1997) *Assessment of boring activity in Porites lutea from Aqaba (Red Sea) using computed tomography* Vol. 2, pp 1813–1818.

[82] Beuck L, Vertino A, Stepina E, Karolczak M, Pfannkuche O (2007) Skeletal response of *Lophelia pertusa* (scleractinia) to bioeroding sponge infestation visualised with micro-computed tomography. *Facies* 53:157–176.

[83] Schönberg CH, Shields G (2008) in *Current Developments in Bioerosion* (Springer), pp 147–164.

[84] Lowe RJ, Falter JL, Monismith SG, Atkinson MJ (2009) A numerical study of circulation in a coastal reef-lagoon system. *J. Geophys. Res.* 114:C06022.

[85] Smith SV, Kimmerer WJ, Laws EA, Brock RE, Walsh TW (1981) Kaneohe Bay sewage diversion experiment- perspectives on ecosystem responses to nutritional perturbation. *Pac. Sci.* 35:279–402.

[86] Hauss H, Franz J, Sommer U (2012) Changes in N: P stoichiometry influence taxonomic composition and nutritional quality of phytoplankton in the Peruvian upwelling. *J Sea Res* 73:74–85.

[87] Dickson A, Sabine C, Christian JR (2007) *Guide to Best Practices for Ocean CO_2 Measurements.* eds Dickson A, Sabine C, Christian JR (PICES Special Publication 3).

[88] van Heuven S, Pierrot D, Rae J, Lewis E, Wallace D (2011) *MATLAB Program Developed for CO2 System Calculations. ORNL/CDIAC-105b.* (Carbon Dioxide Information Analysis Center, Oak Ridge National Laboratory, U.S. Department of Energy, Oak Ridge, Tennessee.).

[89] Mehrbach C (1973) Measurement of the apparent dissociation constants of carbonic acid in seawater at atmospheric pressure. *Limnol. Oceanogr.* 18:897–907.

[90] Dickson A, Millero F (1987) A comparison of the equilibrium constants for the dissociation of carbonic acid in seawater media. *Deep Sea Research Part A. Oceanographic Research Papers* 34:1733–1743.

[91] Uppström LR (1974) *The boron/chlorinity ratio of deep-sea water from the Pacific Ocean* Vol. 21, pp 161–162.

[92] Dickson AG (1990) Standard potential of the reaction:$AgCl(s) + 12H2(g) = Ag(s) + HCl(aq)$, and and the standard acidity constant of the ion HSO_4^- in synthetic sea water from 273.15 to 318.15 k. *The Journal of Chemical Thermodynamics* 22:113–127.

[93] Goring DG, Nikora VI (2002) Despiking acoustic doppler velocimeter data. *Journal of Hydraulic Engineering* 128:117–126.

[94] Wahl TL (2003) Discussion of "despiking acoustic doppler velocimeter data" by derek g. goring and vladimir i. nikora. *Journal of Hydraulic Engineering* 129:484–487.

[95] McLelland SJ, Nicholas AP (2000) A new method for evaluating errors in high-frequency adv measurements. *Hydrological Processes* 14:351–366.

[96] Bluteau CE, Jones NL, Ivey GN (2011) Estimating turbulent kinetic energy dissipation using the inertial subrange method in environmental flows. *Limnology and Oceanography: Methods* 9:302–321.

[97] Lumley J, Terray E (1983) Kinematics of turbulence convected by a random wave field. *Journal of Physical Oceanography* 13:2000–2007.

[98] Mattes D, Haynor D, Vesselle H, Lewellen TK, W E (2001) Non-rigid multimodality image registration. *Medical Imaging 2001: Image Processing* pp 1609–1620.

[99] Styner M, Brechbuhler C, Szckely G, Gerig G (2000) Parametric estimate of intensity inhomogeneities applied to mri. *Medical Imaging, IEEE Transactions on* 19:153–165.

[100] Legland D, Kiêu K, Devaux MF (2011) Computation of minkowski measures on 2d and 3d binary images. *Image Analysis & Stereology* 26:83–92.

CHAPTER 4

A MULTI-SCALE ANALYSIS OF CORAL REEF ACCRETION-EROSION RATES AND BIOERODER COMMUNITIES

ABSTRACT

Management efforts to sustain coral reefs often focus on coral health and growth, but reef resilience also depends on bioerosion rates and their response to local and global human impacts. A persistent challenge is to distinguish the effects of climate change from other forms of environmental variation, and to understand how environmental variation impacts accretion-erosion processes across different spatial scales. In this study, we used a natural environmental gradient to test how accretion rates by secondary calcifiers, erosion rates by borers and grazers, and net change rates respond to natural environmental variability across a range of spatial scales in the Hawaiian Archipelago. Highly accurate erosion, secondary calcification, and percent change in volume rates were calculated from micrometer-scale 3D images of $CaCO_3$ blocks from year-long deployments at 29 reefs across Hawai‘i. We correlated these rates with a suite of co-measured chemical, biological, and physical datasets compiled from multiple data sources and determined the strongest drivers of accretion and erosion at each spatial scale. There are three major outcomes from this study: 1) accretion and erosion rates were driven by different environmental parameters, 2) the bulk of the variability in accretion and erosion rates were at the smallest within-reef spatial scale, and 3) the strongest correlates of accretion and erosion differed across spatial scales. This dataset highlights the significance of spatial scale in understanding reef dynamics and, further, the need to recognize both reef accretion and erosion processes in order to predict net coral reef response to future environmental change.

1. INTRODUCTION

Worldwide, declines in coral cover and shifts in coral reef community composition (Hughes 1994; Bellwood et al. 2004) have raised concerns about reef persistence and whether reef accretion will continue to exceed reef erosion. The anthropogenic impacts influencing reef

decline act at a range of spatial scales, from global impacts on ocean temperature and acidity to local impacts of overfishing, eutrophication, and sedimentation. These anthropogenic impacts interact with physical, chemical, and biological processes that influence accretion and erosion at a range of spatial and temporal scales. The management of coral reefs requires an understanding of environmental drivers of reef accretion and erosion and how these drivers interact at different scales.

Corals and other calcifying organisms build reefs through the accretion of calcium carbonate ($CaCO_3$) skeletons while a diverse community of bioeroders erode reefs through grazing on and boring into $CaCO_3$ reef substrate (Neumann 1966). The accretion-erosion balance is influenced by a variety of environmental processes and these processes may vary at different spatial scales. Chemical drivers, such as ocean acidity, can increase erosion (Tribollet et al. 2009; Wisshak et al. 2012; Fang et al. 2013; Reyes-Nivia et al. 2013; Wisshak et al. 2013; Silbiger et al. 2014; DeCarlo et al. 2015; Enochs et al. 2015; Silbiger and Donahue 2015) by making it easier for chemical eroders to dissolve the $CaCO_3$ skeleton and can decrease accretion (Hoegh-Guldberg et al. 2007; Jokiel et al. 2008; Diaz-Pulido et al. 2012; Johnson and Carpenter 2012; Comeau et al. 2013) through metabolic stress. Several studies show increased erosion in eutrophic relative to oligotrophic conditions (reviewed in Le Grand and Fabricius 2011) suggesting that erosion rates are particularly sensitive to nutrients, perhaps because many macroborers are filter feeders. However, studies that examined the impact of nutrients and ocean acidity on erosion simultaneously found different responses at different spatial scales. A local-scale within reef study (~30 m) found that ocean acidity was the best predictor of reef erosion when compared to resource availability (nutrients and chlorophyll), temperature, depth, and distance from shore (Silbiger et al. *in review* and Silbiger et al. (2014)). A much broader Pacific

basin (~16,000 km) study found that the relationship between erosion rates and ocean acidity was enhanced at higher nutrient concentrations (DeCarlo et al. 2015). Physical parameters, like hydrodynamics, can enhance accretion through transport and removal of nutrients and metabolic wastes (Hearn et al. 2001) or decrease accretion through dislodgement and abrasion (Madin and Connolly 2006). In a Lizard Island study (~5 km), accretion of crustose coralline algae and corals was highest at sites with the highest wave energy (Hamylton et al. 2013). Conversely, in much broader Pacific-wide study (~8000 km), coral cover declined with increasing wave energy (Williams et al. 2015). Lastly, biological parameters, like grazing pressure by herbivorous fish, can directly influence erosion by removing $CaCO_3$ substrate while grazing for algae (Hutchings 1986) and can indirectly influence accretion by removing fleshy algae and relieving competitive interactions with CCA (Harley et al. 2012). These studies all highlight the complex interactions between the accretion-erosion balance and chemical, physical, and biological parameters at different spatial scales. To predict the impact of environmental change on coral reefs, we need to have a better understanding of the different drivers of the accretion-erosion balance and the relative influence of each of these drivers at different spatial scales.

Erosion rates are also influenced by bioeroder community composition (Kiene and Hutchings 1994). Bioeroding organisms may be classified into three functional groups: grazers (e.g., urchins and parrotfish), microborers (e.g., endoliths), and macroborers (e.g., sponges, polychaetes, and bivalves). Grazers erode reefs externally by scraping $CaCO_3$ while foraging on the overlying algal or coral tissue. Micro- and macroborers erode reefs internally by boring into the reef framework. Among these three functional groups, macroborers are most diverse, consisting of hundreds of polychaete, sipunculan, sponge, and bivalve species with a range of life history strategies and morphological and chemical mechanisms for boring (Hutchings 1986).

The macroborer community composition is shaped by physical, chemical and biological processes (Hutchings 1986; Hutchings et al. 1992; Hutchings and Peyrot-Clausade 2002). For example, boring sponges and bivalves respond positively to eutrophication, while the response of polychaetes is more variable (Le Grand and Fabricius 2011). Filter feeding sponges and bivalves are positively correlated with eutrophic sites in the Bahamas (Rose and Risk 1985), Barbados (Holmes et al. 2000), the Red Sea (Kleemann 2001), the Great Barrier Reef (Osorno et al. 2005; Tribollet and Golubic 2005) and the eastern Pacific (Fonseca et al. 2006); bivalve abundances are also correlated with high water velocity (Cantera et al. 2003; Londono-Cruz et al. 2003). In contrast, deposit feeding polychaetes in the Great Barrier Reef are more abundant at eutrophic sites (Osorno et al. 2005), while suspension feeding polychaetes are more abundant in oligotrophic sites (Le Bris et al. 1998). The interaction between the macroborer community and the environment ultimately drives patterns in bioerosion rates on coral reefs.

In this study, we describe spatial patterns in accretion-erosion rates from of experimental blocks, as well as spatial patterns in macroborer communities from benthic samples, and relate these patterns to chemical, physical, and biological data from long-term monitoring and remote sensing at multiple spatial scales. We use a newly developed µCT methodology (Silbiger et al 2014, Silbiger et al in review) to measure *in situ* accretion, erosion, and percent change in volume rates from experimental blocks across the Hawaiian Archipelago. Using µCT to calculate accretion, erosion, and percent change in volume is superior to previously described methods (Silbiger et al. *in review*) because it is a high resolution analysis that can separately identify accretion and erosion processes from the same experimental substrate (Silbiger et al. *in review*) and also calculate a highly accurate percent change in volume (Silbiger et al. 2014) to determine if blocks are net accreting (positive change) or net eroding (negative change) over a known

deployment time. Further, it allows for the 3D visualization of accretion and erosion (Silbiger et al. 2014, Silbiger et al *in review*). Here, we use µCT to calculate accretion rates from secondary calcifiers and erosion rates from borers and grazers from an early successional community after a one-year deployment period. This study is the first broad-scale application of this method.

2. MATERIALS AND METHODS

2.1 Study Sites: This study was conducted at 29 forereef sites (8-16 m depth) across six islands/atolls in the Hawaiian Archipelago (Fig. 1). Kure Atoll (KUR), Pearl and Hermes Atoll (PHR), Lisianski Atoll (LIS), and French Frigate Shoals (FFS), are atolls in the Northwestern Hawaiian Islands (NWHI) and protected by the Papahānaumokuākea Marine National Monument (PMNM), one of the largest and most remote marine protected areas in the world. O‘ahu and Maui are populated, volcanic islands in the Main Hawaiian Islands (MHI). Twenty-seven of these sites were co-located with long-term monitoring sites maintained by the NOAA Coral Reef Ecosystem Division (CRED) to take advantage of pre-existing environmental data and research cruise logistics. The remaining two sites, O‘ahu-KBay and Maui-A27, were selected with similar depth and exposure characteristics.

2.2 Accretion, Erosion, and Percent Change in Volume Rates: Five blocks (5 x 5 x 2.5 cm) cut from dead *Porites lobata* were deployed at each site for approximately one year (Fig. S1 and Table S1). Blocks were deployed at FFS, LIS, and PHR sites in July/August 2011 on NOAA cruise HA1103 and retrieved in August 2012 on NOAA cruise HA1204; at KUR sites in August 2012 on NOAA cruise HA1204 and retrieved in July 2013 on NOAA cruise SE1305; and at O‘ahu and Maui sites in September/October 2012 on NOAA cruise SE1207 and retrieved September/October 2013 with small boat operations (Table S1). We recovered 143 of the 145

deployed experimental blocks and 122 had adequate quality before/after µCT scans for data analysis.

Accretion rate, erosion rate, and percent changes in volume were calculated for each block by comparing before and after µCT scans (Silbiger et al. 2014; Silbiger et al *in review*). µCT is an X-ray technology that non-destructively images the external and internal structures of solid objects, resulting in a three-dimensional array of object densities. We used an eXplore CT120 µCT (GE Healthcare Xradia, Inc) at the Cornell University Imaging Multiscale CT Facility to scan blocks before and after deployment (voltage = 100kV, current = 50mA). A three-dimensional array of isotropic voxels at 50 μm^3 resolution was generated using the GE Console Software and were averaged to 100 μm^3 for data analysis. We used a threshold of 200 Hounsfield Units to separate coral from air (Silbiger et al. 2014).The number of voxels exceeding this threshold was multiplied by the voxel size $(100\ \mu m)^3$ to give the total volume of $CaCO_3$ for pre and post-deployment blocks. The pre and post-deployment scans were then aligned using an intensity-based registration technique from the MATLAB R2014b Image Processing Toolbox, converted to binary, and subtracted from one another resulting in a matrix of 0's, 1's, and -1's. All positive values were new pixels added to the post-deployment scan which indicate accretion, negative values were pixels that were lost and indicate erosion, and zeros meant there was no change at that pixel between the two scans. All values were summed and multiplied by the resolution of the scan to obtain the volume lost (erosion) or gained per block (accretion).

Prior studies highlight the need to analyze both accretion and erosion independently (Silbiger and Donahue 2015, Silbiger et al *in review*), but net change rates are also necessary for understanding the net growth of coral reefs (i.e. are reefs net accreting or net eroding; Silbiger et

al. 2014). Here, we calculated accretion rates, erosion rates, and the percent change in volume of experimental blocks over the one year deployment time. Accretion rates are typically presented in mm yr^{-1}(e.g, Payri 1995; Tribollet et al. 2006) and erosion rates are presented as kg m^{-2} yr^{-1} (e.g., Tribollet and Golubic 2005; Wisshak et al. 2012) in the literature. Because accretion and erosion rates were in different units to stay consistent with literature values, they could not simply be added together to determine the net rate of the block; thus, we used percent change in volume of the block to determine whether blocks were net accreting (positive change) or net eroding (negative change). Erosion and accretion rates were calculated using the following equations:

$$\text{Erosion Rate (kg m}^{-2}\text{ yr}^{-1}) = (\Delta Vol_i \times \rho_i)/(SA_i \times Time) \quad (1)$$

$$\text{Accretion Rate (mm yr}^{-1}) = 1000 \times (\Delta Vol_i)/(SA_i \times Time)\,, \quad (2)$$

where i represents an individual block, ΔVol is the volume lost (erosion) or gained (accretion) in m^3, SA is the surface area of the pre-deployment blocks (m^2), ρ is the skeletal density of the pre-deployment block (kg m^{-3}), and $Time$ is the deployment time (years). Accretion rates were multiplied by 1000 to convert from m to mm yr^{-1}. Surface area was calculated from the µCT scans following methods by Legland et al. (2011). Skeletal density of the blocks was calculated by converting intensity values from the µCT scans to bulk skeletal density following methods in DeCarlo et al. (2015). Percent change in volume per year was calculated as:

$$\text{Percent change in volume (\% y}^{-1}) = 100 \times (Vol_{t2} - Vol_{t1})/(Vol_{t1} \times Time)\,. \quad (3)$$

Where Vol_{t2} and Vol_{t1} were the volumes of the blocks at time 2 (post-deployment) and time 1 (pre-deployment), respectively.

2.3 Community Data: At each site, we characterized the infaunal community, including polychaetes, sipunculans, echinoids, and bivalves but excluding sponges, by extracting organisms from samples of dead coral substrate (Table S2). We excluded bioeroding sponges from this analysis because they are difficult to extract and quantify. Using a hammer and chisel, we collected 983 ± 96 cm^3 (mean ± SE) of dead massive *Porites* spp. reef substrate at each site. The average skeletal density of the rubble was 1.82 ± 0.03 (mean ± SE) and there was no relationship between rubble skeletal density and bioeroder abundances. Samples were collected and immediately placed into a plastic bag and sealed underwater. Samples were collected at all NWHI sites between July and August, 2012 on NOAA cruise HA1204 and all the MHI sites between September and October, 2013 using small boat operations (Table S1). Rubble from each site was transferred into individual buckets filled with approximately 10 L of seawater. To each bucket, we added 5 ml of a 95% ethanol and 5% clove oil solution and left the rubble to soak in the solution for 2-3 hours. This solution coerces mobile organisms out of the interstitial spaces of the rubble without compromising the integrity of the organisms, easing later identification. At the end of the soak period, we sieved the seawater from each bucket through a 100 µm mesh sieve, extracted the organisms and preserved them in 95% ethanol. All rubble pieces were broken apart and carefully inspected for any other organisms that were not extracted using the solution. We calculated the volume of all reef substrate pieces via volume displacement to normalize the organism abundances to the total volume of rubble from each site. Polychaeta, Sipuncula, Echinometra, and Bivalvia were counted and identified to the lowest possible taxonomic unit by taxonomic experts (co-authors Scott Godwin and Holly Bolick) as potential macroborers, but were pooled by family for data analysis. These groups include both macroborers and non-eroders (Table S2). All species from these groups were used in the community analyses. Some species

within these groups were identified as known macroborers (pers. com. S. Godwin; Table S2) and were pooled to test for relationships between macroborer abundances and erosion rates.

2.4 Environmental Data: We compiled data describing the chemical, physical, and biological characteristics of each site (Table 1) from NOAA CRED, Hawai‘i Department of Aquatic Resources (DAR), NOAA satellite data, NOAA global wave models, and *in situ* sampling. Detailed methods and collections protocols are described in the supplemental material.

2.5 Statistical Analysis:

2.5.1 Environmental data: There were three specific groups of predictor variables: chemical drivers, biological drivers, and physical drivers (Table 1). We used separate principle components analyses (PCA) for each group of predictor variables as well as a summary PCA with all 23 variables to summarize the spatial patterns in the environment (Figs. 2 and 3).

2.5.2 Accretion, erosion, and percent change in volume rates: To evaluate the contribution of variance at each spatial scale (regions, islands, sites, within sites). We used a variance components analysis, where site in island in region are all considered random effects. To compare means at each level, we used a nested analysis of variance (ANOVA) with a Tukey Honestly Significant Difference (HSD) *post-hoc*, where sites, islands, and regions were all fixed effects. Because secondary calcification can inhibit erosion (White 1980; Tribollet and Payri 2001), we also tested for a relationship between accretion and erosion rates with a non-linear regression. Accretion and erosion rates were both log-transformed to meet assumptions of normality.

To determine environmental drivers of accretion-erosion rates, we used a model selection approach by ranking Akaike Information Criterion (AIC) values from simple linear models that correlate environmental predictors with accretion, erosion, and percent change in volume rates. Models with the smallest AIC value ($\Delta AIC = 0$) are the 'best' of the models considered, but models with an ΔAIC value of <4 have some empirical support and models with a ΔAIC value greater than 10 to 12 are less plausible (Anderson 2007). To test if the relationship between the environmental predictors and accretion-erosion is conserved across spatial-scale, we also constructed individual models for each region (MHI and NWHI). All environmental data were transformed to fit a normal distribution (Table 1).

2.5.3. Community analysis: To test whether infaunal community composition varied by region or island, we used a nested multivariate generalized linear model with a negative binomial distribution (*mvabund* package in *R*; Wang et al. (2012)). We did not collect within site community replicates and, therefore, compared community composition only at the region and island levels. We used volume of the rubble as a covariate to account for minor differences in collection volume across sites. We chose a multivariate generalized linear model approach, rather than a distance-based approach (e.g., ANOSIM, SIMPER) because there was a strong mean-variance relationship in the abundance data (Fig. S2; $F_{28,1}=399$, $p<0.0001$, $R^2=0.94$) and mean-variance relationships confound region and dispersion effects in distance-based approaches (Warton et al. 2012). To visualize the data, we used a non-metric multi-dimensional scaling analysis (nMDS) with a Bray-Curtis dissimilarity index (*Vegan* package in *R;* Oksanen et al. (2007)).

We used a model selection approach by ranking AIC values to determine the best environmental predictors of macroborer community composition. Because this is a multivariate

analysis, we reduced the dimensionality of the data by using the first and second PC axes from each of the four PCAs as our independent variables in the models instead of individual parameters. Multivariate generalized linear models with a negative binomial distribution were used to test the relationship between environmental models (PC axes) and macroborer community composition (*mvabund* package in *R*; Wang et al. (2012)); rubble volume was also included as a covariate in these analyses. We did not have enough statistical power to construct individual models for the community data across region and, therefore, did not test to see if patterns were conserved across spatial scales. Because the bioeroder community ultimately drives patterns in erosion rates, we also examined the relationship between the macroborer community and erosion rates with a simple linear regression (Table S2).

3. RESULTS

3.1 Environmental drivers: For the chemistry data, changes in carbonate chemistry (loadings = 0.33 - 0.51) explained the majority of the variance in PC1, while phosphate and silicate (loadings= 0.57 - 0.64; Fig. 2a and 3a) explained the majority of the variance in PC2 (loadings= 0.57 - 0.64; Fig. 2a and 3a). The first principal component in the biological data accounted for herbivore biomass (loadings = 0.49) and turf algae (loadings = 0.53), where sites in the negative direction had the highest herbivorous fish biomass and the lowest % cover of turf algae (Figs. 2b and 3b). The second principal component was driven by a coral (loadings = 0.56) – macroalgae gradient (loadings = 0.72): sites in the negative direction had the highest coral cover while sites in the positive direction had the highest macroalgal cover (Figs. 2b and 3b). For the physical data, max wave energy described the majority of the variance in PC1 (loadings =0.42) and std SST described the majority of the variance in PC2 (loadings = 0.40; Figs. 2c and 3c). Lastly, in

the model with all 23 parameters, min SST (loadings = 0.35) and std SST (loadings = 0.34) explained the majority of the variance in PC1, while N+N (loadings = 0.30) and TA (loadings = 0.36) explained the majority of the variance in the PC2 (Figs. 2d and 3d).

3.2 Accretion, erosion, and percent change in volume rates:

3.2.1 Spatial patterns in accretion, erosion and percent change in volume: We compared rates of accretion, erosion, and the percent change in block volume at between regions, between islands within regions, and between sites within islands. We found variation in erosion rates at the region and site scale (Table 2 and Figs. 4c and 5b), variation in accretion at the island and site scale (Table 2 and Figs. 4b and 5a), and variation in percent change in volume at the island and site scale (Table 2 and Figs. 4f and 5c). All three measures had substantial within-site variability (Table 2 and Figs. 5 and 6). In fact, the highest portion of variance in the data was attributed to the smallest (within sites) spatial scale, explaining between 47 and 72% of the variance in accretion, erosion, and percent change in volume rates (Fig. 6). The two largest spatial-scales, region and island, explained substantially less of the variation (<0.01 – 18%) for all rates (Fig. 6).

Overall, accretion, erosion, and percent change in volume rates ranged from 0.16 – 6.5mm y^{-1}, 0.012 – 0.46 kg m^{-2} y^{-1}, and -13 – 16% y^{-1}, respectively, and 73% of all the experimental blocks were net accreting after the one year deployment. There was also a significant exponential relationship between accretion and erosion rates ($F_{120,2}$ = 99, $p<0.001$, R^2 = 0.19; Fig. S3). Erosion rates were 39% higher at the MHI sites than the NWHI sites (Table 2, Figure 3c), while accretion rates were similar between regions (Table 2, Fig 4a); percent change in volume was not significantly higher in the NWHI than the MHI (Fig. 4e and Table 3).

Accretion rates varied at the island scale, driven primarily by exceptionally high accretion at LIS (nearly double the accretion rate of other NWHI sites, Table 3, Fig. 4d); percent change in volume also varied by site, with a similar pattern for LIS (Fig. 4f). In contrast, there were only marginal differences in erosion at the island scale (Table 3, Fig. 4d). Lisianski had the highest average percent change in volume, the highest accretion rate, and second lowest erosion rate. O‘ahu had the most blocks that were net eroding (46%), had the lowest average percent change in volume, coupled with the second lowest accretion rate and highest erosion rate (Fig. 4b,d,f and Table 3). Site level variation was significant for erosion, accretion, and percent change in volume (Fig. 5 and S4, and Table 2). For all sites, MauiA27 (Kahekili, Maui) had the highest average erosion rate (0.35 kg m^{-2} y^{-1} ± 0.03) and the lowest percent change in volume (-8.2% ±1.97), while LIS18 had the highest accretion rate (3.68 ± 0.57 mm y^{-1}) (Fig. 5 and S4).

3.2.2 Environmental drivers of accretion, erosion and percent change in volume: We compared models with parameters that represented the chemical, biological, and physical environment as drivers of accretion, erosion, and percent change in volume. The highest ranking models for accretion and erosion were always different from each other (Fig. 7 and Tables S3 and S4). The highest ranking models for percent change in volume were similar to erosion models in the Hawaiian Archipelago and the MHI and to accretion models in the NWHI (Fig. 7, Table S5). Relationships between environmental parameters and accretion, erosion, and percent change in volume were not conserved across space; the highest ranking models were always different between the MHI and NWHI sites (Fig. 7 and Tables S3-5).

For accretion, carbonate chemistry parameters were the most parsimonious models for the Hawaiian Archipelago (Fig. 7a, Table S3) and for the NWHI (Fig. 7c, Table S3) while physical and biological parameters were the most parsimonious for the MHI (Fig. 7b, Table S3).

TA was the highest ranking model in the Hawaiian Archipelago ($R^2 = 0.17$) and the NWHI ($R^2 = 0.29$) while macroalgae ($R^2 = 0.14$) was the highest ranking model in the MHI (Figure 7a-c, Table S3).

For erosion, biological and physical models were the most parsimonious for the Hawaiian Archipelago (Fig. 7d and Table S4), while biological and chemical models were the most parsimonious for the MHI (Fig. 7e and Table S4) and the NWHI (Fig. 7f and Table S4). Herbivore biomass was the highest ranking model for the Hawaiian Archipelago ($R^2 = 0.14$) and the MHI ($R^2 = 0.28$), while benthic cover descriptors (% other: mainly bare substrate, cyanobacteria, and sessile invertebrates) ranking highest ($R^2 = 0.11$; Fig. 7d-f and Table S3).

Lastly, for percent change in volume, biological and chemical models were the most parsimonious in the Hawaiian Archipelago (Fig. 7g and Table S5), chemical models were the most parsimonious in the NWHI (Fig. 7i and Table S5), and chemical, physical, and biological parameters all had models with ΔAIC values of < 4 in the MHI (Fig. 7h and Table S5). Herbivore biomass ranked highest for percent change in volume in the Hawaiian Archipelago ($R^2 = 0.08$; Fig. 7g and Table S5), macroalgae ranked highest in the MHI ($R^2 = 0.16$; Fig. 7h and Table S5), but herbivore biomass only had a ΔAIC of 0.36 and explained nearly the same amount of variance in the data ($R^2 = 0.15$; Fig. 7h, Table S4), and DIC ranked highest in the NWHI ($R^2 = 0.16$; Fig. 7i and Table S4).

3.3 Community data:

3.3.1 Spatial patterns in infaunal community: We collected 2073 organisms from 29 different families (Table S2) from the phyla Sipuncula, Annelida, Mollusca, and Echinodermata. The most common and abundant organisms were from the Eunicidae family followed by organisms from

the Syllidae, Aspidosiphonidae and Mytilidae families (Fig. S5 and Table S2). There was a significant difference in the community across regions ($F_{27,1}$ = 139.51, p = 0.001; Figs. 6 and S6 and Table 4) and across islands ($F_{22,10}$ = 16.94, p = 0.001; Fig. 8 and Table 4). MHI communities were clustered, but there was greater community variation throughout the NWHI (Fig. 8).

3.1.2 Environmental drivers of infaunalcommunity: When testing for relationships between the community and environmental models, we found that the chemical model ranked highest in model parsimony (Table 5). The second best model, the biological model, had a ΔAIC of 17.1, explaining substantially less of the variation in the data. We also tested for a relationship between the macroborer abundances (Table S2) and erosion rates and found that erosion rates were highest at sites with the highest abundance macroborers ($F_{27,1}$ = 9.45, p = 0.005, and R^2 = 0.26; Fig. 9).

4 DISCUSSION

4.1 Spatial patterns of accretion, erosion, and percent change in volume

Ecological patterns are incontrovertibly entwined with scale (Hutchinson 1953; Levin 1992), and the present study evokes this classic ecological phenomenon. Across the 2500 km linear extent of our study, accretion and percent change rates vary among islands (Fig 4c,f) and sites within islands (Fig. 5a,c), but not between regions (Fig 4a,e). Conversely, erosion rates differed across regions and sites (Fig. 4b and Fig. 5b), but not islands (Fig. 4d). At the regional or island-scale, differences may be driven by large climatic gradients, recruitment pulses in bioeroders and calcifiers, ocean circulation, or major disturbances such as storm events. However, for all factors investigated here, the smallest scale of variation (within sites) holds a disproportionately higher amount of variance than any other spatial scale in this study.

Although many processes interact at multiple scales to shape patterns in the accretion-erosion balance (e.g., Tribollet et al. 2002; Tribollet and Golubic 2005; Tribollet et al. 2006; Silbiger et al. 2014; DeCarlo et al. 2015), these data provide compelling evidence that local variability is important in shaping the accretion-erosion balance (Silbiger et al. 2014; Silbiger et al in review). The within-site spatial scale was the highest source of variance in the data, responsible for 71.8%, 47.4%, and 65.6% of the variation in accretion, erosion, and percent change in volume, respectively (Fig 6). This high within-site variance indicates that individual blocks within a site were more different than blocks 2500 km apart. The relative importance of local-scale variance is not restricted to Hawai‘i and its isolated location in the Pacific. For example, on the Great Barrier Reef (GBR), over 65% of the variance in coral cover was explained by local, within site differences (Hughes et al. 2012). Within-site variability at backreef sites also accounted for the highest amount of variance in Scarid (bioeroding parrotfish) biomass and abundance across multiple spatial scales on the GBR (Gust et al. 2001). Both broad and local scale gradients in biological and physicochemical drivers are likely interacting to shape patterns in these studies.

4.2 Environmental drivers of accretion, erosion, and percent change in volume rates

Our data indicate that chemical parameters are the strongest drivers of accretion (Fig. 7a) while biological and physical parameters are the strongest drivers of erosion when analyzed for the entire Hawaiian Archipelago (Fig. 7d). These results corroborate previous work showing that accretion and erosion are influenced by different environmental parameters (Silbiger et al. *in review*, Silbiger and Donahue 2015). Though it is clear which categories of environmental parameters ranked highest for accretion and erosion, the top five highest-ranking models often

had ΔAIC values of <4, indicating empirical support for several models. We anticipated interactive effects among parameters because all environmental parameters used in this study were known drivers of accretion and/or erosion; however, we wanted to test if these parameters separate on our a spatial gradient, given the large differences in geography, chemistry, hydrodynamics, and community structure across this 2500 km transect (Figs. 2 and 3).

The strongest drivers of accretion and erosion were different in the MHI and NWHI. Physical parameters dominated the accretion models in the MHI (though the macroalgae model was ranked highest; Fig. 7b), while carbonate chemistry parameters dominated the accretion models in the NWHI (Fig. 7c), likely because there was a larger range in the carbonate chemistry in the NWHI (mostly driven by Lisianksi Atoll) than the MHI (Fig. 2a and 3a). For erosion, herbivore biomass was the best model in the MHI while benthic cover descriptors were the best models in the NWHI which was likely driven by considerable differences in fish biomass between NWHI and MHI (Williams et al. 2010). Herbivorous fish are abundant at all NWHI sites because of the inaccessibility and special protection status of the PMNM (Williams et al. 2010), whereas there is a strong gradient in fish biomass throughout the MHI due to varying fishing pressures (Williams et al. 2008). The highest ranking models for percent change in volume rates also differed between the MHI and the NWHI sites. In the MHI, the highest ranking models were similar to the erosion models which were most strongly influenced by herbivorous fish and % cover of macroalgae, but in the NWHI, the highest ranking models most closely resembled to the accretion models which were most strongly influenced by carbonate chemistry parameters (Fig. 7). Further, erosion rates were much higher in the MHI than the NWHI (Fig 4c); these patterns indicate that erosion rates have a higher impact on percent change in volume rates in the MHI than the NWHI. A prior Pacific Basin study also found that the relationship between

environmental models and reef characteristics (coral, CCA, and macroalgal cover) were not conserved across space (Williams et al. 2015). Williams et al (2015) split sites between populated and unpopulated islands, found that biophysical parameters had higher explanatory power at unpopulated islands, and concluded that local human impacts decouple biophysical relationships on coral reefs. The MHI versus NWHI comparison is similarly populated versus unpopulated, and differences between sites could be driven by local human impacts; however, there are also several other major differences between these regions that may be more directly related (e.g., high vs low islands, benthic habitat differences, etc.).

The carbonate chemistry models had the highest explanatory power for accretion in the Hawaiian Archipelago ($R^2 = 0.17$; Fig. 7a) and the NWHI ($R^2 = 0.29$; Fig. 7c). The carbonate chemistry models also had the highest explanatory power for percent change in volume in the NWHI ($R^2 = 0.16$; Fig. 7i). Both erosion and secondary accretion are sensitive to changes in carbonate chemistry: typically erosion rates increase (Tribollet et al. 2009; Wisshak et al. 2012; Fang et al. 2013; Reyes-Nivia et al. 2013; Wisshak et al. 2013; Silbiger et al. 2014; Enochs et al. 2015; Silbiger and Donahue 2015) and secondary accretion rates decrease (Jokiel et al. 2008; Diaz-Pulido et al. 2012; Johnson and Carpenter 2012; Comeau et al. 2013), though some studies have found parabolic responses with increasing CO_2 (Ries et al. 2009; Silbiger and Donahue 2015).

The biological models, specifically herbivorous fish, had the highest explanatory power for erosion rates in the Hawaiian Archipelago overall ($R^2 = 0.14$; Fig. 7d) and the MHI specifically ($R^2 = 0.28$; Fig. 7e). The biological models were also the highest ranking models for percent change in volume for the Hawaiian Archipelago and MHI (Fig. 7a,b). Herbivorous fish can directly influence erosion by removing $CaCO_3$ substrate while grazing for algae and they can

indirectly influence accretion by removing fleshy algae and relieving competitive interactions with CCA (Harley et al. 2012). Because the presence of secondary calcifiers, mainly CCA, can inhibit the settlement of bioeroders by sealing off the substrate and making it difficult for borers to penetrate (White 1980; Tribollet and Payri 2001), herbivore biomass can also indirectly influence erosion rates. Notably, we saw a negative exponential relationship between accretion and erosion (Fig S3) and a negative relationship between herbivore biomass and erosion (Fig. 7e), suggesting that there is a complex interaction between herbivorous fish, secondary calcifiers, and erosion.

4.3 Spatial patterns in infaunal communities along the Hawaiian Archipelago

Variation in infaunal community composition also differed across spatial-scales. The community composition was significantly different across islands and across regions (Figs. 8 and S6), but the community was highly variable in the NWHI, likely due to the fact that the NWHI has much higher habitat variation between sites than the MHI (Friedlander et al. 2005; Friedlander et al. 2008).We did not collect community replicates within each site so we could not assess the importance of within site variability to macroborer communities. Hutchings et al. (1992) proposed that many mobile macroborers have strong site preferences, suggesting that broad-scale environmental processes can have a strong influence on recruitment. Although not addressed in this study, we would expect high within-site variability in the infaunal community as well because they are sensitive to differences in substrate type (Enochs 2012; Enochs and Manzello 2012); dead corals typically have a higher richness of cryptic organisms than live corals (Enochs and Manzello 2012).

4.3 Environmental drivers of infaunal communities

The chemical parameters ranked highest for the infaunal communities. The infaunal community structure could be affected by nutrients and resource availability because many infaunal organisms are filter feeders (reviewed in Le Grand and Fabricius 2011). The carbonate chemistry parameters could also influence infaunal macroborers because macro-bioerosion is sensitive to pH (Wisshak et al. 2012; Silbiger and Donahue 2015). We were not surprised to find that erosion rates and infaunal communities had different environmental predictors. Indeed, erosion rates on our experimental blocks were controlled by organisms in addition to macroborers such as microborers and grazers which is likely responsible for this difference. Further, we used a late successional community that included both macroborers and non-eroders in our community analysis (samples were collected from dead substrate), while the erosion rates were from an early successional community of bioeroders that only appear during the first year. Still, there was a significant relationship between abundances of macroborers (Table S2) and erosion rates (Fig. 9).

4.4 Constraints

There are some limitations to this study that should be carefully considered when interpreting the results. First, the temporal scales of the environmental variables differ and, particularly in the case of water chemistry, are disconnected from the block deployment period (Table S1 and S6). While fish and benthic community data are generally stable over a year-long time frame, water chemistry data are not (Guadayol et al. 2014; Silbiger et al. 2014). Chemistry data in this analysis were from single data points collected between spring and summer during daylight hours. This ignores differences in diel or seasonal variation across sites. In some

instances, diel variance is a stronger predictor of secondary accretion than the mean (Price et al. 2012), and this could not be accounted for in our analysis. The sampling intensity reported here reflects the data available for these remote sites. If more, higher-frequency data were available then we may have seen stronger or different relationships between the chemical parameters and accretion-erosion rates.

Second, the highest spatial resolution of the environmental data was at the site level, but the majority of the variance in the accretion-erosion data was within sites. The low R^2 values for all environmental models (highest R^2 value was 0.29) are likely in response to the highly variable accretion-erosion data. Prior studies examining within site environmental variability and accretion-erosion rates had markedly higher explanatory power between accretion-erosion rates and environmental parameters (Silbiger et al. 2014; Silbiger et al. in review), further highlighting the importance of local-scale environmental variability to the accretion-erosion balance of coral reefs. Monitoring protocols are typically in place to track broad environmental trends; however, a better understanding of local-scale variability is necessary to predict how environmental change will impact the accretion-erosion balance.

Last, there are some limitations to the μCT analysis: i) blocks need a long deployment time to quantify late successional stage bioeroders; it may take up to three years for sponges to fully colonize dead substrates (Tribollet and Golubic 2005), ii) the accretion rates exclude adult corals, but include secondary calcifiers such as calcifying algae and sessile invertebrates, and iii) it does not distinguish between different types of eroders or secondary calcifiers (though this analysis could be developed). Given these limitations, though, our analysis is currently the highest resolution analysis that allows for the simultaneous measurement of accretion and erosion from the same experimental substrate.

4.5 Management considerations

Within the United States, long-term coral reef monitoring efforts have been implemented by the NOAA and other state and federal agencies to track reef response to changing ocean conditions, but the large spatial extent (~10,000 km^2) of coral reefs within U.S. waters make this challenging. Coral reef managers often do not have the capabilities to monitor environmental conditions and reef response at fine temporal and spatial scales due to time, money, and logistical constraints, especially in remote management zones such as those in the central Pacific. Still, there are several modes of data acquisition currently being used to monitor coral reefs across a range of spatial and temporal scales. Using stationary buoys, managers can collect high temporal resolution data over small areas of reef. With satellite data, managers can monitor broad areas at a high temporal resolution, but with low spatial resolution (the best satellite data available is at a 1km grid cell). Using *in situ* monitoring protocols on research cruises, managers can collect information over a broad spatial-scale, but at a low temporal resolution. In the present study, we used a combination of data from these monitoring protocols to describe patterns in accretion, erosion, and percent change in volume rates and macroborer communities across multiple spatial scales, and, further, test whether monitoring data can adequately predict patterns in accretion-erosion rates and macroborer communities. While we did find significant patterns between rates, communities, and environmental drivers, there was low explanatory power. It is clear that local, small-scale variability is more important in driving accretion-erosion patterns than broad-scale differences in the environment—the data resolution captured currently through monitoring. A better understanding of the local-scale variability is necessary to identify mechanisms driving these patterns and to predict how reefs will respond to a changing environment.

This is the first study that used μCT to quantify accretion, erosion and percent change in volume rates over large spatial scales. Using this method, we highlight the importance of spatial scale in interpreting patterns in accretion-erosion data and infaunal communities. Our results and those from previous studies (Silbiger et al. 2014; Silbiger et al. in review) provide compelling evidence that local-scale environmental variability is particularly important to the coral reef accretion-erosion balance. We also demonstrate that the relationships between explanatory and response variables are not conserved across space, as there were differences in the highest ranking environmental models between the MHI and NWHI datasets. NOAA is currently using similar μCT methods to monitor bioerosion rates at sites throughout the Pacific and the Caribbean. The differing relationships between environmental variability and accretion-erosion data should be taken into consideration when interpreting those results and in future management decisions on coral reefs.

REFERENCES:

Anderson DR (2007) Model based inference in the life sciences: a primer on evidence. Springer Science & Business Media

Bellwood DR, Hughes TP, Folke C, Nyström M (2004) Confronting the coral reef crisis. Nature 429:827-833

Cantera JRK, Orozco C, Londono-Cruz E, Toro-Farmer G (2003) Abundance and distribution patterns of infaunal associates and macroborers of the branched coral (*Pocillopora damicornis*) in Gorgona Island (eastern tropical Pacific). Bulletin of Marine Science 72:207-219

Comeau S, Edmunds PJ, Spindel NB, Carpenter RC (2013) The responses of eight coral reef calcifiers to increasing partial pressure of CO_2 do not exhibit a tipping point. Limnol Oceanogr 58:388-398

DeCarlo TM, Cohen AL, Barkley HC, Cobban Q, Young C, Shamberger KE, Brainard RE, Golbuu Y (2015) Coral macrobioerosion is accelerated by ocean acidification and nutrients. Geology 43:7-10

Diaz-Pulido G, Anthony K, Kline DI, Dove S, Hoegh-Guldberg O (2012) Interactions between ocean acidification and warming on the mortality and dissolution of coralline alge. Journal of Phycology 48:32-39

Enochs IC (2012) Motile cryptofauna associated with live and dead coral substrates: implications for coral mortality and framework erosion. Marine biology 159:709-722

Enochs IC, Manzello DP (2012) Species richness of motile cryptofauna across a gradient of reef framework erosion. Coral reefs 31:653-661

Enochs IC, Manzello DP, Carlton RD, Graham DM, Ruzicka R, Colella MA (2015) Ocean acidification enhances the bioerosion of a common coral reef sponge: implications for the persistence of the Florida Reef Tract. Bulletin of Marine Science 91:000-000

Fang JKH, Mello-Athayde MA, Schönberg CHL, Kline DI, Hoegh-Guldberg O, Dove S (2013) Sponge biomass and bioerosion rates increase under ocean warming and acidification. Global Change Biology 19:3581-3591

Fonseca EAC, Dean HK, Cortes J (2006) Non-colonial coral macro-borers as indicators of coral reef status in the south Pacific of Costa Rica. Revista De Biologia Tropical 54:101-115

Friedlander A, Aeby G, Brainard R, Clark A, DeMartini E, Godwin S, Kenyon J, Kosaki R, Maragos J, Vroom P (2005) The state of coral reef ecosystems of the Northwestern

Hawaiian Islands. The state of coral reef ecosystems of the United States and Pacific freely associated states 73:263-306

Friedlander A, Aeby G, Brainard R, Brown E, Chaston K, Clark A, McGowan P, Montgomery T, Walsh W, Williams I (2008) The state of coral reef ecosystems of the main Hawaiian Islands. The state of coral reef ecosystems of the United States and Pacific freely associated states:222-269

Guadayol Ò, Silbiger NJ, Donahue MJ, Thomas FIM (2014) Patterns in Temporal Variability of Temperature, Oxygen and pH along an Environmental Gradient in a Coral Reef. PloS one 9:e85213

Gust N, Choat JH, McCormick MI (2001) Spatial variability in reef fish distribution, abundance, size and biomass: a multi-scale analysis. Marine Ecology Progress Series 214:237-251

Hamylton SM, Pescud A, Leon JX, Callaghan DP (2013) A geospatial assessment of the relationship between reef flat community calcium carbonate production and wave energy. Coral reefs 32:1025-1039

Harley CDG, Anderson KM, Demes KW, Jorve JP, Kordas RL, Coyle TA, Graham MH (2012) Effects of climate change on global seaweed communities. Journal of Phycology 48:1064-1078

Hearn C, Atkinson M, Falter J (2001) A physical derivation of nutrient-uptake rates in coral reefs: effects of roughness and waves. Coral Reefs 20:347-356

Hoegh-Guldberg O, Mumby PJ, Hooten AJ, Steneck RS, Greenfield P, Gomez E, Harvell CD, Sale PF, Edwards AJ, Caldeira K, Knowlton N, Eakin CM, Iglesias-Prieto R, Muthiga N, Bradbury RH, Dubi A, Hatziolos ME (2007) Coral reefs under rapid climate change and ocean acidification. Science 318:1737-1742

Holmes KE, Edinger EN, Hariyadi, Limmon GV, Risk MJ (2000) Bioerosion of live massive corals and branching coral rubble on Indonesian coral reefs. Marine Pollution Bulletin 40:606-617

Hughes TP (1994) Catastrophies, phase-shifts, and large-scale degradation of a Caribbean coral-reef. Science 265:1547-1551

Hughes TP, Baird AH, Dinsdale EA, Moltschaniwskyj NA, Pratchett MS, Tanner JE, Willis BL (2012) Assembly rules of reef corals are flexible along a steep climatic gradient. Current Biology 22:736-741

Hutchings PA (1986) Biological destruction of coral reefs- a review. Coral Reefs 4:239-252

Hutchings PA, Peyrot-Clausade M (2002) The distribution and abundance of boring species of polychaetes and sipunculans in coral substrates in French Polynesia. Journal of Experimental Marine Biology and Ecology 269:101-121

Hutchings PA, Kiene WE, Cunningham RB, Donnelly C (1992) Spatial and temporal patterns of non-colonial boring organisms (Polychaetes, Sipunculans and Bivalve molluscs) in Porites at Lizard Island , Great Barrier Reef. Coral Reefs 11:23-31

Hutchinson GE (1953) The concept of pattern in ecology. Proceedings of the Academy of Natural Sciences of Philadelphia:1-12

Johnson MD, Carpenter RC (2012) Ocean acidification and warming decrease calcification in the crustose coralline alga *Hydrolithon onkodes* and increase susceptibility to grazing. J Exp Mar Biol Ecol 434:94-101

Jokiel PL, Rodgers KS, Kuffner IB, Andersson AJ, Cox EF, Mackenzie FT (2008) Ocean acidification and calcifying reef organisms: a mesocosm investigation. Coral Reefs 27:473-483

Kiene WE, Hutchings PA (1994) Bioerosion experiments at Lizard-Island, Great Barrier Reef. Coral Reefs 13:91-98

Kleemann K (2001) The pectinid bivalve *Pedum spondyloideum* (Gmelin 1791): Amount of surface and volume occupied in host corals from the Red Sea. Marine Ecology-Pubblicazioni Della Stazione Zoologica Di Napoli I 22:111-133

Le Bris S, Le Campion-Alsumard T, Romano JC (1998) Characteristics of epilithic and endolithic algal turf exposed to different levels of bioerosion in French Polynesian coral reefs. Oceanologica Acta 21:695-708

Le Grand HM, Fabricius KE (2011) Relationship of internal macrobioeroder densities in living massive Porites to turbidity and chlorophyll on the Australian Great Barrier Reef. Coral Reefs 30:97-107

Legland D, Kiêu K, Devaux M-F (2011) Computation of Minkowski measures on 2D and 3D binary images. Image Analysis & Stereology 26:83-92

Levin SA (1992) The problem of pattern and scale in ecology: the Robert H. MacArthur award lecture. Ecology 73:1943-1967

Londono-Cruz E, Cantera JR, Toro-Farmer G, Orozco C (2003) Internal bioerosion by macroborers in *Pocillopora* spp. in the tropical eastern Pacific. Marine Ecology-Progress Series 265:289-295

Madin JS, Connolly SR (2006) Ecological consequences of major hydrodynamic disturbances on coral reefs. Nature 444:477-480

Neumann AC (1966) Observations on coastal erosion in Bermuda and measurements of boring rate of sponge *Cliona lampa.* Limnology and Oceanography 11:92-108

Oksanen J, Kindt R, Legendre P, O'Hara B, Stevens MHH, Oksanen MJ, Suggests M (2007) The vegan package. Community ecology package

Osorno A, Peyrot-Clausade M, Hutchings PA (2005) Patterns and rates of erosion in dead Porites across the Great Barrier Reef (Australia) after 2 years and 4 years of exposure. Coral Reefs 24:292-303

Payri CE (1995) Production carbonatée de quelques algues calcifiées sur un récif corallien de Polynésie française. Bulletin de la Societe Geologique de France 166:77-84

Price NN, Martz TR, Brainard RE, Smith JE (2012) Diel Variability in Seawater pH Relates to Calcification and Benthic Community Structure on Coral Reefs. PloS one 7:e43843-e43843

Reyes-Nivia C, Diaz-Pulido G, Kline D, Guldberg O-H, Dove S (2013) Ocean acidification and warming scenarios increase microbioerosion of coral skeletons. Global Change Biology 19:1919-1929

Ries JB, Cohen AL, McCorkle DC (2009) Marine calcifiers exhibit mixed responses to CO_2-induced ocean acidification. Geology 37:1131-1134

Rose CS, Risk MJ (1985) Increase in *Cliona delitrix* infestation of *Montastrea cavernosa* heads on an organically polluted portion of the Grand Cayman fringing-reef. Marine Ecology-Pubblicazioni Della Stazione Zoologica Di Napoli I 6:345-363

Silbiger NJ, Donahue MJ (2015) Secondary calcification and dissolution respond differently to future ocean conditions. Biogeosciences 12:567-578

Silbiger NJ, Guadayol, xd, Thomas FIM, Donahue MJ (2014) Reefs shift from net accretion to net erosion along a natural environmental gradient. Marine Ecology Progress Series 515:33-44

Tribollet A, Payri C (2001) Bioerosion of the coralline alga *Hydrolithon onkodes* by microborers in the coral reefs of Moorea, French Polynesia. Oceanologica Acta 24:329-342

Tribollet A, Golubic S (2005) Cross-shelf differences in the pattern and pace of bioerosion of experimental carbonate substrates exposed for 3 years on the northern Great Barrier Reef, Australia. Coral Reefs 24:422-434

Tribollet A, Decherf G, Hutchings PA, Peyrot-Clausade M (2002) Large-scale spatial variability in bioerosion of experimental coral substrates on the Great Barrier Reef (Australia): importance of microborers. Coral Reefs 21:424-432

Tribollet A, Langdon C, Golubic S, Atkinson M (2006) Endolithic microflora are major primary producers in dead carbonate substrates of Hawaiian coral reefs. Journal of Phycology 42:292-303

Tribollet A, Godinot C, Atkinson M, Langdon C (2009) Effects of elevated $pCO_{(2)}$ on dissolution of coral carbonates by microbial euendoliths. Global Biogeochemical Cycles 23:GB3008

Wang Y, Naumann U, Wright ST, Warton DI (2012) mvabund–an R package for model-based analysis of multivariate abundance data. Methods in Ecology and Evolution 3:471-474

Warton DI, Wright ST, Wang Y (2012) Distance-based multivariate analyses confound location and dispersion effects. Methods in Ecology and Evolution 3:89-101

White J (1980) Distribution, recruitment and development of the borer community in dead coral on shallow Hawaiian reefs. University of Hawaii at Manoa,

Williams GJ, Gove JM, Eynaud Y, Zgliczynski BJ, Sandin SA (2015) Local human impacts decouple natural biophysical relationships on Pacific coral reefs. Ecography

Williams ID, Walsh WJ, Schroeder RE, Friedlander AM, Richards BL, Stamoulis KA (2008) Assessing the importance of fishing impacts on Hawaiian coral reef fish assemblages

along regional-scale human population gradients. Environmental Conservation 35:261-272

Williams ID, Richards BL, Sandin SA, Baum JK, Schroeder RE, Nadon MO, Zgliczynski B, Craig P, McIlwain JL, Brainard RE (2010) Differences in reef fish assemblages between populated and remote reefs spanning multiple archipelagos across the central and western Pacific. Journal of Marine Biology 2011

Wisshak M, Schönberg CHL, Form A, Freiwald A (2012) Ocean acidification accelerates reef bioerosion. Plos One 7:e45124-e45124

Wisshak M, Schönberg CHL, Form A, Freiwald A (2013) Effects of ocean acidification and global warming on reef bioerosion—lessons from a clionaid sponge. Aquatic Biology 19:111-127

Table 1: Environmental parameters grouped by chemical (a), physical (b), and biological (c) drivers. Parameters is environmental parameter, transformation is data transformation, data source is the agency, satellite, or model source for the data, and method is collection method for each parameter.

	Parameters	Transformation	Data Source	Method
(a) Chemical				
	PO_4^{3-}	log(X)	CRED/Silbiger[1]	Water Sample
	Si	log(X)	CRED/Silbiger[1]	Water Sample
	$NO_3^- + NO_2^-$	log(X)	CRED/Silbiger[1]	Water Sample
	Ω_{arag}	log(X)	CRED/Silbiger[1]	CO2SYS
	pH	log(X)	CRED/Silbiger[1]	CO2SYS
	TA (salinity normalized)	log(X)	CRED/Silbiger[1]	Water Sample
	DIC (salinity normalized)	log(X)	CRED/Silbiger[1]	Water Sample
(b) Physical				
	Depth	NA	CRED	Dive computer
	mean(SST)	NA	G1SST	Satellite
	max(SST)	NA	G1SST	Satellite
	min(SST)	NA	G1SST	Satellite
	std(SST)	log(X)	G1SST	Satellite
	mean(Wave Energy)	log(X)	Wave Watch III	Satellite
	max(Wave Energy)	log(X)	Wave Watch III	Satellite
	sum(Wave Energy)	NA	Wave Watch III	Satellite
	std(Wave Energy)	log(X)	Wave Watch III	Satellite
(c) Biological				
	Fish herbivore biomass	log(X)	CRED/DAR[2]	BLT/nSPC
	% Coral cover	log(X)	CRED/DAR[2]	LPI/Photoquad[3]
	% Calcified algae	log(X+1)	CRED/DAR[2]	LPI/Photoquad[3]
	% Macroalgae	log(X+1)	CRED/DAR[2]	LPI/Photoquad[3]
	% Turf algae	log(X)	CRED/DAR[2]	LPI/Photoquad[3]
	% Sand	log(X+1)	CRED/DAR[2]	LPI/Photoquad[3]
	% Other	log(X+1)	CRED/DAR[2]	LPI/Photoquad[3]

[1] Nutrient samples from O‘ahu sites and carbonate chemistry samples from Maui, OahuKB, and OahuKN were collected by Silbiger. All other data were collected by CRED. N+N, Si, or PO data are not available for MauiA27.
[2] MauiA27 fish and benthic data were collected by DAR; biological data at all other sites were collected by CRED
[3] Photoquads were used for benthic cover estimates only at OahuKBay, OahuKN, Oahu10, Oahu4, and MauiA27

Table 2: Heirarchical ANOVA for accretion (a), erosion (b), and percent change in volume rates (c) across regions, islands, and sites. DF is degrees of freedom, SS is sum of squares, Mean SS is mean sum of squares, F is the F-test, and p is the p-value. Bold values represent statistically significant differences at $\alpha < 0.05$.

Model	DF	SS	Mean SS	F	p
a) Accretion					
Region	1	0.025	0.25	1.26	0.27
Island:Region	4	5.48	1.37	7.03	**<0.001**
Site:Island:Region	23	8.55	0.37	1.91	**0.01**
Residuals	93	18.11	0.19		
b) Erosion					
Region	1	7.15	7.15	20.18	**<0.001**
Island:Region	4	3.41	0.85	2.4	0.055
Site:Island:Region	23	35.6	1.55	4.37	**<0.001**
Residuals	93	32.96	0.35		
c) Percent change in volume					
Region	1	65.1	65.14	2.76	0.1
Island:Region	4	374.2	93.56	3.97	**0.005**
Site:Island:Region	21	1641.7	71.38	3.03	**<0.001**
Residuals	93	2215.1	23.57		

Table 3: Means and standard errors for erosion, accretion, and percent change in volume rates across regions (a) and sites (b).

	Accretion (mm y^{-1})		Erosion (kg m^{-2} y^{-1})		Net Change (% y^{-1})	
	Mean	**Std**	**Mean**	**Std**	**Mean**	**Std**
(a) Region						
MHI	1.72	0.12	0.15	0.02	1.29	1.06
NWHI	1.86	0.11	0.092	0.009	2.82	0.60
(b) Site						
MAI	1.98	0.20	0.15	0.03	2.87	1.94
OAH	1.52	0.14	0.15	0.02	0.05	1.11
FFS	1.49	0.13	0.12	0.02	0.79	1.31
LIS	2.92	0.34	0.074	0.02	6.3	1.62
PHR	1.65	0.17	0.094	0.01	2.23	1.12
KUR	1.64	0.09	0.072	0.007	2.82	0.30

Table 4: ANOVA table for hierarchical multivariate generalized linear model with negative binomial distribution for community across regions and islands. Volume is the rubble volume from each site. Bold values indicate statistical significance at $\alpha < 0.05$.

Model	**Residual DF**	**DF**	**F**	**p**
Community data				
Region	27	1	139.4	**0.001**
Island:Region	22	10	16.9	**0.001**
Volume	26	1	38.8	0.231
Intercept	28			

Table 5: Model selection for infaunal community composition versus chemical, biological, physical, and all environmental parameters. Models outputs are from multivariate GLMs with a negative binomial distribution. *Vol* is volume of rubble from each site. *PC1* is the first PC axis and *PC2* is the second PC axis from the chemical (Fig 2a and 3a), biological (Fig 2b and 3b), physical (Fig 2c and 3c) and all data (Fig 2d and 3d) PCAs. k is the number of parameters in the model, -ʟ is the sum of all the log likelihoods across all families, AIC is the sum of all the AIC values across families, ΔAIC is the difference from the lowest AIC value, and rank is the rank of the model with 1 being the best.

Model	k	-ʟ	AIC	ΔAIC	Rank
Chemical *Y ~ Vol + PC1 + PC2*	150	955.09	2210.17	0	1
Biological *Y ~ Vol + PC1 + PC2*	150	993.64	2227.28	17.1	2
Full *Y ~ Vol + PC1 + PC2*	150	969.01	2238.02	27.84	3
Physical *Y ~ Vol + PC1 + PC2*	150	975.12	2250.25	40.07	4

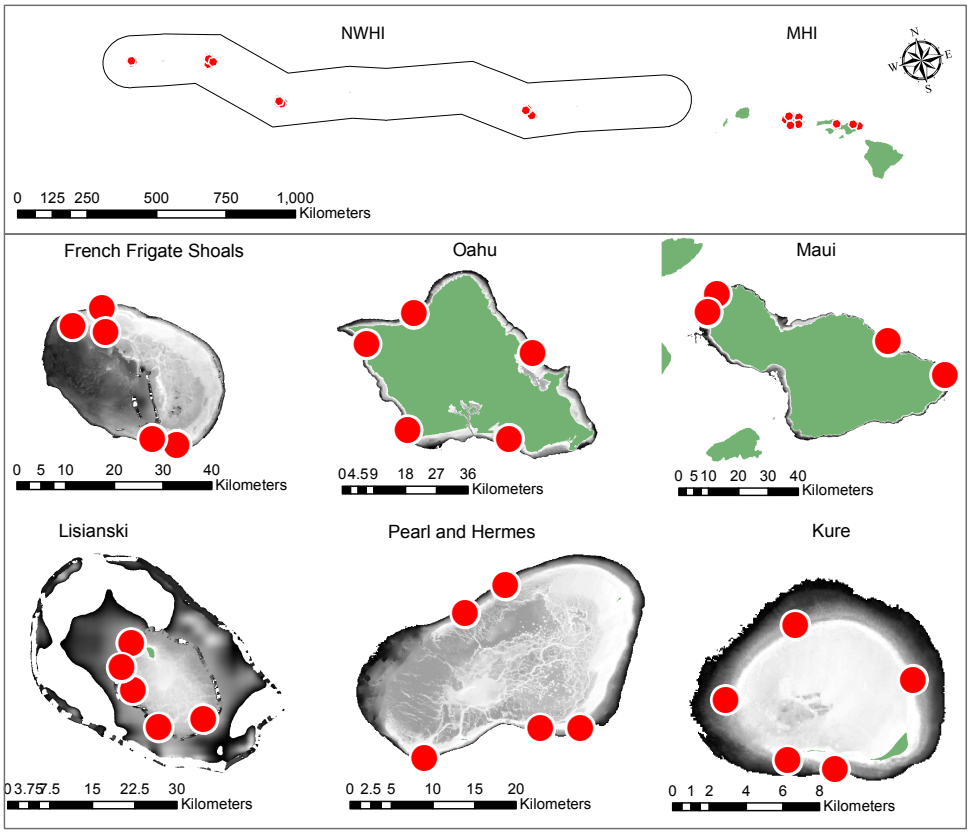

Figure 1: Map of 29 forereef sites across the Hawaiian Archipelago. Top inset shows the extent of the Hawaiian Archipelago (area outlined in black is the Papahānaumokuākea Marine National Monument). Maui and O‘ahu are in the Main Hawaiian Islands region and French Frigate Shoals, Lisianksi Atoll, Pearl and Hermes Atoll, and Kure Atoll are in the Northwestern Hawaiian Islands region. Red dots are individual sites. Grey areas in maps are 0-40m bathymetry data from NOAA CRED.

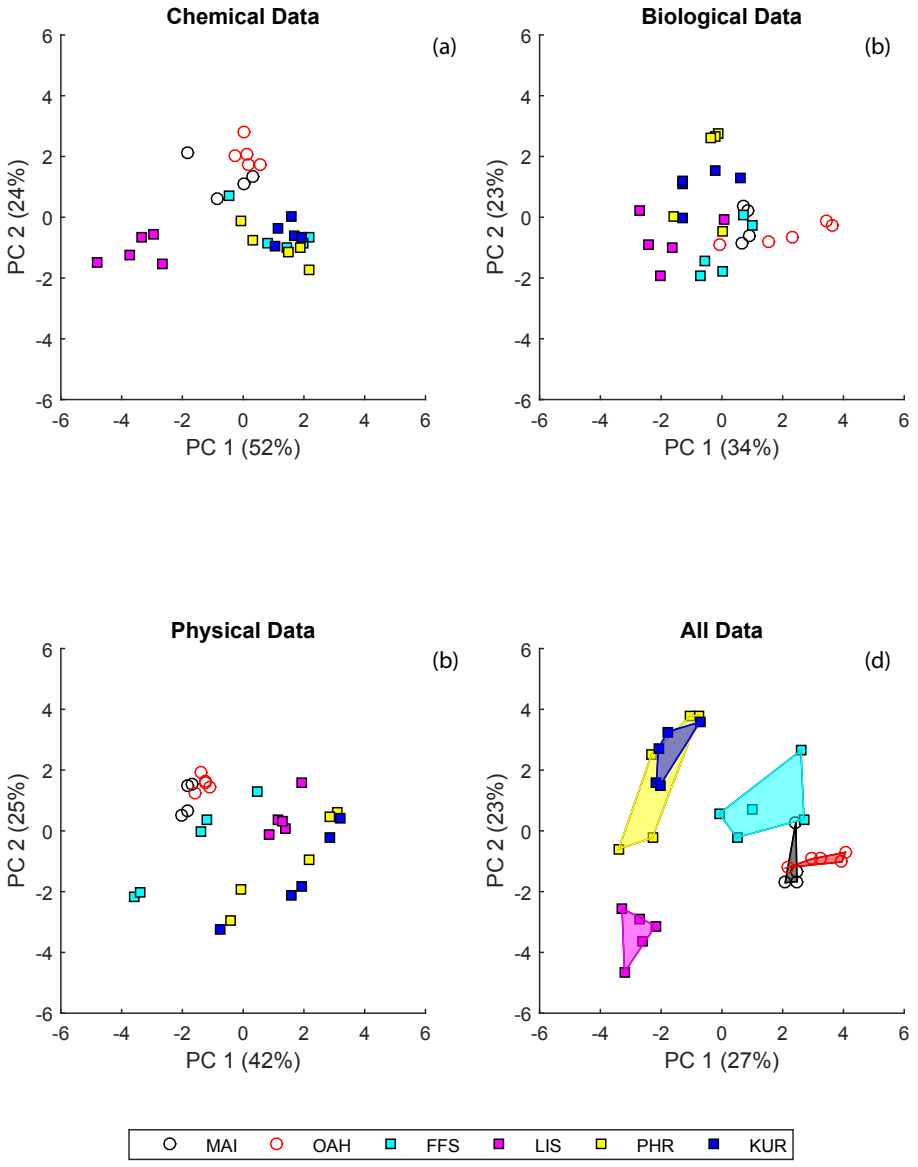

Figure 2: PCA for (a) chemical, (b) biological, (c) physical, and (d) all environmental data. Each PCA is a combination of all environmental parameters for chemical (Table 1a), biological (Table 1c), physical (Table 1b), and all 23 parameters collected. Open circles are sites from the MHI and closed squares are sites from the NWHI. Colors represent different islands. X-axis is the first principal component and y-axis is the second principal component. Numbers in parentheses are the percent of variance explained by each PC axis. Biplots of each PCA are in Fig 3. Polygons in inset (d) represent data from individual islands.

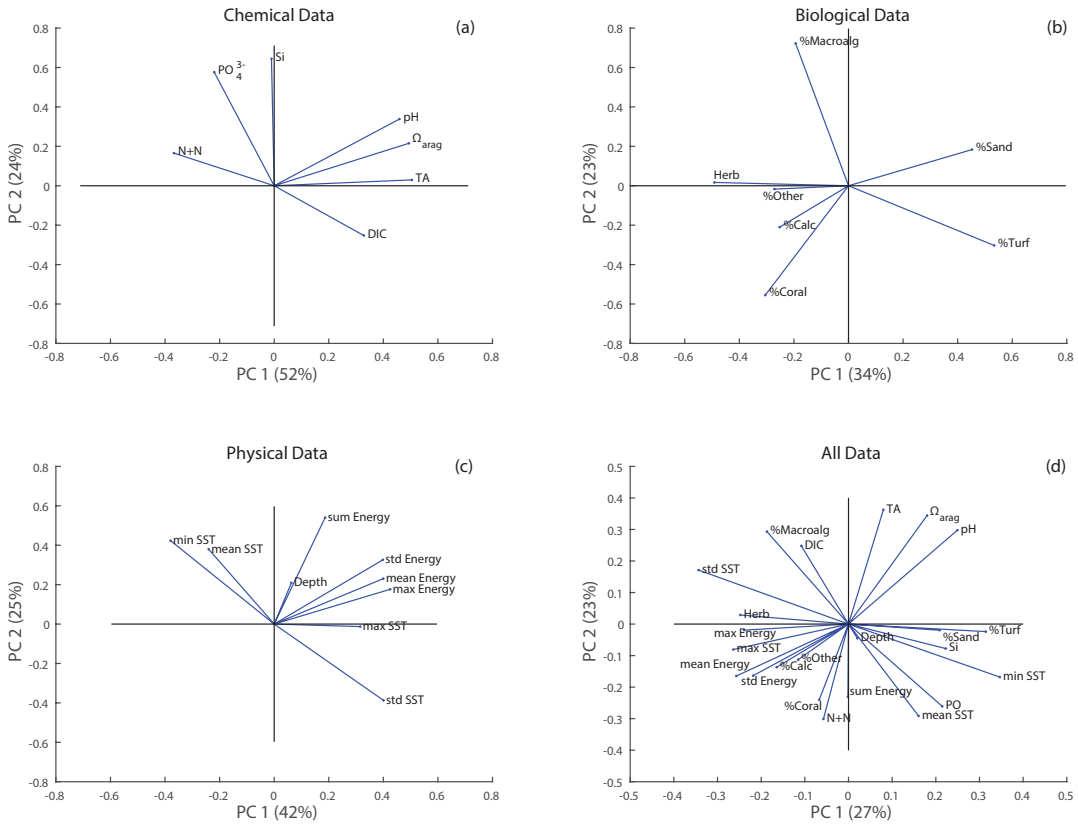

Figure 3: Biplot for (a) chemical, (b) biological, (c) physical, and (d) all environmental data. X-axis is the first principal component and y-axis is the second principal component. Numbers in parentheses are the percent variance explained by each PC axis. Lines are the loadings for each environmental parameter.

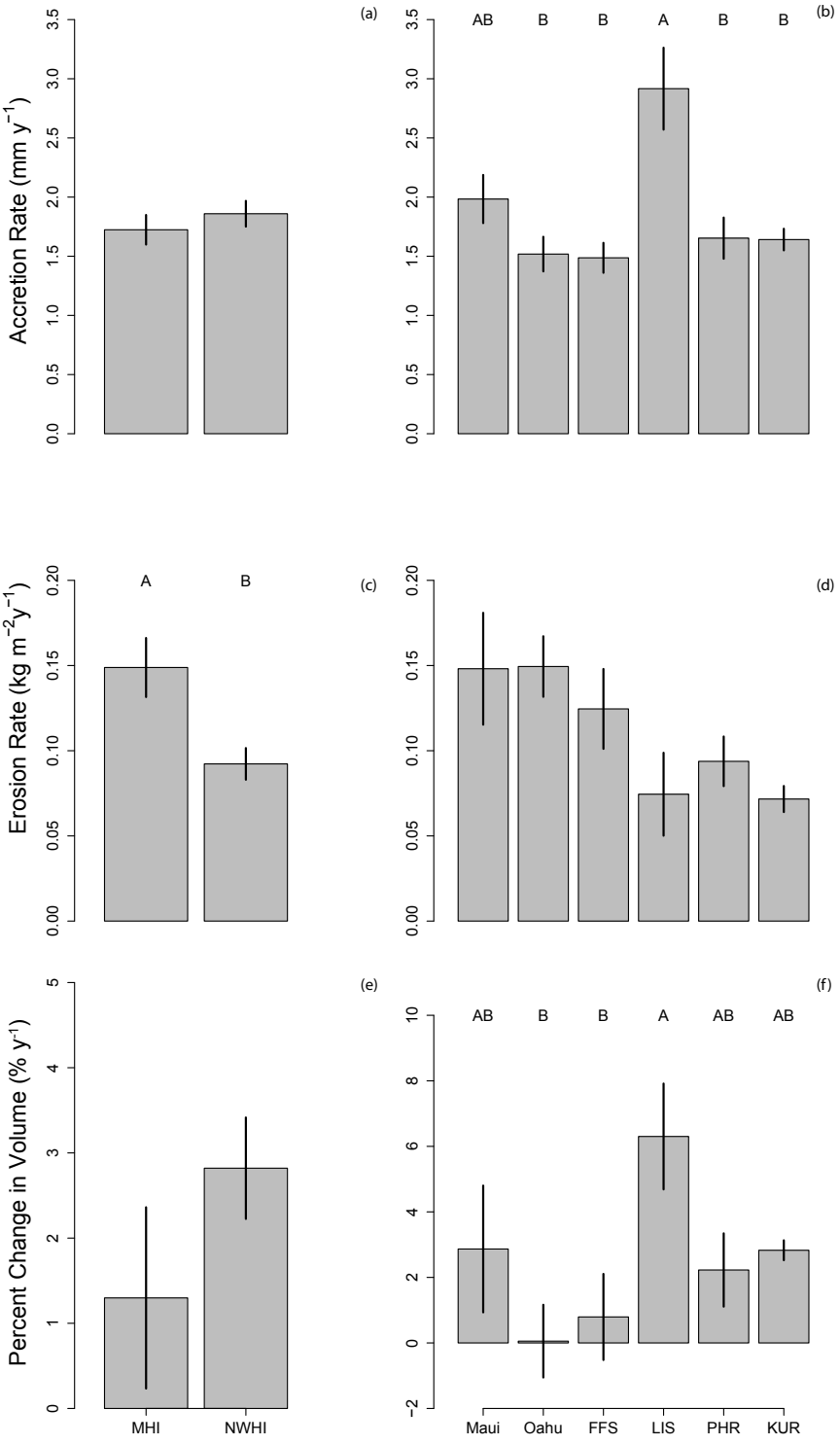

Figure 4: Means ± SE for (a,b) accretion, (c,d) erosion, and (e,f) percent change in volume across (a,c,e) regions and (b,d,f) islands. Data were log-transformed in the analysis and were back-transformed in this figure. There was a significant difference across region for erosion (Table 2b), but not accretion and percent change in volume. There was a significant difference across islands for accretion and percent change in volume (Table 2a,c), but not erosion. Letters are from pairwise comparisons from a TukeyHSD post-hoc test. Means with different letters are statistically different from each other.

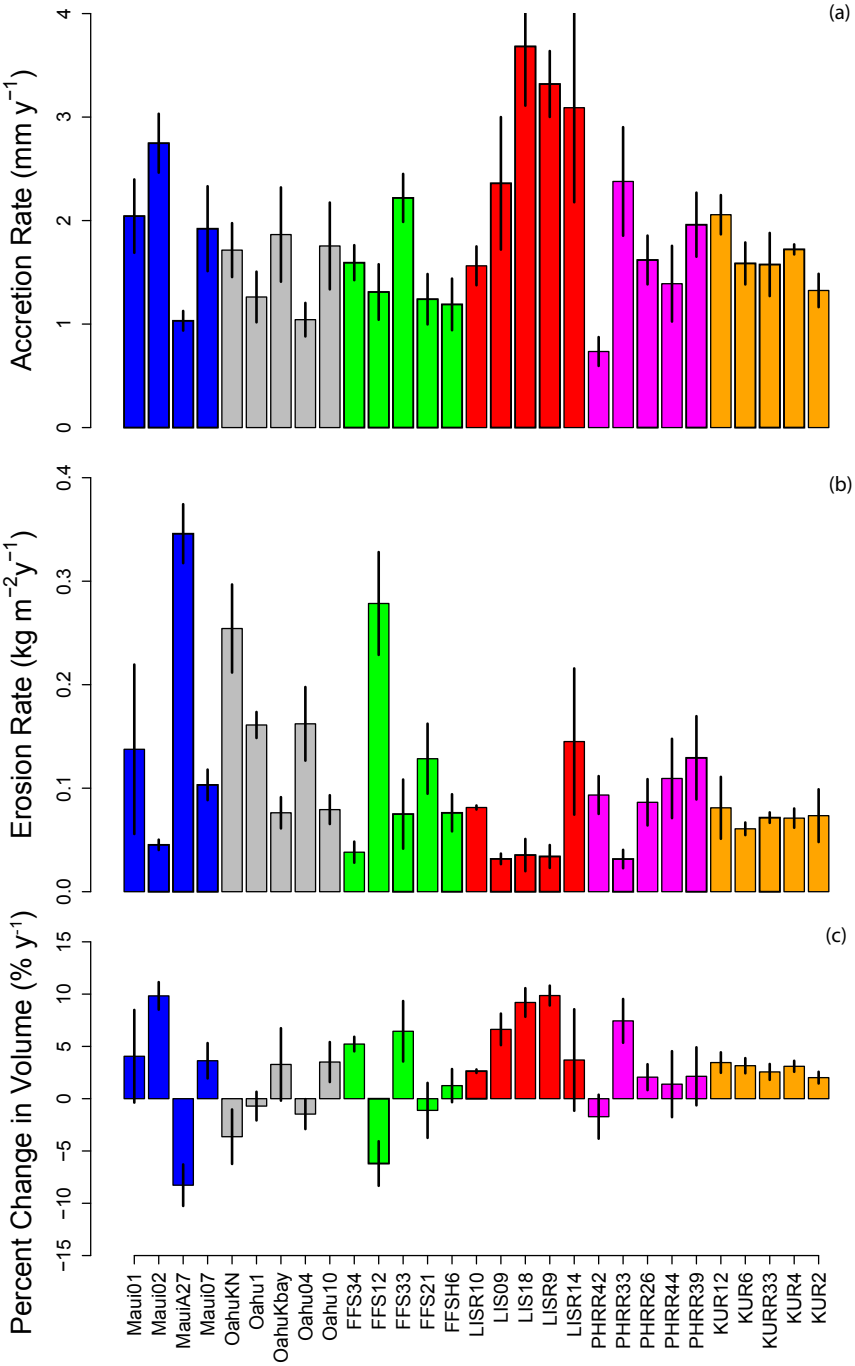

Figure 5: Means ± SE for (a) accretion, (b) erosion, and (c) percent change in volume across sites. Accretion and erosion data are log-transformed in the data analysis and were back-transformed in this figure. Sites are show in order of latitude where bars in blue are from Maui, grey are from O‘ahu, green are from French Frigate Shoals, red are from Lisianski, purple are from Pearl and Hermes, and orange are from Kure. There were statistically significant differences across sites for accretion, erosion, and percent change in volume (Table 2). For percent change in volume, positive values were net accreting while sites with negative values were net eroding over the deployment period

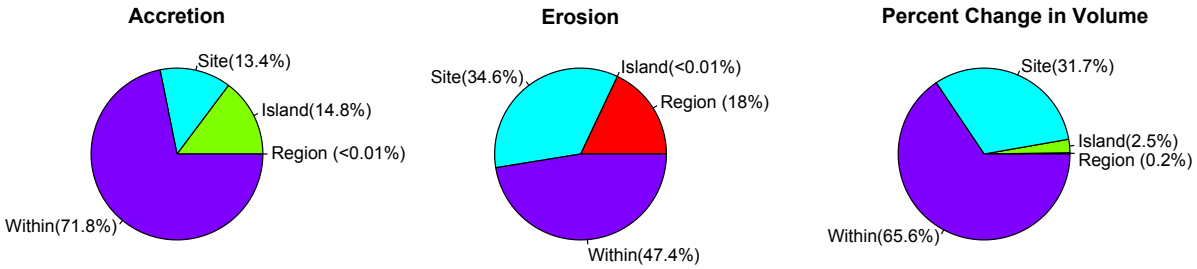

Figure 6: Variance components analysis for accretion, erosion, and percent change in volume across all spatial scales. Dark blue is within site level variation, light blue is site within island variation, green is island within region variation, and red is within region variation. The highest percent of variation in the data was at the within site scale for accretion, erosion, and percent change in volume

Figure 7: ΔAIC values for environmental models versus (a,b,c) accretion, (d,e,f) erosion, and (g,h,i) percent change in volume for (a,d,g) all sites, (b,e,h) the MHI, and (c,f,g) the NWHI. Each inset shows the top five highest ranking models for each model selection with bars representing individual environmental models. Full model selections are available in Tables S3-5. X-axes are the ΔAIC values with 0 being the best model. Models with a ΔAIC of >4 had little to no empirical support. Y-axes list the environmental models. Numbers inside each bar are R^2 values and the signs in the parentheses represent the direction of the relationships from the linear models. Models with a (+) had a positive slope and models with a (-) had a negative slope. Colors represent the environmental group: pink are chemical drivers, yellow are physical drivers, and blue are biological drivers.

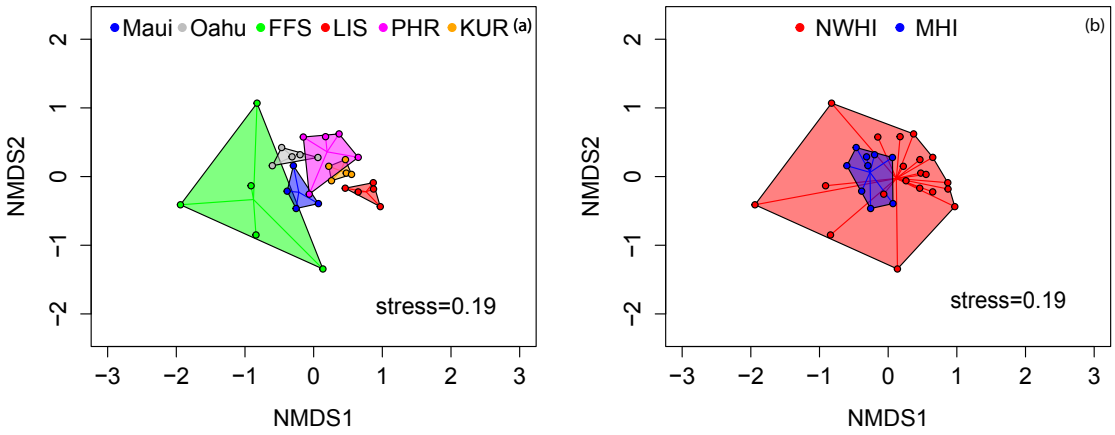

Figure 8: nMDS for macroborer community data by (a) island and (b) region. Communities were significantly different across both islands ($F_{22,10}$=16.9, p=0.001; Table 5) and regions ($F_{27,1}$=139.4, p=0.001; Table 5). In inset (a), colors represent islands where Maui is blue, O‘ahu is grey, French Frigate Shoals is green, Lisianski is red, Pearl and Hermes is purple, and Kure is orange. For inset (b), colors represent regions where the NWHI sites are in red and the MHI sites are in blue. Stress for the nMDS was 0.19.

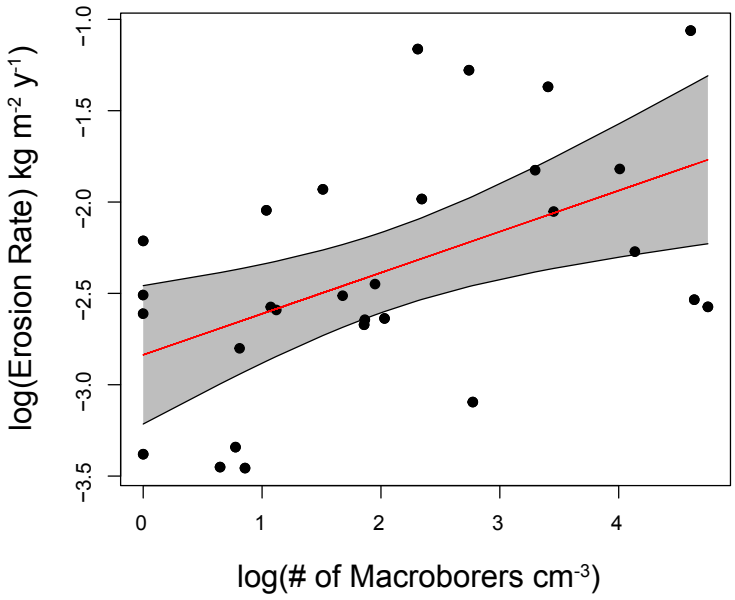

Figure 9: Erosion rate versus bioeroder abundance. Figure shows a linear regression for abundance of bioeroders versus erosion rate. Abundances were log (x+1) transformed and erosion rates were log (x) transformed here and in the analysis. Red line is the best fit line and grey lines are 95 % confidence intervals. There was a significant linear relationship between the abundance of macroborers (Table S2) and erosion rate ($F_{27,1}$ = 9. 45, p=0.005, R^2=0.26, $y \sim 0.22x - 2.83$).

Supplemental Material
Methods for environmental data collection
Tables S1-S6
References
Figures S1-S6

Methods for environmental data collection:

Chemical Data: Discrete water samples for silica (Si), phosphate (PO), nitrate + nitrite (N+N), total alkalinity (TA), dissolve inorganic carbon (DIC), and salinity were collected at each site from benthic water with horizontally oriented 5L Niskin® bottles fired directly above the substrate (Table 1a). At most sites (Table 1), these samples were co-located with conductivity, temperature and depth (CTD) casts. TA and DIC samples were immediately decanted into Tedlar bags or BOD bottles, fixed with $HgCl_2$, and then stored in a cool, dark area until further processing. All nutrient samples were filtered through combusted GF/F filters, stored in acid-washed HDPE bottles, and frozen until processing. Salinity samples were decanted into HDPE bottles, wrapped in parafilm, and stored in a cool, dark location until processing. All NWHI and most MHI samples were collected as part of the NOAA Pacific Reef Assessment and Monitoring Program (RAMP) monitoring efforts from 2008 – 2010 and were collected and analyzed using standard protocols. Some samples from Maui and O‘ahu (Table 1) were collected following similar protocols in 2013 - 2014. All NOAA-RAMP samples were analyzed at NOAA Pacific Marine Environmental Laboratory (PMEL); the remaining samples were analyzed at the University of Hawai‘i SOEST Laboratory for Analytical Chemistry (UH S-LAB) and at the Hawai‘i Institute of Marine Biology. All samples were analyzed using standard protocols (Dickson et al. 2007). pH and aragonite saturation states (Ω_{arag}) for each site were calculated in CO2SYS (van Heuven et al. 2011) with the temperature, salinity, TA, and DIC as parameters.

Any site that had more than one water sample taken during this time period was averaged for data analysis (Table S6).

Physical Data: The physical data includes depth, sea surface temperature (SST) metrics, and wave power (E_f) metrics (Table 1b). Depth was measured by placing a dive computer in the middle of each site and recording the depth. SST data was compiled from ultra-high resolution (1 km grid) satellite data from the G1SST dataset (http://oceanwatch.pfeg.noaa.gov/thredds/dodsC/satellite/JS/ssta/1day.html). The G1SST dataset is a blended (across eight satellites) global dataset produced by the Regional Ocean Modeling System group at the Jet Propulsion Laboratory. We extracted SST data for the deployment period at each site and used an ordinary kriging method with a spherical semivariogram model to average over missing values using ArcGIS (version 10.1). SST data from each site was used to calculate the mean, max, min, and standard deviation in temperature over the deployment period.

Wave power was calculated for the deployment period at each site using a 1-hr output at a 0.5 × 0.5 degree resolution of mean significant wave height (H_s), peak period (t_p) and peak direction (d_p) from the Wavewatch III Global Wave Model (WWIII, http://oos.soest.hawaii.edu/erddap/griddap/NWW3_Global_Best.html). Wave power (*Ef*) in kilowatts per meter (kW m^{-1}) was calculated using the following equation:

$$E_f = \frac{\rho g^2}{64\pi} {H_s}^2 t_p / 1000 \qquad (1)$$

where, ρ is the density of seawater (1024 kg m^{-3}) and g is the acceleration of gravity. Previous studies suggest that wave power, which combines both H_s and t_p, is a more representative metric of wave events than using only H_s and t_p (Storlazzi et al. 2003; Storlazzi et al. 2005; Gove et al. 2013). Wave power statistics (mean, cumulative sum, max, and standard deviation) were

calculated from incident wave angles for each site. Note that this is a conservative method that ignores any wave energy caused by wave-bathymetry interactions (e.g. refraction).

Biological Data: Herbivorous fish biomass and benthic cover (Table 1c) data were used to describe the biological characteristics of each site. Herbivorous fish biomass was estimated from visual surveys of fish size and abundance throughout the MHI and NWHI from 2000-2014 using three different methods: fixed benthic transects by CRED (BLT_CRED), fixed benthic transects by DAR (BLT_DAR), and stratified random stationary point count by CRED (nSPC). CRED methods are described in Williams et al. (2010) and the DAR method is described in Walsh et al. (2010). Fish biomass (kg m^{-2}) for each species was calculated using conversion parameters from the literature (Kulbicki et al. 2005; Froese and Pauly 2010), and fish biomass data were standardized to the BLT_CRED method using conversion factors from M. Donovan (unpub). CRED pools their data by trophic functional group (herbivore, invertivore, apex predator, planktivore, and corallivore) and by depth zone (shallow= 0 - 6 m, mid=6 - 18 m, deep=18 - 30 m). We restricted our analysis to herbivore biomass from the mid depth zone (6 - 18 m) because herbivorous grazers are the functional group most likely to impact accretion-erosion processes and the mid depth zone overlapped with the depth of our sites. To calculate herbivore biomass for each site, we used a distance-weighted average for all fish transects within 3km of our study site for all years:

$$Biomass_x = \sum_{i=1}^{n} Biomass_i/(1 + Distance_{ix}), \quad (2)$$

where $Biomass_x$ is estimated herbivore biomass at site *x*, $Biomass_i$ is the measured herbivore biomass at fish transect *i*, and $Distance_{ix}$ is the distance from sampling site *x* to fish transect *i*

Benthic cover was measured at each site using the least point intercept (LPI) method (collected in 2010 by CRED) or the photoquadrat method (collected in 2010 – 2012 by CRED or DAR). The LPI method uses visual surveys of benthic cover along a 25 m transect. The species (or lowest possible taxonomic unit) that fell directly under the transect tape was recorded every 0.5 m along the transect. For sites where LPI data was unavailable, we used photoquad data (Table 1c; methods described in Walsh et al. (2010)). All benthic data were pooled into 5 categories for data analysis: % coral, % calcified algae, % macroalgae, % turf algae, % sand, and % other (mobile invertebrates, cyanobacteria, and unidentified sessile organisms).

REFERENCES

Dickson AG, Sabine CL, Christian JR (2007) Guide to best practices for ocean CO_2 measurements

Froese R, Pauly D (2010) "FishBase," World Wide Web electronicpublication., http://www.fishbase.org/search.php

Gove JM, Williams GJ, McManus MA, Heron SF, Sandin SA, Vetter OJ, Foley DG (2013) Quantifying climatological ranges and anomalies for Pacific coral reef ecosystems. PloS one 8:e61974

Kulbicki M, Guillemot N, Amand M (2005) A general approach to length-weight relationships for New Caledonian lagoon fishes. Cybium 29:235-252

Storlazzi CD, Logan JB, Field ME (2003) Quantitative morphology of a fringing reef tract from high-resolution laser bathymetry: Southern Molokai, Hawaii. Geological Society of America Bulletin 115:1344-1355

Storlazzi CD, Brown EK, Field ME, Rodgers K, Jokiel PL (2005) A model for wave control on coral breakage and species distribution in the Hawaiian Islands. Coral Reefs 24:43-55

van Heuven S, Pierrot D, Rae JWB, Lewis E, Wallace DWR (2011) MATLAB Program developed for CO2 system calculations Rep ORNL/CDIAC-105b, Carbon Dioxide Inf. Anal.Cent., Oak Ridge Natl. Lab., US DOE, Oak Ridge, Tenn.

Walsh W, Cotton S, Barnett C, Couch C, Preskitt L, Tissot B, Osada-D'Avella K (2010) Long-term monitoring of coral reefs of the Main Hawaiian Islands. Honolulu, Hawaii: Department of Land and Natural Resources 133

Williams ID, Richards BL, Sandin SA, Baum JK, Schroeder RE, Nadon MO, Zgliczynski B, Craig P, McIlwain JL, Brainard RE (2010) Differences in reef fish assemblages between populated and remote reefs spanning multiple archipelagos across the central and western Pacific. Journal of Marine Biology 2011

Table S1: Site information. These are the latitudes, longitudes, and depths for each site and well as the deployment and retrieval dates for experimental blocks and collection dates for rubble used in community analysis. Five blocks were deployed at all sites, but some blocks were not retrieved or did not have adequate quality µCT scans. Sample size is the number of blocks that were used in the analysis from each site.

Site	Latitude	Longitude	Depth (m)	Deployment Date	Retrieval Date	Sample size	Rubble Collection Date
Maui-01	20.762	-155.980	32	9/8/2012	9/30/2013	5	9/30/2013
Maui-02	20.864	-156.151	42	9/8/2012	9/30/2013	5	9/30/2013
Maui-A27	20.951	-156.694	46	9/26/2012	9/29/2013	4	9/29/2013
Maui-07	21.007	-156.668	45	9/9/2012	9/29/2013	5	9/29/2013
O‘ahu-KN	21.289	-157.865	38	10/16/2012	10/8/2013	5	10/8/2013
O‘ahu-1	21.312	-158.127	43	9/13/2012	9/12/2013	5	9/12/2013
O‘ahu-Kbay	21.508	-157.805	47	9/20/2012	9/26/2013	5	9/26/2013
O‘ahu-04	21.534	-158.233	43	9/10/2012	9/12/2013	5	9/12/2013
O‘ahu-10	21.612	-158.111	48	9/2/2012	9/9/2013	4	9/9/2013
FFS-34	23.628	-166.135	30	7/27/2011	8/6/2012	4	7/8/2012
FFS-12	23.639	-166.180	35	7/27/2011	8/4/2012	5	7/8/2012
FFS-33	23.837	-166.267	27	7/28/2011	8/5/2012	4	7/9/2012
FFS-21	23.847	-166.327	40	7/28/2011	8/5/2012	4	7/9/2012
FFS-H6	23.880	-166.273	25	7/28/2011	8/5/2012	5	7/9/2012
LIS-R10	25.945	-173.954	44	8/10/2011	8/17/2012	2	8/17/2012
LIS-09	25.958	-173.882	44	8/10/2011	8/17/2012	3	8/17/2012
LIS-18	26.004	-173.994	27	8/10/2011	8/18/2012	3	8/18/2012
LIS-R9	26.040	-174.012	25	8/11/2011	8/18/2012	3	8/18/2012
LIS-R14	26.078	-173.997	46	8/11/2011	8/18/2012	5	8/18/2012
PHR-R42	27.753	-175.949	45	8/9/2011	8/12/2012	3	7/13/2012
PHR-R33	27.785	-175.824	44	8/9/2011	8/12/2012	3	8/12/2012
PHR-R26	27.786	-175.780	49	8/9/2011	8/12/2012	5	8/12/2012
PHR-R44	27.910	-175.905	42	8/8/2011	8/9/2012	3	7/13/2012
PHR-R39	27.940	-175.861	34	8/8/2011	8/9/2012	5	7/13/2012
KUR-12	28.382	-178.324	33	8/15/2012	7/14/2013	4	7/14/2013
KUR-6	28.387	-178.348	32	8/15/2012	7/13/2013	4	7/13/2013
KUR-R33	28.417	-178.378	50	8/14/2012	7/14/2013	4	7/14/2013
KUR-4	28.427	-178.286	36	8/14/2012	7/13/2013	5	7/13/2013
KUR-2	28.454	-178.344	39	8/14/2012	7/14/2013	5	7/14/2013

Table S2: List of all organisms included in community analysis. If there is a "yes" in the bioeroder column, organisms are known bioeroders (pers. com. S. Godwin). All organisms listed here were used in the community analysis. Only known bioeroders were used in linear regression between erosion rates and macroborers. UNID stands for unidentified. Codes in parenthesis are the 3 letter codes from Fig S6a. Count is the total number of organisms across all sites from each species.

Common Name	Bioeroder?	Family	Genus	Species	Count
Bivalve	Yes	Arcidae (Arc)	*Arca*	*ventricosa*	1
			Barbatia	*divaricata*	45
		Gastrochaenidae (Gas)	*Gastrochaena*	*cuneiformis*	8
				kanaka	2
		Hiatellidae (Hia)	*Hiatella*	*arctica*	7
		Hipponicidae (Hip)	*Hipponix*	*foliaceus*	2
		Mytilidae (Myt)	*Lithophaga*	*fasciola*	168
	No	Mytilidae (Myt)	*Brachidontes*	*crebristriatus*	6
Polychaete	Yes	Eunicidae (Eun)	*Palola*	*siciliensis*	30
		Sabellidae (Sab)	*Hypsicomus*	*phaeotaenia*	32
	No	Dorvellidae (Dor)	*UNID*	*UNID*	2
		Amphinomidae (Amp)	*Eurythoe*	*complanata*	3
			Notopygos	*gregoryi*	1
				UNID	3
			Pherecardia	*striata*	5
			UNID	*UNID*	15
		Capitellidae (Cap)	*UNID*	*UNID*	4
		Chaetopteridae (Cha)	*Mesochaetopterus*	*sagittarius*	2
			Phyllochaetopterus	*socialis*	2
				verrilli	2
			UNID	*UNID*	1
		Chrysopetellidae (Chr)	*UNID*	*UNID*	22
		Cirratulidae (Cir)	*UNID*	*UNID*	8
		Dorvellidae (Dor)	*Dorvillea*	*angolana*	1
			UNID	*UNID*	25
		Eunicidae (Eun)	*Eunice*	*afra*	5
				antennata	9
				australis	4
				cariboea	2
				nicicoformis	1
			Lysidice	*ninetta*	32
			Marphysa	*UNID*	19
			Nematoneris	*unicornis*	227

			UNID	*UNID*	159
		Glyceridae (Gly)	*Glycera*	*tesselata*	6
			UNID	*UNID*	4
		Lumbrineridae (Lum)	*Lumbrineris*	*dentata*	5
			UNID	*UNID*	7
		Maldanidae (Mal)	*UNID*	*UNID*	22
		Nereidae Ner)	*Ceratoneris*	*tentaculata*	2
			Neanthes	*arenaceodonta*	5
			UNID	*UNID*	144
		Opheliidae (Oph)	*UNID*	*UNID*	2
		Phyllodocidae (Phy)	*UNID*	*UNID*	32
		Polynoidae (Pol)	*Iphione*	*muricata*	5
			Lepidasthenia	*alba*	2
			Lepidonotus	*havaicus*	1
			Thormora	*jukesii*	3
				UNID	2
			UNID	*UNID*	67
		Sabellidae Sab)	*Megalomma*	*intermedium*	1
			UNID	*UNID*	10
		Serpulidae (Ser)	*Pomatoleios*	*kraussii*	1
			Spirobranchus	*giganteus corn.*	4
			UNID	*UNID*	8
			Vermilopsis	*torquata*	4
		Spirorbiidae (Spi)	*Neodexiospira*	*foraminosa*	1
			Nidificaria	*dalestraughanae*	1
			UNID	*UNID*	65
		Syllidae (Syl)	*UNID*	*UNID*	418
		Terebellidae (Ter)	*Lysilla*	*ubianansis*	1
			UNID	*UNID*	13
Sipunculid	Yes	Aspidosiphonidae (Asp)	*Aspidosiphon*	*elegans*	279
			Lithacrosiphon	*cristatus*	39
		Phascolosomatidae (Pha)	*Phascolosoma*	*perlucens*	14
				stephensoni	8
				nigrescens	8
				scolops	2
				sp	2
			Antillesoma	*antillarium*	1
Urchin	Yes	Echinometridae (Echt)	*Echinometra*	*mathaei*	3
			Echinostrephus	*aciculatus*	2
	No	Echinoneidae (Ech)	*Echinoneus*	*cyclostomus*	13
		Eucidaridae (Euc)	*Eucidarus*	*metularia*	11

Table S3: Model selection for environmental parameters versus accretion. Pink are chemical parameters, blue are biological parameters, and yellow are physical parameters. The top five models are bolded and a star is next to the highest ranked model.

	Hawaiian Archipelago					MHI					NWHI				
Model	$\mathcal{L}$	**AIC**	**ΔAIC**	**R^2**	**Rank**	$\mathcal{L}$	**AIC**	**ΔAIC**	**R^2**	**Rank**	$\mathcal{L}$	**AIC**	**ΔAIC**	**R^2**	**Rank**
Si	-92.21	188.42	-22.08	0.000	22	-35.37	74.75	-4.20	0.057	8	-54.30	112.59	-26.85	0.001	20
N+N	-90.77	185.55	-19.20	0.023	9	-36.03	76.06	-5.52	0.028	15	-50.00	104.01	-18.27	0.104	6
PO	-92.14	188.28	-21.94	0.001	19	-35.52	75.04	-4.49	0.051	9	-50.80	105.61	-19.86	0.086	8
Ω_{arag}	-81.81	167.63	-1.28	0.157	**2**	-35.68	75.35	-4.80	0.044	10	-43.84	91.68	-5.94	0.233	**3**
pH	-82.54	169.08	-2.73	0.147	**3**	-36.07	76.14	-5.60	0.026	16	-43.90	91.80	-6.06	0.232	**4**
TA	-81.17	166.35	0.00	0.166	**1***	-35.88	75.76	-5.22	0.035	13	-40.87	85.74	0.00	0.289	**1***
DIC	-87.69	179.38	-13.03	0.072	**4**	-36.63	77.27	-6.72	0.000	22	-43.33	90.65	-4.91	0.243	**2**
Herb	-89.90	183.80	-17.46	0.037	7	-35.99	75.98	-5.43	0.030	14	-52.77	109.54	-23.79	0.039	10
%Coral	-92.18	188.36	-22.02	0.001	21	-36.63	77.26	-6.72	0.000	21	-54.33	112.65	-26.91	0.000	21
%Calc	-91.72	187.43	-21.09	0.008	14	-36.47	76.95	-6.40	0.008	18	-54.12	112.23	-26.49	0.006	18
%Macroalgae	-91.53	187.06	-20.72	0.011	13	-33.27	70.55	0.00	0.145	**1***	-54.34	112.69	-26.94	0.000	23
%Turf	-88.86	181.71	-15.37	0.054	6	-35.84	75.68	-5.14	0.036	12	-51.73	107.46	-21.71	0.064	9
%Sand	-92.16	188.31	-21.97	0.001	20	-36.56	77.12	-6.57	0.004	19	-53.78	111.55	-25.81	0.014	13
%Other	-88.44	180.89	-14.54	0.060	**5**	-36.59	77.19	-6.64	0.002	20	-49.93	103.86	-18.11	0.106	**5**
Depth	-90.53	185.05	-18.71	0.027	8	-35.24	74.48	-3.93	0.063	6	-53.73	111.46	-25.71	0.015	12
mean SST	-92.21	188.43	-22.08	0.000	23	-34.16	72.32	-1.77	0.109	**2**	-53.53	111.06	-25.31	0.020	11
max SST	-91.25	186.49	-20.15	0.016	11	-34.56	73.13	-2.58	0.092	**3**	-50.48	104.96	-19.22	0.093	7
min SST	-91.11	186.22	-19.87	0.018	10	-35.79	75.59	-5.04	0.039	11	-53.90	111.79	-26.05	0.011	16
std SST	-91.39	186.77	-20.43	0.014	12	-36.64	77.28	-6.73	0.000	23	-53.90	111.79	-26.05	0.011	15
mean Energy	-91.80	187.61	-21.26	0.007	16	-35.08	74.17	-3.62	0.070	**5**	-53.83	111.67	-25.93	0.013	14
max Energy	-92.08	188.16	-21.81	0.002	18	-36.30	76.60	-6.05	0.016	17	-54.07	112.14	-26.40	0.007	17
sum Energy	-91.80	187.59	-21.25	0.007	15	-34.82	73.64	-3.09	0.081	**4**	-54.33	112.65	-26.91	0.000	22
std Energy	-91.93	187.87	-21.52	0.005	17	-35.28	74.56	-4.01	0.061	7	-54.25	112.49	-26.75	0.002	19

Table S4: Model selection for environmental parameters versus erosion. Pink are chemical parameters, blue are biological parameters, and yellow are physical parameters. The top five models are bolded and a star is next to the highest ranked model.

	Hawaiian Archipelago					MHI					NWHI				
Model	$\mathcal{L}$	**AIC**	**ΔAIC**	**R^2**	**Rank**	$\mathcal{L}$	**AIC**	**ΔAIC**	**R^2**	**Rank**	$\mathcal{L}$	**AIC**	**ΔAIC**	**R^2**	**Rank**
Si	-145.45	294.90	-16.20	0.020	11	-43.88	91.77	-3.62	0.214	**2**	-91.77	187.53	-9.28	0.002	21
N+N	-146.67	297.33	-18.63	0.000	22	-49.01	102.01	-13.86	0.002	21	-91.63	187.26	-9.01	0.005	20
PO	-145.67	295.35	-16.65	0.017	13	-49.05	102.11	-13.96	0.000	23	-90.46	184.91	-6.66	0.034	**5**
Ω_{arag}	-145.66	295.32	-16.62	0.017	12	-48.50	100.99	-12.84	0.026	15	-91.58	187.16	-8.91	0.007	19
pH	-145.03	294.07	-15.37	0.027	10	-49.05	102.10	-13.95	0.000	22	-91.54	187.07	-8.83	0.008	17
TA	-146.42	296.84	-18.14	0.004	17	-48.82	101.64	-13.49	0.011	17	-90.74	185.48	-7.23	0.028	8
DIC	-146.63	297.26	-18.56	0.001	19	-45.60	95.20	-7.05	0.148	**5**	-88.64	181.27	-3.02	0.078	**2**
Herb	-137.35	278.70	0.00	0.142	**1***	-42.08	88.15	0.00	0.277	**1***	-91.84	187.68	-9.43	0.000	22
%Coral	-146.46	296.93	-18.23	0.004	18	-48.88	101.76	-13.61	0.008	18	-90.32	184.63	-6.39	0.038	**4**
%Calc	-146.67	297.34	-18.63	0.000	23	-48.97	101.94	-13.78	0.004	20	-91.48	186.96	-8.71	0.009	16
%Macroalgae	-140.91	285.82	-7.12	0.090	**5**	-45.31	94.61	-6.46	0.160	**3**	-90.84	185.67	-7.42	0.025	9
%Turf	-140.42	284.84	-6.14	0.098	**3**	-48.24	100.47	-12.32	0.037	14	-90.84	185.69	-7.44	0.025	10
%Sand	-146.37	296.74	-18.04	0.005	16	-48.93	101.85	-13.70	0.006	19	-89.77	183.55	-5.30	0.051	**3**
%Other	-142.09	288.18	-9.48	0.073	6	-47.72	99.45	-11.29	0.060	11	-87.12	178.25	0.00	0.113	**1***
Depth	-142.43	288.85	-10.15	0.068	7	-46.77	97.54	-9.39	0.101	8	-90.96	185.92	-7.67	0.022	11
mean SST	-144.86	293.73	-15.02	0.030	9	-45.98	95.97	-7.82	0.133	6	-91.84	187.68	-9.43	0.000	23
max SST	-146.30	296.60	-17.90	0.006	15	-45.59	95.17	-7.02	0.149	**4**	-91.36	186.72	-8.47	0.012	14
min SST	-139.46	282.92	-4.22	0.112	**2**	-47.01	98.03	-9.87	0.091	9	-90.96	185.93	-7.68	0.022	12
std SST	-140.46	284.92	-6.22	0.097	**4**	-47.63	99.26	-11.10	0.064	10	-91.41	186.81	-8.57	0.011	15
mean Energy	-146.66	297.32	-18.62	0.001	21	-48.22	100.45	-12.30	0.038	13	-91.06	186.13	-7.88	0.020	13
max Energy	-146.65	297.30	-18.60	0.001	20	-46.43	96.85	-8.70	0.115	7	-91.54	187.08	-8.84	0.008	18
sum Energy	-142.83	289.66	-10.96	0.061	8	-48.68	101.35	-13.20	0.017	16	-90.56	185.11	-6.87	0.032	6
std Energy	-146.19	296.38	-17.68	0.008	14	-48.09	100.18	-12.03	0.044	12	-90.72	185.44	-7.19	0.028	7

Table S5: Model selection for environmental parameters versus percent change in volume. Pink are chemical parameters, blue are biological parameters, and yellow are physical parameters. The top five models are bolded and a star is next to the highest ranked model.

	Hawaiian Archipelago					MHI					NWHI				
Model	$\mathcal{L}$	**AIC**	**ΔAIC**	**R^2**	**Rank**	$\mathcal{L}$	**AIC**	**ΔAIC**	**R^2**	**Rank**	$\mathcal{L}$	**AIC**	**ΔAIC**	**R^2**	**Rank**
Si	-390.35	784.69	-9.84	0.000	22	-43.88	91.77	-3.62	0.214	**2**	-243.24	490.48	-13.81	0.000	21
N+N	-389.98	783.96	-9.10	0.006	13	-49.01	102.01	-13.86	0.002	21	-241.04	486.09	-9.43	0.054	7
PO	-390.32	784.65	-9.80	0.000	19	-49.05	102.11	-13.96	0.000	23	-240.00	483.99	-7.33	0.079	**4**
Ω_{arag}	-387.19	778.38	-3.52	0.051	**3**	-48.50	100.99	-12.84	0.026	15	-240.25	484.51	-7.85	0.073	6
pH	-387.24	778.48	-3.62	0.050	**4**	-49.05	102.10	-13.95	0.000	22	-240.08	484.17	-7.51	0.077	**5**
TA	-387.53	779.05	-4.20	0.045	6	-48.82	101.64	-13.49	0.011	17	-238.09	480.19	-3.53	0.122	**2**
DIC	-389.38	782.77	-7.92	0.016	12	-45.60	95.20	-7.05	0.148	**5**	-236.33	476.66	0.00	0.160	**1**
Herb	-385.43	774.85	0.00	0.078	**1***	-42.08	88.15	0.00	0.277	**1***	-243.06	490.13	-13.47	0.004	18
%Coral	-390.16	784.32	-9.47	0.003	16	-48.88	101.76	-13.61	0.008	18	-242.63	489.26	-12.60	0.015	14
%Calc	-390.29	784.57	-9.72	0.001	17	-48.97	101.94	-13.78	0.004	20	-243.24	490.48	-13.82	0.000	22
%Macroalgae	-387.68	779.36	-4.51	0.043	7	-45.31	94.61	-6.46	0.160	**3**	-242.58	489.16	-12.50	0.017	13
%Turf	-386.97	777.95	-3.09	0.054	**2**	-48.24	100.47	-12.32	0.037	14	-241.05	486.10	-9.44	0.054	8
%Sand	-390.34	784.67	-9.82	0.000	20	-48.93	101.85	-13.70	0.006	19	-241.13	486.27	-9.61	0.052	9
%Other	-387.42	778.84	-3.99	0.047	**5**	-47.72	99.45	-11.29	0.060	11	-239.28	482.56	-5.90	0.095	**3**
Depth	-388.22	780.45	-5.59	0.034	9	-46.77	97.54	-9.39	0.101	8	-242.65	489.30	-12.64	0.015	15
mean SST	-390.07	784.15	-9.30	0.005	14	-45.98	95.97	-7.82	0.133	6	-243.13	490.26	-13.60	0.003	20
max SST	-390.12	784.25	-9.39	0.004	15	-45.59	95.17	-7.02	0.149	**4**	-241.38	486.77	-10.10	0.046	10
min SST	-388.11	780.22	-5.37	0.036	8	-47.01	98.03	-9.87	0.091	9	-242.15	488.29	-11.63	0.027	11
std SST	-388.38	780.76	-5.91	0.032	10	-47.63	99.26	-11.10	0.064	10	-242.42	488.85	-12.19	0.020	12
mean Energy	-390.29	784.59	-9.73	0.001	18	-48.22	100.45	-12.30	0.038	13	-243.24	490.48	-13.82	0.000	23
max Energy	-390.35	784.70	-9.85	0.000	23	-46.43	96.85	-8.70	0.115	7	-243.05	490.10	-13.44	0.005	17
sum Energy	-389.23	782.46	-7.61	0.018	11	-48.68	101.35	-13.20	0.017	16	-242.98	489.96	-13.30	0.007	16
std Energy	-390.35	784.69	-9.84	0.000	21	-48.09	100.18	-12.03	0.044	12	-243.10	490.20	-13.54	0.003	19

Table S6: Collections dates for nutrient and carbonate chemistry samples.

Site	Date Collected	Samples collected
Maui-01	10/15/2010	All
	9/30/2013	TA/DIC
Maui-02	10/16/2010	All
	9/30/2013	TA/DIC
Maui-07	10/18/2010	All
	9/29/2013	TA/DIC
Maui-A27	9/29/2013	TA/DIC
O‘ahu-04	9/18/2013	TA/DIC
	11/6/2014	N+N/PO/Si
O‘ahu-1	10/25/2010	All
	11/6/2014	N+N/PO/Si
O‘ahu-10	8/18/2013	TA/DIC
	11/5/2014	N+N/PO/Si
O‘ahu-Kbay	9/26/2013	TA/DIC
	11/10/2014	N+N/PO/Si
O‘ahu-KN	10/8/2013	TA/DIC
	11/5/2014	N+N/PO/Si
FFS-12	9/9/2010	All
FFS-21	9/8/2010	All
FFS-33	10/9/2008	All
FFS-34	9/10/2010	All
FFS-H6	9/8/2010	All
LIS-09	9/24/2010	All
LIS-18	9/23/2010	All
LIS-R10	9/23/2010	All
LIS-R14	9/23/2010	All
LIS-R9	9/24/2010	All
PHR-R26	9/14/2010	All
PHR-R33	9/15/2010	All
PHR-R39	9/15/2010	All
PHR-R42	9/16/2010	All
PHR-R44	9/16/2010	All
KUR-12	9/19/2010	All
KUR-2	9/20/2010	All
KUR-4	9/20/2010	All
KUR-6	9/20/2010	All
KUR-R33	9/19/2010	All

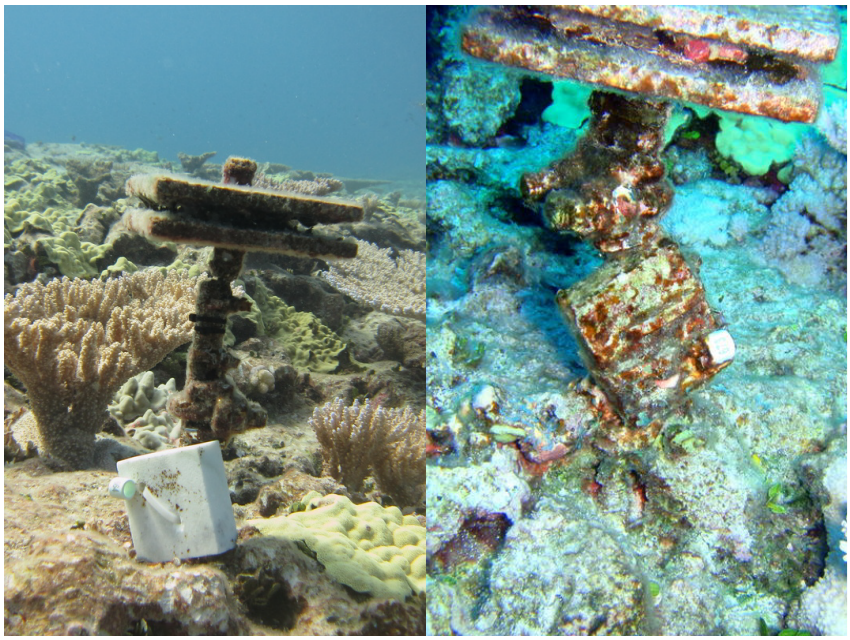

Figure S1:Before (left) and after (right) image of an experimental block.

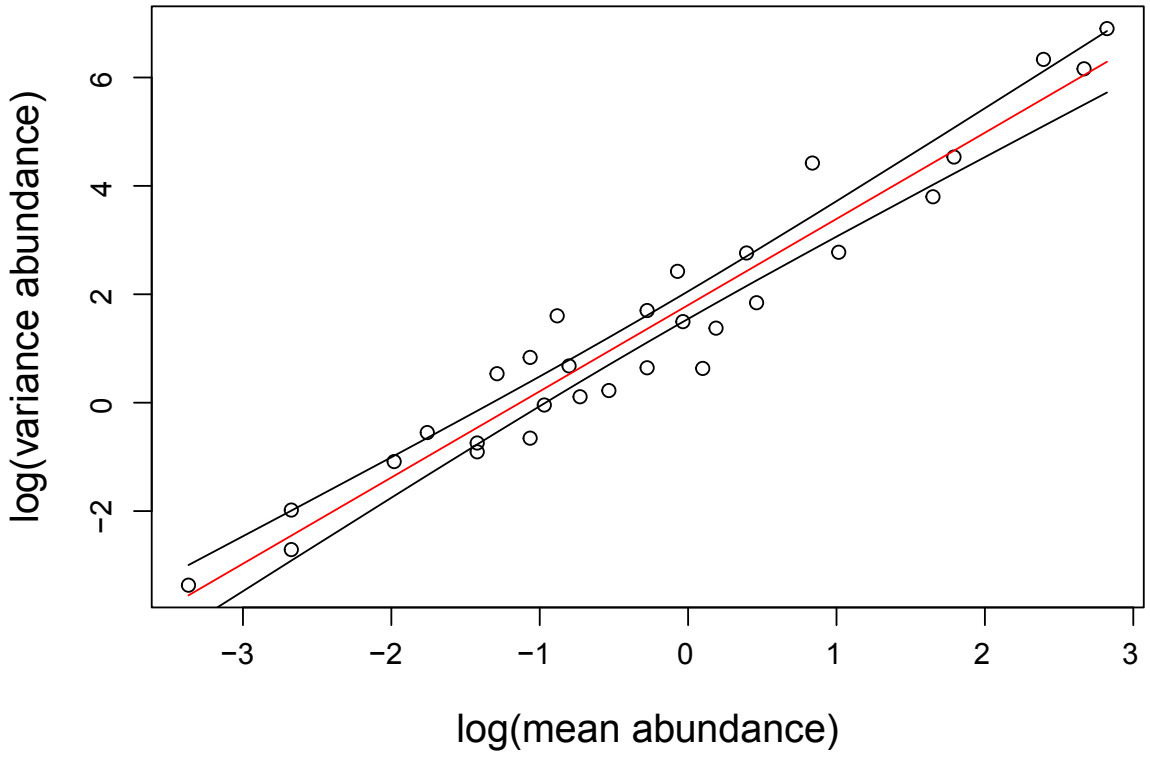

Figure S2: Mean-variation relationship of community data. Data are log-transformed mean and variance for all 29 families across all sites. Log(mean) and log(variance) are highly collinear ($F_{28,1}$=399, p<0.0001, R^2=0.94) suggesting that a negative binomial distribution is most appropriate.

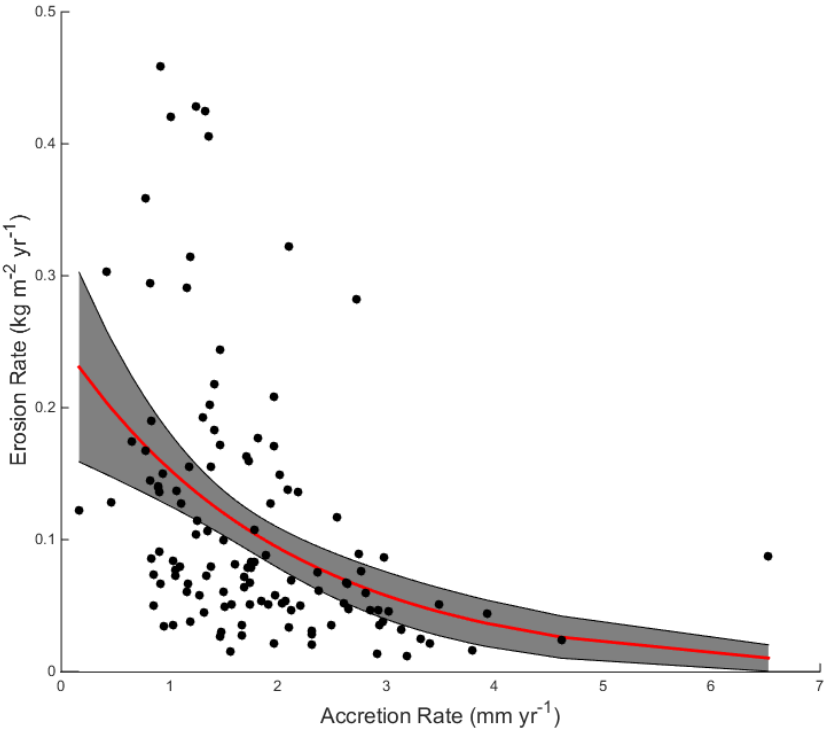

Figure S3: Erosion versus accretion. There was a significant exponential relationship between accretion rate (mm y^{-1}) and erosion rate (kg m^{-2} y^{-1}) across all experimental blocks ($F_{120,2}$ = 99, p<0.001, R^2 = 0.19, $y \sim 0.25 \times e^{(-0.49x)}$). We used a combined error model to account for the heteroscedasticity in the data.

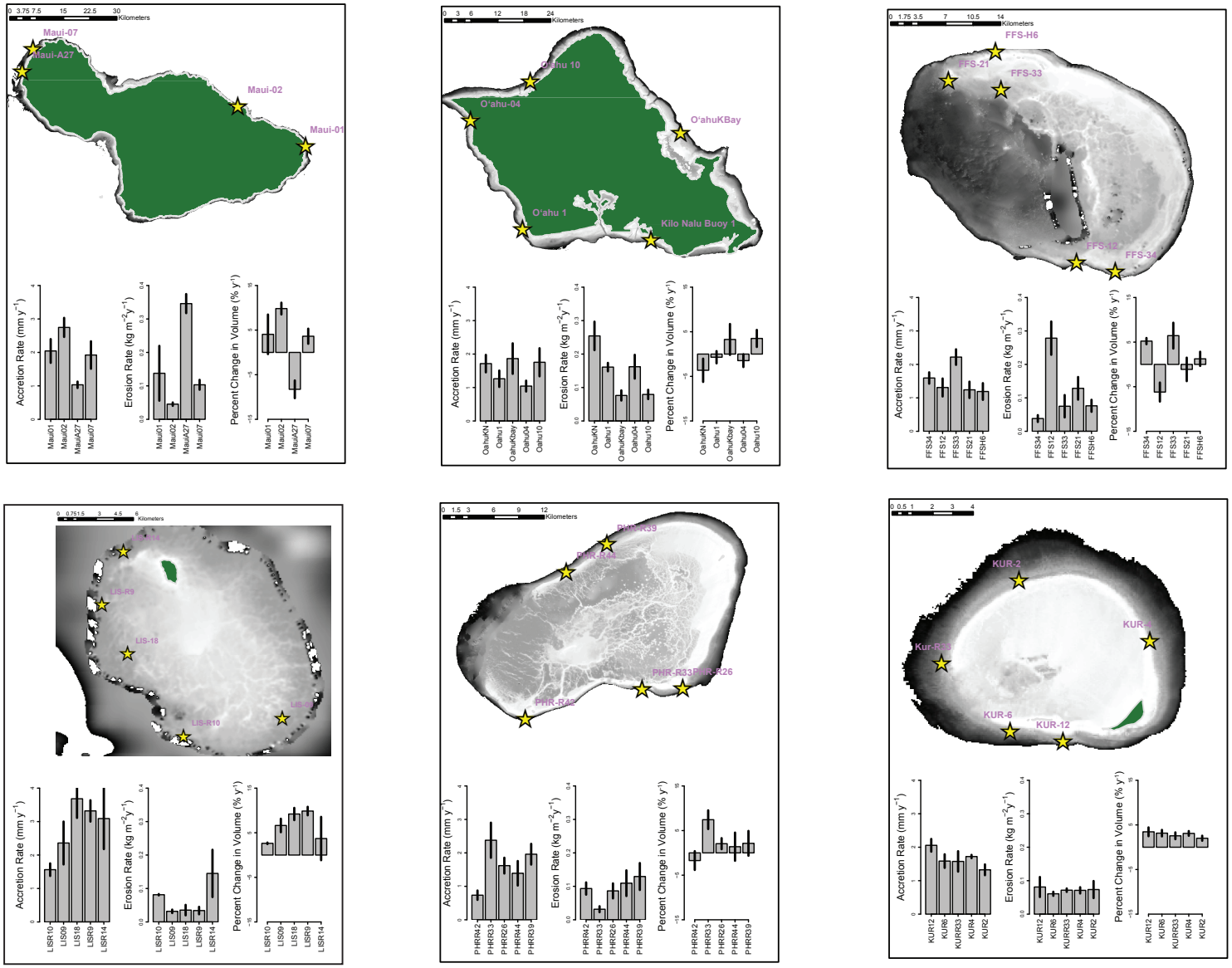

Figure S4: Within island comparison of accretion, erosion, and percent change in volume rates. Data are means ± SE for sites within each island. Data were log-transformed for analysis and back-transformed in this figure.

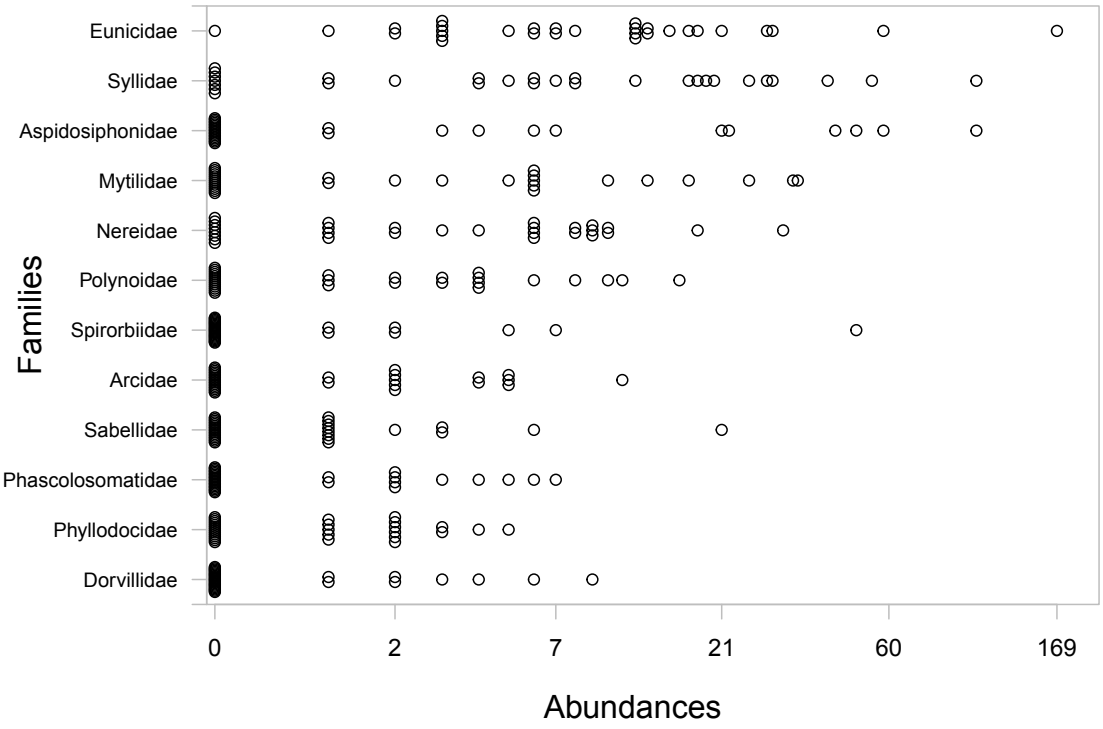

Figure S5: Abundances of infaunal organisms. Data are from the top 12 most abundant families out of the 29 families in the analysis. Each circle represents data from one site.

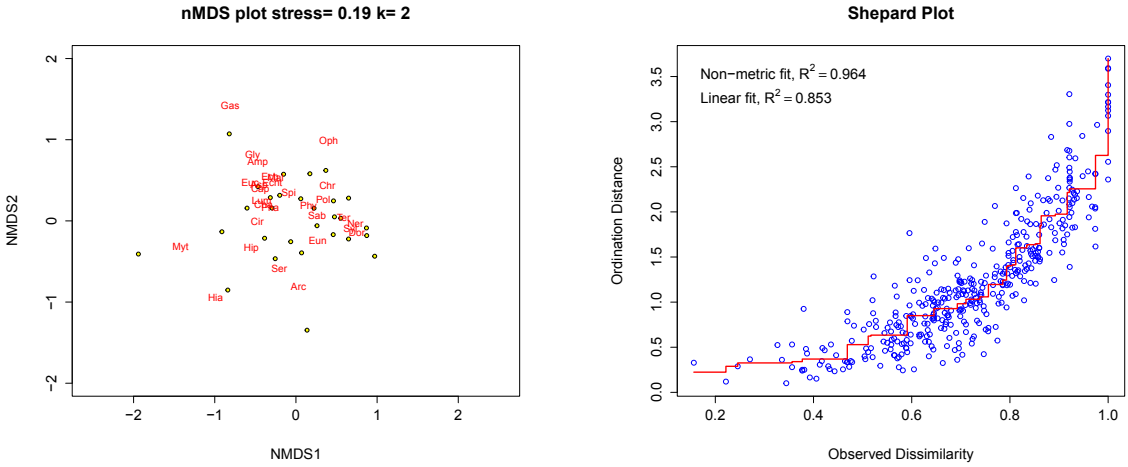

Figure S6: (a) nMDS and (b) Shepard plot for infaunal community. nMDS shows both sites (dots) and families (red). Families are 3 letter codes and the full names are listed in Table S2).

CHAPTER 5

SECONDARY CALCIFICATION AND DISSOLUTION RESPOND DIFFERENTLY TO FUTURE OCEAN CONDITIONS.

Published as: Silbiger, NJ, and Donahue, MJ (2015). Secondary dalcification and dissolution respond differently to future ocean conditions. *Biogeosciences*, 12:567-578

ABSTRACT

Climate change threatens both the accretion and erosion processes that sustain coral reefs. Secondary calcification, bioerosion, and reef dissolution are integral to the structural complexity and long-term persistence of coral reefs, yet these processes have received less research attention than reef accretion by corals. In this study, we use climate scenarios from RCP 8.5 to examine the combined effects of rising ocean acidity and sea surface temperature (SST) on both secondary calcification and dissolution rates of a natural coral rubble community using a flow-through aquarium system. We found that secondary reef calcification and dissolution responded differently to the combined effect of pCO_2 and temperature. Calcification had a non-linear response to the combined effect of temperature-pCO_2: the highest calcification rate occurred slightly above ambient conditions and the lowest calcification rate was in the highest pCO_2-temperature condition. In contrast, dissolution increased linearly with temperature-pCO_2. The rubble community switched from net calcification to net dissolution at +271 µatm pCO_2 and 0.75° C above ambient conditions, suggesting that rubble reefs may shift from net calcification to net dissolution before the end of the century. Our results indicate that (i) dissolution may be more sensitive to climate change than calcification and (ii) that calcification and dissolution have different functional responses to climate stressors; this highlights the need to study the effects of climate stressors on both calcification and dissolution to predict future changes in coral reefs.

1 INTRODUCTION

In 2013, atmospheric carbon dioxide ($CO_{2(atm)}$) reached an unprecedented milestone of 400 ppm (Tans and Keeling, 2013), and this rising $CO_{2(atm)}$ is increasing sea-surface temperature

(SST) and ocean acidity (Caldeira and Wickett, 2003;Cubasch et al., 2013;Feely et al., 2004). Global SST has increased by 0.78°C since pre-industrial times (Cubasch et al., 2013), and it is predicted to increase by another 0.8-5.7°C by the end of this century (Meinshausen et al., 2011;Van Vuuren et al., 2008;Rogelj et al., 2012). The Hawai`i Ocean Time-series detected a 0.075 decrease in mean annual pH at Station ALOHA over the past 20 years (Doney et al., 2009) and there have been similar trends at stations around the world including the Bermuda Atlantic Time-series and the European Station for Time-series Observations in the ocean (Solomon et al. 2007). pH is expected to drop by an additional 0.14-0.35 pH units by the end of the 21st century (Bopp et al., 2013). All marine ecosystems are at risk from rising SST and decreasing pH (Doney et al., 2009;Hoegh-Guldberg et al., 2007;Hoegh-Guldberg and Bruno, 2010), but coral reefs are particularly vulnerable to these stressors (reviewed in Hoegh-Guldberg et al., 2007).

Corals create the structurally complex calcium carbonate ($CaCO_3$) foundation of coral reef ecosystems. This structural complexity is at risk from climate-driven shifts from high-complexity, branched coral species to mounding and encrusting growth forms (Fabricius et al., 2011) and from increases in the natural processes of reef destruction, including bioerosion and dissolution (Wisshak et al., 2012, 2013;Tribollet et al., 2006). While substantial research attention has focused on the response of reef-building corals to climate change (reviewed in Hoegh-Guldberg et al., 2007;Fabricius, 2005;Pandolfi et al., 2011), secondary calcification (calcification by non-coral invertebrates and calcareous algae), bioerosion, and reef dissolution that are integral to maintaining the structural complexity and net growth of coral reefs has received less attention (Andersson and Gledhill, 2013;Andersson et al., 2011;Andersson and Mackenzie, 2012). Bioerosion and dissolution breakdown the reef framework while secondary calcification helps maintain reef stability by cementing the reef together (Adey, 1998; Camoin

and Montaggioni, 1994; Littler, 1973) and producing chemical cues that induce settlement of many invertebrate larvae including several species of corals (Harrington et al. 2004; Price 2010). Coral reefs will only persist if constructive reef processes (growth by corals and secondary calcifiers) exceed destructive reef processes (bioerosion and dissolution). In this study, we examine the combined effects of rising ocean acidity and SST on both calcification and dissolution rates of a natural community of secondary calcifiers and bioeroders.

Recent laboratory experiments have focused on the response of individual taxa of bioeroders or secondary calcifiers to climate stressors. For example, studies have specifically addressed the effects of rising ocean acidity and/or temperature on bioerosion by a *Clionid* sponge (Wisshak et al., 2012, 2013;Fang et al., 2013) and a community of photosynthesizing microborers (Tribollet et al., 2009;Reyes-Nivia et al., 2013). These studies found that bioerosion increased under future climate change scenarios. Several studies have focused on tropical calcifying algae and have found decreased calcification (Semesi et al., 2009; Johnson et al., 2014; Comeau et al., 2013;Jokiel et al., 2008;Kleypas and Langdon, 2006) and increased dissolution (Diaz-Pulido et al., 2012) with increasing ocean acidity and/or SST. However, the bioeroding community is extremely diverse and can interact with the surrounding community of secondary calcifiers: for example, crustose coralline algae (CCA) can inhibit internal bioerosion (White, 1980;Tribollet and Payri, 2001). To understand the combined response of bioeroders and secondary calcifiers, we take a community perspective and examine the synergistic effects of rising SST and ocean acidity on a natural community of secondary calcifiers and bioeroders. Using the total alkalinity anomaly technique, we test for net changes in calcification during the day and dissolution (most of which is caused by bioeroders; Andersson and Gledhill, 2013) at night. Our climate change treatments are modelled after the Representative Concentration

Pathway (RCP) 8.5 climate scenario (Van Vuuren et al., 2011;Meinshausen et al., 2011), one of the high emissions scenarios used in the most recent Intergovernmental Panel on Climate Change (IPCC) report (Cubasch et al., 2013). The RCP 8.5 scenario predicts an increase in temperature of 3.8 – 5.7°C (Rogelj et al., 2012) and an increase in atmospheric CO_2 of 557 ppm by the year 2100 (Meinshausen et al., 2011). We use the RCP 8.5 scenario because the current CO_2 concentrations are tracking just above what this scenario predicts (Sanford et al., 2014). While prior studies have focused on the contributions of individual community members to increased temperature and CO_2; here, we examine the community response to the RCP 8.5 climate scenario and measure calcification, dissolution, and net community production rates.

2 MATERIALS AND METHODS

2.1 Collection Site

All collections were made on the windward side of Moku o Loʻe (Coconut Island) in Kāneʻohe Bay, Hawaiʻi adjacent to the Hawaiʻi Institute of Marine Biology. This fringing reef is dominated by *Porites compressa* and *Montipora capitata*, with occasional colonies of *Pocillopora damicornis*, *Fungia scutaria*, and *Porites lobata*. Kāneʻohe Bay is a protected, semi-enclosed embayment; the residence time can be >1 month long in the protected southern portion of the Bay (Lowe et al., 2009a;Lowe et al., 2009b) that is coupled with a high daily variance in pH (Guadayol et al., 2014). The wave action is minimal (Smith et al., 1981;Lowe et al., 2009a;Lowe et al., 2009b) and currents are relatively slow (5cm s^{-1} maximum) and wind-driven (Lowe et al., 2009a;Lowe et al., 2009b).

2.2 Sample Collection

We collected pieces of dead *Porites compressa* coral skeleton (hereafter, referred to as rubble) as representative communities of bioeroders and secondary calcifiers. Rubble was collected with a hammer and chisel from a shallow reef flat (~1m depth) in November, 2012. Only pieces of rubble without any live coral were collected. The rubble community in Kāneʻohe Bay is comprised of secondary calcifiers, including CCA from the genera *Hydrolithon, Sporolithon,* and *Peyssonnelia* and non-coral calcifying invertebrates (e.g. boring bivalves (*Lithophaga fasciola* and *Barbatia divaricate*), oysters (*Crassostrea gigas*), and small crustaceans); filamentous and turf algae; and internal bioeroders, including boring bivalves (*L. fasciola* and *B.divaricate*), sipunculids (*Aspidosiphon elegans*, *Lithacrosiphon cristatus*, *Phascolosoma perlucens*, and *Phascolosoma stephensoni*), phoronids (*Phoronis ovalis*), sponges (*Cliona* spp.) and a diverse assemblage of polychaetes (White, 1980). All rubble pieces were combined after collection and maintained in a 100L flow-through tank with ambient seawater from Kāneʻohe Bay until random assignment to treatments.

2.3. Experimental Design

The Hawaiʻi Institute of Marine Biology (HIMB) hosts a mesocosm facility with flow-through seawater from Kāneʻohe Bay and controls for light, temperature, pCO_2, and flow rate. The facility is comprised of 24 experimental aquaria split between four racks; each rack has a 150L header tank which feeds 6 experimental aquaria, each 50L in volume (Figure 1).

Before adding rubble to the experimental aquaria, we collected day and night samples of pH, total alkalinity (TA), temperature, and salinity from all aquaria to demonstrate the consistency of water conditions across aquaria without any rubble present (Table 1). The long-

term temporal stability of the mesocosm system is reported in Putnam (2012). We then conducted "control" and "treatment" experiments to determine how RCP 8.5 predictions affect daytime calcification and nighttime dissolution rates in a natural rubble community. The first "control experiment" characterized baseline calcification and dissolution in each aquarium caused by differences in rubble communities. In the second "treatment experiment", we manipulated pCO_2 and temperature to simulate four climate scenarios (pre-industrial, present day, 2050, and 2100) and tested the response of calcification, dissolution, and net community production. Each experiment used the TA anomaly method (Smith and Key, 1975; Andersson et al., 2009). This method calculates net calcification from changes in total alkalinity, and calculates net community production from changes in total dissolved inorganic carbon (DIC) adjusted for changes in carbon due to calcificaiton. Because estimates of calcification are based on changes in TA, this method does not account for mechanical erosion (e.g., small chips of $CaCO_3$ produced by sponge erosion). However, given the short duration of the experiment and the types of bioeroders present, we expect that chemical dissolution captured a significant proportion of the erosion in the system.

Approximately 1.2L of rubble (3-4 pieces of weight 499 ± 148 g and skeletal density 1.53 ± 0.1 g cm^{-3} (mean ± SD, n=85)) were placed in each of the 24 experimental aquaria and acclimated to tank conditions in ambient seawater for three days. On the fourth day, we performed the control experiment, calculating daytime calcification and nighttime dissolution for rubble in ambient seawater conditions using the TA anomaly technique. The next day we manipulated seawater pCO_2 and temperature to replicate four climate scenarios for the treatment experiment: pre-industrial (-1±0.057°C and -205±11.9 µatm), present day (natural Kāneʻohe Bay seawater 24.8±0.09 °C, 614±15.6 µatm), 2050 (+1.4±0.09 °C and +255±31 µatm), and 2100

(+2.4±0.08 and +433±40 µatm). Note that all changes in temperature and pCO_2 were made relative to present day Kāneʻohe Bay seawater conditions: pCO_2 in Kāneʻohe Bay is consistently high relative to the open ocean and can range from 196-976 µatm in southern Kāneʻohe bay depending on conditions (Drupp et al., 2013). The yearly average pCO_2 at our collection site ranged from 565-675 µatm (Silbiger et al., 2014). After an acclimation time of seven days, we sampled the treatment experiment, calculating daytime calcification and nighttime dissolution over a 24 hour period.

During both experiments, TA, pH, salinity, temperature, and dissolved inorganic nutrient (DIN) samples were collected every 12 hours over a 24 hour period: just before lights-on in the morning (time 1) and just before lights-off at night (time 2) to capture light conditions, and then again before lights-on the next morning (time 3) to capture dark conditions. Flow into each aquarium was monitored and adjusted every three hours to ensure a consistent flow rate over the 24 hour experiment. We calculated net ecosystem calcification and net community production using a simple box model (Andersson et al., 2009) and normalized all our calculations to the surface area of the rubble in each tank. Surface area of the rubble was calculated using the wax dipping technique (Stimson and Kinzie III, 1991) at the end of the experiment.

2.4 Mesocosm Set-up

The mesocosm facility (Figure 1) is supplied with ambient seawater from Kāneʻohe Bay, which is filtered through a sand filter, passed through a water chiller (Aqualogic Multi Temp MT-1 Model # 2TTB3024A1000AA), and then fed into one of the four header tanks. pCO_2 was manipulated using a CO_2 gas blending system (see Fangue et al., 2010; Johnson and Carpenter, 2012). Each target pCO_2 concentration was created by mixing CO_2-free atmospheric air with

pure CO_2 using mass flow controllers (C100L Sierra Instruments). Output pCO_2 was analyzed using a calibrated infrared CO_2 analyzer (A151, Qubit Systems). CO_2 mixtures were then bubbled into one of the four header tanks and water from each individual header tank fed into the six individual treatment aquaria (Figure 1). The pCO_2 in each treatment aquarium was estimated with CO2SYS (Van Heuven et al., 2011) using pH and TA as the parameters.

Temperature was manipulated in each treatment aquarium using dual-stage temperature controllers (Aqualogic TR115DN). The temperature was continuously monitored with temperature loggers (TidbiT v2 Water Temperature Data Logger, sampling every 20 min) and point measurements were taken during every sampling period with a handheld digital thermometer (Traceable Digital Thermometer, Thermo Fisher Scientific; precision = 0.001 °C). Light was controlled by positioning an oscillating pendant metal-halide light (250 W) over a set of three aquaria and was programmed to emit an equal amount of light to each tank (~500µE of light). Lights were set to a 12h:12h hour photoperiod and were monitored using a LI-COR spherical quantum PAR sensor. Flow rate was maintained at 115±1 ml min^{-1}, resulting in a residence time of 7.3±0.07 hours per tank. Each aquarium was equipped with a submersible powerhead pump (Sedra KSP-7000 powerhead) to ensure that the tank was well-mixed.

2.5 Seawater Chemistry

All sample collection and storage vials were cleaned in a 10% HCl bath for 24 hours and rinsed three times with MilliQ water before use and rinsed three times with sample water during sample collection and processing.

2.5.1 Total Alkalinity

Duplicate TA samples were collected in 300 ml borosilicate sample containers with glass stoppers. Each sample was preserved with 100µL of 50% saturated $HgCl_2$ and analyzed within 3 days using open cell potentiometric titrations on a Mettler T50 autotitrator (Dickson et al., 2007). A Certified Reference Material (CRM - Reference Material for Oceanic CO_2 Measurements, A. Dickson, Scripps Institution of Oceanography) was run at the beginning of each sample set. The accuracy of the titrator never deviated more than ±0.8% from the standard, and TA measurements were corrected for these deviations. The precision was 3.55µEq (measured as standard deviation of the duplicate water samples). During the 24-hour control experiment the average changes in TA were 37µEq over the day and 20µEq over the night (day and night TA changes were of larger magnitude in the treatment experiments): these are measurable changes given the precision and accuracy of the TA measurements.

2.5.2 pH_t (total scale)

Duplicate pH_t samples were collected in 20ml borosilicate glass vials, brought to a constant temperature of 25ºC in a water bath, and immediately analyzed using an m-cresol dye addition spectrophotometric technique (Dickson et al., 2007). Accuracy of the pH was tested against a Tris buffer of known pH_t from the Dickson Lab at Scripps Institution of Oceanography (Dickson et al., 2007). Our accuracy was better than ±0.04%, and the precision was 0.004 pH units (measured as standard deviation of the duplicate water samples). *In situ* pH and the remaining carbonate parameters were calculated using CO2SYS (Van Heuven et al., 2011) with the following measured parameters: pH_t, TA, temperature, and salinity. The K1K2 apparent

equilibrium constants were from Mehrbach (1973) and refit by Dickson & Millero (1987) and HSO_4^- dissociation constants were taken from Uppström (1974) and Dickson (1990).

2.5.3 Salinity

Duplicate salinity samples were analyzed on a Portasal 8410 portable salinometer calibrated with an OSIL IAPSO standard (accuracy = ±0.003, precision = ±0.0003).

2.5.4 Nutrients

Nutrient samples were collected with 60ml plastic syringes and immediately filtered through combusted 25mm glass fiber filters (GF/F 0.7µm) and transferred into 50ml plastic centrifuge tubes. Nutrient samples were frozen and later analyzed for $Si(OH)_4$, NO_3^-, NO_2^-, NH_4^+, and PO_4^{3-} on a Seal Analytical AA3 HR Nutrient Analyzer at the UH SOEST Lab for Analytical Chemistry.

2.6 Measuring Net Ecosystem Calcification

We assumed that the mesocosms were well mixed systems; thus, we calculated net ecosystem calcification and net communtity photosynthesis following the simple box model presented in Andersson et al. (2009). TA was normalized to a constant salinity (35) to account for changes due to evaporation and then corrected for dissolved inorganic nitrogen and phosphate to account for their small contributions to the acid-base system (Wolf-Gladrow et al., 2007). Net ecosystem calcification, or G, was calculated using the following equation:

$$G = \left[F_{TAin} - F_{TAout} - \frac{d\mathrm{TA}}{dt}\right]/2 \qquad \text{Eq. 1}$$

where F_{TAin} is the rate of TA flowing into an aquarium (= average TA in the header tank times the inflow rate), F_{TAout} is the rate of TA flowing out of an aquarium (= average TA in the aquarium times the outflow rate), and , $\frac{dTA}{dt}$ is the change in TA in an aquarium during the measurement period (change in TA normalized to the volume of water and the surface area of the rubble); specific calculations are given in the supplemental material. The equation is divided by two because one mole of $CaCO_3$ is precipitated or dissolved for every two moles of TA removed or added to the water column. Here, G represents the sum of all the calcification processes minus the sum of all the dissolution processes in mmol $CaCO_3$ m^{-2} hr^{-1}; thus, all positive numbers are net calcification, and all negative numbers are negative net calcification (i.e., net dissolution). Net daytime calcification (G_{day}) is calculated from the first 12 hour sampling period in the light, net nightime dissolution (G_{night}) is calculated from the second 12 hour sampling period in the dark, and total net calcification (G_{net}) is calculated from the full 24 hour cycle ($G_{day} + G_{night}$). G_{day}, G_{night}, and G_{net} are converted from hourly to daily rates and presented as mmol $CaCO_3$ m^{-2} d^{-1}.

2.7 Measuring Net Community Production and Respiration

Net community production (NCP) was calculated by measuring changes in DIC (Gattuso et al., 1999). DIC was normalized to a constant salinity (35) to account for any evaporation over the 24 hour period. We used a simple box model to calculate NCP:

$$NCP = \left[F_{\mathrm{DIC}in} - F_{\mathrm{DIC}out} - \frac{d\mathrm{DIC}}{dt}\right] - G \qquad \text{Eq. 2}$$

$F_{\mathrm{DIC}in}$, $F_{\mathrm{DIC}out}$, and $\frac{d\mathrm{DIC}}{dt}$ are the rates of DIC flowing into the aquaria, flowing out of the aquaria, and the change in DIC in the aquaria per unit time in mmol C m^{-2} hr^{-1}, respectively. To measure

NCP, we subtract G to remove any change in carbon due to inorganic processes. NCP represents the sum of all the photynthetic processes minus the sum of all the respiration processes, thus all positive numbers are net photosynthesis and all negative numbers are negative net photosynthesis (i.e., net respiration). Net daytime NCP (NCP_{day}) is calculated from the first 12 hour sampling period in the light, net nightime NCP (NCP_{night}) is calculated from the second 12 hour sampling period in the dark, and total NCP (NCP_{net}) is calculated from the full 24 hour cycle (NCP_{day} + NCP_{night}). All rates are presented as mmol C m^{-2} d^{-1}.

2.8 Statistical Analysis

Each aquarium contained a slightly different rubble community because of the randomization of rubble pieces to each treatment. To ensure there were no systematic differences in rubble communities between racks (rack effects) before the experimental treatments were applied, we tested for differences in calcification and NCP between racks in the control experiment using an ANOVA (Figure A2).

In the treatment experiment, we first tested for feedbacks in carbonate chemistry due to the presence of rubble: using a paired t-test, we compared the day-night difference in measured pCO_2 in each aquarium with rubble, $\left(pCO_{2,day} - pCO_{2,night}\right)_{rubble}$, and without rubble, $\left(pCO_{2,day} - pCO_{2,night}\right)_{no\ rubble}$.

Although we imposed four discrete temperature-pCO_2 scenario treatments on each tank (Table 1), random variation between treatments and the feedback between the rubble communities and the water chemistry resulted in near-continuous variation in temperature-pCO_2 treatments across aquaria (Figures 2 and A1). To capture this continuous variation in

temperature-pCO_2 in the analysis, we used the measured temperature-pCO_2 seawater condition as a continuous independent variable in a regression rather than the four categorical treatment conditions in an ANOVA (an analysis of G and NCP using the ANOVA approach is included in Figures A3, A4 and Tables A1, A2). The regression approach allowed us to better capture the quantitative relationships between net calcification (G) or NCP and the temperature-pCO_2 treatment. We created a single, continuous variable, Standardized Climate Change (SCC), from a linear combination of temperature and pCO_2 values in each aquarium. A simple linear combination was used because pCO_2 increased linearly with temperature (Figure 2), as imposed by our treatments. We first calculated the relationship between ΔTemp (Eq 3) and ΔpCO_2 (Eq 4) using linear regression. The coefficients from this regression (slope: α = 0.0031; y-intercept: β = - 0.078) were used to combine pCO_2 and temperature onto the same scale, as a measure of Standardized Climate Change (Eq 5):

$$\Delta Temp_i = Temp_{trt,i} - Temp_{cont,i} \quad \text{Eq. 3}$$

$$\Delta pCO_{2_i} = pCO_{2_{trt,i}} - pCO_{2_{cont,}} \quad \text{Eq. 4}$$

$$SCC_i = \Delta Temp_i + \alpha * \Delta pCO_{2_i} + \beta \quad \text{Eq. 5}$$

This synthetic temperature-pCO_2 axis, SCC, is centered on the ambient (control) conditions such that a value of 0 corresponds to present day Kāneʻohe Bay conditions, a negative value corresponds to water that is colder and less acidic (pre-industrial) and a positive value corresponds to water that is warmer and more acidic (future conditions) compared to background seawater. (The independent relationships between G and NCP with ΔTemp and ΔpCO_2 are shown in Figures A5 and A6 and are similar to the relationship with SCC.)

With SCC as a continuous, independent variable, we used a regression to test for linear and non-linear relationships between day, night, and net calcification (G_{day}, G_{night}, and G_{net}) and NCP (NCP_{day}, NCP_{night}, and NCP_{net}) versus SCC. For a simple test of nonlinearity in the response of calcification to SCC, we included a quadratic term (SCC^2) in the model. For G_{day}, we used weighted regression (weight function: $w_i=1/(1+|r_i|)$, where w_i = weight and r_i = residual, Fair, 1974) to account for heteroscedasticity. All other data met assumptions for a linear regression. Lastly, we used a linear regression to test the relationship between G and NCP.

3 RESULTS

3.1 Control Experiment

For rubble in ambient seawater conditions, the average G_{day}, G_{night}, and G_{net} in the control experiment were 3.4±0.16 mmol m^{-2} d^{-1}, -2.4±0.15 mmol m^{-2} d^{-1}, and 0.96±0.20 mmol m^{-2} d^{-1}, respectively. There was no significant difference in G_{day} ($F_{3,23}$=0.68, p=0.58), G_{night} ($F_{3,23}$=1.52, p=0.24), or G_{net} ($F_{3,23}$=1.38, p=0.28) between racks in the control experiment (Figure A2). NCP rates also did not show any racks effects. Average NCP rates were 23.2±1.4 mmol m^{-2} d^{-1} ($F_{3,23}$=0.07, p=0.94) during the day, -20.7±1.9 mmol m^{-2} d^{-1} ($F_{3,23}$=1.95, p=0.15) during the night, and 2.5±2.1 mmol m^{-2} d^{-1} ($F_{3,23}$=1.5, p=0.25) over the entire 24 hour period.

3.2 Treatment Experiment

The rubble communities significantly altered the seawater chemistry, with higher pCO_2 than the applied pCO_2 manipulation, particularly at night (Figure A1). The mean difference between day and night pCO_2 for all treatments was 134.4 ± 39 µatm without rubble and was 438.5 ± 163.9 µatm when rubble was present (t_{23}= -7.23, p<0.0001; Figure 2).

Standardized Climate Change was a significant predictor for G_{day}, G_{night}, and G_{net} (Table 2; Figure 3). G_{day} had a non-linear relationship with Standardized Climate Change (Table 2, Figure 3a), increasing to a threshold and then rapidly declining. G_{night}, however, had a strong linear relationship with Standardized Climate Change (Table 2; Figure 3c), suggesting that joint increases in ocean pCO_2 and temperature will increase nighttime dissolution of coral rubble. Lastly, G_{net} had a strong negative relationship with Standardized Climate Change (Table 2; Figure 3e) and the rubble community switched from net calcification to net dissolution at an increase in pCO_2 and temperature of 271 µatm and 0.75° C, respectively. Standardized Climate Change was also a significant predictor of NCP: Day, night, and net NCP rates all declined with standardized climate change (Table 2; Figure 3b,d,f).

Net ecosystem calcification increased with net community production ($F_{1,46}$ = 260, $p<0.0001$, R^2=0.85; Figure 4). In general, communities were net photosynthesizing and net calcifying during the day (Figure 4a: squares in the upper right quadrant) and were net respiring and net dissolving at night (Figure 4a: circles in the lower left quadrant). The exception was communities in the most extreme temperature-pCO_2 treatment: these communities were net respiring during the day while holding a positive, yet very low, calcification rate (Figure 4a: squares in the upper left quadrant).

4 DISCUSSION

4.1 Carbonate Chemistry Feedbacks

The rubble communities in the aquaria significantly altered the seawater chemistry, particularly at night (t_{23}= -7.23, $p<0.0001$; Figure 2, Figure A1). This day-night difference in

seawater chemistry increased under more extreme climate scenarios, as predicted by Jury *et al.* (2013). This large diel swing in pCO_2 is not uncommon on shallow coral reef environments. pCO_2 ranged from 480 to 975µatm over 24 hours on a shallow reef flat adjacent to our collection site (Silbiger et al. 2014) and from 450 to 742 µatm on a Moloka‘i reef flat dominated by coral rubble (Yates and Halley, 2006). Here, pCO_2 had an average difference of 438 µatm between day and night with a range of 412 µatm in the pre-industrial treatment to 854 µatm in the most extreme temperature-pCO_2 treatments (Figure 2). In our study, we incorporated these feedbacks into the statistical analysis by using the actual, sampled pCO_2 (and temperature) in each aquaria (Figure 3) rather than using the intended pCO_2 (and temperature) treatments in an ANOVA (Tables A1, A2 and Figures A3, A4), better reflecting the pCO_2 experienced by organisms in each aquarium.

4.2 Calcification, Dissolution, and Net Community Production in a High CO_2 and Temperature Environment

Our results suggest that as pCO_2 and temperature increase over time, rubble reefs may shift from net calcification to net dissolution. In our study, this tipping point occurred at a pCO_2 and temperature increase of 271 µatm and 0.75° C. Further, our results showed that G_{day} and G_{night} in a natural coral rubble community have different functional responses to changing pCO_2 and temperature (Figure 3). The ranges in G_{day} and G_{night} in our aquaria were similar to *in situ* rates on Hawaiian rubble reefs. Yates & Halley (2006) saw G_{day} values between 3.3 to 11.7 mmol $CaCO_3$ m^{-2} d^{-1} and G_{night} values between -2.4 to -24 mmol $CaCO_3$ m^{-2} d^{-1} on a Moloka‘i reef flat with only coral rubble (Note that Yates and Halley calculated G over a 4 hour timeframes and the data was multiplied by 3 here to show G in mmol m^{-2} d^{-1}. Also note that we

normalized our rates to the surface area of the rubble while Yates and Halley (2006) normalized their rates to planar surface area.). G_{day} and G_{night} in our experiment ranged from 1.9 to 9.4 and -1.3 to -10.5 mmol $CaCO_3$ m^{-2} d^{-1}, respectively, across all treatment conditions. The higher dissolution rates in the *in situ* study by Yates and Halley (2006) are likely due to dissolution in the sediment, which was not present in our study.

G_{day} had a non-linear response to Standardized Climate Change. G_{day} increased with temperature-pCO_2 until slightly above ambient conditions, and then decreased under more extreme climate conditions (Figure 3a). This mixed response, increasing and then decreasing with Standardized Climate Change, is reflected in prior experiments. We suggest three possible mechanisms to explain why calcification increases in slightly higher temperature-pCO_2 than ambient conditions. 1) Some calcifiers can maintain and even increase their calcification rates in acidic conditions (Kamenos et al., 2013;Findlay et al., 2011;Rodolfo-Metalpa et al., 2011;Martin et al., 2013) by either modifying their local pH environment (Hurd et al., 2011) or partitioning their energetic resources towards calcification (Kamenos et al., 2013). For example, in low, stable pH conditions the coralline algae, *Lithothamnion glaciale,* increased its calcification rate relative to a control treatment but, did not concurrently increase its rate of photosynthesis (Kamenos et al., 2013). Kamenos et al (2013) suggest that the up-regulation of calcification may limit photosynthetic efficiency. In the present study, the increase in G_{day} coincided with a decrease in net photosynthesis (Figure 3a,b). Photosynthesizing calcifiers in the community may be partitioning their energetic resources more towards calcification and away from photosynthesis in order to maintain a positive calcification rate (Kamenos et al., 2013). Notably, turf algae likely have a major control over the NCP in this community which would not have any impact on calcification. 2) An alternative hypothesis is that the calcifiers may be adapted or

acclimatized to high pCO_2 conditions (Johnson et al., 2014) and have not yet reached their threshold because the rubble was collected from a naturally high and variable pCO_2 environment (Guadayol et al., 2014; Silbiger et al. 2014). 3) In this study, the calcifiers experienced a combined increase in both pCO_2 and temperature and, thus, the non-linear response in G_{day} may also be due a metabolic response. In a typical thermal performance curve, organisms increase their metabolism until they have reached a thermal maximum and then rapidly decline (Huey and Kingsolver, 1989; Pörtner et al., 2006), and we see this response in our results. A recent study found a similar nonlinear response to temperature and pCO_2 in the coral *Siderastrea sidera* (Castillo et al. 2014). While they attribute the pCO_2 response to photosynthesis being neutralized (we did not see this response in our non-coral community), they suggest that the thermal response is due to both changes in metabolism and thermally-driven changes in aragonite saturation state (Castillo et al. 2014).

We saw a decline in both calcification and NCP in the extreme temperature-pCO_2 condition (Figure 3). Calcification has been shown to decline with climate stressors and the magnitude of decline differs across species (Kroeker et al., 2010;Pandolfi et al., 2011;Ries et al., 2009;Kroeker et al., 2013). The concurrent decline in NCP and calcification (Figure 3a,b & 4) suggests that non-photosynthesizing invertebrates in the community (such as bivalves) might be dominating the calcification signal in these conditions. This hypothesis would explain the pattern that we see in Figure 4, where communities in the most extreme pCO_2 and temperature conditions are net respiring during the day while still maintaining a small, positive calcification rate (Figure 4a: five points in the upper left quadrant).

G_{night} rates are more straightforward, decreasing linearly with pCO_2 and temperature (Figures 3c and 4). NCP_{night} rates also decreased linearly with pCO_2 and temperature (Figure 3d).

Similarly, Andersson et al. (2009) saw an increase in dissolution under acidic conditions in a community of corals, sand, and CCA. Previous studies on individual bioeroder taxa have also found higher rates of bioerosion or dissolution in more acidic, higher temperature conditions (Wisshak et al., 2013;Fang et al., 2013;Reyes-Nivia et al., 2013;Tribollet et al., 2009;Wisshak et al., 2012). There are several mechanisms that could be mediating the increased dissolution rates in the high temperature-pCO_2 treatments: 1) Higher temperatures could increase the metabolism of the bioeroder community, thus increasing borer activity (e.g., Davidson et al. 2013). 2) Because many boring organisms excrete acidic compounds to erode the skeletal structure (Hutchings 1986), reduced pH in the overlaying water column may reduce the metabolic cost to the organisms, making it easier for eroders to breakdown the $CaCO_3$. 3) Higher dissolution rates could be mediated by an increase in the proportion of dolomite in the skeletal structure of CCA on the rubble. A recent study found a 200% increase in dolomite in CCA that were exposed to high pCO_2 and temperature conditions; this increase in dolomite resulted in increased bioerosion by endolithic algae (Diaz-Pulido et al., 2014). However, it is unlikely that changes in the mineralogy of the CCA indirectly increased dissolution here given the short time-scale of our study. In the present study, we used the TA anomaly method to calculate chemical dissolution as a proxy for bioerosion. Future studies should also include measures of mechanical breakdown (e.g. the production of sponge chips) in addition to chemical dissolution for a more complete picture of the impacts of climate stress on reef breakdown. Studies, including the present one, which focused on community-level responses, have consistently found that ocean acidification will increase dissolution rates on coral reefs (Andersson and Gledhill, 2013).

Standardized Climate Change explained more of the variance in dissolution than in calcification in our rubble community: ($R^2_{G_{night}} = 0.64 > R^2_{G_{day}} = 0.33$; Table 2) this result is not surprising. Bioerosion, an important driver of dissolution, may be more sensitive to changes in ocean acidity than calcification, leading to net dissolution in high CO_2 waters. Many boring organisms excrete acidic compounds, which may be less metabolically costly in a low pH environment. Erez et al. (2011) hypothesize that increased dissolution, rather than decreased calcification, maybe be the reason that net coral reef calcification is sensitive to ocean acidification. The results of this study support this hypothesis. Although G_{net} declines linearly with temperature- pCO_2, calcification (G_{day}) and dissolution (G_{night}) have distinct responses to Standardized Climate Change: G_{day} had a non-linear response while G_{night} declined linearly with Standardized Climate Change. Our results highlight the need to study the effects of climate stressors on both calcification and dissolution.

Author contributions:

Conceived and designed the experiments: NJS MJD. Performed the experiments: NJS. Analyzed the data: NJS MJD. Wrote the paper: NJS MJD.

Acknowledgements

Thanks to I Caldwell, R Coleman, J Faith, K Hurley, J Miyano, R Maguire, D Schar, JM Sziklay, and MM Walton for help in field collections and lab analyses and to R. Briggs from UH SOEST Lab for Analytical Chemistry. MJ Atkinson, R Gates, C Jury, H Putnam, and R Toonen gave thoughtful advice throughout the project. Comments by F Mackenzie and our two anonymous reviewers improved this manuscript. This project was supported by a NOAA Dr. Nancy Foster Scholarship to NJS, a PADI Foundation Grant to NJS, and Hawaii SeaGrant 1847 to MJD. This

paper is funded in part by a grant /cooperative agreement from the National Oceanic and Atmospheric Administration, Project R/IR-18, which is sponsored by the University of Hawaii Sea Grant College Program, SOEST, under Institutional Grant No. NA09OAR4170060 from NOAA Office of Sea Grant, Department of Commerce. The views expressed herein are those of the author(s) and do not necessarily reflect the views of NOAA or any of its subagencies. This is HIMB contribution #1607, Hawai‘i SeaGrant contribution # UNIHI-SEAGRANT-JC-12-19, and SOEST contribution #9237.

REFERENCES

Adey, W.H. Review—coral reefs: algal structures and mediated ecosystems in shallow turbulent, alkaline waters. Journal of Phycology, 34, 393-406, 1998.

Andersson, A. J., Kuffner, I. B., Mackenzie, F. T., Jokiel, P. L., Rodgers, K. S., and Tan, A.: Net Loss of $CaCO_3$ from a subtropical calcifying community due to seawater acidification: mesocosm-scale experimental evidence, Biogeosciences, 6, 1811-1823, 2009.

Andersson, A. J., Mackenzie, F. T., and Gattuso, J.-P.: Effects of ocean acidification on benthic processes, organisms, and ecosystems, in: Ocean Acidification, edited by: Gattuso, J.-P., and Hansson, L., Oxford University Press, 122-153, 2011.

Andersson, A. J., and Mackenzie, F. T.: Revisiting four scientific debates in ocean acidification research, Biogeosciences, 9, 893-905, 2012.

Andersson, A. J., and Gledhill, D.: Ocean Acidification and Coral Reefs: Effects on Breakdown, Dissolution, and Net Ecosystem Calcification, Annual Review of Marine Science, Vol 5, 5, 321-348, 2013.

Bopp, L., Resplandy, L., Orr, J. C., Doney, S. C., Dunne, J. P., Gehlen, M., Halloran, P., Heinze, C., Ilyina, T., Séférian, R., Tjiputra, J., and Vichi, M.: Multiple stressors of ocean ecosystems in the 21st century: projections with CMIP5 models, Biogeosciences, 10, 3627-3676, 2013.

Caldeira, K., and Wickett, M. E.: Oceanography: anthropogenic carbon and ocean pH, Nature, 425, 365-365, 2003.

Camoin, G.F., Montaggioni, L.F., High energy coralgal-stromatolite frameworks from Holocene reefs (Tahiti, French Polynesia), Sedimentology, 41, 656-676, 1994.

Castillo, K.D., Ries, J.B., Bruno, J.F., Westfield, I.T., The reef-building coral *Siderastrea siderea* exhibits parabolic responses to ocean acidification and warming. Proc. R. Soc. B., 281, 20141856, 2014

Comeau, S., Edmunds, P. J., Spindel, N. B., and Carpenter, R. C.: The responses of eight coral reef calcifiers to increasing partial pressure of CO_2 do not exhibit a tipping point, Limnol. Oceanogr, 58, 388-398, 2013.

Cubasch, U., Wuebbles, D., Chen, D., Facchini, M. C., Frame, D., Mahowald, N., and Winther, J.-G.: Climate Change 2013: The Physical Science Basis. Contribution of Working Group I to the Fifth Assessment Report of the Intergovernmental Panel on Climate Change Cambridge, United Kingdom and New York, NY, USA., 119-158 , 2013.

Davidson, T.M., de Rivera, C.E., Carlton, J.T., Small increases in temperature exacerbate the erosive effects of a non-native burrowing crustacean, Journal of Experimenal Marine Biology and Ecology, 446, 115-121, 2013.

Diaz-Pulido, G., Anthony, K., Kline, D. I., Dove, S., and Hoegh-Guldberg, O.: Interactions between ocean acidification and warming on the mortality and dissolution of coralline alge, Journal of Phycology, 48, 32-39, 2012.

Diaz-Pulido, G., Nash, M.C., Anthony, K.R.N., Bender. D., Opdyke, B.N., Reyed-Nivia, C.,

Troitzsch, U., Greenhouse conditions induce mineralogical changes and dolomite accumulation in coralline algae on tropical reefs, Nature Communications, 5, 3310, DOI:10.1038/ncomms4310, 2014

Dickson, A. G., and Millero, F. J.: A comparison of the equilibrium constants for the dissociation of carbonic acid in seawater media, Deep Sea Research Part A. Oceanographic Research Papers, 34, 1733-1743, 1987.

Dickson, A. G.: Standard potential of the reaction: AgCl (s)+ $12H_2$(g)= Ag (s)+ HCl (aq), and and the standard acidity constant of the ion HSO_4^- in synthetic sea water from 273.15 to 318.15 K, The Journal of Chemical Thermodynamics, 22, 113-127, 1990.

Dickson, A. G., Sabine, C. L., and Christian, J. R.: Guide to best practices for ocean CO_2 measurements, Sidney, BritishColumbia, North Pacific Marine Science Organization, PICES Special Publication 3, 2007.

Doney, S. C., Fabry, V. J., Feely, R. A., and Kleypas, J. A.: Ocean Acidification: The Other CO_2 Problem, Annual Review of Marine Science, 1, 169-192, 2009.

Drupp, P. S., De Carlo, E. H., Mackenzie, F. T., Sabine, C. L., Feely, R. A., and Shamberger, K. E.: Comparison of CO_2 dynamics and air–sea gas exchange in differing tropical reef environments, Aquatic Geochemistry, 19, 371-397, 2013.

Erez, J., Reynaud, S., Silverman, J., Schneider, K., and Allemand, D.: Coral calcification under ocean acidification and global change, in: Coral Reefs: an ecosystem in transition, edited by: Dubinski, Z., and Stambler, N., Springer, 151-176, 2011.

Fabricius, K., Langdon, C., Uthicke, S., Humphrey, C., Noonan, S., De'ath, G., Okazaki, R., Muehllehner, N., Glas, M., and Lough, J.: Losers and winners in coral reefs acclimatized to elevated carbon dioxide concentrations, Nature Climate Change, 1, 165-169, 2011.

Fabricius, K. E.: Effects of terrestrial runoff on the ecology of corals and coral reefs: review and synthesis, Mar. Pollut. Bull., 50, 125-146, 2005.

Fair, R. C.: On the robust estimation of econometric models, in: Annals of Economic and Social Measurement, Volume 3, number 4, NBER, 117-128, 1974.

Fang, J. K. H., Mello-Athayde, M. A., Schönberg, C. H. L., Kline, D. I., Hoegh-Guldberg, O., and Dove, S.: Sponge biomass and bioerosion rates increase under ocean warming and acidification, Global Change Biology, 19, 3581-3591, 2013.

Fangue, N. A., O'Donnell, M. J., Sewell, M. A., Matson, P. G., MacPherson, A. C., and Hofmann, G. E.: A laboratory-based, experimental system for the study of ocean acidification effects on marine invertebrate larvae, Limnology and Oceanography: Methods, 8, 441-452, 2010.

Feely, R. A., Sabine, C. L., Lee, K., Berelson, W., Kleypas, J., Fabry, V. J., and Millero, F. J.: Impact of anthropogenic CO_2 on the $CaCO_3$ system in the oceans, Science, 305, 362-366, 2004.

Findlay, H. S., Wood, H. L., Kendall, M. A., Spicer, J. I., Twitchett, R. J., and Widdicombe, S.: Comparing the impact of high CO_2 on calcium carbonate structures in different marine organisms, Marine Biology Research, 7, 565-575, 2011.

Gattuso, J.-P., Frankignoulle, M., and Smith, S. V.: Measurement of community metabolism and significance in the coral reef CO_2 source-sink debate, Proceedings of the National Academy of Sciences, 96, 13017-13022, 1999.

Guadayol, Ò., Silbiger, N. J., Donahue, M. J., and Thomas, F. I. M.: Patterns in temporal variability of temperature, oxygen and pH along an environmental gradient in a coral reef, PloS one, 9, e85213, DOI:10..1371/journal.pone.0085213, 2014.

Harrington, L., Fabricius, K., De'ath, G., Negri, A., Recognition and selection of settlement substrata determine post-settlement survival in corals. Ecology, 84-3428-3437, 2004.

Hoegh-Guldberg, O., Mumby, P. J., Hooten, A. J., Steneck, R. S., Greenfield, P., Gomez, E., Harvell, C. D., Sale, P. F., Edwards, A. J., Caldeira, K., Knowlton, N., Eakin, C. M., Iglesias-Prieto, R., Muthiga, N., Bradbury, R. H., Dubi, A., and Hatziolos, M. E.: Coral reefs under rapid climate change and ocean acidification, Science, 318, 1737-1742, 2007.

Huey, R.B., Kingsolver, J.G. Evolution of thermal sensitivity of ecotherm performance. Trends Ecol. Evol., 4,131-135, 1989

Hutchings, P.A., Biological destruction of coral reefs, Coral Reefs, 4, 239-252, 1986.

Hoegh-Guldberg, O., and Bruno, J. F.: The impact of climate change on the world's marine ecosystems, Science, 328, 1523-1528, 2010.

Hurd, C. L., Cornwall, C. E., Currie, K., Hepburn, C. D., McGraw, C. M., Hunter, K. A., and Boyd, P. W.: Metabolically induced pH fluctuations by some coastal calcifiers exceed projected 22nd century ocean acidification: a mechanism for differential susceptibility?, Global Change Biology, 17, 3254-3262, 2011.

Johnson, M. D., and Carpenter, R. C.: Ocean acidification and warming decrease calcification in the crustose coralline alga *Hydrolithon onkodes* and increase susceptibility to grazing, J. Exp. Mar. Biol. Ecol., 434, 94-101, 2012.

Johnson, M. D., Moriarty, V. W., and Carpenter, R. C.: Acclimatization of the Crustose Coralline Alga *Porolithon onkodes* to Variable pCO_2, PLOS ONE, 9, e87678, DOI: 10.1371/journal.pone.0087678, 2014.

Jokiel, P. L., Rodgers, K. S., Kuffner, I. B., Andersson, A. J., Cox, E. F., and Mackenzie, F. T.: Ocean acidification and calcifying reef organisms: a mesocosm investigation, Coral Reefs, 27, 473-483, 2008.

Jury, C. P., Thomas, F. I. M., Atkinson, M. J., and Toonen, R. J.: Buffer Capacity, Ecosystem Feedbacks, and Seawater Chemistry under Global Change, Water, 5, 1303-1325, 2013.

Kamenos, N. A., Burdett, H. L., Aloisio, E., Findlay, H. S., Martin, S., Longbone, C., Dunn, J., Widdicombe, S., and Calosi, P.: Coralline algal structure is more sensitive to rate, rather than the magnitude, of ocean acidification, Global Change Biology, 19, 3621-3628, 2013.

Kleypas, J., and Langdon, C.: Coral reefs and changing seawater chemistry, in: Coral Reefs and Climate Change: Science and Management., edited by: Phinney, J., Skirving, W., Kleypas, J., and Hoegh-Guldberg, O., American Geophysical Union, Washington D.C., pp. 73-110, 2006.

Kroeker, K. J., Kordas, R. L., Crim, R. N., and Singh, G. G.: Meta-analysis reveals negative yet variable effects of ocean acidification on marine organisms, Ecology Letters, 13, 1419-1434, 2010.

Kroeker, K. J., Kordas, R. L., Crim, R., Hendriks, I. E., Ramajo, L., Singh, G. S., Duarte, C. M., and Gattuso, J. P.: Impacts of ocean acidification on marine organisms: quantifying sensitivities and interaction with warming, Global Change Biology, 19, 1884-1896, 2013.

Littler, M.M.m The population and community structure of Hawaiian fringing-reef crustose corallinaceae (Rhodophyta, Cryptonemiales), Journal of Experimental Marine Biology and Ecology, 11, 103-120, 1973.

Lowe, R. J., Falter, J. L., Monismith, S. G., and Atkinson, M. J.: A numerical study of circulation in a coastal reef-lagoon system, Journal of Geophysical Research-Oceans, 114, C06022, 2009a.

Lowe, R. J., Falter, J. L., Monismith, S. G., and Atkinson, M. J.: Wave-driven circulation of a coastal reef-lagoon system, J. Phys. Oceanogr., 39, 873-893, 2009b.

Martin, S., Cohu, S., Vignot, C., Zimmerman, G., and Gattuso, J. P.: One-year experiment on the physiological response of the Mediterranean crustose coralline alga, *Lithophyllum cabiochae*, to elevated pCO_2 and temperature, Ecology and evolution, 3,636-693, DOI: 10.1029/2008JC005081, 2013.

Mehrbach, C.: Measurement of the apparent dissociation constants of carbonic acid in seawater at atmospheric pressure, Limnol. Oceanogr., 18, 897-907, 1973.

Meinshausen, M., Smith, S. J., Calvin, K., Daniel, J. S., Kainuma, M. L. T., Lamarque, J. F., Matsumoto, K., Montzka, S. A., Raper, S. C. B., and Riahi, K.: The RCP greenhouse gas concentrations and their extensions from 1765 to 2300, Climatic Change, 109, 213-241, 2011.

Pandolfi, J. M., Connolly, S. R., Marshall, D. J., and Cohen, A. L.: Projecting coral reef futures under global warming and ocean acidification, Science, 333, 418-422, 2011.

Price, N., Habitat selection, facilitation, and biotic settlement cues affect distribution and performance of coral recruits in French Polynesia, Oecologia, 163, 747-758, 2010.

Pörtner, H.O., Bennet, A.F., Bozinovic, F., Clarke, A., Lardies, M.A., Lucassen, M., Pelster, B., Schiemer, F., Stillman, J.H., Trade-offs in therman adaptation: the need for molecular ecological integration, Phys. Biochem. Zool., 79, 295-313, 2006.

Putnam, H.M. Resilience and acclimatization potential of reef corals under predicted climate change stressors, PhD, Zoology, University of Hawaii at Manoa, Honolulu, 2012

Reyes-Nivia, C., Diaz-Pulido, G., Kline, D., Guldberg, O.-H., and Dove, S.: Ocean acidification and warming scenarios increase microbioerosion of coral skeletons, Global Change Biology, 19, 1919-1929, 2013.

Ries, J. B., Cohen, A. L., and McCorkle, D. C.: Marine calcifiers exhibit mixed responses to CO_2-induced ocean acidification, Geology, 37, 1131-1134, 2009.

Rodolfo-Metalpa, R., Houlbrèque, F., Tambutté, É., Boisson, F., Baggini, C., Patti, F. P., Jeffree, R., Fine, M., Foggo, A., and Gattuso, J. P.: Coral and mollusc resistance to ocean acidification adversely affected by warming, Nature Climate Change, 1, 308-312, 2011.

Rogelj, J., Meinshausen, M., and Knutti, R.: Global warming under old and new scenarios using IPCC climate sensitivity range estimates, Nature Climate Change, 2, 248-253, 2012.

Sanford, T., Frumhoff, P. C., Luers, A., and Gulledge, J.: The climate policy narrative for a dangerously warming world, Nature Climate Change, 4, 164-166, 2014.

Semesi, I. S., Kangwe, J., and Björk, M.: Alterations in seawater pH and CO_2 affect calcification and photosynthesis in the tropical coralline alga, *Hydrolithon* sp.(Rhodophyta), Estuarine, Coastal and Shelf Science, 84, 337-341, 2009.

Silbiger, N., Guadayol, Ò., Thomas, F. I.M., and Donahue, M.: Reefs shift from net accretion to net erosion along a natural environmental gradient, Marine Ecology Progress Series, 515, 33-44, 2014.

Smith, S. V., and Key, G. S.: Carbon dioxide and metabolism in marine environments, Limnol. Oceanogr, 20, 493-495, 1975.

Smith, S. V., Kimmerer, W. J., Laws, E. A., Brock, R. E., and Walsh, T. W.: Kaneohe Bay sewage diversion experiment- perspectives on ecosystem responses to nutritional perturbation, Pacific Science, 35, 279-402, 1981.

Solomon, S., Qin. D., Manning. M. Chen. Z., Marquis, M., et al. Climate Change 2007: The physical Science Basis: Contributions of Working Group I to the Fourth Assessment Report of the Intergovernmental Panel on Climate Change., New York, Cambridge Univ. Press, 2007.

Stimson, J., and Kinzie III, R. A.: The temporal pattern and rate of release of zooxanthellae from the reef coral *Pocillopora damicornis* (Linnaeus) under nitrogen-enrichment and control conditions, Journal of Experimental Marine Biology and Ecology, 153, 63-74, 1991.

Tans, P., and Keeling, R.: NOAA/ESRL, www.esrl.noaa.gov/gmd/ccgg/trends/, 2013.

Tribollet, A., and Payri, C.: Bioerosion of the coralline alga *Hydrolithon onkodes* by microborers in the coral reefs of Moorea, French Polynesia, Oceanologica Acta, 24, 329-342, 2001.

Tribollet, A., Atkinson, M. J., and Langdon, C.: Effects of elevated $pCO_{(2)}$ on epilithic and endolithic metabolism of reef carbonates, Global Change Biology, 12, 2200-2208, 2006.

Tribollet, A., Godinot, C., Atkinson, M., and Langdon, C.: Effects of elevated $pCO_{(2)}$ on dissolution of coral carbonates by microbial euendoliths, Global Biogeochemical Cycles, 23, GB3008, DOI: 10.1029/2008GB003286, 2009.

Uppström, L. R.: The boron/chlorinity ratio of deep-sea water from the Pacific Ocean, Deep Sea Research and Oceanographic Abstracts, 21,1974, 161-162.

Van Heuven, S., Pierrot, D., Lewis, E., and Wallace, D. W. R.: MATLAB Program developed for CO_2 system calculations, Rep. ORNL/CDIAC-105b, 2011.

van Heuven, S., Pierrot, D., Rae, J. W. B., Lewis, E., and Wallace, D. W. R.:MATLAB program developed for CO_2 system calculations, ORNL/CDIAC-105b, Carbon Dioxide Inf. Anal. Cent., Oak Ridge Natl. Lab., US DOE, Oak Ridge, Tenn., DOI:10.3334/CDIAC/otg.CO2SYS_MATLAB_v1.1, 2011

Van Vuuren, D. P., Meinshausen, M., Plattner, G. K., Joos, F., Strassmann, K. M., Smith, S. J., Wigley, T. M. L., Raper, S. C. B., Riahi, K., and De La Chesnaye, F.: Temperature increase of 21st century mitigation scenarios, Proceedings of the National Academy of Sciences, 105, 15258-15262, 2008.

Van Vuuren, D. P., Edmonds, J., Kainuma, M., Riahi, K., Thomson, A., Hibbard, K., Hurtt, G. C., Kram, T., Krey, V., and Lamarque, J.-F.: The representative concentration pathways: an overview, Climatic Change, 109, 5-31, 2011.

White, J.: Distribution, recruitment and development of the borer community in dead coral on shallow Hawaiian reefs, Ph.D., Zoology, University of Hawaii at Manoa, Honolulu, 1980.

Wisshak, M., Schönberg, C. H. L., Form, A., and Freiwald, A.: Ocean acidification accelerates reef bioerosion, Plos One, 7, e45124-e45124, DOI: 10.1371/journal.pone.0045124, 2012.

Wisshak, M., Schönberg, C. H. L., Form, A., and Freiwald, A.: Effects of ocean acidification and global warming on reef bioerosion—lessons from a clionaid sponge, Aquatic Biology, 19, 111-127, 2013.

Wolf-Gladrow, D.A., Zeebe, R.E., Klass, C., Körtzinger, A., Dickson, A.G.,: Total Alkalinity: The explicit conservative expression and its application to biogeochemical processes, Marine Chemistry, 106, 287-300, 2007.

Yates, K. K., and Halley, R. B.: CO_3^{2-} concentration and pCO_2 thresholds for calcification and dissolution on the Molokai reef flat, Hawaii, Biogeosciences, 3, 357-369, 2006.

Table 1: Means and standard errors of all measured parameters by rack. pCO_2, HCO_3^-, CO_3^{2-}, DIC, and Ω_{arag} were all calculated from the measured TA and pH samples using CO2SYS. Each table entry is the mean of 12 water samples: one daytime sample and one nighttime sample for six aquaria within a rack. Data are all from the imposed treatment conditions with no rubble inside the aquaria.

Rack	**Pre-industrial**	**Present Day**	**2050 prediction**	**2100 prediction**
Temp (°C)	23.8±0.07	24.8±0.08	26.2±0.06	27.2±0.08
Salinity	35.65±0.01	35.71±0.02	35.62±0.02	35.71±0.02
TA (µmol kg^{-1})	2137±1.7	2138±2.3	2139±2.0	2142±1.9
pH_t	8.02±0.02	7.87±0.01	7.74±0.02	7.67±0.02
pCO_2 (µatm)	409±20.0	614±15.6	868±33.0	1047±38.7
HCO_3^- (µmol kg^{-1})	1692±16.9	1815±7.3	1894±7.8	1939±6.6
CO_3^{2-} (µmol kg^{-1})	194.20±6.7	147.08±2.8	113.98±3.8	99.24±3.3
DIC (µmol kg^{-1})	1898±10.9	1980±5.1	2032±5.0	2067±4.5
Ω_{arag}	3.06±0.1	2.32±0.04	1.80±0.06	1.57±0.05
NO_2^- (µmol L^{-1})	0.082 ± 0.0028	0.078 ±0.0045	0.074 ± 0.0047	0.070 ± 0.0051
PO_4^{3-} (µmol L^{-1})	0.017 ±0.014	0.0097 ±0.0081	0.033 ±0.016	0.018±0.0061
$Si(OH)_4$ (µmol L^{-1})	3.60 ±0.58	3.64 ±0.61	3.88 ± 0.49	3.78 ± 0.52
NH_4^+ (µmol L^{-1})	0.45 ±0.30	0.19 ±0.067	0.23 ±0.15	0.34 ± 0.14
NO_3^-(µmol L^{-1})	2.13±0.20	2.25±0.21	2.55±0.10	2.48±0.11

Table 2: Regression results for the treatment experiments: G_{day}, G_{night}, and G_{net} versus Standardized Climate Change (Figure 3a,c,e) and NCP_{day}, NCP_{night}, and NCP_{net} versus Standardized Climate Change (Figure 3b,d,f). Bold values indicate a statistically significant p-value at an $\alpha < 0.05$.

	SS	df	F	p	R^2
G_{day}					
Standardized Climate Change	3.79	1	1.45	0.06	
(Standardized Climate Change)^2	23.63	1	9.04	**0.007**	
Error	54.89	21			0.33
G_{night}					
Standardized Climate Change	67.80	1	39.14	**<0.0001**	
Error	38.11	22			0.64
G_{net}					
Standardized Climate Change	88.01	1	19.49	**<0.001**	
Error	99.35	22			0.47
NCP_{day}					
Standardized Climate Change	5687.2	1	57.36	**<0.0001**	
Error	2181.4	22			0.72
NCP_{night}					
Standardized Climate Change	3816.1	1	52.06	**<0.0001**	
Error	1612.6	22			0.70
NCP_{net}					
Standardized Climate Change	17925	1	121.47	**<0.0001**	
Error	3246.4	22			0.85

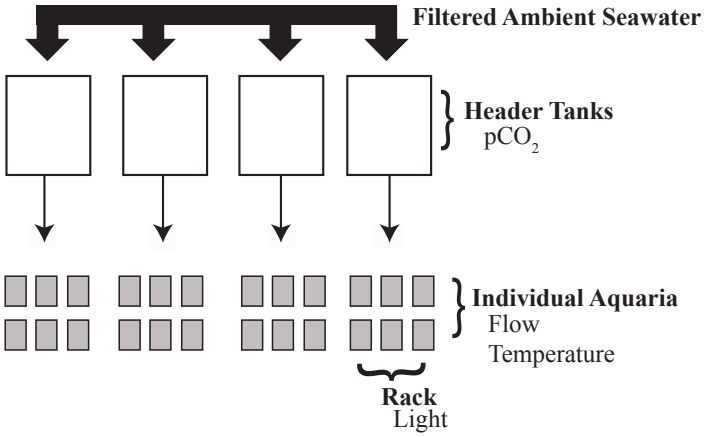

Figure 1: A schematic of the mesocosm system at the Hawai‘i Institute of Marine Biology. Ambient seawater is pumped into the system from a nearby fringing reef in Kāne‘ohe Bay. The seawater is filtered with a sand trap filter, passed through a water chiller and then fed into one of four header tanks. pCO_2 is manipulated in each header tank by bubbling a mixture of CO_2-free air and pure CO_2 to the desired concentration. The water from one header tank flows into 6 aquaria (a rack). Light is controlled by rack with metal-halide lights. There are two metal-halide lights per rack with each light oscillating over a set of three aquaria. Flow and temperature are controlled in each individual aquarium with flow valves and aquarium heaters and coolers, respectively.

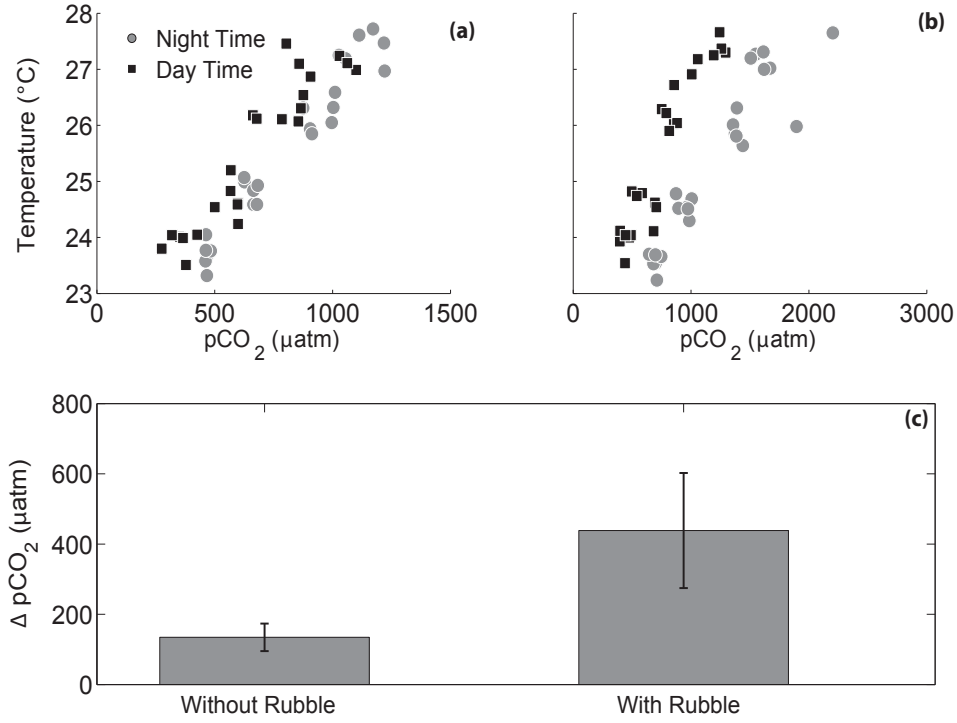

Figure 2: pCO_2 and temperature in each aquarium (a) without any rubble present and (b) with rubble present. Daily variability in pCO_2 was higher when rubble was present due to feedbacks from the rubble community (note the different x-axis scales in panels a and b). Panel (c) shows the mean difference between day and night pCO_2 with and without rubble present with observations paired by aquarium (error bars are standard error) (t_{23}= -7.23, p<0.0001).

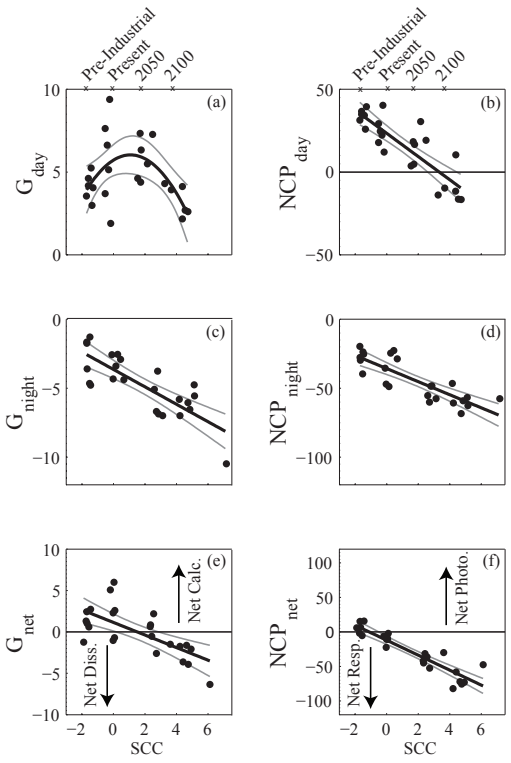

Figure 3: Net ecosystem calcification ((a) G_{day}, (c) G_{night}, (e) and G_{net}) and net community production ((b) NCP_{day}, (d) NCP_{night}, and (f) NCP_{net}) versus Standardized Climate Change (SCC). Each point represents net ecosystem calcification (left panel) or net community production (right panel) calculated from an individual aquarium. Standardized Climate Change was centered around background seawater conditions such that a value of 0 indicated that there was no change in pCO_2 or temperature. Positive values indicate an elevated pCO_2 and temperature condition relative to background and negative values represent lower pCO_2 and temperature conditions. G_{day} had a non-linear relationship with Standardized Climate Change ($y = -0.27x^2 + 0.59x + 5.7$), while G_{night} ($y = -0.63x - 3.6$) and G_{net} ($y = -0.76x + 1.1$) each had a negative linear relationship with Standardized Climate Change (Table 2). NCP_{day} ($y = -7.01x + 23.4$), NCP_{night} ($y = -35.76 - 4.74$), and NCP_{net} ($y = -12.07x - 10.85$) all had significant negative relationships with Standardized Climate Change. Black lines are best fit lines for each model with 95 % confidence intervals in gray. The x's on the top panel represent the imposed conditions for Pre-industrial, Present Day, 2050, and 2100. The black horizontal line in in panels (b), (e) and (f) shows the point where G and NCP = 0. Points above the line are net calcifying (e) or net photosynethsizing (f) and points below the line are net dissolving (e) or net respiring (f) over the entire 24 hour period.

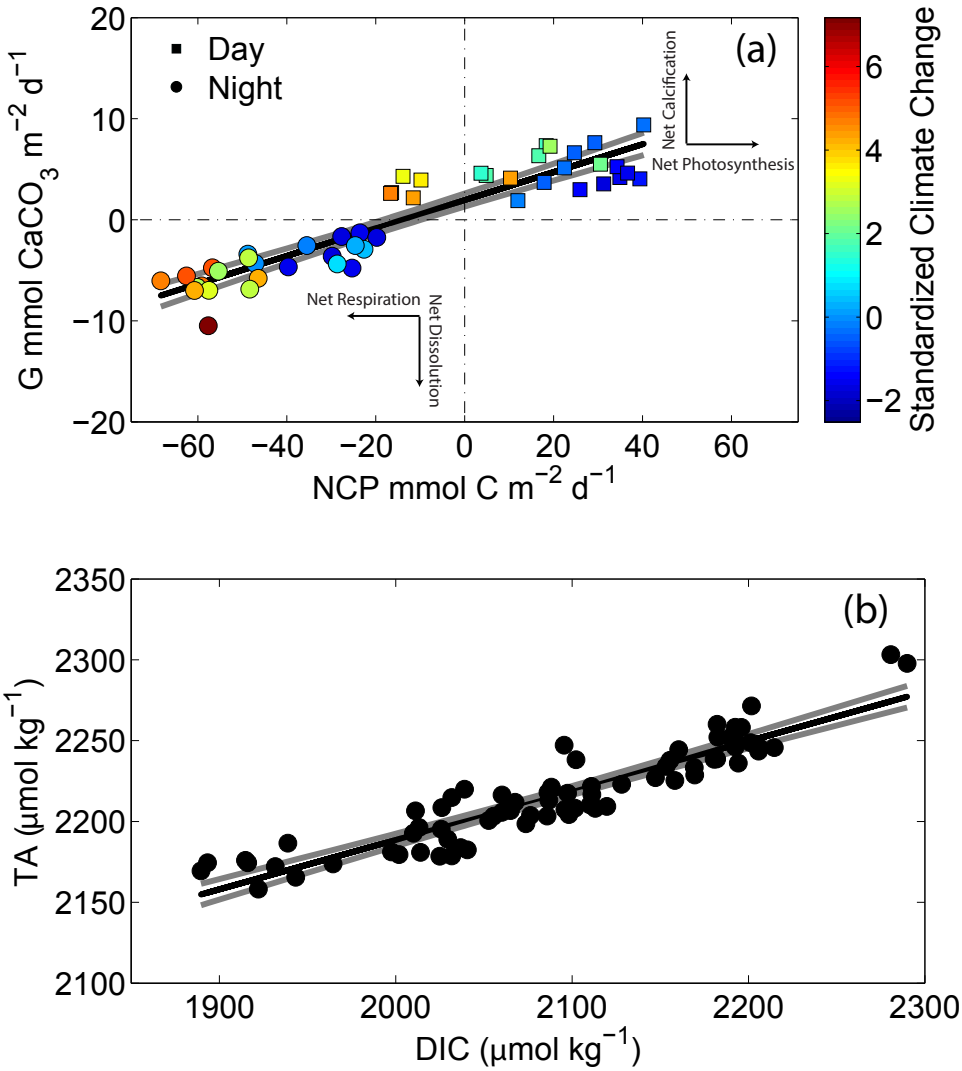

Figure 4: (a) Calculated G and NCP rates for all treatment aquaria. Squares are data collected during light (day) conditions and circles represent data collected during dark (night) conditions, and the color represents Standardized Climate Change (color bar). There is a strong positive relationship between G and NCP ($y = 0.14x + 1.9$, p<0.0001, R^2=0.85). Negative and positive y-values are net dissolution and net calcification, respectively; negative and positive x-values are net respiration and net photosynthesis, respectively. (b) TA versus DIC: There is a strong positive relationship between TA and DIC ($y = 0.31x + 1577.4$, p<0.0001, R^2=0.85). Black and gray lines represent the best-fit line and 95 % confidence intervals, respectively. As expected, the slope of TA versus DIC (0.31) is approximately twice that of G versus NCP (0.14).

SUPPLEMENTAL MATERIAL:

Tables S1-S2
G and NCP calculations:
Figures S1-S6

Table S1: Analysis of variance for G_{day}, G_{night}, and G_{net} across the four climate scenario treatments (Figure S3).

	SS	df	MS	F	p
G_{day}					
Treatment	28.83	3	9.81	3.65	**0.030**
Error	52.61	20	2.63		
Total	81.45	23			
G_{night}					
Treatment	60.39	3	20.13	8.84	**<0.0001**
Error	45.53	20	2.28		
Total	105.92	23			
G_{net}					
Treatment	104.31	3	34.77	8.37	**<0.0001**
Error	83.05	20	4.15		
Total	197.36	23			

Table S2: Analysis of variance for NCP_{day}, NCP_{night}, and NCP_{net} versus climate scenario treatments (Figure S4).

	SS	df	MS	F	p
NCP_{day}					
Treatment	6265.3	3	2088.4	26.0	**<0.0001**
Error	1603.2	20	80.2		
Total	7868.6	23			
NCP_{night}					
Treatment	4145.2	3	1381.7	21.5	**<0.0001**
Error	1283.4	20	64.2		
Total	5428.6	23			
NCP_{net}					
Treatment	1936.8	3	6456.0	71.6	**<0.0001**
Error	1803.4	20	90.17		
Total	2117.1	23			

G and NCP calculations: Below are the specific calculations for G and NCP for Equations 1 and 2 in the text (in mmol C m^{-2} hr^{-1}). For comparisons with existing literature, G and NCP were both multiplied by 12 hr/day to get mmol m^{-2} d^{-1}.

Equation 1 (equations modified from Andersson et al. 2009):

$$G = \left[F_{TAin} - F_{TAout} - \frac{d\mathrm{TA}}{dt}\right]/2 \quad \text{(S1)}$$

F_{TAin} is the rate of TA flowing into the aquaria in mmol $CaCO_3$ m^{-2} hr^{-1}:

$$F_{TAin} = ((TA_{H,t2} + TA_{H,t1})\frac{1}{2} * FlowRate_{aq})/1000 \quad \text{(S2)}$$

F_{TAout} is the rate of TA flowing out of the aquaria in mmol $CaCO_3$ m^{-2} hr^{-1}:

$$F_{TAout} = ((TA_{aq,t2} + TA_{aq,t1})\frac{1}{2} * FlowRate_{aq})/1000 \quad \text{(S3)}$$

$\frac{d\mathrm{TA}}{dt}$ is the change in TA in each aquaria in mmol $CaCO_3$ m^{-2} hr^{-1}:

$$\frac{d\mathrm{TA}}{dt} = \frac{\frac{TA_{aq,t2} - TA_{aq,t1}}{\Delta t * SA} * Vol * \rho}{1000} \quad \text{(S4)}$$

Each equation is divided by 1000 to convert from µmol of $CaCO_3$ to mmol of $CaCO_3$

Parameters:

$TA_{H,t1}$ = Total alkalinity in the header tank at the first sampling time point (µEq kg^{-1}).

$TA_{H,t2}$ = Total alkalinity in the header tank at the second sampling time point (µEq kg^{-1}).

$TA_{aq,t1}$ = Total alkalinity in the aquarium at the first sampling time point (µEq kg^{-1}).

$TA_{aq,t2}$ = Total alkalinity in the aquarium at the second sampling time point (µEq kg^{-1}).

Δt = Time between first and second sampling time point (h)

SA = Surface area of the rubble in the aquarium (m^{-2})

Vol= Volume of water in the aquarium (L)

ρ = Density of seawater (kg L^{-1})

$FlowRate_{aq}$ = Flow rate of the water coming into the aquarium in kg m^{-2} h^{-1} (equal to flow rate of the water leaving the aquarium)

NCP is net community production rate in mmol C m^{-2} d^{-1} :

$$NCP = \left[F_{\mathrm{DIC}in} - F_{\mathrm{DIC}out} - \frac{d\mathrm{DIC}}{dt}\right] - G \qquad \text{(S5)}$$

$F_{\mathrm{DIC}in}$, $F_{\mathrm{DIC}out}$, $\frac{d\mathrm{DIC}}{dt}$ are calculated in the same way as, F_{TAin}, F_{TAout}, and $\frac{d\mathrm{TA}}{dt}$ in Equations S2-S4), replacing Total Alkalinity with Dissolved Inorganic Carbon.

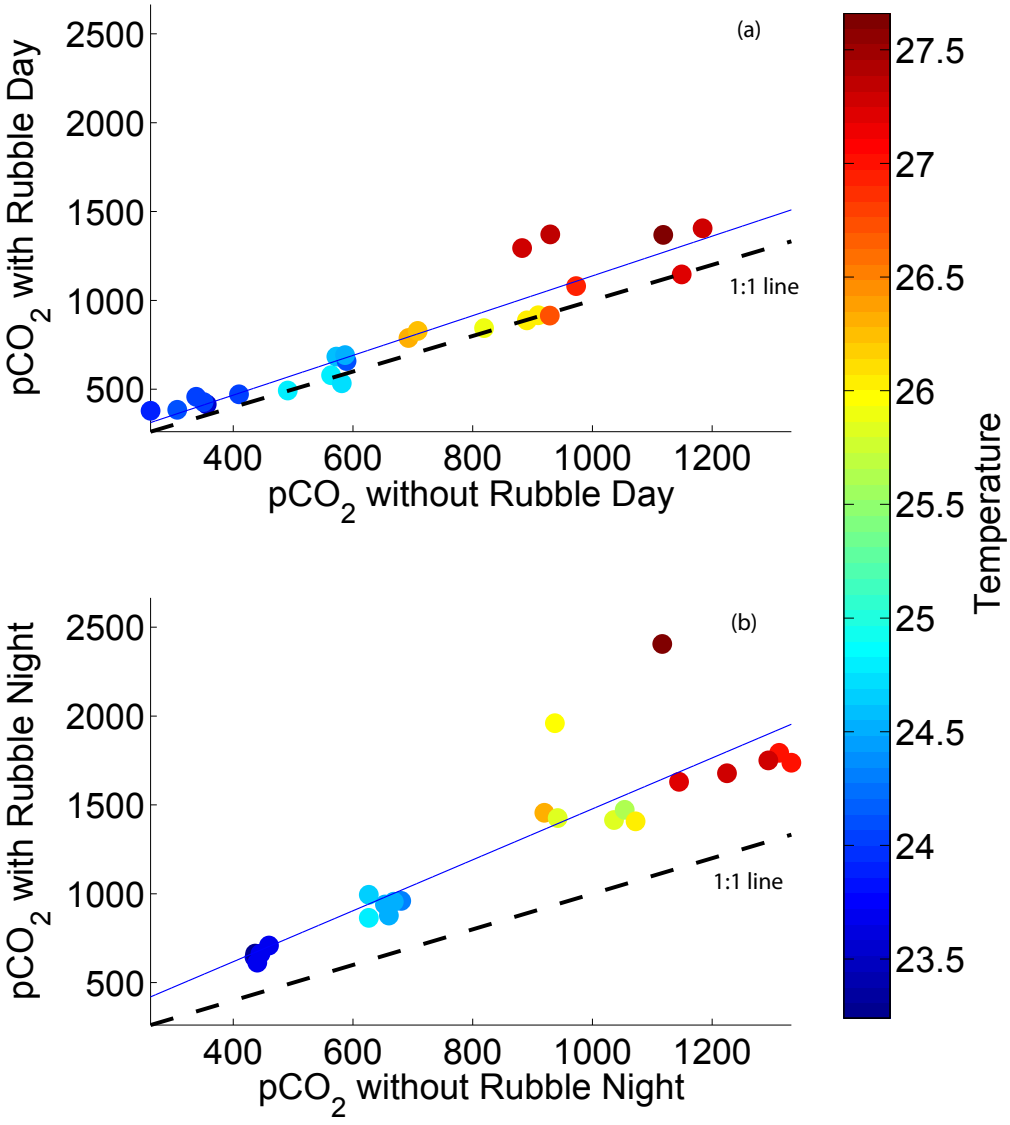

Figure S1: Feedbacks in seawater chemistry caused by the presence of rubble during the (a) day and (b) night. X-axis is pCO_2 in seawater without any rubble and y-axis is pCO_2 in seawater with rubble present. Color represents temperature. The black dashed line is a 1:1 line and the blue line is a regression line. The pCO_2 conditions drift farther away from the manipulated conditions during the night. The slopes from each regression analysis were both greater than one (Day: $y = 1.12x + 19.83$, Night: $y = 1.43x + 44.54$) meaning that the biological feedbacks were greater at more extreme treatments and greater during the night than the day.

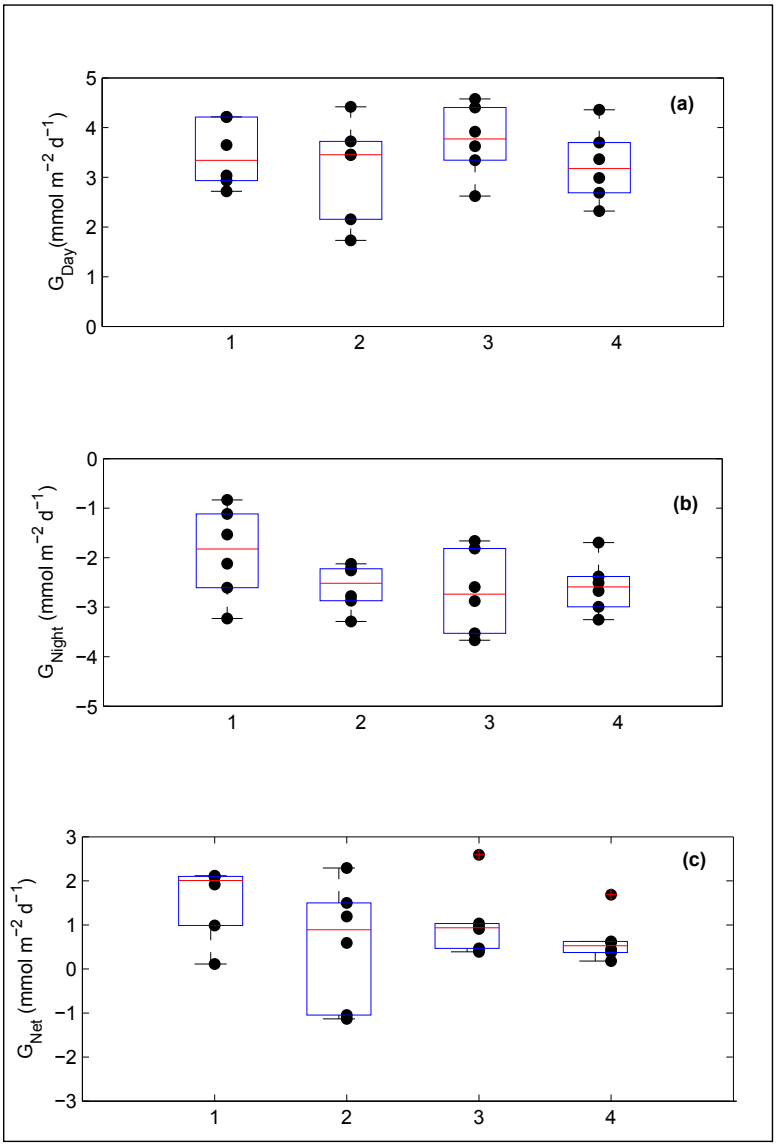

Figure S2: Boxplots for (a) G_{day} , (b) G_{night} , and (c) G_{net} for the control experiment separated by rack. We used an ANOVA to test for differences across racks and found no significant difference in G_{day} ($F_{3,23}$=0.68, p=0.58), G_{night} ($F_{3,23}$=1.52, p=0.24), or G_{net} ($F_{3,23}$=1.38, p=0.28).

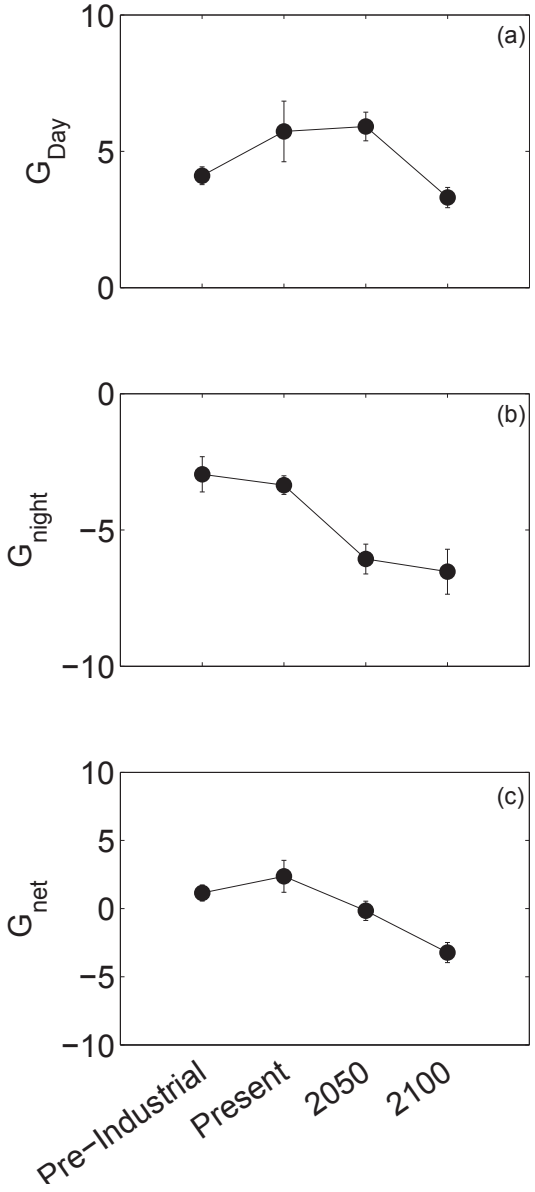

Figure S3: Means and standard error bars for (a) G_{day}, (b) G_{night}, and (c) G_{net} in mmol m^{-2} d^{-1} in the four climate scenario treatment categories. There were significant differences between treatments for G_{day} (p=0.03), G_{night} (p<0.0001), and G_{net} (p<0.0001) (Table S1).

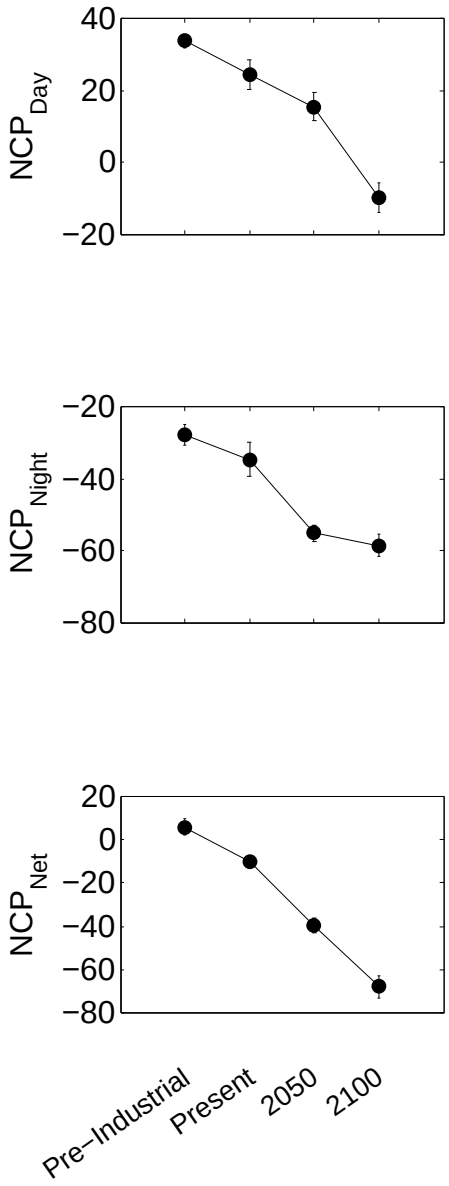

Figure S4: Means and standard error bars for (a) NCP$_{day}$, (b) NCP$_{night}$, and (c) NCP$_{net}$ in mmol m^{-2} d^{-1} across the four climate scenario treatments. There were significant differences across treatments for NCP$_{day}$ (p<0.0001), NCP$_{night}$ (p<0.0001), and NCP$_{net}$ (p<0.0001) (Table S2).

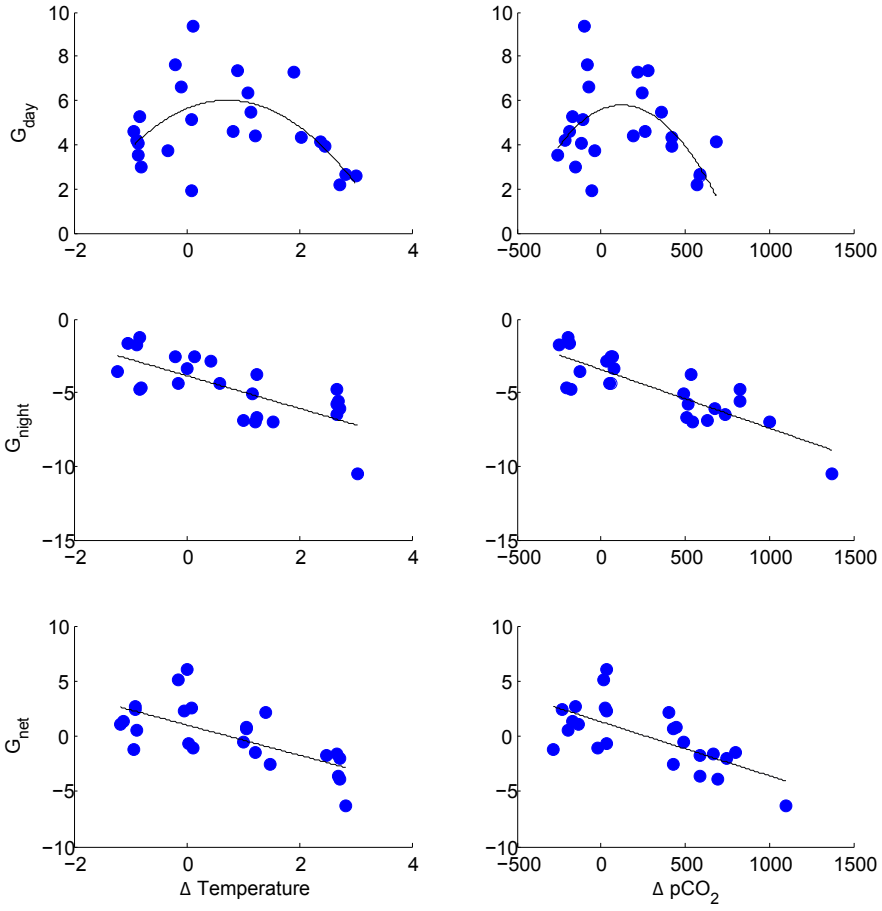

Figure S5: Net ecosystem calcification (G_{day}, G_{night}, and G_{net}) versus ΔTemperature (left panel) and ΔpCO_2 (right panel). Lines are best fit lines. G_{day} has a significant non-linear relationship ΔpCO_2 (p=0.04) and ΔTemperature (p=0.01). $_{night}$, (ΔTemp: p<0.001, ΔpCO_2: p<0.001) and G_{net} (ΔTemp: p<0.001, ΔpCO_2: p<0.001) both have significant linear relationships with ΔpCO_2 and ΔTemperature.

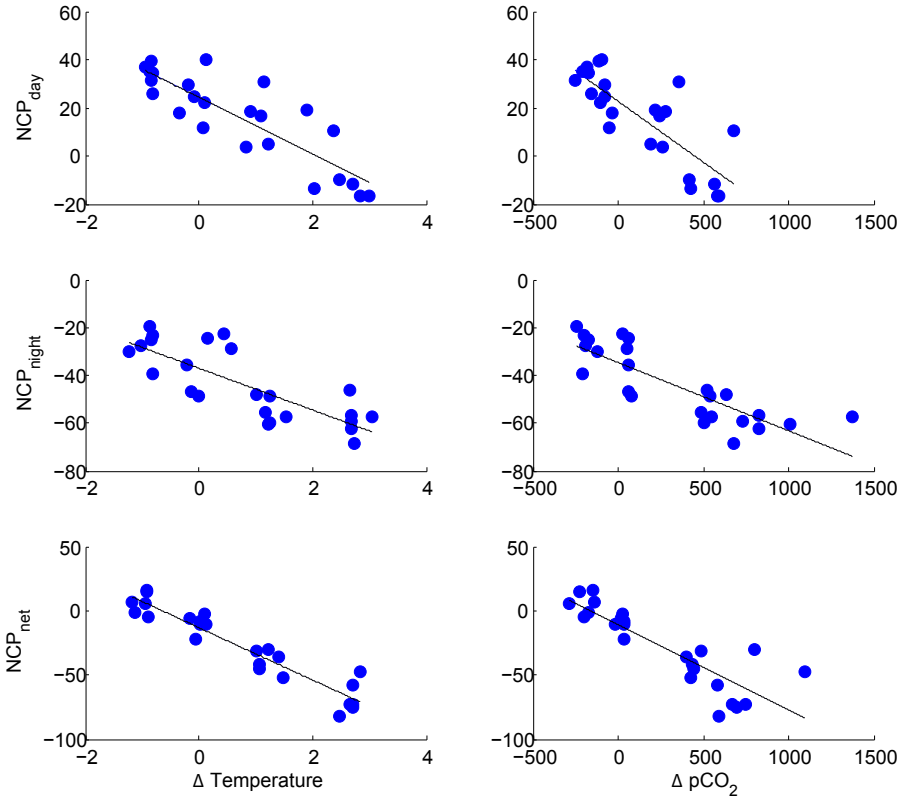

Figure S6: Net community production (NCP$_{day}$, NCP$_{night}$, and NCP$_{net}$) versus ΔTemperature (left panel) and ΔpCO$_2$ (right panel). Lines are best fit lines. NCP$_{day}$ (ΔTemp: p<0.001, ΔpCO$_2$: p<0.001), NCP$_{night}$, (ΔTemp: p<0.001, ΔpCO$_2$: p<0.001) and NCP$_{net}$t (ΔTemp: p<0.001, ΔpCO$_2$: p<0.001) all have significant linear relationships with ΔpCO$_2$ and ΔTemperature.

CHAPTER 6

SUMMARY AND SYNTHESIS

SUMMARY

General Summary

Coral reefs live in a balance between reef growth (accretion) and reef breakdown (erosion) and both processes are necessary to maintain the integrity of the coral reef framework. If the balance shifts, and erosion becomes excessive, the complex structural reef framework will cease to exist. In this dissertation, I explore different facets of the accretion-erosion balance and make inferences for how the balance may shift under predicted ocean conditions. Corals have been the primary focus of research on the drivers and stressors influencing net reef growth (see, Hoegh-Guldberg et al. 2007; Pandolfi et al. 2011). However, "secondary" calcification and erosion processes are critical to net reef growth and comparatively understudied. Thus, to showcase an underrepresented area of research, I focused only on secondary accretion (hereafter, "accretion") and erosion. Using a combination of natural and controlled environmental conditions, I aimed to answer three fundamental questions about the coral reef accretion-erosion balance:

1) What are the dominant environmental drivers of accretion-erosion rates and of bioeroder community composition?

2) Is the relationship between environmental drivers and accretion-erosion rates conserved across different spatial scales?

3) How will predicted changes in sea surface temperature (SST) and ocean acidity impact the accretion-erosion balance?

To answer these questions, I measured accretion and erosion rates across natural environmental gradients ranging from within a single reef (~30m) to across an archipelago (~2500 km). Using new methods for visualizing and analyzing accretion and erosion, I determined how different environmental parameters drive accretion and erosion at different spatial scales. Taking an

experimental approach, I used a controlled laboratory setting to simulate the impact of climate change scenarios on calcification and dissolution rates by a natural community of borers and encrusters.

Summary of experimental findings

In Chapter 2, I characterized the spatial and temporal variability in pH, temperature, and resource availability (DIN:DIP and chorophyll *a*) at 21 sites along a 34m onshore to offshore reef transect. Using a model selection approach, I compared the means and variances of these environmental parameters along with depth and distance from shore as potential predictors of net reef erosion (calculated as the % change in volume of experimental $CaCO_3$ blocks). There were steep gradients in the means and variances of pH along the transect. In fact, several of the 21 sites experience natural, daily pH variation that exceeds the predicted range for mean pH in the 21st century (Bopp et al. 2013). pH was the best predictor of net reef erosion with net erosion being highest at the most acidic sites. This chapter highlights pH variation at small spatial scales (<1m) in coastal systems and the importance of micro-habitat variation for net reef erosion. My findings also suggest that increases in reef erosion, combined with expected decreases in calcification (Hoegh-Guldberg et al. 2007; Kroeker et al. 2010; Pandolfi et al. 2011), could accelerate the shift of coral reefs to an erosion-dominated system in a high-CO_2 world.

In Chapter 3, I used a more sophisticated analysis of the µCT data presented in Chapter 2 to separate accretion and erosion rates along the same environmental gradient. I also highlighted the applicability of µCT as a novel method for quantifying accretion and erosion rates. In Chapter 2, I used µCT to calculate net erosion as a percent change in volume of experimental blocks, but, in Chapter 3, I advanced this technique and separated accretion and erosion

processes using before and after μCT scans. There were two major outcomes from this chapter: 1) accretion and erosion were driven by different environmental parameters: distance from shore drove patterns in accretion and pH drove patterns in erosion and 2) erosion was more sensitive to pH than accretion.

Chapter 4 assessed the patterns and drivers of accretion-erosion rates and macroborer communities across the Hawaiian Archipelago. For this chapter, I deployed bioerosion blocks and sampled bioeroder communities in natural substrate at 29 sites from Maui to Kure. Using a hierarchical framework, I described spatial patterns in accretion-erosion rates and macroborer communities and determined the source of variance across four spatial scales (regions, islands, sites, within sites). In all cases, the highest source of variance in the data was from the within-site spatial scale, highlighting the importance of small-scale variability to accretion-erosion processes. Using existing data from state and federal agencies, I compiled a suite of chemical, physical, and biological datasets that described the environment at each site. I found, again, that accretion and erosion were driven by different environmental parameters. The chemical parameters (which included carbonate chemistry and nutrients) ranked highest for the macroborer communities. I also tested relationships between environmental parameters and accretion-erosion rates across spatial scales and found that the relationships were not conserved across space; there were different dominant drivers for all accretion-erosion rates between the Main Hawaiian Island and Northwestern Hawaiian Island models.

Chapter 5 focused on the impacts of rising SST and ocean acidity on calcification and dissolution on the community of borers and secondary calcifiers living on and in dead coral rubble. In a controlled laboratory setting, I manipulated pCO_2 and temperature to expose these rubble communities to pre-industrial, present day, 2050, and 2100 ocean conditions based on the

RCP 8.5 climate scenario (Meinshausen et al. 2011; Rogelj et al. 2012). Secondary reef calcification and dissolution responded differently to the combined effect of pCO_2 and temperature. Calcification had a non-linear response to pCO_2 and temperature: the highest calcification rate occurred slightly above ambient conditions and the lowest calcification rate was in the highest temperature– pCO_2 condition. In contrast, dissolution increased linearly with temperature– pCO_2. These results indicate that dissolution may be more sensitive to climate change than calcification and that calcification and dissolution have different functional responses to climate stressors.

SYNTHESIS

There were several themes that arose from my dissertation:

1) Accretion and erosion are driven by different environmental parameters. At a small, within-reef scale (Ch 2-3), pH was the best predictor for erosion, while distance from shore was the best predictor for accretion. At a large scale (Ch 4), chemical parameters were the strongest drivers of accretion while biological and physical parameters were the strongest drivers of erosion. Even in the controlled laboratory study, where only temperature and ocean acidity were manipulated, accretion (or calcification) responded differently from erosion (or dissolution). Previous studies that examined accretion and erosion individually have, similarly, found different responses to environmental stress. For example, coral calcification and bioerosion have different functional relationships with land-based pollution on Indonesian reefs (Edinger et al. 2000). Laboratory experiments focusing on temperature and ocean acidity have found linear relationships with erosion (Tribollet et al. 2009; Wisshak et al. 2012; Fang et al. 2013; Reyes-

Nivia et al. 2013) and both linear (Pandolfi et al. 2011; Comeau et al. 2013) and parabolic (Pandolfi et al. 2011; Comeau et al. 2013; Castillo et al. 2014) relationships with calcification. These complex responses to environmental variation highlight the need to examine both accretion and erosion when predicting reef response to environmental stress.

2) Erosion is more sensitive to ocean acidity than accretion. Erosion, and dissolution, was more sensitive to ocean acidity than accretion in response to natural and manipulated pH variability. In Chapter 3, pH ranked highest when compared to other environmental models and explained 54% of the variation in erosion. For accretion, pH ranked second and only explained 13% of the variance in the data. Complementary to these findings, dissolution had a sharp negative relationship with pH (and temperature) while calcification had a weak, parabolic response to pH (and temperature) in the manipulation experiment. Reef erosion (and dissolution), rather than reef accretion, may be driving the negative relationship between ocean acidification and net calcification of coral reefs (Erez et al. 2011), and recent studies support this hypothesis (Rodolfo-Metalpa et al. 2011). My results and those from previous studies (Tribollet et al. 2009; Wisshak et al. 2012; Fang et al. 2013; Silbiger et al. 2014; DeCarlo et al. 2015; Silbiger and Donahue 2015) provide compelling evidence that erosion rates will increase under future ocean conditions.

3) Local-scale variability is important to the accretion-erosion balance. Coral reefs are embedded in highly variable coastal ecosystems (Gagliano et al. 2010, Hofmann et al. 2011, Guadayol et al. 2014) where restricted water motion, terrestrial influences, and feedbacks between benthic productivity and calcification strongly influence the physicochemical

environment (Yates et al. 2007, Drupp et al. 2011, Massaro et al. 2012, Duarte et al. 2013, Smith et al. 2013). In Chapters 2 & 3, we characterized the spatiotemporal variability in pH, nutrients, chlorphyll *a*, and temperature along a 34m reef transect. Local-scale differences in pH drove patterns in accretion-erosion rates and had high explanatory power: net reef erosion (% change in volume) had an R^2 of 0.64 and erosion rates had an R^2 of 0.54, suggesting that local-scale physicochemical differences in microhabitats strongly influence accretion-erosion rates. Further, in the broad scale study (Chapter 4), the within-site spatial scale had the highest amount of variability in the data. These data provide compelling evidence that local-scale environmental variability is particularly important to the coral reef accretion-erosion balance and may pose challenges for predicting reef response.

4) µCT is a good tool for measuring accretion-erosion rates. In Chapters 2-4, I used before and after µCT scans to calculate accretion rates, erosion rates, and percent change in volume in experimental blocks of $CaCO_3$. In prior studies using experimental substrates, pre and post deployment buoyant weights have been used to calculate changes in density, mass, or volume, but buoyant weights are unable to distinguish between accretion and erosion processes. Imaging methodologies in 2-dimensions and, more recently, 3-dimensions (CT and µCT) can separate accretion and erosion on slabs or cores of reef, but rates are difficult to estimate because the period of exposure is unknown. Here, I developed a new analysis that uses µCT to separate reef accretion and erosion with a micrometer-scale resolution from the same experimental substrate exposed to the same environmental variation over the same time-scale. This µCT method also allows for a 3D visualization of the experimental blocks that highlights specific areas of

accretion and erosion. The development of this technique will advance the understanding of accretion-erosion beyond the limits imposed by traditional methods.

5) Ocean acidity could tip the balance. Although there are many environmental drivers of accretion-erosion, there is a consistent pattern of higher erosion rates with higher ocean acidity. Erosion rates have shown an increase with rising ocean acidity on small spatial scales (Silbiger et al. 2014), large spatial scales (DeCarlo et al. 2015), and in laboratory studies (Tribollet et al. 2009; Wisshak et al. 2012; Fang et al. 2013; Reyes-Nivia et al. 2013; Wisshak et al. 2013; Enochs et al. 2015; Silbiger and Donahue 2015). Though we did not find pH to be a strong predictor in secondary accretion, several studies have shown that coral calcification decreases with increasing CO_2 (Hoegh-Guldberg et al. 2007; Kroeker et al. 2010; Pandolfi et al. 2011). Could ocean acidity tip the accretion-erosion balance? Previous studies on coral reefs have shown shifts from net accretion to erosion after major disturbances, such as El Niño-Southern Oscillation events or hurricanes (Perry et al. 2008). The data from this dissertation indicate that pH is a significant driver of reef erosion and that, as mean pH decreases, erosion rates will increase. The combination of slower coral growth (Hoegh-Guldberg et al. 2007; Kroeker et al. 2010; Pandolfi et al. 2011) and higher erosion rates (Tribollet et al. 2009; Wisshak et al. 2012; Fang et al. 2013; Reyes-Nivia et al. 2013; Wisshak et al. 2013; Enochs et al. 2015; Silbiger and Donahue 2015) in response to ocean acidification could act synergistically to hinder reef growth. Further, given the strong relationship between bioerosion and local anthropogenic impacts like sedimentation and nutrient runoff (Edinger et al. 2000; Le Grand and Fabricius 2011), the combined effect of these local impacts with decreases in pH in the global oceans could be devastating to reefs worldwide.

Manuscript publications

Chapter 2: Silbiger NJ, Guadayol, Ó, Thomas FIM, Donahue MJ (2014) Reefs shift from net accretion to net erosion along a natural environmental gradient. *Marine Ecology Progress Series* 515:33-44

Chapter 3: Silbiger NJ, Guadayol, Ó, Thomas FIM, Donahue MJ (*submitted)* Ranking the impact of multiple environmental stressors on coral reef erosion and secondary accretion.

Chapter 4: Silbiger NJ, Donahue MJ (2015) Secondary calcification and dissolution respond differently to future ocean conditions. *Biogeosciences* 12:567-578

Chapter 5: Silbiger, NJ, Donahue, MJ et al. (*in prep*). A multi- scale analysis of coral reef accretion-erosion rates and bioeroder communities.

References

Bopp L, Resplandy L, Orr JC, Doney SC, Dunne JP, Gehlen M, Halloran P, Heinze C, Ilyina T, Séférian R, Tjiputra J, Vichi M (2013) Multiple stressors of ocean ecosystems in the 21st century: projections with CMIP5 models. Biogeosciences 10:3627-3676

Castillo KD, Ries JB, Bruno JF, Westfield IT (2014) The reef-building coral *Siderastrea siderea* exhibits parabolic responses to ocean acidification and warming. Proceedings of the Royal Society B: Biological Sciences 281:20141856

Comeau S, Edmunds PJ, Spindel NB, Carpenter RC (2013) The responses of eight coral reef calcifiers to increasing partial pressure of CO_2 do not exhibit a tipping point. Limnol Oceanogr 58:388-398

DeCarlo TM, Cohen AL, Barkley HC, Cobban Q, Young C, Shamberger KE, Brainard RE, Golbuu Y (2015) Coral macrobioerosion is accelerated by ocean acidification and nutrients. Geology 43:7-10

Edinger EN, Limmon GV, Jompa J, Widjatmoko W, Heikoop JM, Risk MJ (2000) Normal coral growth rates on dying reefs: Are coral growth rates good indicators of reef health? Marine Pollution Bulletin 40:404-425

Enochs IC, Manzello DP, Carlton RD, Graham DM, Ruzicka R, Colella MA (2015) Ocean acidification enhances the bioerosion of a common coral reef sponge: implications for the persistence of the Florida Reef Tract. Bulletin of Marine Science 91:000-000

Erez J, Reynaud S, Silverman J, Schneider K, Allemand D (2011) Coral calcification under ocean acidification and global change. In: Dubinski Z, Stambler N (eds) Coral Reefs: an ecosystem in transition. Springer,

Fang JKH, Mello-Athayde MA, Schönberg CHL, Kline DI, Hoegh-Guldberg O, Dove S (2013) Sponge biomass and bioerosion rates increase under ocean warming and acidification. Global Change Biology 19:3581-3591

Hoegh-Guldberg O, Mumby PJ, Hooten AJ, Steneck RS, Greenfield P, Gomez E, Harvell CD, Sale PF, Edwards AJ, Caldeira K, Knowlton N, Eakin CM, Iglesias-Prieto R, Muthiga N, Bradbury RH, Dubi A, Hatziolos ME (2007) Coral reefs under rapid climate change and ocean acidification. Science 318:1737-1742

Kroeker KJ, Kordas RL, Crim RN, Singh GG (2010) Meta-analysis reveals negative yet variable effects of ocean acidification on marine organisms. Ecology Letters 13:1419-1434

Le Grand HM, Fabricius KE (2011) Relationship of internal macrobioeroder densities in living massive Porites to turbidity and chlorophyll on the Australian Great Barrier Reef. Coral Reefs 30:97-107

Meinshausen M, Smith SJ, Calvin K, Daniel JS, Kainuma MLT, Lamarque JF, Matsumoto K, Montzka SA, Raper SCB, Riahi K (2011) The RCP greenhouse gas concentrations and their extensions from 1765 to 2300. Climatic Change 109:213-241

Pandolfi JM, Connolly SR, Marshall DJ, Cohen AL (2011) Projecting coral reef futures under global warming and ocean acidification. Science 333:418-422

Perry CT, Spencer T, Kench PS (2008) Carbonate budgets and reef production states: a geomorphic perspective on the ecological phase-shift concept. Coral Reefs 27:853-866

Reyes-Nivia C, Diaz-Pulido G, Kline D, Guldberg O-H, Dove S (2013) Ocean acidification and warming scenarios increase microbioerosion of coral skeletons. Global Change Biology 19:1919-1929

Rodolfo-Metalpa R, Houlbrèque F, Tambutté É, Boisson F, Baggini C, Patti FP, Jeffree R, Fine M, Foggo A, Gattuso JP (2011) Coral and mollusc resistance to ocean acidification adversely affected by warming. Nature Climate Change 1:308-312

Rogelj J, Meinshausen M, Knutti R (2012) Global warming under old and new scenarios using IPCC climate sensitivity range estimates. Nature Climate Change 2:248-253

Silbiger NJ, Donahue MJ (2015) Secondary calcification and dissolution respond differently to future ocean conditions. Biogeosciences 12:567-578

Silbiger NJ, Guadayol, O, Thomas FIM, Donahue MJ (2014) Reefs shift from net accretion to net erosion along a natural environmental gradient. Marine Ecology Progress Series 515:33-44

Tribollet A, Godinot C, Atkinson M, Langdon C (2009) Effects of elevated $pCO_{(2)}$ on dissolution of coral carbonates by microbial euendoliths. Global Biogeochemical Cycles 23:GB3008

Wisshak M, Schönberg CHL, Form A, Freiwald A (2012) Ocean acidification accelerates reef bioerosion. Plos One 7:e45124-e45124

Wisshak M, Schönberg CHL, Form A, Freiwald A (2013) Effects of ocean acidification and global warming on reef bioerosion—lessons from a clionaid sponge. Aquatic Biology 19:111-127